Analysis of Ureteric Bud Morphogenesis by Reassociation of Fetal Kidney Cells

Kevin Leclerc

Submitted in partial fulfillment of the requirements for the degree of Doctor of Philosophy

under the Executive Committee

of the Graduate School of Arts and Sciences

COLUMBIA UNIVERSITY

2016

ABSTRACT

Analysis of Ureteric Bud Morphogenesis by Reassociation of Fetal Kidney Cells

Kevin Leclerc

While the genetic control of ureteric bud (UB) morphogenesis has been extensively studied, the cellular basis of this process remains unclear. The renal organoid system is a novel technique in which embryonic kidneys are dissociated into single cells and then reaggregated, where they reassociate to form organotypic structures. This system may be very beneficial for investigating the cellular basis of ureteric bud development. Here, we first used a fluorescent UB marker, Hoxb7:myrVenus, and time-lapse microscopy to characterize the cellular and tissue-level events during self-organization and UB morphogenesis of E12.5 or E14.5 renal organoids. Briefly, we found that UB structures self-assembled by aggregation of individual cells that sent out long cell processes. The cellular aggregates grew and elongated into epithelial tubes that displayed characteristic ampullae, bifurcated, and appropriately expressed UB tip markers analogous to their *in vivo* counterparts. We also found that cap mesenchymal cells are attracted to newly formed epithelial structures early in renal organoid development, and were later found in cell clusters surrounding new branches.

RET is a trans-membrane tyrosine kinase receptor (RTK), expressed in ureteric bud cells, whose expression is gradually restricted to the tips of the growing ureteric tree. We demonstrate that the renal organoid system can be used, as an alternative to the generation of *in vivo* chimeric embryos, to study Ret-dependent cell rearrangements previously shown

to establish and maintain the UB tip progenitor domain. Chimeric renal organoids that juxtaposed wild-type cells with *Sprouty1*$^{-/-}$ mutant cells (higher Ret-signaling) or with Ret$^{51/cre}$ (lower Ret-signaling) mutant cells recapitulated the cell sorting pattern observed in similar *in vivo* chimeras. The cells with higher Ret-signaling preferentially sorted to, and were maintained in, the forming and growing tips of these mosaic ureteric bud structures, out-competing cells with lower Ret-signaling.

We then used the mosaic organoid system to ask if fibroblast growth factor receptor 2 (Fgfr2), another RTK expressed in the ureteric bud and important for its development, also mediates individual cell rearrangements that generate and maintain the UB tips. UB cells null for *Fgfr2* were largely unable to compete with wild-type cells for occupancy of the UB tips in chimeric renal organoids. Using the innovative MASTR (Mosaic Mutant Analysis with Spatial and Temporal Control of Recombination) technique *in vivo*, mosaic homozygous deletion of *Fgfr2* in newly formed ureteric buds also revealed that mutant cells were slightly deficient in their ability to contribute to *Fgfr2* heterozygous UB tips. This demonstrates a novel, cell-autonomous role of *Fgfr2* in ureteric bud development.

Matrix metalloproteinase 14 (MMP14) is a membrane-bound protein known to participate in a wide variety of cell functions including degradation of the extracellular matrix (ECM), cell signaling, and cell-autonomous cell migration. It is expressed in the UB and was discovered to act downstream of Ret-signaling. Although needed in the ureteric epithelium for ECM degradation and proper UB morphogenesis, its specific function in the UB has not been thoroughly investigated. In generating *in vivo* chimeras, we discovered that *Mmp14* null cells could contribute to wild-type ureteric bud tips at E12.5 and E14.5,

demonstrating that, despite its documented role in UB branching, *Mmp14* does not have a cell-autonomous role in the cell rearrangements observed during UB morphogenesis.

Table of Contents

Figures and Tables **iv**

Chapter 1: Introduction **1-18**

Mammalian Kidney Morphogenesis 2

Development of the Wolffian Duct 3

Ureteric Bud Morphogenesis 6

Signals and Receptors Controlling UB Morphogenesis 8

Cellular Mechanisms of UB branching 13

Renal organoid system 16

Chapter 2: Characterizing Ureteric Bud Morphogenesis in a Renal Organoid System **19-49**

Introduction 19

Cellular dynamics during the self-assembly of ureteric bud structures 24

Characterizing UB morphogenesis in renal organoids 28

Cell proliferation during renal organoid UB morphogenesis 30

Characterizing the tip domain of UB structures in renal organoids 33

Investigating metanephric mesenchyme interactions with UB structures in renal organoids 36

Exploring the potential utility of E14.5 renal organoids for the study of UB morphogenesis 40

Discussion 42

Experimental Procedures 46

Chapter 3: The Use of Chimeric Renal Organoids for the Study of Ret-Dependent Cell Rearrangements During UB Morphogenesis 49-79

Introduction 49

Global *Spry1*$^{-/-}$ renal organoids display a phenotype similar in vivo mutants 54

Cellular dynamics during the self-organization of UB cells in *Spry1*$^{-/-}$ renal organoids 57

Spry1$^{-/-}$⇔WT chimeric renal organoids recapitulate the *in vivo* chimera phenotypes 60

Ret$^{51/Cre}$⇔WT chimeric renal organoids recapitulate similar *in vivo* chimera phenotypes 68

Discussion 74

Experimental Procedures 78

Chapter 4: The Cell-Autonomous Role of Fgfr2 During Ureteric Bud Morphogenesis 80-110

Introduction 80

Global *Fgfr2*$^{UB-/-}$ renal organoids display a severe reduction in UB morphogenesis 85

Wildtype cells preferentially occupy the UB tips of *Fgfr2*$^{UB-/-}$ ⇔WT renal organoid chimeras 87

Cells lacking *Fgfr2* become slightly less abundant in heterozygous UB tips. 95

Discussion 101

Experimental Procedures 107

CHAPTER 5: The Role of Matrix Metalloproteinase 14 in Early Kidney Development 109-135

Introduction 109

Testing the requirement for Mmp14 during cellular rearrangements in the Wolffian duct and ureteric bud 114

Exploring the role of MMP14 in promoting ureteric bud growth by gain-of-function studies 118

Discussion 126

Experimental Procedures 131

CHAPTER 6: Discussion 136-140

REFERENCES 141-152

APPENDIX 153-195

FIGURES AND TABLES

Figure 1.1 Development of the Wolffian duct and renal collecting duct system 5

Figure 1.2 Expression pattern of Ret and GNDF during UB morphogenesis 7

Figure 1.3 RTK signaling and the downstream genetic network that control ureteric bud branching 10

Figure 1.4 RTK-signaling dependent cell movements that may establish and maintain the progenitor tip domain of the UB 14

Figure 1.5 Schematics illustrating the methods used to create renal organoids and chimeric renal organoids for the study of UB morphogenesis, based on *Unbekandt et al. (2010)* 16

Figure 2.1 Cellular dynamics during the self-assembly of UB structures in the renal organoid system 26

Figure 2.2 Individual cells self-assemble to form UB spheroids and "pseudo-branched" UB tubules during the first 24 hours of culture 27

Figure 2.3 Renal organoids undergo ureteric bud branching morphogenesis with some features similar to *in vivo* developing kidneys 29

Figure 2.4 Proliferation is a major driver of UB morphogenesis in renal organoids 32

Figure 2.5 The ends of renal organoid UB tubules contain organotypic tip domains. 34

Figure 2.6 Renal organoid Ret mRNA expression recapitulates the *in vivo* Ret expression pattern 35

Figure 2.7 Cap mesenchymal cells surround established UB structures within the first 24 hours of renal organoid cultures 37

Figure 2.8 Renal organoid UB tubules elongate and branch in regions enriched in Six2-lineage and Six2+ mesenchyme (MM) 39

Figure 2.9 E14.5 and E12.5 renal cells show a similar potential for UB morphogenesis in renal organoids 41

Figure 3.1 *Sprouty1* mutant renal organoids display large, broad cystic masses of UB epithelia that contain multiple UB outbuddings 56

Figure 3.2 Cellular dynamics during the self-assembly of *Spry1*$^{-/-}$ renal organoids 59

Figure 3.3 Generation of *Sprouty1*$^{-/-}$⇔WT and WT⇔WT chimeric renal organoids 61

Figure 3.4 *Spry1*$^{-/-}$ cells preferentially occupy the tips of chimeric renal organoid structures at the expense of WT cells. 64

Figure 3.5 *Sprouty1*$^{-/-}$ cells outcompete WT cells for residence at the tips of growing and branching chimeric renal organoid structures 66

Figure 3.6 Distribution of wild-type and mutant cells in tip and trunk regions in *Sprouty1*$^{-/-}$⇔WT and WT⇔WT chimeric UB structures 67

Figure 3.7 Generation of *Ret*$^{51/cre}$⇔WT and WT⇔WT chimeric renal organoids. 70

Figure 3.8 *Ret*$^{51/cre}$ cells show a preference for residence of the tips of branching chimeric renal organoid structures at the expense of WT cells 71

Figure 3.9 Distribution of wild-type and mutant cells in tip and trunk regions in *Ret*$^{51/cre}$⇔WT and WT⇔WT chimeric UB structures 73

Figure 4.1 Time course of *Fgfr2*$^{UB-/-}$ mutant renal organoids 86

Figure 4.2 Generation of *Fgfr2*$^{UB-/-}$ ⇔WT and WT⇔WT chimeric renal organoids 88

Figure 4.3 Wildtype cells show a preference for residence of the tips of chimeric renal organoid structures at the expense of *Fgfr2*$^{UB-/-}$ cells,

after 2-3 days of culture 90

Figure 4.4 Wildtype cells show a preference for residence of the tips of chimeric renal organoid structures at the expense of *Fgfr2*$^{UB-/-}$ cells, after 3-4 days of culture 92

Figure 4.5 Color profiles of tip and trunk regions in *Fgfr2*$^{UB-/-}$ ⇔WT and WT⇔WT chimeric UB structures 94

Figure 4.6 Prevalence of recombinant cells in *R*$^{FlpoER/MASTR}$;*Fgfr2*$^{lox/-}$ and *R*$^{FlpoER/MASTR}$;*Fgfr2*$^{+/-}$ UB tips 98

Table 4.1 The distribution of recombinant UB cells in *R*$^{FlpoER/MASTR}$;*Fgfr2*$^{lox/-}$ and *R*$^{FlpoER/MASTR}$;*Fgfr2*$^{+/-}$ kidneys 99

Figure 4.7 The fraction of recombinant UB cells in the UB tips of *R*$^{FlpoER/MASTR}$; *Fgfr2*$^{lox/-}$ and *R*$^{FlpoER/MASTR}$;*Fgfr2*$^{+/-}$ kidneys 100

Figure 5.1 Distribution of *Mmp14*$^{-/-}$ cells in chimeric Wolffian duct and ureteric bud epithelium at E12.5 115

Figure 5.2 Distribution of *Mmp14*$^{-/-}$ cells in chimeric ureteric bud epithelium at E14.5 117

Figure 5.3 Transfection of retroviral vectors reveals functional plasmids that can overexpress MMP14 119

Figure 5.4 Infection of HEK293 cells with MMP14 and Venus Control virus reveals functional virus and viral infectablility 121

Table 5.1 Troubleshooting retroviral infection of UB epithelia for the overexpression of MMP14 122

Figure 5.5 Infection of renal organoid cultures demonstrates the infectablitly of primary renal cells. 123

Figure 5.6 The disintegration of renal organoid cultures infected with MMP14 and Venus Control virus 125

Acknowledgements

I've always had a strong interest in huge, dynamic urban environments, languages, and cosmology. It wasn't until later in life, however, that I realized the underlying motif that connected all these seemingly disparate domains. It's the idea that out of the chaos comes order. Little tiny modules (be they people, buildings, morphemes, or sub-atomic particles) all making their own "decisions" unaware of the general pattern they help to create overall. So it should be of absolutely no surprise that when I had my first real biology course in middle school, it totally swept me off my feet. It was like magic! I yearned for as much information as I could get. I relished in it. And now, many years later, it's an incredible feeling to be a producer of information, to discover patterns of my own. To achieve this, however, would not have been possible without my amazing support.

I would like to thank Frank for being a great and insightful mentor. He's an incredible scientist who challenges me to ask very difficult questions pertaining to my line of research. I appreciate his enthusiasm, rigor, and dedication, and I whole-heartedly thank him for his support throughout my doctoral studies. I'd also like to especially thank my former mentor and current committee member, Lori Sussel, who has always been rooting for me all along the way, and has always tried to ensure my success. I hold her in very high regard.

I'd like to give thanks my lab mates who often provided much needed comic relief in and out of the lab and were always there to help with experiments or to bounce ideas off of.

To my gigantic family that has always provided me with comfort and support, and their major contribution in molding me into the person I am today

To my bestest of friends, who daily inspire me to live a life full of joy and laughter. They've given me the opportunity to be silly *or* serious, and to feel the warmth of a true connection.

To my boyfriend, who has given me the confidence to pursue dreams thought unimaginable, and believed in me, and has enriched my life daily.

To my aunt, and second mother, Danielle, who nourished my intellectual spirit as a child and immensely facilitated success in all aspects of life.

And no amount of words can describe how greatful I am for my mother. Her unwavering support and love are why I'm here today. She is *still* my main source of encouragement to living this 'ordered chaos' we call 'life' to its fullest potential!

To my mother, who always dreamed of calling me ‘Doctor’….

CHAPTER 1

Introduction

The kidneys are paired organs with several functions. They serve homeostatic functions such as the regulation of electrolytes or maintenance of acid-base balance and also secrete various hormones such as erythropoietin to stimulate red blood cell production or renin to regulate blood pressure (Schedl, 2007; Bunn, 2013; Sparks et al., 2014). As an essential part of the urinary system though, their main function is to filter wastes from the blood that are then diverted to the bladder via the ureter for excretion (Saxen, 1987; Schedl, 2007). Currently more than 26 million Americans are suffering from Chronic Kidney Disease (CKD; National Kidney Foundation, https://www.kidney.org), a gradual loss in kidney function that may go on to result in permanent kidney failure and is a major cause of heart disease (Santos-Araújo et al., 2015). At present the only way to treat severe cases of CKD and other kidney diseases is through kidney dialysis or kidney transplants. For end-stage kidney failure, dialysis is usually considered a holding measure until a kidney transplant can be performed. Renal transplants, however, are impeded by the scarcity of appropriate donor organs or rejection of the transplant by the recipient's immune system. One potential alternative therapy that has gained recent focus is tissue regeneration by directing stem cells to take on the fate of various kidney cell types. The ability to develop new therapies for CKD and other kidney diseases will therefore rely on a complete grasp of the cellular and molecular factors that guide kidney development.

Mammalian Kidney Morphogenesis

One fundamental aspect of development biology is the concept of morphogenesis: understanding how a group of multipotent cells organize and differentiate into a complex organ. In murine kidney development, morphogenetic events lead to the formation of thousands of nephrons, the functional units of the kidney (Merlet-Bénichou et al., 1999), each of which consists of a glomerulus, Bowman's capsule, proximal tubule, loop of Henle, distal tubule and connecting tubule. Nephrons are connected to the renal collecting ducts, a branched network of ducts that serve as a conduit to deliver the filtrate (urine) to the renal pelvis and ureter of the kidney and ultimately to the bladder (**Figure 1.1L** and **M**; Saxen, 1987). These two separate compartments of the kidney, the collecting ducts and the nephrons, arise mostly from two different embryonic tissues, the Wolffian duct (WD; also called the nephric duct) and the bordering metanephric mesenchyme (MM), respectively (Saxen, 1987; Costantini et al., 2010). During early organogenesis (around E10.5 in the mouse), the MM produces inductive signals that cause the adjacent region of the Wolffian duct to evaginate, forming the ureteric bud (UB) **(Figure 1.1H**; Saxen, 1987**)**. The UB grows into the MM and undergoes a series of branching events that give rise to the adult collecting system of the kidney (**Figure 1.1I-M**; Short et al., 2014). At the same time, the tips of the branching UB induce the surrounding MM to undergo a mesenchymal-to-epithelial transition, thereby generating complex epithelial structures that form a connection to the UB tips and later become nephrons (Quaggin et al., 2008). This reveals a reciprocal inductive relationship whereby the mesenchyme induces branching and growth of the UB and the UB induces the mesenchyme to differentiate into nephrons. This reciprocal induction is critical for proper kidney development as the final nephron number is highly

dependent on UB branching (Cebrian et al., 2004). In fact, nephron number in humans can vary by more than 10-fold, and low nephron number is believed to be a significant risk factor for development of hypertension and chronic kidney disease (Hoy et al., 2008). It is therefore important that we study the mechanisms involved in UB branching morphogenesis if we want to improve the health outcomes of at-risk populations.

Development of the Wolffian Duct

We are only beginning to unravel the spatiotemporal requirements of the many morphogenetic and key signaling events necessary for the development of the WD, the UB, and ultimately development of the whole kidney. Early in development (E8.5-E9.5), the WD and the adjacent nephrogenic chord (which gives rise to the MM) both derive from the intermediate mesoderm (IM), a narrow stripe of tissue that runs along the anterior-posterior axis between the paraxial somitic mesoderm and the lateral plate mesoderm (**Figures 1.1A-E**; Barak et al., 2005; Costantini et al., 2010). In response to signals from these tissues and the overlying ectoderm, the Wolffian duct coalesces and elongates caudally, transitioning from a loose group of mesenchymal-like cells to a polarized, epithelial tube (Costantini et al., 2010). The extending WD interacts with the nephrogenic cord to initially produce the pronephric and (more caudally) the mesonephric tubules, which are transient structures that contribute only to male sex accessory tissues in higher vertebrates (Saxen, 1987).

There has been a lot of interest surrounding the cellular mechanisms involved in WD elongation. Cells at the caudal end of the Wolffian duct have been observed to extend large filopodia, a feature that is associated with cell migration and appears to be very

important (Chia et al., 2011; Weiss et al., 2014). Migration and chemoattraction are two processes that have also been shown to be important for WD formation in other, lower vertebrate species as well (Drawbridge et al., 2000). Around E9.5, the caudal WD finally inserts into and fuses with the cloaca, the future bladder (Chia et al., 2011).

The formation and extension of the Wolffian duct require its expression of the transcription factors *Pax2*, *Pax8* and *Lhx1,* among others (Bouchard et al., 2002; Costantini et al., 2010). Pax2 and Pax8, along with b-catenin/Wnt signaling, then activate transcription of the downstream Gata3, which is necessary for the proper elongation of the WD (**Figure 1.1C-E**; Bouchard et al., 2002; Grote et al., 2006). Gata3, in turn and in tandem with retinoic acid signaling from the stroma, positively regulates expression of the receptor tyrosine kinase (RTK) Ret in the extending WD (Costantini et al., 2010; Grote et al., 2008). As such, the lack of either Gata3 or the major retinoic acid-synthesizing enzyme, *Adlh1a2,* causes a great reduction in Ret expression and a degeneration of the WD (Grote et al., 2008; Chia et al., 2011; Rosselot et al., 2010). Gata3 may also have the separate function of suppressing premature differentiation of WD cells (Grote et al., 2008). While Ret is expressed in the WD and is important for later UB development (Costantini and Shakya, 2006), its absence has no visible effect on the WD (Chi et al., 2009), except for failure to fuse with the cloaca and an absence of the filopodia at the caudal end of the extending WD described above (Chia et al., 2011).

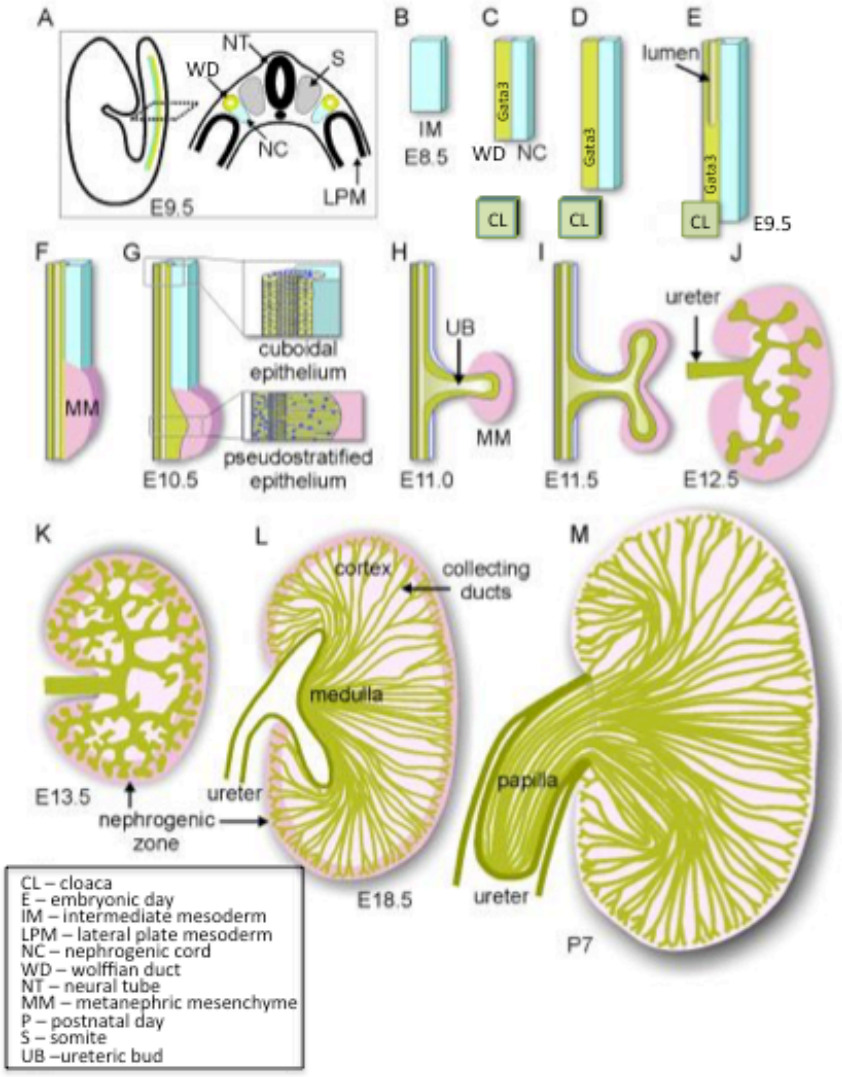

Figure 1.1 – Development of the Wolffian duct and renal collecting duct system. (A-M) illustrate the general morphogenesis of the kidney from E8.5 to P7. The Wolffian duct (in green) and the nephrogenic chord (in blue) are situated at the caudal end of the embryo and run along the anterior-posterior axis between the lateral plate mesoderm and the paraxial somatic mesoderm (A). Both tissues form from the intermediate mesoderm (in blue) after E8.5 (B). From E8.5 to E9.5, the ND, expressing Gata3, extends caudally towards and fuses with the cloaca while coalescing and organizing into an epithelial tube (C-E). The caudal region of the NC develops into a specialized region called the metanephric mesenchyme (G) and the adjacent caudal region of the WD begins to swell in the direction of the MM, producing a pseudostratified pattern of epithelium in the process (G). The ureteric bud then evaginates from the WD and enters the MM by E11 (H) and undergoes its first bifurcation by E11.5 (I). By E12.5 the UB has undergone two or three rounds of branching and the primary UB will develop into the ureter (J). Several more rounds of branching lead to the elaboration of the collecting ducts and a reorganization of previous branch generations into the medulla and papilla (K-M). From the emergence of the primary

UB until neonate stage the MM compartment is restricted to surround the tips of the branching epithelium in the nephrogenic zone (H-L). Adapted from *Costantini and Kopan, 2010*.

After fusion with the cloaca at E9.5, the caudal Wolffian duct begins to swell to form a pseudo-stratified epithelium at the site of emergence of the ureteric bud **(Figure 1.1G)**. Adjacent to this swelling is the metanephric mesenchyme that has differentiated from the nephrogenic chord and now expresses GDNF, a secreted protein and ligand of the Ret receptor (**Figure 1.1F** and **G**). GDNF/Ret signaling does not induce the formation of the pseudo-stratified epithelium, however, as caudal WD swelling is still observed in Ret-/- mutants (Chi et al., 2009), indicating that there are other factors regulating the onset of UB morphogenesis.

Ureteric Bud Morphogenesis

The development of the metanephric kidney begins definitively with the emergence of the ureteric bud from the caudal WD around E10.5. As mentioned before, ureteric bud growth and branching are critical for normal renal development and their failure produces birth defects such as renal agenesis, hypoplasia, or congenital obstructive uropathy (Costantini, 2006; Dressler, 2006; Schedl, 2007; Shah et al., 2004). The bud quickly emerges and undergoes the first dichotomous branching event within the MM at E11.5, forming the T-stage kidney (**Figure 1.1H** and **I**). Subsequently, the ureter lengthens and multiple branching cycles ensue (**Figure 1.1J**; Dressler, 2006). By this early stage (E11.5), the kidney can be explanted, cultured on a filter at an air-medium interface, and imaged with time-lapse microscopy. The kidney will grow for about 7 days and during this time, the

early phases of UB branching morphogenesis and nephrogenesis closely approximate in vivo development (although at a lower rate; Srinivas et al. 1999a; Watanabe et al., 2004). Studies with these kidneys have revealed that the UB can branch in three different manners: terminal bifid, terminal trifid, or lateral branching. Most UB branching events are terminal bifurcations where the tip first grows to form a swollen, rounded ampulla that is then gradually remodeled into a laterally elongated structure, and finally resolves into two new branches. Both terminal trifurcation (where the ampulla into three branches) and lateral branching (the outgrowth of a new segment from an existing branch) occur much less frequently and usually during the first few branch generations (Watanabe et al., 2004; Majumdar et al., 2003). Around E15.5, the ureteric tree enters a phase during which the branch segments of the 6th–8th branch generation start to elongate extensively, giving rise to the long unbranched collecting ducts of the medulla and papilla required for urine concentration (**Figure 1.1L** and **M**; Cebrian et al., 2004; Short et al., 2014).

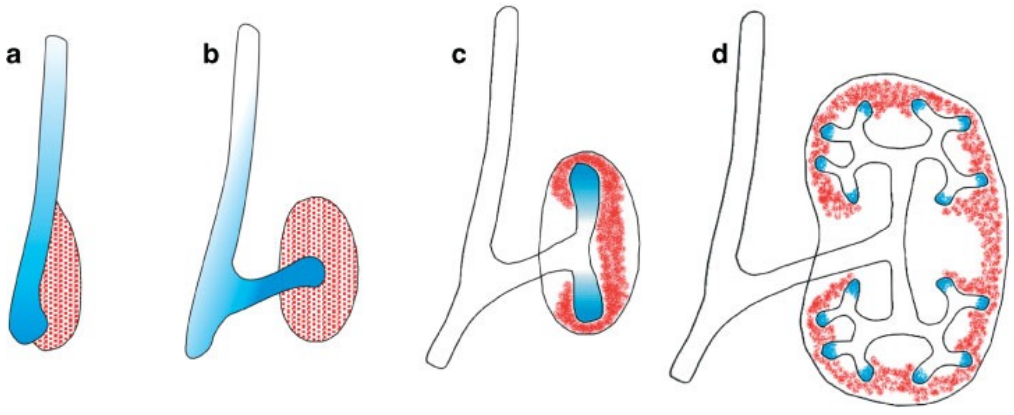

Figure 1.2 – Expression pattern of Ret and GNDF during UB morphogenesis. (a) Before UB outgrowth, Ret is expressed in the WD (blue) and GDNF in a broad, adjacent region of metanephric mesenchyme (red). As the UB emerges from the WD (b) and begins to branch (c, d), Ret is gradually restricted to just the tips of the branching epithelium and GDNF is restricted to the undifferentiated mesenchyme at the periphery of the kidney. Adapted from *Costantini and Shakya, 2006.*

Signals and Receptors Controlling UB Morphogenesis

The signals involved in UB morphogenesis have been extensively studied (Costantini and Kopan, 2010; Dressler, 2006; Bates, 2011). The initial outgrowth of the UB is dependent on many of the same signals that later control branching morphogenesis within the developing kidney. A major inducer is GDNF, emanating from the MM **(Figures 1.2 and 1.3)**, as mice lacking GDNF, its epithelial receptor Ret, or its co-receptor Gfrα1, frequently exhibit failure to form the ureteric bud, which leads to renal agenesis (Costantini and Shakya, 2006). Conversely, mutations in genes that usually limit the expression domain of GDNF (e.g., *Slit2, Robo2, Foxc2*) or that render the WD epithelium more sensitive to GDNF/Ret signaling (*Spry1*) tend to display ectopic and supernumerary UBs that can lead to multiplex kidneys (Costantini, 2006; Uetani et al., 2009). As the UB begins to branch within the MM, the Ret receptor (and co-receptor, GFRα1) becomes down-regulated in the trunks of the UB and restricted to the tips, while GDNF expression becomes restricted to the undifferentiated mesenchyme surrounding the UB tips (also called cap mesenchyme), and this pattern is maintained throughout kidney development **(Figure 1.2)**. In fact, the cells in this specialized tip domain are the primary progenitors of the entire ureteric tree and future collecting ducts (Shakya et al., 2005; Paul Riccio, unpublished). In addition to its important role in the emergence of the primary UB, GDNF/Ret signaling is also crucial for continued UB branching morphogenesis. Loss-of-function experiments that reduce the amount of GDNF/Ret signaling (but do not ablate it) in *in vivo* and explanted kidneys show a reduction of UB growth and branching (de Graaff et al., 2001; Jijiwa et al., 2004; Ehrenfels et al., 1999). Similarly, gain-of-function experiments in which exogenous GDNF is added to

cultured kidneys show an increase in growth and branching (Vega et al., 1996; Pepicelli et al., 1997).

Fgf/Fgfr2 signaling

Although Ret- or GDNF-null mutants are commonly associated with renal agenesis, the primary UB can still form at the correct position, however, in ~20-40% of mutants (Schuchardt et al., 1996), suggesting that there are other major signals that contribute to UB morphogenesis. Indeed, several investigators have established roles for FGF (fibroblast growth factor) ligands in inducing ureteric morphogenesis. Early studies in either isolated rat UB cultures or in intact rat embryonic kidney explants showed that Fgf2, Fgf7, and Fgf10 stimulated growth and differentially affected ureteric branching (Qiao et al., 2001; Qiao et al 1999). In addition, overexpression of FGF2 or FGF7 in developing rodent kidneys *in vivo* led to cystic dilation of collecting ducts (Li et al., 2006; Nguyen et al., 2006). Conversely, global deletion of Fgf7 (produced by cortical stromal cells) or Fgf10 (expressed in the MM) resulted in viable mice with a reduction in ureteric branch number and, as a secondary effect, fewer nephrons (Qiao et al., 1999; Ohuchi et al., 2000). Additionally, whereas *Fgf10*$^{+/-}$ or *Gdnf*$^{+/-}$ heterozygote mice had, respectively, no or low frequency (7-10%) of defective UB morphogenesis, double heterozygotes (*Fgf10*$^{+/-}$;*Gdnf*$^{+/-}$) exhibited frequent renal agenesis or severe hypoplasia (Michos et al., 2010). This reveals how Fgf10 and GDNF cooperate to support UB outgrowth and kidney development **(Figure 1.3)**.

The major receptor for these FGFs is another receptor tyrosine kinase, FGFR2 (the *IIIb* isoform expressed in the UB), as deletion of this receptor in the UB (*Fgfr2*$^{UB-/-}$) resulted in small kidneys with ureteric defects, including longer branches and significantly fewer

ampullary tips. *Fgfr2*$^{UB-/-}$ post-natal kidneys also displayed ~70% reduction of nephrons (Sims-Lucas et al., 2009; Zhao et al., 2004). Earlier, *Fgfr2* also plays an important role in WD development, where it is essential for maintenance and proliferation of its caudal portion (Okazawa 2015). Other RTKs may also be implicated in UB morphogenesis. While neither the epithelial receptors Met or Egfr, nor their activating ligands produced by the MM (HGF and EGF, respectively), show an overt effect on UB growth and branching, a double knockout of these two RTKs exhibit a significant branching defect (Ishibe et al., 2009; **Figure 1.3**).

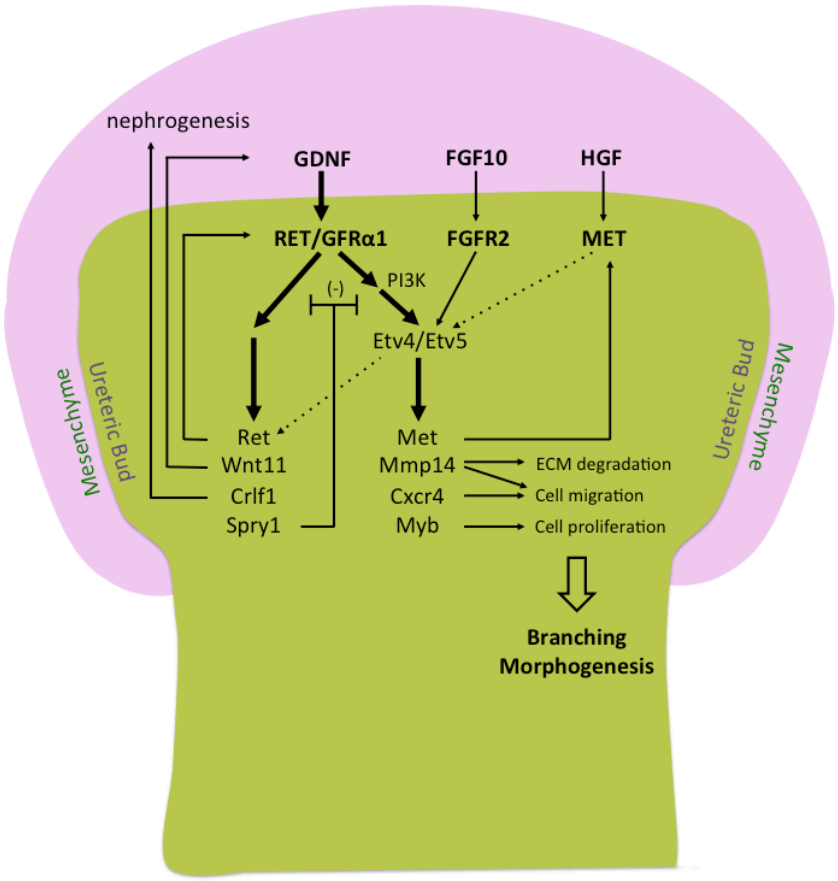

Figure 1.3 – RTK signaling and the downstream genetic network that control ureteric bud branching. Mesenchymal GDNF signals to the UB via RET and the co-receptor GFRa1, therefore regulating a set of downstream genes (bold arrows), including the transcription factors, Etv4 and Etv5. FGF10 signaling normally has a lesser role in regulating Etv4/Etv5 expression in the UB. Genes downstream of Ret that are regulated by Etv4 and Etv5 include

Met, Mmp14, Cxcr4, and Myb. Other GDNF-induced genes (e.g., Ret, Wnt11, Crlf1, Spry1) are relatively insensitive to Etv4/Etv5 levels (dashed arrow) and are likely regulated via other mechanisms. Collectively, these downstream genes compose part of a regulatory network that promotes UB branching morphogenesis, and other aspects of kidney development. In three positive feedback loops, Ret signaling positively regulates its own expression, Wnt11 upregulates Gdnf, and Met encodes the receptor for HGF, which may also upregulate Etv4/Etv5 (dotted arrow). Spry1 is an inhibitor of RTK signaling that provides negative feedback. Crlf1 may participate in nephrogenesis. Mmp14, Cxcr4, and Myb may contribute to cellular processes important for UB morphogenesis. **Diagram** adapted from *Costantini and Kopan, 2010.*

Signaling downstream of Ret and other RTKs

Downstream of the RTKs, Ret and Fgfr2 (among other RTKs), are at least three well-described signaling pathways critical to UB growth and branching: the Ras/Erk MAP kinase, PI3-kinase/Akt, and PLC-γ pathways. Inhibiting either PI3-kinase or PLC-γ severely inhibits UB growth and branching (Tang et al., 2002; Jain et al., 2006), while inhibiting the Erk pathway reduces the rate of branching and mildly inhibits elongation (Fisher et al., 2001; Watanabe et al., 2004). GDNF/Ret signaling has been shown to transcriptionally activate a set of genes that allow for normal function of Ret-expressing tip cells. Among the genes upregulated are Ret, itself, and Wnt11, another tip-specific gene and secreted protein that signals to the MM to promote GDNF production. Here is revealed a positive feedback loop that that reinforces the tip-specific expression Ret along with the downstream signaling components. There are negative regulators of this feedback loop, however. Sprouty1 (*Spry1*) is an intracelleular protein whose expression is simultaneously induced by RTK signaling and inhibits RTK signaling. *Spry1*$^{-/-}$ mutants develop multiple ectopic UBs, increased branch number, and multiplex kidneys, but this phenotype can be partially rescued by the additional removal of either Ret (*Ret*$^{-/-}$*;Spry1*$^{-/-}$) or GDNF (*Gdnf*$^{-/-}$*;Spry1*$^{-/-}$)(Basson et al., 2005; Basson et al., 2006; Michos et al., 2010), indicating that proper

branching morphogenesis in the kidney requires a finely tuned balance of tyrosine kinase activity. The additional removal of Fgf10 in these double mutants results in renal agenesis, reinforcing the idea that Fgf/Fgfr2 signaling acts as a secondary, alternative signaling pathway that synergizes with the GDNF/Ret signaling pathway (Michos et al., 2010). A diagram of some of the downstream components of RTK-signaling can be found in **Figure 1.3**.

Etv4 and Etv5

In an effort to further elucidate the gene regulatory network that is activated by GDNF, and hence responsible for branching morphogenesis, *Lu et al., 2010* conducted a genome-wide analysis of mRNA expression in isolated ureteric buds cultured with or without GDNF. They identified two ETS transcription factors, *Etv4* and *Etv5* that are jointly required for kidney development and seem to mediate the effects of extracellular cues on UB formation and branching morphogenesis. These two genes show overlapping expression in the WD at E9.5 and the subsequent UB tips, a profile that is reminiscent of Ret expression. Unlike Ret, however they are also mildly expressed in the metanephric mesenchyme (Lu et al., 2010). Mice that are missing both genes show a complete absence of kidney development, whereas mice that lack both alleles of *Etv4* and one of *Etv5* have a very high frequency of renal agenesis or hypodysplasia. Indeed, many of the genes previously identified as downstream components of Ret-signaling (Ret, Wnt11, and Spry1) were shown to be mediated by *Etv4* and *Etv5* (Lu et al., 2010; **Figure 1.3**).

Cellular Mechanisms of UB branching

While the molecular control of ureteric bud (UB) branching during kidney development has been extensively studied, the detailed cellular events underlying this process remain poorly understood. What are the cell behavior changes that may be needed for the UB epithelium to grow and change shape while remaining intact, and which genes carry out these specific functions? In order to form a branch point, cells may need to proliferate, move in relation to each other, and/or change their shape as well as adhesive properties. Although the full extent of gene targets for Etv4/5 are yet to be defined, several downstream targets (whether direct or indirect) that may mediate these cell behaviors have been identified including, Myb (a transcription factor having a defined role in the proliferation of progenitor populations), Cxcr4 (a chemokine receptor implicated in cell migration in many situations), and Mmp14 **(Figure 1.3)**. The latter is a matrix metalloproteinase which may promote branching morphogenesis by local remodeling of the extracellular matrix (ECM), by releasing bound growth factors, or by a novel, signaling mechanism that promotes cell migration of individual cells (Mori et al., 2009). In the kidney, MMP14 is indeed involved UB branching in culture (Pohl et al., 2000) and *Mmp14*$^{-/-}$ mice have UB branching defects (Riggins et al., 2010).

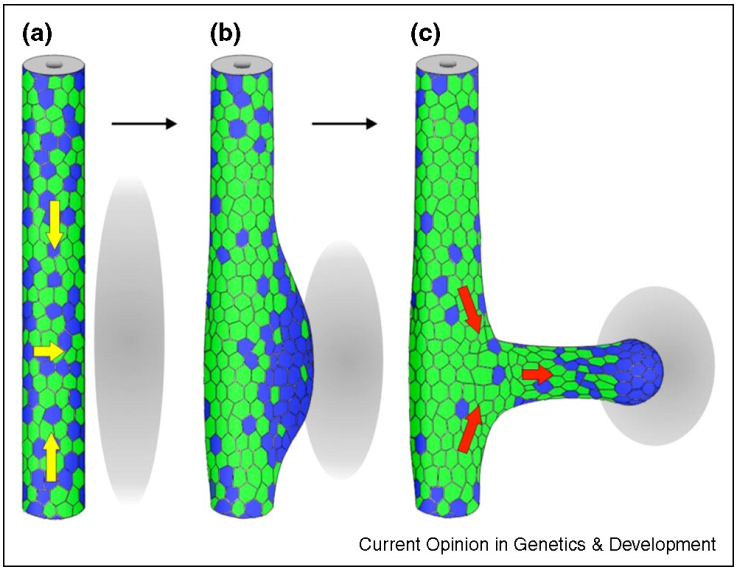

Figure 1.4 – RTK-signaling dependent cell movements that may establish and maintain the progenitor tip domain of the UB – (a-c) Schematic model of UB morphogenesis demonstrating the independent cell movements that may occur based on the level of RTK signaling in the WD. (a) High RTK signaling cells (blue) and low RTK-signaling cells (green) in the WD are initially randomly distributed and evenly dispersed. (b) Cells with high RTK-signaling migrate (yellow arrows) to the site of UB evagination adjacent to MM (gray ovals), establishing the primary tip domain. (c) The primary tip domain then evaginates from the WD, with high RTK signaling cells taking the lead and forming the UB tip and lower RTK-signaling cells following behind and forming part of the trunk (red arrows). Reproduced from *Chi et al., 2009*.

The generation of chimeric kidneys, for the study of cell-autonomous effects of particular mutations, has been crucial in the analysis of complex phenotypes of mutant mice and the underlying complex cell behaviors involved. Previous chimera studies have shown that during UB branching morphogenesis, RET is required for cell rearrangements in the caudal WD that generate a particular epithelial domain that later emerges as the tip of the primary ureteric bud, and that independent cell movements occur during this process (Shakya et al, 2005b; Chi et al., 2009). Other chimeric analyses using, *Sprouty1* mutant, *Etv4/5* mutant, and *Ret*-hypomorph alleles revealed that the level of Ret-signaling, not necessarily the presence of a functional RET gene itself, helps determine a cell's

position within the primary ureteric bud and the branching ureteric tree. Indeed, cells with high Ret-signaling are preferentially found in the swollen tip domain of the Wolffian duct (the site of UB evagination) and in the subsequent, branching epithelial tips at the expense lower Ret-signaling cells (Chi et al., 2009; Kuure et al., 2010; **Figure 1.4**). Furthermore, yet other mosaic kidneys have demonstrated that Ret and Etv4 are important for individual cells to be maintained in the progenitor tip domain during later UB branching (Paul Riccio, manuscript submitted; Cristina Cebrian et al., unpublished). These mosaic analyses suggest that directed cell migration of epithelial cells may play a pivotal role in establishment and maintenance of the tip domain in the WD and during branching morphogenesis **(Figure 1.4)**. Independent cell motility has been observed in the WD and in UB branches (Chi et al., 2009; Shakya et al., 2006b), and varying levels of Ret-signaling have been observed among adjacent cells in wild-type Wolffian ducts (Chi et al., 2009). In addition, cultured cells expressing Ret display chemotaxis towards a GDNF source (Tang et al., 1998), suggesting that GDNF may promote and/or guide these cell movements *in vivo*. It remains to be seen, however, whether other RTKs, in addition to Ret, play a role in the cell rearrangements observed during establishment and maintenance of the progenitor tip domain. Furthermore, identification of the many downstream effectors that mediate the cell-autonomous cell behavior changes will be needed to enhance our understanding of UB morphogenesis.

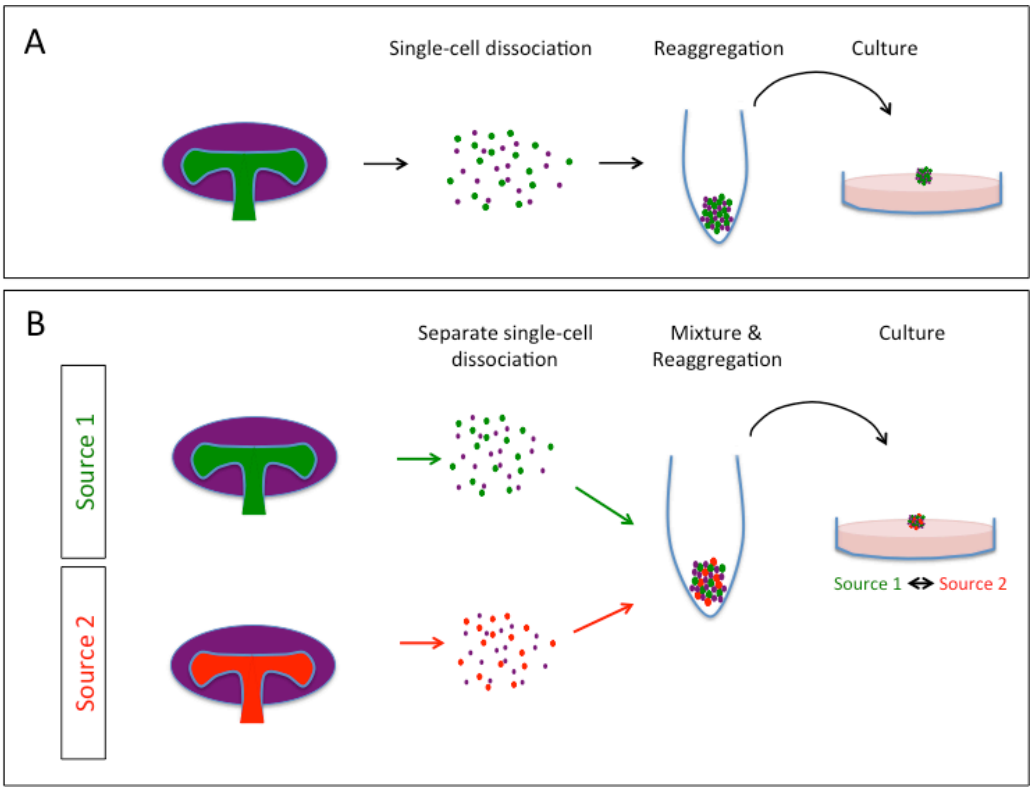

Figure 1.5 – Schematics illustrating the methods used to create renal organoids and chimeric renal organoids for the study of UB morphogenesis, based on *Unbekandt et al. (2010)*. (A) To produce renal organoids, E11.5 or E12.5 kidneys are dissociated into a single-cell suspension containing a mixture of ureteric bud cells (green), mesencymal cells and other renal cells (purple). 80,000-200,000 cells are then reaggregated by centrifugation in an Eppendorf tube and subsequently cultured for 4-7 days. Renal cells reassociate to form organotypic renal structures. (B) In the typical scheme to generate chimeric renal organoids from two different sources, kidneys from one source (green UB) and kidneys from a second source (red UB) are separately dissociated into single cells and each cell population counted by hemocytometer. Cells from each source are then mixed in an Eppendorf tube at the desired ratio to form a mosaic cell suspension, which is reaggregated by centrifugation. The mosaic pellet is then cultured for 4-7 days. The metanephric mesenchyme, other renal compartments, and their corresponding cells are indicated in purple.

Renal organoid system

UB morphogenesis and kidney development have been investigated using a variety of experimental methods including: dissection and analysis of the whole kidney at various

fixed embryonic stages (al-Awqati et al., 1998), explanted whole kidneys or isolated UBs cultured for time-lapse microscopy (Davies, 1994; Watanabe et al., 2004; Riccio et al., 2012), and primary or immortalized UB cell cultures for studying cell migration, cell adhesion, or growth factor requirements (Liang et al., 2007; Kuure et al., 2000b; Montesano et al., 1991; Sakurai et al., 1997; Derman et al., 1995). Also, the visualization and analysis of UB branching has been greatly facilitated by the use of a transgenic strain that expresses eGFP (enhanced green fluorescent protein) specifically in the UB epithelium, under the Hoxb7 promoter (Srinivas et al., 1999a). Recently a novel method of generating renal organoids from a single-cell suspension of fetal kidney cells **(Figure 1.5A)** has proven to hold great potential for both the study of kidney development (Unbekandt et al., 2010; Xinaris et al., 2012) and regenerative medicine (Xinaris et al., 2012; Xia et al. 2013). In this new system, the formation of ureteric bud-derived epithelial structures and nephrogenesis is observed, but the extent to which UB morphogenesis recapitulates *in vivo* UB development remains unclear. Of particular interest is the potential use of renal organoids for studying the important RTK-signaling-dependent cell rearrangements that occur during UB morphogenesis (Shakya et al., 2006b; Chi et al., 2009; Kuure et al., 2010). Producing chimeric renal organoids for mosaic analysis is a straightforward, timesaving process that involves the simple mixing of dissociated renal cells from different sources before they are reconstituted to form renal structures **(Figure 1.5B)**. A validation of this new experimental approach to studying UB morphogenesis can set the stage for the high-throughput, streamlined generation of chimeras, a process that is often long and laborious *in vivo*, and greatly aid in forming a detailed understanding of complex cellular events that occur during UB branching.

In this thesis, I first (Chapter 2) use kidneys expressing fluorescent proteins in specific cell lineages, together with time-lapse microscopy, to examine in more detail some of the cellular events and morphogenetic processes that occur during the formation of renal organoids from dissociated kidney cells. In Chapter 3, I investigate the potential use of this new system to study cellular rearrangements known to occur in the ureteric epithelium that help form and maintain the progenitor tip domain during kidney UB morphogeneis. I then (Chapter 4) use mosaic renal organoids to explore the cell-autonomous role Fgfr2 may have in establishing and sustaining these domains. And finally, in Chapter 5, I consider whether a downstream component of RTK-signaling, MMP14, has cell-autonomous functions in the ureteric bud similar to its upstream regulators.

CHAPTER 2

Characterizing Ureteric Bud Morphogenesis in a Renal Organoid System

Introduction

During vertebrate kidney organogenesis, the primary ureteric bud (UB) emerges from the Wolffian duct in response to signals primarily emanating from the adjacent metanephric mesenchyme. It then undergoes a series of reiterative branch events that gives rise to the urinary collecting system (collecting ducts, calyces, pelvis and ureter) of the adult kidney (Shah et al., 2009; Dressler, 2006). This UB branching morphogenesis is essential for the development of the mouse renal system as, in a reciprocal fashion, the tips of the branching UB induce the surrounding mesenchyme to differentiate into nephrons (Saxen, 1987; Costantini, 2012). As such, many research groups have focused on the morphogenetic events that lead to the growth and development of the ureteric bud, and have done so using a variety of methods. Most of our broad knowledge of renal branching morphogenesis has been determined from embryonic kidneys that were dissected and studied at different, fixed gestational stages (al-Awqati et al., 1998). While these methods can provide an accurate picture of the status of branching at any given time, they cannot unambiguously describe the sequence of morphogenetic events that gave rise to a particular structure.

Consequently, other means of studying UB branching morphogenesis have been devised. In explant organ culture, for example, the intact metanephric kidneys can be

explanted to culture and grown at an air-medium interface (Davies, 1994; Watanabe et al., 2004; Riccio et al., 2012). This is one of the most useful tools for studying kidney development, as many aspects of its development, particularly branching morphogenesis of the collecting duct system, can be elucidated with high resolution via time-lapse microscopy. Moreover, the administration of some pharmacological agents can be performed without concerns about their effects on other aspects of mouse physiology (Kanwar et al., 1997; Fisher et al., 2001; Watanabe et al., 2004).

Similarly, primary ureteric bud epithelial cell cultures too have routinely been used to study cell motility and cell adhesion, among other important aspects of UB morphogenesis. Primary cell cultures obtained from UB epithelium can be used for the classical scratch assay, for example, to measure cells' motility (Liang et al., 2007; Kuure et al., 2010b). In this system, the metanephric mesenchymes of early embryonic kidneys are separated from the developing ureteric bud by light proteolysis and physical manipulation. The isolated ureteric bud is then plated on fibronectin, where it transforms into a confluent monolayer culture of cells that can be challenged to move by the creation of an artificial gap in the monolayer, the so-called scratch. The cells on the edge of the newly produced gap are activated, and start moving toward the opening to close the scratch. This movement/migration occurs until the edges meet again and the cells are able to establish new cell–cell contacts (Kuure, 2012). This system has also proven to be useful for comparing the motility between cells of different origins, such as those derived from mutant versus wildtype kidneys (Kuure et al., 2010b).

Immortalized kidney cell lines, such as the popular Madin-Darby Canine Kidney

epithelial (MDCK) cells (Montesano et al., 1991), murine inner medullary collecting duct (mIMCD3; Barros et al., 1995; Cantley et al., 1994), and immortalized ureteric bud cell lines (Sakurai et al., 1997) have proven useful as well. Since these cell lines can be induced, under certain conditions, to undergo "branching tubulogenesis", they have served as a simple and quick system to study the growth factors and signaling cascades that affect this process (Derman et al., 1995; Montesano et al., 1991; Santos et al., 1993b). They have also provided a platform for introducing pharmacological manipulations or performing antibody inhibition assays that are sometimes very inefficient *in vivo* (Santos et al., 1993a; Sakurai et al., 1997). However, the morphological aspects of "branching" in this system are very different from branching of the UB *in vivo* or in organ cultures, which limits its utility.

With these investigative tools, a considerable amount of knowledge on molecular and cellular control of ureteric bud branching has been accumulating during the past few decades, but they each have their drawbacks. Explanted kidneys lose their three-dimensional shape and assume a flattened "pancake" shape. This causes deviations from normal, 3-dimensional kidney morphogenesis (Watanabe et al., 2004). And the delivery of siRNAs, antibodies or other large molecular agents have a serious problem of penetration (Lee et al., 2008). On the other hand, although primary and immortalized kidney epithelial cell cultures may be highly amenable to manipulation, they greatly lack the morphology of explanted (and, of course, *in vivo*) kidneys, and the techniques used that lead to cell immortality unfortunately often lead to dedifferentiation or highly irregular gene expression profiles (Santos et al., 1993b; Okada et al., 1997; Strutz et al., 1995; Elberg et al., 2007).

In a new tactic, Auerbach and Grobstein in 1958 demonstrated that the metanephric mesenchyme, when isolated from the ureteric bud, dissociated to single cells, and recombined with dissociated spinal cord, was still competent to produce nephron-like patterned structures (Auerbach et al., 1958). This suggested a considerable potential for self-organization of dissociated renal cells. While tissue dissociation and reaggregation was effective in the context of heterologous recombination (spinal cord/metanephric mesenchyme), reaggregation of single cells derived from the whole embryonic kidney has had a very limited success for reconstitution and self-organization (Coles et al., 1993; Unbekandt et al., 2010). In these previous studies, it was discovered that dissociated and reagreggated embryonic kidneys cells can form epithelial structures in a very limited fashion, but the further development of these structures is limited by widespread cell death without pharmacological intervention. In this situation, the reassociated ureteric bud structures appear to lose much of their capacity to branch and induce adjacent metanephric mesenchyme. A key new step has been added to this method, however, opening up a revolutionary new approach to studying kidney development. *Unbekandt et al., 2010* found that inhibition of Rho-associated kinase (ROCK) enhances embryonic kidney cell survival, which leads to the formation and development of ureteric bud epithelial structures. If the ROCK inhibitor is left in the culture, nephrons fail to form. However, when the ROCK inhibitor was removed after 24 hours of culture, not only did the ureteric bud continue to grow and branch but nephrons also formed in the cultures. Rho-associated kinases are effectors for the small GTPase Rho and participate in diverse cellular processes, including actin cytoskeleton dynamics and the regulation of gene expression (Laeno et al., 2013). Recently, ROCK inhibitors have been demonstrated to inhibit apoptosis of human

embryonic stem cells induced by dissociation (Watanabe K et al., 2007). In addition, Y27632 (a ROCK inhibitor) has previously been shown to enhance ureteric bud growth in explant cultures (Meyer et al., 2006).

Investigating ureteric bud branching morphogenesis with this "dissociation/reaggregation" system affords many of the advantages of a cell culture system, but in a more realistic and organotypic context. By including a stage in which cells are in a single-cell suspension, this presents the opportunity for the easy mixing of cells from different sources or cells that have been submitted to various treatments. For instance, via cell-mixing, chimeric organoids can easily be generated at the desired level of mosaicism in order to study the cell-autonomous nature of mutations that affect ureteric bud morphogenesis. Generating chimeras *in vivo,* on the other hand, is an arduous, time-consuming process that involves establishing embryonic stem cell lines, the manipulation of blastocysts, and mouse surgery (Shakya et al., 2005b; Chi et al., 2009). In contrast, stem cells and other cells can easily be added to the single-cell suspension to analyze their developmental potential during renal organogenesis (Unbekandt et al., 2010, Hendry et al., 2013). Additionally, siRNAs and other macromolecules have excellent access to ureteric bud and other renal cells at the stage when the kidney cells have been dissociated but not yet reaggregated (Unbekandt et al., 2010, Davies and Unbekandt, 2012). Thus the renal organoid system is in many ways intermediate in its advantages and disadvantages between the *in vivo* or explanted whole kidney system and the primary ureteric bud or immortalized ureteric bud cell culture system for the study of ureteric bud morphogenesis.

In this chapter, we use time-lapse microscopy to analyze the cellular events during

the reformation of epithelial tubules from disassociated ureteric bud cells during the early development of renal organoids, and we characterize the subsequent morphogenesis of ureteric bud structures and their interaction with the mesenchymal compartment. These characterizations reveal the extent to which ureteric bud morphogenesis in renal organoids recapitulates *in vivo* kidney development and form a baseline for future studies on mutant kidneys and renal organoids with defects in ureteric bud morphogenesis.

RESULTS

Cellular dynamics during the self-assembly of ureteric bud structures

In order to visualize the ureteric bud cells as they form ureteric bud structures in the renal organoids, E12.5 mouse kidneys containing the ureteric bud marker *Hoxb7:GFP* or *Hoxb7:myrVenus* (expressing a membrane-bound form of YFP) were dissociated into a single-cell suspension and then reaggregated. Briefly (see Experimental Procedures for details), the kidneys were incubated with trypsin and the cells were physically dissociated by trituration; the cells were then counted and concentrated by centrifugation, and the cell pellet was placed on a Transwell filter and cultured under conditions similar to those used for whole kidney culture. To visualize individual cell behaviors, kidney culture was performed in an environmental chamber on the stage of an epifluorescence microscope, and images were captured every 20-30 minutes.

This time-lapse imaging revealed that, over the first 24 hours of culture, individual ureteric bud (UB) cells came together to re-form ureteric bud structures. Early in the cultures, the individual UB cells, as well as UB cells within UB structures (on their periphery), extended long cellular processes that established cell-cell contact with other UB cells, and this lead to the re-formation epithelial UB structures **(Figure 2.1)**. In this regard, the dissociated UB cells resemble cells at the tip of the nephric duct during nephric duct elongation, which have not yet formed an epithelial tube, and which are thought to be involved in the caudal migration of the duct tip (Chia et al., 2011; Weiss et al., 2014). This suggests that dissociated UB cells transiently revert to an earlier developmental state in this culture system, leading to the reformation of epithelial tubules.

By 24 hours, the accretion of most UB cells into multicellular structures was complete, and two types of UB structures were visible: spheroids and tubules **(Figure 2.2A)**. These early UB tubules either took the form of simple tubules or else presented as more elaborate, "pseudo-branched" tubules. We call these "pseudo-branched" because they did not form through conventional bifurcation but instead by the fusion of several pre-existing tubular structures. These pseudo-branched tubular structures sometimes fused with each other to form yet even larger branched structures that went on to grow and bifurcate after this initial self-association process. Moreover, when a single-cell suspension containing cells with two different color UB markers was reaggregated, the resulting UB structures that formed during the first 24 hours were mosaic; individual red and green cells could be seen to aggregate to form a multicellular structure. This further confirmed that these multicellular structures formed primarily by the aggregation of cells and not only by the proliferation of single cells **(Figure 2.2B)**.

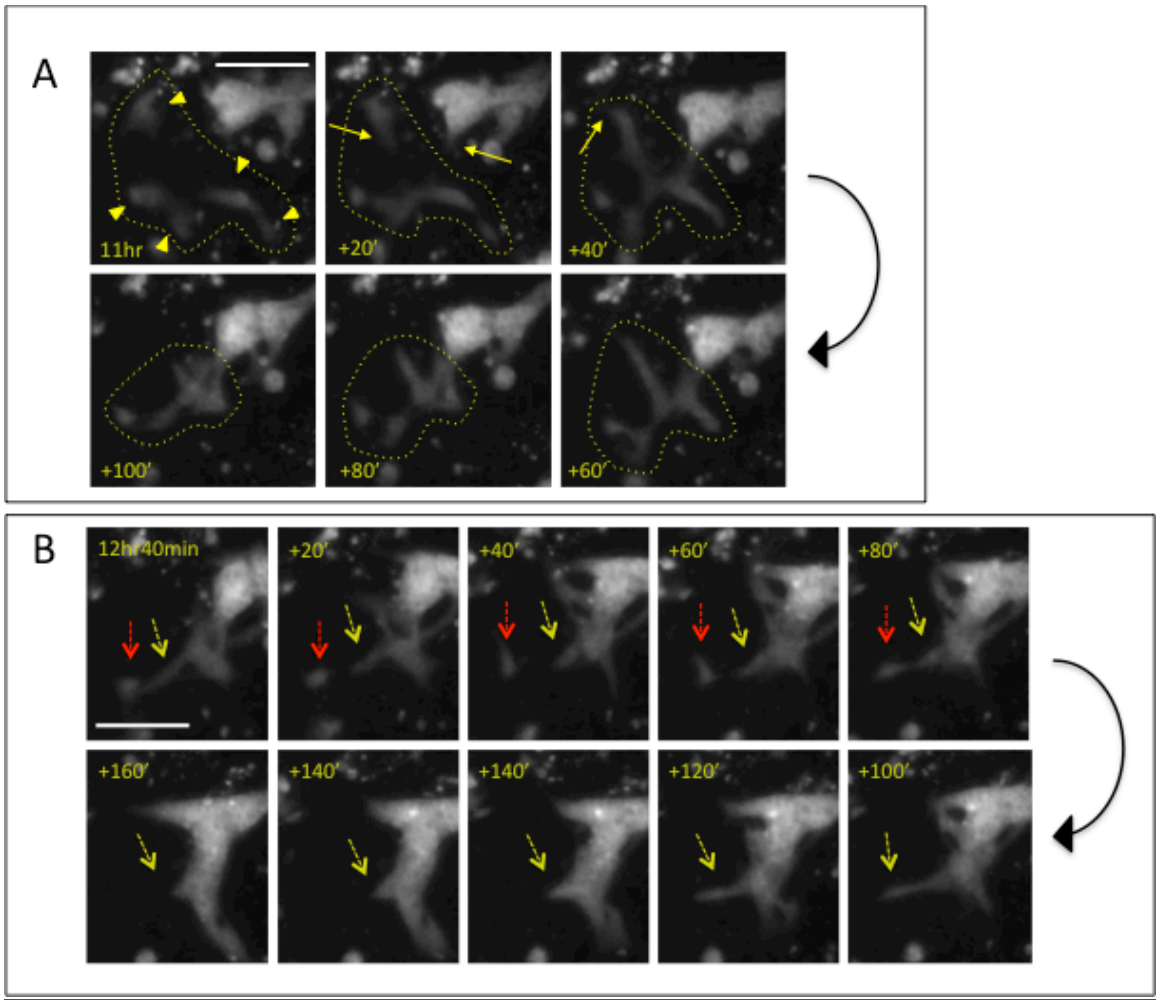

Figure 2.1 - Cellular dynamics during the self-assembly of UB structures in the renal organoid system. Reaggregated renal cells from E12.5 *Hoxb7:GFP* kidneys were used to specifically visualize UB cells and reveal the initial steps of the self-assembly of UB structures. Although the kidney mesenchyme cells were present in the cultures, they were not labeled with GFP and so were not visible. (A) shows a time-lapse over 100 minutes and demonstrates individual cells (yellow arrowheads) and/or small groups of cells (within the yellow, dotted lines) extending cellular processes (yellow arrows at 20 and 40 min) until cell-cell contact is established. Cells maintain contact while retracting the processes, thus reaggregating to form part of a larger UB structure. (B) shows a 160-minute time-lapse sequence in which one UB cell (red arrows) becomes incorporated into a larger UB structure (yellow arrows). From 0 min – 40 min, one or a few cells within the UB structure can be seen extending and retracting long processes. During the 40 min – 80 min period, the individual cell can also be seen extending processes and one or a few cells within the UB structure extending from the same location again until contact is made. The extensions then retract and the individual cell is incorporated into the whole structure (100 min -160 min). Scale bars equal 100 microns.

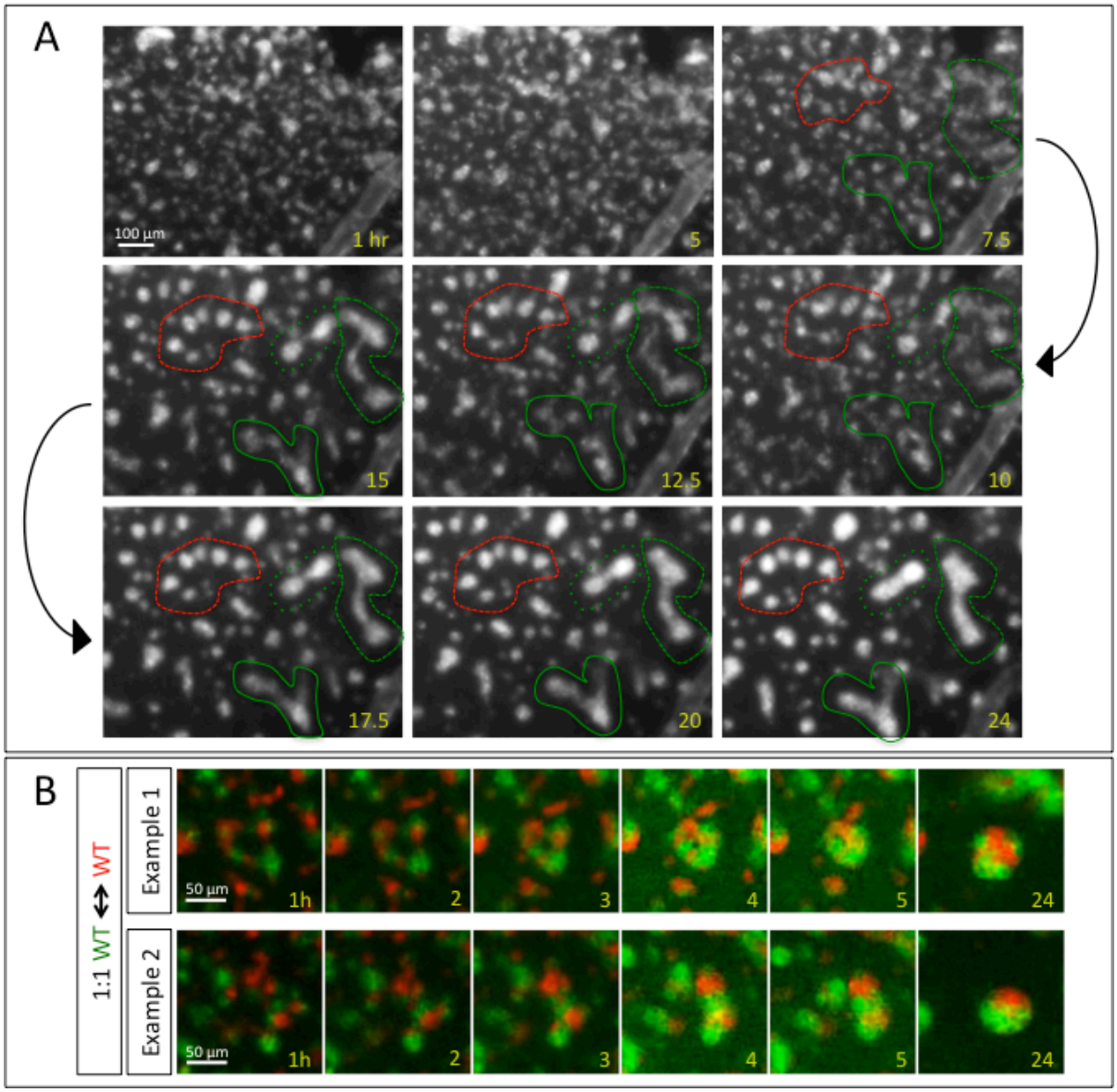

Figure 2.2 – Individual cells self-assemble to form UB spheroids and "pseudo-branched" UB tubules during the first 24 hours of culture. (A) shows the same region in selected frames from a 24-hour time-lapse of reaggregated renal cells derived from E12.5 *Hoxb7:GFP* kidneys. They reveal the self-assembly of UB spheroids (within the red dotted line), UB tubules (within green dotted lines), and "pseudo-branched" UB tubules (within the green solid line). Two examples in (B) show selected frames from a 24-hour time-lapse of a 1:1 mixture of *Hoxb7:myrVenus* and *Hoxb7cre;Rosa26*$^{Tomato/Tomato}$ cells that have been reaggregated and cultured. Both cells types are initially well dispersed and evenly distributed amongst each other at 1 hr of culture, and demonstrate that the formation of UB spheroids is from an amalgamation of cells, not the proliferation of one or a few cells.

Characterizing UB morphogenesis in renal organoids

Beyond the first 24 hours of culture, the UB structures then underwent morphogenetic changes reminiscent of *in vivo* kidney development, including tubule elongation, ampulla formation, branching, and cell proliferation. By day 2 (48 hours), many of the UB spheroids elongated to form more oblong shapes with distinct ends and most of the simple and "pseudo-branched" UB tubules formed from self-assembly in the early culture had started to branch **(Figures 2.3A, B, and F)**. From day 2 to 3, many of these elongated UB tubules (derived from UB spheroids) started to undergo *bona-fide* branching (defined as the growth of new branches from an existing tubule, rather than by fusion of two or more tubules) **(Figure 2.3B, C, and F)**. The UB tubules grew, formed ampullae, and some of the ampullae bifurcated to form new structures with numerous branches that, themselves, sometimes elongated and branched. As such, by 6 days in culture, some UB structures had undergone multiple rounds of branching **(Inset 1 in Figure 2.3),** and despite these elaborate branches growing in many directions, they rarely contacted each other, which is another characteristic observed in *in vivo* developing kidneys **(Figures 2.3E-E'')**.

In vivo, once the arborized UB has been established, extensive remodeling of early branch generations continues to occur in order to generate the adult medullary collecting ducts and renal pelvis, the funnel-like dilation essential for channeling urine to the ureter. Previous studies have shown that that in the initial stage of pelvis formation (E15.5), there is a 4-fold volume increase of the first branch generation and a corresponding increase in length of later branch generations (Short et al., 2014). Similarly, late stage renal organoids

(6 day-old) indeed show a substantial thickening and remodeling of the earliest trunk portions (compare **Figures 2.3B**, **C**, and **D**; compare **Figures 2.3C'** and **D'**), and also show a substantial lengthening of adjacent, newer trunk segments in UB tubules **(Figures 2.3E-E')**.

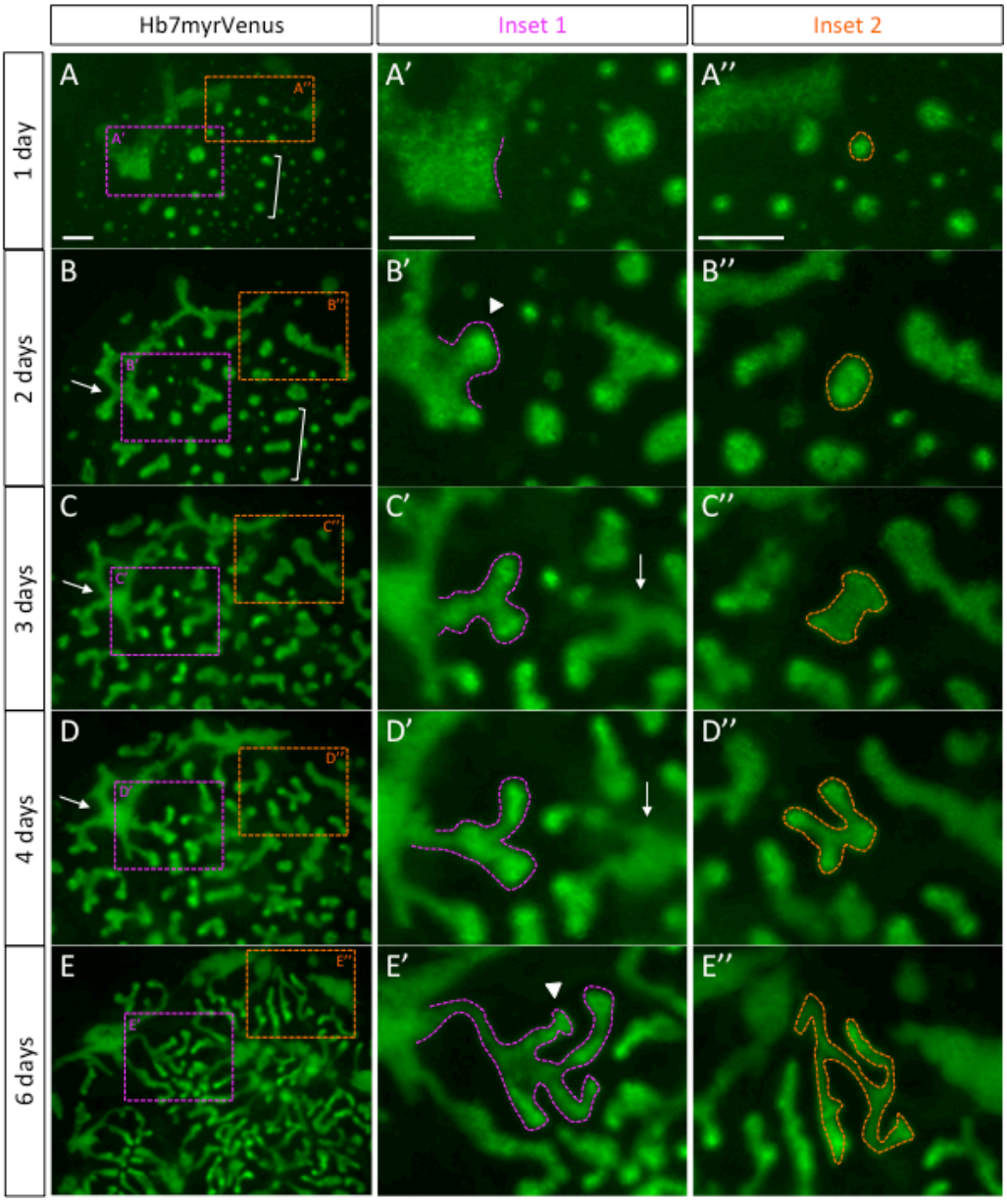

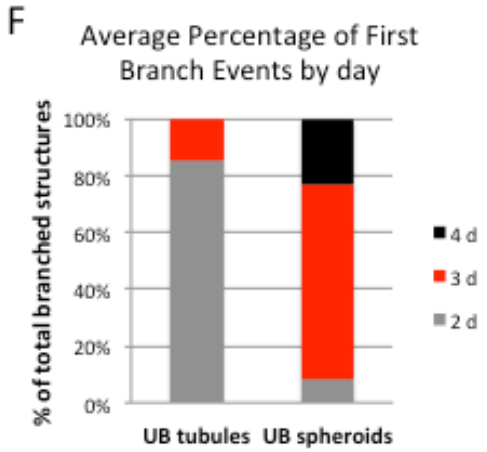

Figure 2.3 – Renal organoids undergo ureteric bud branching morphogenesis with some features similar to *in vivo* developing kidneys. (A-E'') show a 6-day time course of *Hoxb7:myrVenus* renal organoids generated from E12.5 kidneys. (A'-E') and (A''- E'') are enlarged images of the regions shown in Insets 1 and 2, respectively. UB spheroids elongate from 1 day to 2 days (brackets in [A] and [B]).
Bona fide branching among UB tubules (purple dotted lines in Inset 1 images) and UB spheroids (orange dotted line in Inset 2 images) can be observed beginning on day 2. The UB structure in Inset 1 can also be seen undergoing a second round of branching in (E, E'). Arrows in (B-D) and (C',D') show a thickening of the oldest trunk or base portions of UB structures, and (E) shows substantial lengthening of UB tubules after 4 days of culture. Ampulla formation is observed throughout renal organoid development as exemplified in (B') and (E')(arrowheads). Scale bars equal 200 microns.
(F) shows the relative proportion (as a percentage of total branching UB structures) of first branching events by day. The overwhelming majority of simple and "pseudo-branched" UB tubules exhibit *bona fide* branching by 2 days, while most UB spheroids start branching by day 3 of culture. (99 branched UB structures assessed from 3 separate renal organoid time courses; One-way ANOVA; $p<0.001$ for both structure types)

Cell proliferation during renal organoid UB morphogenesis

Cell proliferation makes a significant contribution to UB morphogenesis *in vivo* (Michael et al., 2004). Abundant proliferation is observed at multiple stages of renal organoid morphogenesis. At day 1 (24 hours) UB spheroids and non-UB tissues exhibit actively dividing cells, as demonstrated by phospho-Histone H3 immunofluorescence **(Figures 2.4A, A')**. Additionally, two- and three-day cultures also exhibit active cell

proliferation in elongating and branching ureteric branching structures, and even display cell division occurring in the lumens of single-layered UB tubules as has recently been characterized in the in vivo kidney during early branching morphogenesis (Packard et al., 2013; **Figures 2.4B-C'**). Furthermore, when reaggregated cells at the start of culture are treated with Mitomycin C to arrest cell proliferation, UB cells were still able to self-assemble into UB spheroids and UB tubules, but did not continue to elongate and branch thereafter **(Figures 2.4D-D4)**. When Mitomycin C was instead administered on day 1, after the self assembly of UB structures, the same result was observed, supporting the idea that the lack of typical morphogenetic behaviors stems from the absence of proliferation, and not from other detrimental, secondary effects of mitomycin C treatment (data not shown), although removal of mitomycin C and a subsequent resumption of UB morphogeneis would confirm this. Dissociated and reaggregated renal cells that were concurrently cultured with no Mitomycin C treatment displayed relatively normal growth **(Figures 2.4E-E4).** As a whole, these data further corroborate that, similar to *in vivo* UBs, UB branching morphogenesis in the renal organoid system is primarily driven by an innate proliferative capacity and not by the further aggregation of UB cells or UB structures.

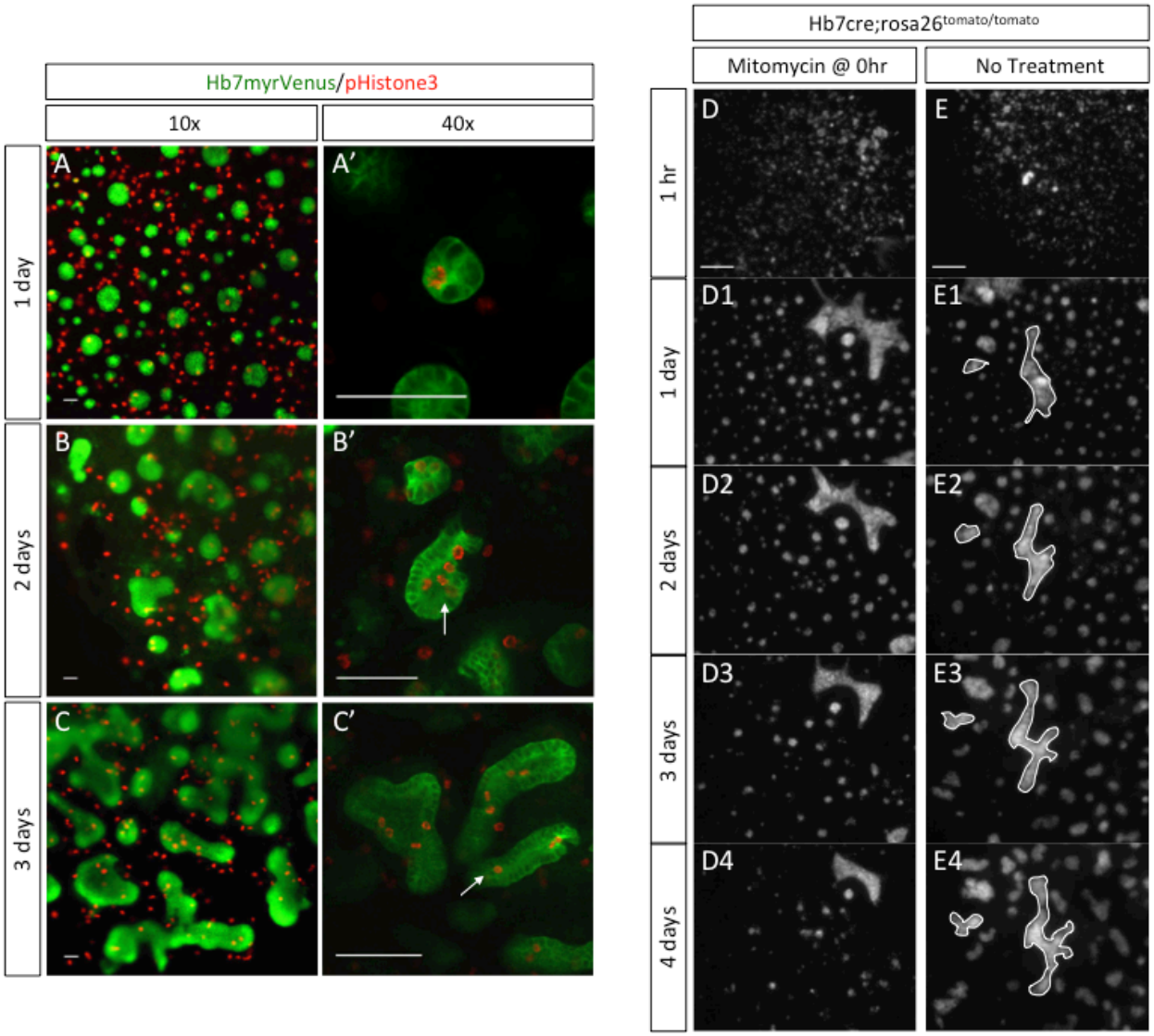

Figure 2.4 – Proliferation is a major driver of UB morphogenesis in renal organoids. (A-C') phospho-Histone H3 immunofluorescence shows abundant mitotic cells in UB and non-UB structures of 1-day (A, A'), 2-day (B, B'), and 3-day (C, C') renal organoid cultures derived from E12.5 *Hoxb7:myrVenus* kidneys. (A'-C') are 40x single-optical section confocal images of the cultures in (A-C). Arrows in (B', C') show mitotic cells in the lumens of single-layered UB tubules. Scale bars equal 50 microns.

In (D-D4), 10µg/ml Mitomycin C was administered to E12.5 reaggregates at the start of culture (0hr). UB tubules and UB spheroids formed by 24 hours and persist, but no further morphogenesis was observed during a 4-day time-course. Non-treated E12.5 reaggregates (E-E4), however, showed relatively normal UB morphogenesis among UB tubules and UB spheroids (solid white lines). Scale bars equal 200 microns.

Characterizing the tip domain of UB structures in renal organoids

A hallmark and essential characteristic of *in vivo* kidney development is the existence of a specialized domain at the tips of the branching UB where most of the epithelial growth and branching occurs (Michael et al., 2004; Watanabe et al., 2004). This progenitor tip domain has been shown to express many specific markers critical for its proper function, including Ret (Pachnis et al., 1993) and Wnt11 (a secreted protein that maintains normal GDNF expression levels in the MM; Majumdar et al., 2003), while these genes are not expressed in the UB trunks. Using gene expression reporter mice for these two genes (Ret^{GFP} and $Wnt11^{RFP\text{-}IRES\text{-}Cre}$, respectively), the presence of a tip domain was investigated during the UB morphogenesis of renal organoids. Robust expression of both Ret and Wnt11 was visible at the ends of tubules and branches starting at three days of culture **(Figures 2.5C-E', F-J')**. Although there was a small minority of tubule ends that lacked tip marker expression, these tended to be tubules that were stagnant throughout the time course, lacking growth and branching (Arrows in **Figures 2.5C-E**). Conversely, extensive UB tubule growth and branching occured in tubules with strong expression of *Ret* and *Wnt11* in the UB tubule tips, and tip marker expression was maintained in the tips of new branches, recapitulating the *in vivo* expression pattern. *Ret* reporter expression differed from the *Wnt11* reporter expression in that the Ret expression pattern appeared to be more broad, extending partially into the "trunk" regions of the UB tubules, rather than the Wnt11 pattern which was more compact and restricted to the extreme ends of the tubules and branches. This may be the result of a long half-life of the Green Fluorescent

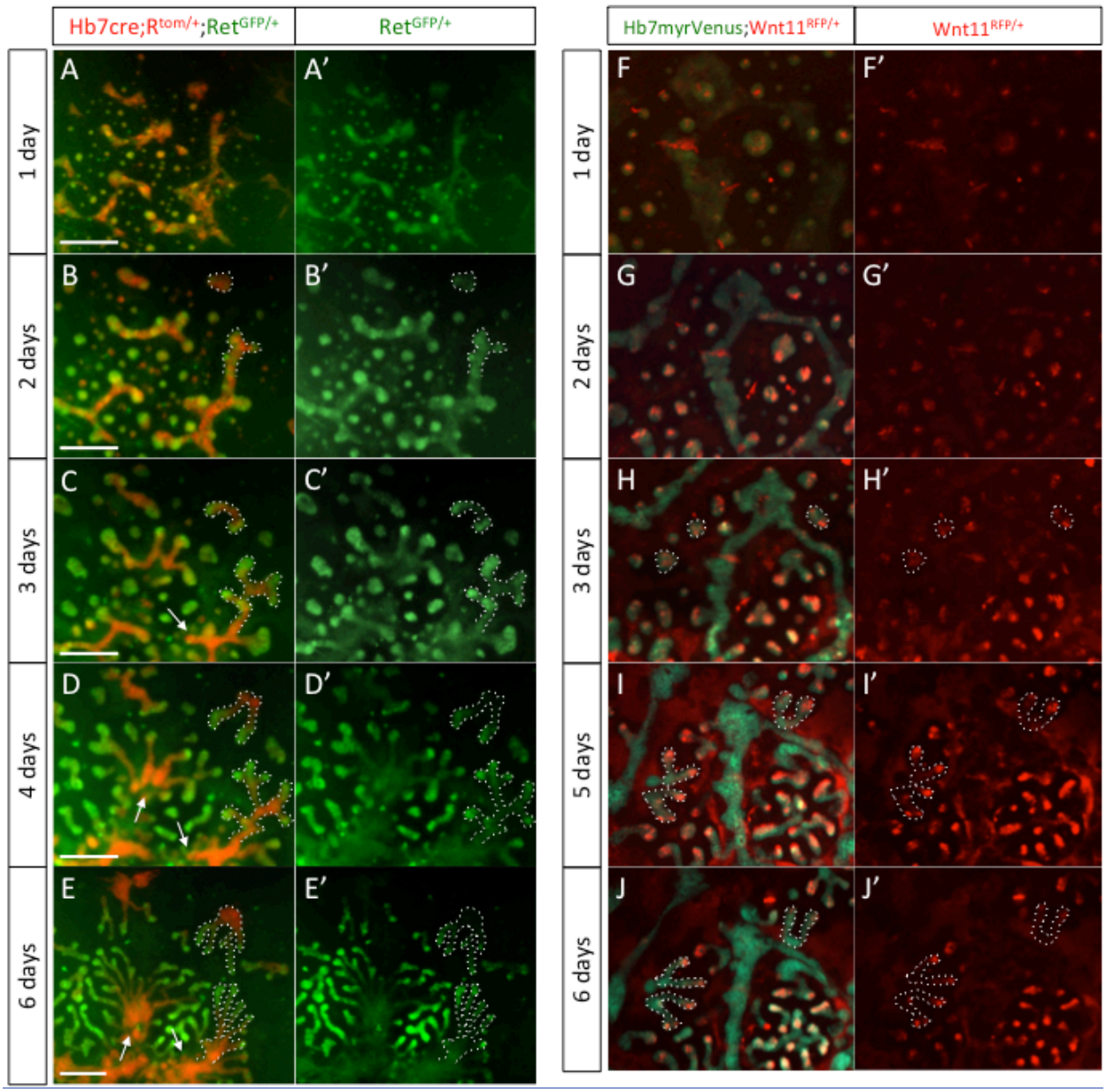

Figure 2.5 – The ends of renal organoid UB tubules contain organotypic tip domains. (A-E') shows a 6-day time course of renal organoids generated from E12.5 *Hoxb7cre;Rosa26*$^{Tomato/+}$*;Ret*$^{GFP/+}$ kidneys. Recombination of *Rosa26*^{Tomato} by *Hoxb7cre* causes the red fluorescent protein Tomato to be expressed throughout the ureteric bud epithelium. GFP fluorescence (green) can be seen at the ends of many UB tubules (red) from 2 days and onwards. (A'-E') shows the GFP channel only of the same images in (A-E). Ret-expressing tips can be seen undergoing dramatic morphogenesis, exhibiting elongation and branching (dotted white lines in B-E'), while non-Ret-expressing tips exhibit very limited or no growth (arrows in C-E).
(F-J') shows a 6-day time course of renal organoids generated from E12.5 *Hoxb7myrVenus;Wnt11*$^{creRFP/+}$ kidneys. Green fluorescence from *Hoxb7myrVenus* marks the

entire UB, while RFP fluorescence (red) can be seen at the ends of many UB tubules (green) from 2 days and onwards. (F'-J') shows the RFP channel only of the same images in (F-J). Wnt11-expressing tips can be seen undergoing dramatic morphogenesis, exhibiting elongation and branching (dotted white lines in F-J'). Scale bars equal 200 microns.

Protein used as the reporter of *Ret* expression (Corish et al., 1999), which could continue to mark "trunk" cells that recently descended from tip cells. Indeed, when the *Ret* mRNA expression pattern was investigated by *in situ* hybridization, Ret appeared more restricted to the ends of the UB tubules, and the tubules that elongated and bifurcated maintained a restricted Ret expression pattern at their branch tips **(Figure 2.6)**.

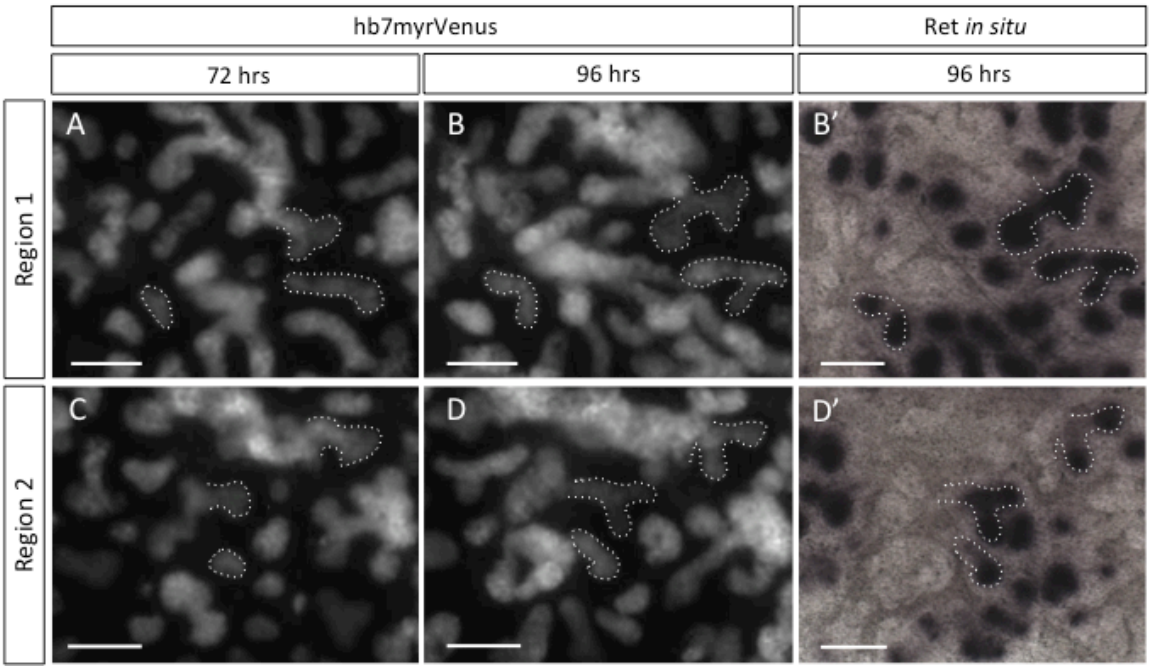

Figure 2.6 – Renal organoid Ret mRNA expression recapitulates the *in vivo* Ret expression pattern. (A, B) and (C, D) show two different regions of *Hoxb7:myrVenus* renal organoids at 72 hrs (A, C) and 96 hrs (B, D). (B') and (D') show a Ret *in situ* hybridization of the same fields in (B) and (D), respectively, and at the same time point. Ret-expressing regions exhibited elongation and branching (white dotted lines). Scale bar is 100 microns.

Investigating metanephric mesenchyme interactions with UB structures in renal organoids

It has been demonstrated that renal organoids display extensive nephrogenesis, developing renal vesicles, comma-shaped bodies, and S-shaped bodies, morphologies typical of the normal sequence of nephron development *in vivo* (Unbekandt. et al., 2010, Hendry et al., 2013). The distal pole of some nephron structures were also observed to connect to mature UB structures, in a manner similar to intact kidneys. However, the very initial steps in the interaction between forming UB tubules and nephron progenitor cells remained to be investigated. Using a lineage marker for the cap mesenchyme (*Six2*$^{creGFP/+}$;*Rosa26*$^{Tomato/+}$) in conjunction with a ureteric bud marker (*Hoxb7:myrVenus*$^{+}$) has allowed us to visualize the cap mesenchyme cells and their interaction with UB cells during the self-organization of renal organoids, and during the later growth and branching of the ureteric bud structures. We observed that Six2-lineage mesenchyme cells were initially widely dispersed **(Figure 7 A'')** but began to robustly envelop most UB structures after the latter finished forming **(Figures 2.7D-G')**. This process generally started during the latter half of the initial 24-hour self-assembly process of UB structures, and by 24 hours of culture, the majority of Six2-lineage mesenchyme cells could be found in "caps" closely surrounding the UB structures **(Figure 2.7G-G')**. As UB tubule morphogenesis continued, Six2-lineage cell clusters could be found closely associated with specific points of UB elongation and branching, as demonstrated by time-lapse microscopy **(Figure 2.8A-A''')**. Indeed, in 5-day old cultures, Six2-expressing cap cells could be found in clusters around UB branches and tips that were previously elongating and dividing, as opposed to regions of the UB devoid of Six2+ cells, where there was limited UB growth **(Figure 2.8B-E''')**.

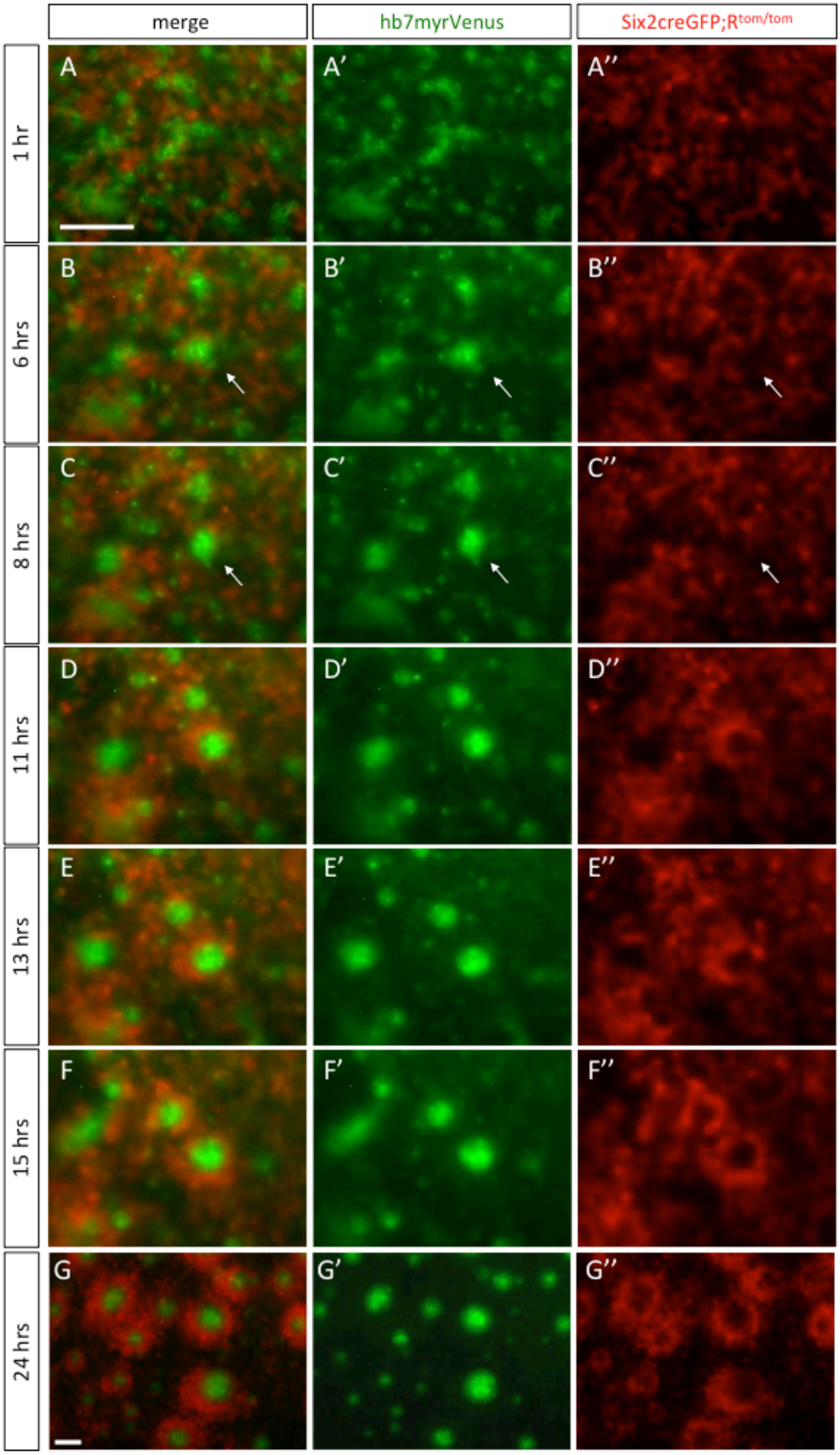
merge
hb7myrVenus
Six2creGFP;Rtom/tom
1 hr
6 hrs
8 hrs
11 hrs
13 hrs
15 hrs
24 hrs
A
A'
A''
B
B'
B''
C
C'
C''
D
D'
D''
E
E'
E''
F
F'
F''
G
G'
G''

Figure 2.7 – Cap mesenchymal cells surround established UB structures within the first 24 hours of renal organoid cultures. (A-G'') show selected frames from 24-hour time lapse image series of dissociated and reaggregated cells derived from E12.5 *Hoxb7:myrVenus;Six2*$^{creGFP/+}$*;Rosa26*$^{Tomato/+}$ kidneys. From an initial mixture of UB cells (green) and metanephric mesenchymeal (MM) cells (red)(A-A''), UB cells self-assemble into UB spheres at 6 and 8 hours of culture (B-C''), and are situated in a field of MM cells that is still evenly distributed (arrows in B-C''). Six2-lineage metanephric mesenchyme cells subsequently start to robustly surround established UB structures (D-F''), and by 24 hours of culture most MM cells are found completely or partially encircling UB spheres. Panels (G-G'') are from a separate culture and time lapse series. (2 cultures analyzed) Scale bar is 100 microns.

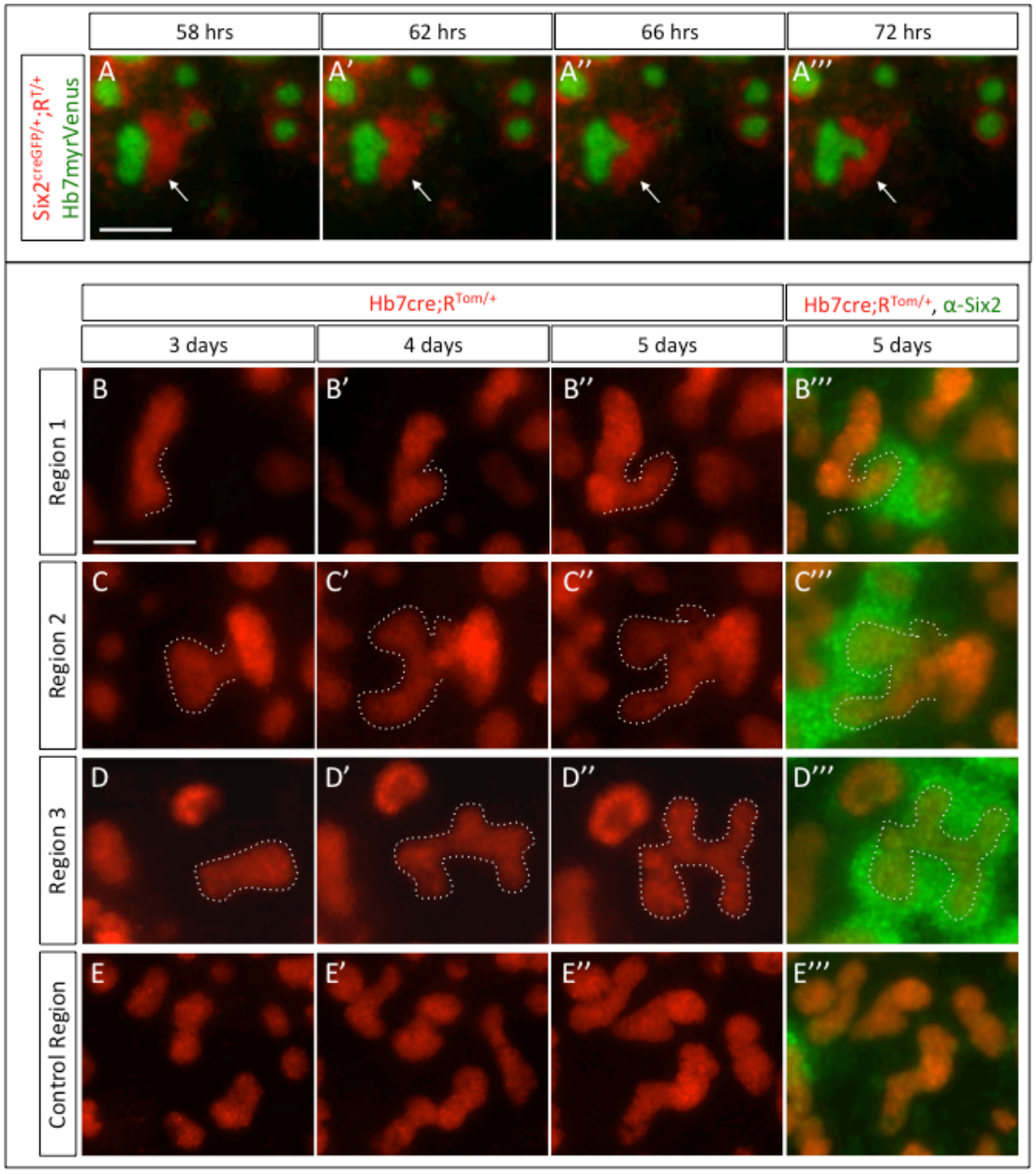

Figure 2.8 – Renal organoid UB tubules elongate and branch in regions enriched in Six2-lineage and Six2+ mesenchyme (MM) cells. (A-A''') show selected frames of a time-lapse from 58 to 72 hrs of renal organoids derived from E12.5 *Hoxb7:myrVenus;Six2$^{creGFP/+}$;Rosa26$^{Tomato/+}$* kidneys. Arrows show a cluster of Six2-lineage MM cells on one side of an elongating UB tubule. The UB tubule can be observed branching into the MM cell cluster. (B-E''') show 4 regions of *Hoxb7cre;Rosa26$^{Tomato/Tomato}$* reaggregates of E12.5 kidneys during a time course from 3 to 5 days. (B-D'') The UB segments (red) that elongate and/or branch correlate with surrounding clusters of Six2^{+} cap mesenchymal cells (green) when Six2 immunofluorescence is performed on the 5-day old cultures (B'''-D'''). Conversely, UB tubules that show limited or no growth (E-E'') lack Six2 cap mesenchymal enrichment (E'''). (3 cultures assessed) Scale bar = 100 microns.

Exploring the potential utility of E14.5 renal organoids for the study of UB morphogenesis

We wanted to probe whether UB cells from older embryonic kidneys had the same or similar developmental potential as the standard E12.5 kidneys or previously reported E11.5 kidneys (Unbekandt et al., 2012). E14.5 *Hoxb7:myrVenus* kidneys were thus dissociated and reaggregated in identical fashion to the younger embryonic kidneys and cultured for numerous days **(Figure 2.9A)**. As with E12.5 UB cells, E14.5 UB cells self-assembled into UB spheroids and UB tubules by 24 hours of culture, and these UB structures were subsequently able to grow, elongate, and bifurcate during a 5-day time-course **(Figure 2.9B)**. Because the process of dissociation and reaggregation of renal cells allows for the easy mixture of cells from different sources at the single-cell suspension stage, we were able to further compare the developmental potential of older and younger embryonic renal cells. To this end, renal cells were harvested from E12.5 and E14.5 kidneys harboring different color UB markers (Tomato and myrVenus, respectively) and then mixed together at a 1:1 ratio just before reaggregation, yielding a well dispersed and even mixture of both cell types in the start of culture **(Figure 2.9C)**. Images taken during a 3-day time-course show that UB cells from both embryonic stages self-organize into mosaic UB structures that subsequently elongate and bifurcate. There was no apparent preference for E12.5 or E14.5 UB cells to form part of the renal organoids as demonstrated by the salt-and-pepper patterning within UB structures throughout the time-course **(Figure 7D)**. This supports the idea that E14.5 UB cells retain a similar developmental potential as their younger, E12.5 counterparts and that older embryonic kidneys can also be used to generate renal organoids for the study of UB branching morphogenesis.

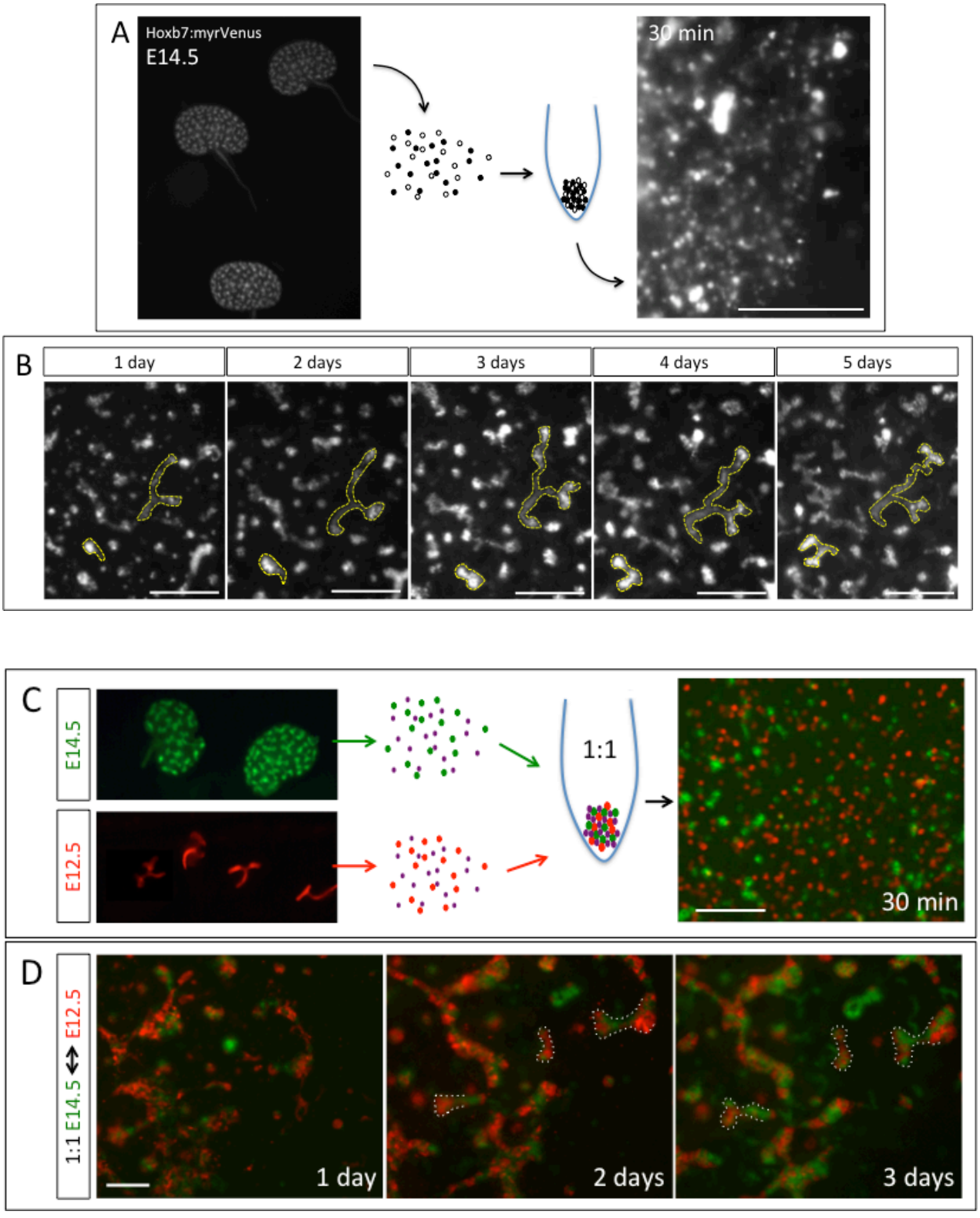
A
Hoxb7:myrVenus
E14.5
30 min
B
1 day
2 days
3 days
4 days
5 days
C
E14.5
E12.5
1:1
30 min
D
1:1 E14.5 ↔ E12.5
1 day
2 days
3 days

Figure 2.9 – E14.5 and E12.5 renal cells show a similar potential for UB morphogenesis in renal organoids. (A, B) shows the development of whole renal organoids composed of *Hoxb7myrVenus* E14.5 cells. (A) illustrates the scheme used to create these E14.5 renal organoids; white dots indicate UB cells and black dots indicate other non-UB renal cells. Identically to E12.5 renal organoids, kidneys were dissociated into a single-cell suspension and ~100,000 were then reaggregated by centrifugation and cultured. (B) displays a 5-day time course with UB structures able to undergo branching morphogenesis (yellow dotted lines)(5 cultures assessed). (C, D) shows the development of chimeric renal organoids composed of a 1:1 ratio of E12.5 and E14.5 kidney cells. (C) illustrates the generation of chimeric renal organoids where green or red dots symbolize UB cells and purple dots symbolize other non-UB renal cells. *Hoxb7myrVenus* E14.5 kidneys and *Hoxb7cre;Rosa26*$^{Tomato/Tomato}$ E12.5 kidneys were separately dissociated into single cells and counted with a hemocytometer. Cells from each stage were then mixed to produce a 1:1 ratio that was then reaggregated by centrifugation and cultured. At 30 min of culture there is a well dispersed and evenly distributed mixture of E14.5 (green) and E12.5 (red) cells. (D) shows a 3-day time course (from 1 to 3 days) of UB structures undergoing morphogenesis. A salt-and-pepper pattern of red and green cells is apparent throughout most structures, indicating that 14.5 UB cells had the ability to form part of developing UBs as effectively as E12.5 UB cells. (2 cultures assessed)

DISCUSSION

Previous studies using renal organoids have focused on its use for studying nephrogenesis (Unbekandt et al., 2010; Xinaris et al., 2012). The utility of this method in studying UB morphogenesis has been less clear and is dependent on the extent to which it recapitulates UB morphogenesis *in vivo*. From our findings, we believe this method has great potential to be used as a model of kidney organogenesis in general and UB morphogenesis in particular. Using fluorescent reporters controlled by regulatory elements from the *Hoxb7* gene, a ureteric bud marker, we were able to easily visualize the self-organization process of UB cells after reaggregation of renal cells from a single-cell suspension. We were also able to analyze many of the morphogenetic events that occurred

in the resulting UB structures in time-lapse studies and compare them to UB development *in vivo*. In the presence of transient (24 hr) Rho-kinase inhibition to prevent cell death, UB cells efficiently self-assemble into spheroids and tubules that are subsequently surrounded by Six2^{+} nephron progenitor cells. The encircling of early UB structures by these mesenchymal cells has previously been reported (Xinaris et al., 2012), but here we reveal that robust condensation of mesenchymal cells begins only after the UB structures have already formed. It is likely that reformed UB structures create a niche from which concentrated signals are released to bring mesenchymal cells into proximity and promote their survival and proliferation. Recent studies have unraveled many candidates of the UB-derived niche signals, which include Fgfs [2 and 9] (Brown et al., 2011; Barak et al., 2012), BMP7 (Blank et al., 2009) and Wnt9b (Karner et al., 2009). Also, it may be the case that UB structures stop amassing cells or adjoining each other because they become surrounded by cap mesenchyme responding to potential niche signals. Indeed, the very few UB structures that join together relatively late in cultures (after 24 hours) were ones that lacked or were deficient in surrounding Six2-lineage mesenchymal cells (data not shown).

Ureteric bud structures subsequently grow in size, elongate, and bifurcate similarly to *in vivo* and cultured kidneys, even displaying characteristic ampullae and T-shaped branches. We conlcuded that the majority of first branching events occur by day two of culture among individual UB tubules, and by day three among individual UB spheroids, forming a fundamental basis for the future study of mutant branching phenotypes using this system. Also analogous to the development of the intact kidney, renal organoid growth and branching occurs mostly in UB segments that express the established tip markers Ret and Wnt11 and in UB segments that are embedded in cap mesenchymal cell clusters. Time-

lapse microscopy revealed that there is very limited aggregation of cells and UB structures after 24 hours of culture, so the observed UB growth and branching morphogenesis after this time depends on the proliferative capacity of the UB cells. Consistently, abundant cell division was observed throughout UB structures at various renal organoid stages, and Mitomycin C treatment (used to prevent proliferation) inhibited the elongation and branching of UB structures. We also report the potential use of older embryonic kidneys for the study of UB morphogenesis in renal organoids. When competing with E12.5 UB cells, E14.5 UB cells had comparable ability to form part of both trunk and tip portions of UB structures, and renal organoids composed entirely of E14.5 cells were to grow, elongate, and undergo branching morphogenesis.

Although the new system produces many small collecting duct "tree-lets" rather than a single connected tree and there in no global corticomedullary organization, as would occur in *in vivo* or explant kidneys, the spatial organization of individual, late-stage renal organoids is quite similar to intact kidneys. Thick trunk-like regions that appear to have undergone remodeling lead into thin, elongated tubules that lead into branching tips and developing nephrons.

In this experimental system, kidneys dissociated to single cells are able to reaggregate and re-form complex kidney-like structures. One important application is that this will allow the generation of *in vitro* chimeras derived from genetically heterogeneous sources, to test for the cell-autonomous nature of mutations, for instance. In addition, previous efforts to target embryonic kidney tissues using siRNAs, plasmids, and other macromolecules have encountered serious problems of tissue penetration and have been

disappointing (Lee et al., 2008). This may be largely due to the poor accessibility of the ureteric bud and the metanephric mesenchyme, which are buried underneath a layer of stromal cells. With the dissociation of the kidney into single-cells, the need for tissue penetration is eliminated, and a more even dispersal of the introduced molecules through the resulting 'tissue' formed after reaggregation can be attained. As a first step toward this application, *Unbekandt et al., 2010* transfected single-cell suspensions with siRNA targeting the transcription factor WT1, which is known to be critical for metanephric mesenchyme differentiation. When they subsequently reaggregated the renal cells, they observed a marked knockdown of WT1 and a cell-autonomous inhibitory effect on nephron differentiation from metanephric mesenchyme (WT1 knocked-down cells had a decreased ability to contribute to developing nephrons when mixed with untreated cells). We should expect knockdown of genes in the UB to be as efficient and, with this detailed characterization of UB morphogenesis in renal organoids, any potential effect observed should be relevant to *in vivo* UB development and can be interpreted accordingly.

This new system for creating renal organoids through the dissociation and reaggregation of embryonic kidneys represents perhaps one of the simplest and most accessible systems for the study of UB morphogenesis and mesenchymal–epithelial interactions relevant to early kidney development. While possessing its own particular limitations, the *in vitro* organoid system can be used to complement genetic or organ culture approaches using intact kidneys. To the extent that this kind of approach reflects events occurring *in vivo* during development, it can be used to gain mechanistic insights into complex morphogenetic processes.

EXPERIMENTAL PROCEDURES

Dissociation of embryonic kidneys. E12.5 or E14.5 mouse embryonic kidneys were harvested and dissected in CO_2-Independent media (Life Technologies: Cat# 18045-088). The embryonic rudiments were then placed in .025% Trypsin/EDTA (Life Technologies: Cat# 25200) for 5 min at 37°C. Organs were stabilized in 200-500µl Kidney Culture Media (KCM; DMEM [Life Technologies] + 10% fetal bovine serum + 1% Penicillin/Streptomycin) for 10 min at 37°C then dissociated by trituration (using a standard plastic pipette tip attached to a Gilson 20 or 200µl Pipetman) and filtered through a 40mm cell strainer (BD Falcon, Oxford, UK) by gravity. The degree of dissociation was monitored by dissection microscope. The cells were then sometimes counted using a hemocytometer. One wild-type E12.5 kidney typically yielded about 40,000 cells.

Culture of reassociated kidney cell pellets. 80,000-200,000 dissociated cells in KCM were lightly centrifuged in 1.5ml Eppendorf tubes at 1600g for 8min. A Wiretrol® (Drummond Scientific) glass pipette was then used to carefully dislodge the pellet from the walls of the Eppendorf tube and subsequently to gently extract the pellet. The pellet was then placed on a 0.4µm polyester membrane Transwell filter (Costar 3450). The pellet was cultured on the filter in a 6-well plate at the air–medium interface, in a humidified incubator at 37°C and 5% CO2. The culture medium used was KCM with 10mmol/l Y27632 ROCK inhibitor (Sigma) or 1.25 mmol/l Glycyl-H1152 dihydrochloride (another ROCK inhibitor used successfully on renal organoids [Unbekandt., et al 2010]; Tocris, Bristol, UK). After 24 hrs, the well was washed (2x) with PBS and fresh KCM was added. KCM was thereafter replaced with fresh KCM every 2 days.

Chimeric Pellet Culture. Kidneys from different sources were dissociated separately and these separate single-cell suspensions were counted with a hemocytometer as described above. The single-cell suspensions from different sources were then mixed to produce 1:1 cell ratios before centrifugation at 1600g for 8 min. Pellet culture then proceeded as described above.

Immunofluorescence Staining. Renal organoid cultures were fixed by adding 4% paraformaldehyde (PFA) (1 hr, 4°C) above and below the filter, and washed 3x in PBS. Samples were then incubated in 10% NDS (Normal Donkey Serum) in TSP (0.1% Triton X-100, 0.05% Saponin, PBS)(3x, 10min, room temperature) before incubation in the following primary antibodies: Goat anti-Six2 (Invitrogen, 1:200) and Rabbit anti-phospho-Histone H3 (Invitrogen, 1:200). Primary antibody was diluted in TSP and 10% Normal Donkey Serum (NDS) and incubation was overnight at 4°C followed by TSP washes (3x, 10min, RT). Secondary antibodies (Cy2 Donkey anti-Goat, Cy3 Donkey anti-Rabbit, respectively; Jackson ImmunoResearch) were diluted in TSP and 10% NDS and samples were incubated for 3 hours at RT followed by TSP washes (3x, 10min, RT). Samples were then mounted onto slides using Fluoro-gel and imaged using a Zeiss AxioObserver Z1 microscope.

Mitomycin Treatment. Mitomycin C was added to the KCM at a standard concentration of 10μg/ml to inactivate mitosis at 0 hr of culture (just after placing the pellet on the filter) or at 24 hours. Mitomycin was continuously added to fresh media when replacing old media.

In situ hybridization. Renal organoids were fixed in 4% paraformaldehyde overnight at 4 °C. Whole-mount Ret in situ hybridization was carried out using digoxigenin-labeled probes as described in *Schaeren-Wiemers et al., 1993*.

Time course and Time-lapse movies. Renal organoid cultures were placed on 0.4µm pore Transwell inserts (Costar 3450) in six-well plates (Falcon: 353046) filled with KCM (with additional 10 mmol/l Y27632 or 1.25 mmol/l H1152 for the first 24 hrs) and pictures were taken once every day for the time course. For time-lapse experiments, pictures were taken every 20 min, every 30 min, or every hour for 3 or 4 days using a time-lapse microscope (Zeiss AxioObserver Z1) equipped with an incubation chamber at 37°C, 100% humidity, and 5% CO_2.

Mouse strains. Mouse strains used were on a 129X1/S, 129S/6, or C57BL/6 background and included *Hoxb7/myr-Venus* (MGI:4415296), *Ret*^{GFP} (MGI:2449909), *Wnt11-myrTagRFP-IRES-CE* (MGI:5435691), *Hoxb7-cre* (MGI:2675121), *Rosa26*^{Tomato} (MGI:3809523), and *Six2-GFPcre* (MGI:3848345).

CHAPTER 3

The Use of Chimeric Renal Organoids for the Study of Ret-Dependent Cell Rearrangements During UB Morphogenesis

INTRODUCTION

Kidney development begins when the primary ureteric bud (UB) emerges from the caudal Wolffian duct (WD) in response to signals emanating from the adjacent metanephric mesenchyme (MM; Dressler, 2006). The UB grows into this surrounding mesenchyme and proceeds to undergo a series of branching events along with tubule elongation and other morphogenetic changes, eventually giving rise to the collecting system of the kidney. The most important of these inducing signals is GDNF, a soluble molecule secreted by the mesenchymal cells and a ligand of the RET Tyrosine kinase receptor, which is found on the cell surface of WD and UB cells (Dressler, 2006; Costantini, 2012). RET activation then leads to complex intracellular signaling events that ultimately change the behavior of WD/UB cells (Chi et al., 2009). From its very early bud stage, the UB is divided into subpopulations, the so-called tip and trunk domains, which are characterized by different morphogenetic behaviors, gene expression patterns, and cell proliferation rates. Indeed, the tip domain is the site of increased proliferation, growth, and branching (Lin et al., 2001; Michael et al., 2004; Watanabe et al., 2004).

During branching morphogenesis, RET and other critical genes become restricted to just the progenitor domain at the tips of the growing ureteric tree and without RET or its

ligand, GDNF, renal agenesis occurs (Schuchardt et al., 1994; Sánchez et al., 1996; Pichel et al., 1996). But specifically how GDNF/RET signaling alters the behavior of Wolffian duct and UB cells to promote branching remained unclear. Agenesis or other complex malformations of kidney mutants during development often precludes a thorough elucidation of the full impact of the mutation. As a result, important functional roles and the primary cellular targets of the gene may be missed. Chimera analysis can offer a complementary experimental approach to the straightforward assessment of phenotype. The generation of chimeric kidneys, for the study of cell-autonomous effects of particular mutations, has been crucial in the analysis of complex phenotypes of mutant mice. Previous chimera studies have shown that during UB branching morphogenesis, RET is required for cell rearrangements in the caudal WD that generate a particular epithelial domain that later emerges as the tip of the primary ureteric bud, and that independent cell movements occur during this process (Shakya et al., 2005b; Chi et al., 2009).

Further investigation revealed that a wild-type *Ret* gene, itself, was not an absolute requirement for UB cells to contribute to the tip domain, but instead the level of RET signaling caused cells to compete for residence of the tip. These studies made use of the Sprouty1 (*Spry1*) null allele that increases RET signaling, and a *Ret* hypomorphic allele that decreases it. Sprouty1 is an antagonist of RTK signaling and is a feedback inhibitor downstream of GDNF/RET signaling in the developing kidney (Basson et al., 2005; Basson et al., 2006). Mice that are mutant for *Spry1* exhibit increased mesenchymal GDNF expression and, as such, develop multiple UBs, and display irregular branching morphogenesis characterized by both increased number and size of ureteric bud tips (Basson et al., 2006). When chimeras are generated with *Spry1*$^{-/-}$ cells mixed with WT cells,

the mutant *Spry1* cells (with increased Ret signaling) are initially interspersed among WT cells in the Wolffian duct, but end up outcompeting the WT cells for residence of the UB tip domain as development progresses. Even as the UB grows and branches, $Spry^{-/-}$ cells are preferentially found at the tips. This in contrast to $Ret^{-/-}$ <-> WT chimeras where WT cells outcompete mutant cells for residence at the tips (Chi et al., 2009).

To further drive home the point of Ret-signaling–dependent cell rearrangements in UB development, *Chi et al., 2009* also made use of a Ret hypomorphic allele (in which the cDNA of the RET51 isoform replaces the *Ret* gene, so the modified allele only expresses RET51, and not the other major isoform, RET9) to generate chimeras. $Ret^{51/51}$ homozygotes have a milder renal phenotype, hypoplasia and reduced branching, when compared to $Ret^{-/-}$ mice, which usually lack kidneys (de Graaff et al., 2001). When *Ret* null cells ($Ret^{-/-}$) were juxtaposed with *Ret* hypomorphic cells ($Ret^{51/51}$) in the developing kidney, *the* Ret null cells were able to contribute to the UB tips more extensively than when they were mixed with WT cells in other chimeras (Chi et al., 2009; Shakya et al., 2005b). This indicated that the difference in signaling levels between *Ret* null and hypomorphic cells is not great enough for the hypomorphic cells to fully out-compete the null cells. Thus, the fate of individual cells in a chimeric UB is highly dependent on the level of RTK signaling it possesses. Those with increased signaling will outcompete those with lower signaling for residence at the progenitor tip domains during UB morphogenesis. Indeed, it was shown that even in WT animals, WD cells exhibit a large degree of heterogeneity with regards to RTK signaling levels, which likely affects their ability to form part of the UB tip domain and ultimately the tips of the branching UB (Chi et al., 2009). This opens the door for other growth factors and signaling molecules to be involved in modifying the levels of RTK signaling among UB cells.

FGF10/FGFR2 signaling, for instance, has been shown to induce UB branching and synergize with the Ret signaling pathway (Michos et al., 2010). Thus, generating chimeras for other critical kidney developmental genes can further elucidate the cell-autonomous morphogenetic behaviors that are potentially very important during UB formation and branching.

Currently, however, genetic labeling of individual UB epithelial cells, or even cell clusters, for *in vivo* or explant studies is very challenging due to technical restrictions and time concerns. For example, generating chimeric kidneys, in which a subset of cells are mutant, necessitates the isolation of mutant embryonic stem cell lines, proper stem cell culture techniques, manipulation of blastocysts during stem cell injection, surgery on pseudo-pregnant mothers for the insertion of chimeric embryos, and also is limited by the frequency of obtaining a viable chimeric embryos at the desired level of chimerism (Shakya et al., 2005b; Chi et al., 2009). The whole process can take many months, or longer, and therefore the use of such chimeric embryos to study the effects of specific genes on cell migration or other behaviors in the living organs can be very difficult and time consuming.

The newly devised renal organoid system may potentially be used as an alternative to generating *in vivo* chimeras. Kidneys can be dissociated into single-cell suspensions that are then reaggregated and go on to form organotypic structures, including UB structures and developing nephrons. The UB structures elongate, form ampullae and bifurcate similarly to intact UBs in the mouse fetal kidney. Additionally, and importantly, UB tubules in the renal organoid system express the typical UB tip markers (Ret and Wnt11) at most of their ends, and this expression pattern is maintained during the *bona fide* branching

observed in this system (**Chapter 2, Figures 2.5** and **2.6**). By virtue of the dissociation of kidneys into single cells, cells from different sources can be mixed before reaggregation to easily and swiftly create fine-grained chimeras. As long as the cells from the two sources are differentially marked (e.g., by expression of different fluorescent proteins in the UB), the ability of one group to form part of the resulting structures can be compared to the other; moreover, the relative level of mosaicism can be adjusted to suit the investigator's need. One published study has generated mosaic renal organoids by mixing wild-type renal cells with renal cells that carry siRNAs against WT1, a mesenchymal gene crucial for nephron development (Davies et al., 2004). They showed a reduction in the ability of WT1 knocked-down cells to contribute developing nephrons (Unbekandt et al., 2010). Although this system seems to be suitable for studying the cell-autonomous nature of mutations in the developing nephron, it remained to be demonstrated whether this system is appropriate for the study of important, Ret-signaling-dependent cell rearrangements that occur during UB morphogenesis. To this end, once having shown that global knockouts of Sprouty1 in this culture system essentially mimic reported *in vivo* results, we go on to generate chimeric renal organoids using *Sprouty1*$^{-/-}$ and WT cells or *Ret*$^{51/-}$ and WT cells. Any cell sorting or cell competition occurring for residence of the UB tips of these renal organoid chimeras can then be compared to the results of previously published, *in vivo* chimeras produced with the same or similar genetic scheme. In doing so, we find that chimeras generated using the new system phenocopy their *in vivo* counterparts, and this may allow for higher-throughput experimentation to test for the cell-autonomous nature of new mutations.

RESULTS

Global *Spry1*$^{-/-}$ renal organoids display a phenotype similar *in vivo* mutants

To test the use of the renal organoid system in investigating cell rearrangements that occur in mosaic UBs during branching morphogenesis, we wanted to generate *Spry1* chimeras in the new system as a proof-of-principle study, since data on *in vivo Spry1* chimeras has already been published (Chi et al., 2009). Before making the chimeric organoids, however, we first checked if a global knockout of *Spry1* yielded a similar phenotype in the renal organoid system as in a conventional whole-kidney knockout. *Sprouty1* is expressed in the epithelial cells of the ureteric tree and at much lower levels in the condensing mesenchyme of the developing metanephric kidney (Basson et al., 2006; Gross et al., 2003). *Spry1*$^{-/-}$ mutants show a widespread defect during the development of the ureteric tree. This includes the formation of supernumerary buds from the WD, which develop into multiplex ureters and kidneys, a large increase in the number and diameter of UB branches, and a highly irregular branching pattern, at least at early states (Basson et al., 2005; Basson et al., 2006). During whole-kidney explant culture, instead of undergoing mostly standard bifurcation as seen in normal UB branching, *Spry1*$^{-/-}$ mutants exhibitwide ureteric bud stalks and tips formed multiple outbuddings resulting in highly irregular structures (Basson et al., 2006).

To create *Sprouty1* mutant renal organoids, we used E12.5 *Sprouty1*$^{-/-}$ kidneys carrying *Hoxb7:myrVenus* which allowed us to visualize the branching ureteric bud. Before dissociation, the harvested mutant kidneys displayed the previously described phenotypes for *Spry1*$^{-/-}$ mice, with an abnormal branching pattern, an increased number of tips and

wide UB branches, while littermate wild-type control kidneys appeared normal **(Figure 3.1A)**. Kidneys were then pooled by genotype and each group was used separately, following the normal protocol of dissociation into a single-cell suspension, reaggregation by centrifugation, and culture at an air-media interface **(Figure 3.1A)**. While images taken at the start of the culture, just after reaggregation, showed a dispersal of UB cells in both *Spry1*$^{-/-}$ mutant and WT cultures, the initial density UB cells in the mutant seemed higher than that of WT cultures **(Figures 3.1B, C)**, and by the next day cultures formed drastically different ureteric bud structures depending on their genotype. *Spry1*$^{-/-}$ mutant renal organoid cultures formed very large masses of cells that comprised most of the UB cells in the culture and that contained numerous large holes or cysts **(Figure 3.1B', C')**. This mutant phenotype persisted throughout the time course and on day 3 of culture, we observed multiple outbuddings emanating from the large mass of UB cells **(Figure 3.1D)**. This was in sharp contrast with the wild-type control renal organoids, which (as described in Chapter 2) formed UB spheroids and "pseudo-branched" UB tubules, which grew, elongated, and bifurcated in accordance with previously characterized wild-type cultures **(Figures 3.1C, C'', F).** Although whole-kidney *Spry1*$^{+/-}$ heterozygotes were not reported to present a detectably abnormal phenotype (Basson et al., 2006; Michos et al., 2010), we found that *Spry1*$^{+/-}$ renal organoids seem to present abnormalities intermediate between wild-type and homozygous mutant renal organoids in terms of the expansive UB epithelial regions and the number of individual UB structures formed (compare **Figure 3.1E** to **Figures 3.1D** and **F**). The formation of dilated, almost cystic ureteric bud structures with multiple outbuddings in our mutants is remarkably similar to anomalies during whole-kidney ureteric bud branching in *Spry1*$^{-/-}$ mutants (Basson et al., 2005). Moreover, both

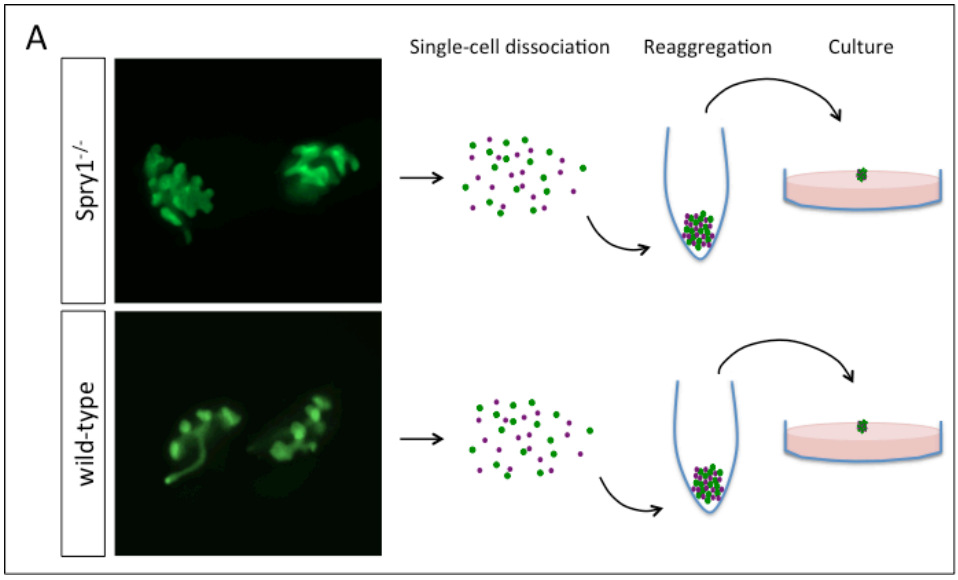
A
Single-cell dissociation
Reaggregation
Culture
Spry1-/-
wild-type

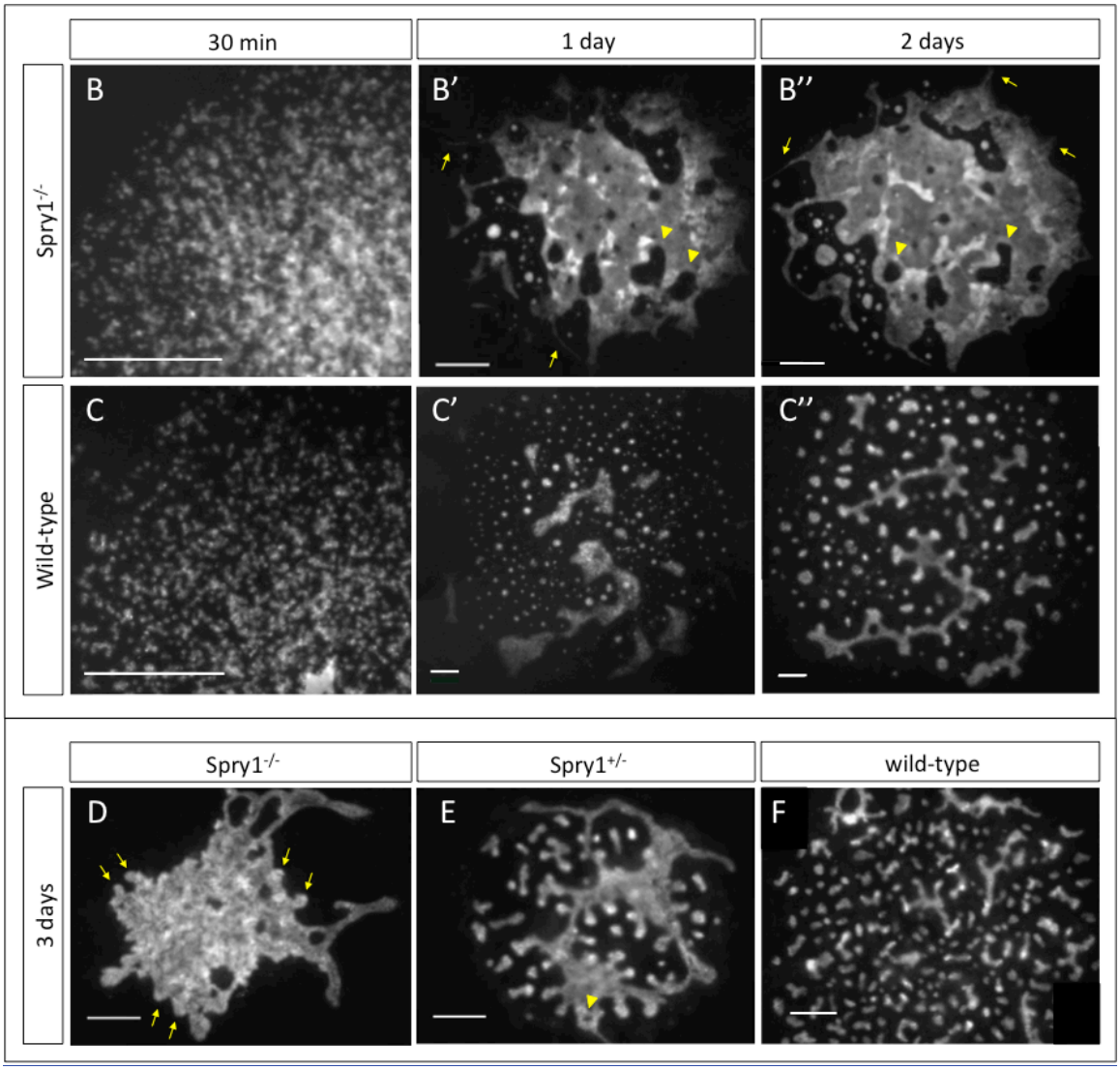
30 min
1 day
2 days
Spry1-/-
Wild-type
B
B'
B''
C
C'
C''
Spry1-/-
Spry1+/-
wild-type
3 days
D
E
F

Figure 3.1 – *Sprouty1* mutant renal organoids display large, broad cystic masses of UB epithelia that contain multiple UB outbuddings. (A) illustrates the scheme used to create WT and *Spry1*$^{-/-}$ global mutant renal organoids, where green dots represent UB cells and purple dots represent other non-UB renal cells. E12.5 kidneys containing *Hoxb7myrVenus* were pooled according to genotype and these groups were dissociated in parallel into single-cell suspensions. Approximately 100,000 cells were then reaggregated by centrifugation and cultured. (B-C'') show images of 30 min, 1-, and 2-day cultures of *Spry1*$^{-/-}$ (B-B''),and WT (C-C'') renal organoids. (D-F) show images of separate 3-day cultures of *Spry1*$^{-/-}$ (D), *Spry1*$^{+/-}$ (E), and WT (F) renal organoids.
(B) demonstrates the seemingly higher density and appropriate dispersion UB cells just after reaggregation and (B'), (B''), and (D) display UB cells forming large, cystic (yellow arrowheads) masses of UB epithelia at 1, 2, and 3 days of *Spry1*$^{-/-}$ culture, respectively. Many cell extensions still persist at these relatively late time points in the mutant (yellow arrows in B', B'')[n=4 cultures analyzed]. WT renal organoids grow normally, with a well-dispersed distribution of UB cells at the beginning of culture (C), the formation of discrete UB spheroids and UB tubules (C'), and UB morphogenesis thereafter (C'', F)[n=2 cultures analyzed. In (E), *Spry1*$^{+/-}$ heterozygote cultures seem to display an intermediate phenotype [n=2].

renal organoids and whole kidney mutants resembled the phenotype produced upon implantation of GDNF beads into normal kidney explants (Pepicelli et al., 1997), with dilated UB stalks and tips and fusion of separate branches to form large, broad areas of UB epithelia. These results are therefore consistent with an upregulation of GDNF/Ret signaling in the absence of *Sprouty1,* as has directly been shown in whole kidneys.

Cellular dynamics during the self-organization of UB cells in *Spry1*$^{-/-}$ renal organoids

Time-lapse imaging was also employed to explore the dynamics of the self-assembly of mutant UB structures during the early portions of *in vitro* renal organoid culture. Three renal organoid cultures are presented in **Figure 3.2**: (A-F) and (G-L) show the self-organization of *Spry1*$^{-/-}$ UB cells and (M-R) of wild type cells. Note that in both mutant cases

the density of UB cells was greater than that of the WT case, although similar numbers of cells were used to establish the cultures . This is consistent with the accelerated growth, increased branch number and size, and increased proliferation observed in the epithelial compartment of whole kidney mutants (Basson et al., 2006). During a 24-hour culture period, UB cells in control renal organoids swiftly organized themselves into UB spheroids via a moderate number of cell extensions that, in general, cease within the first 15 hours of culture as observed previously (**Figures 3.2M-R**; **Chapter2, Figure 2.1**). Mutant cells, however, self-assembled into large UB structures that continued to aggregate with each other to form yet even larger masses of UB cells. During this process the number of cell extensions present at any given time-point was much more extensive in mutant cultures than was observed in WT cultures, and these cell extensions and protrusions endured past 48 hours, even after the majority of free UB cells and smaller UB structures had been expended (**Figures 3.2A-L**; arrows in **Figure 3.1B', B"**).

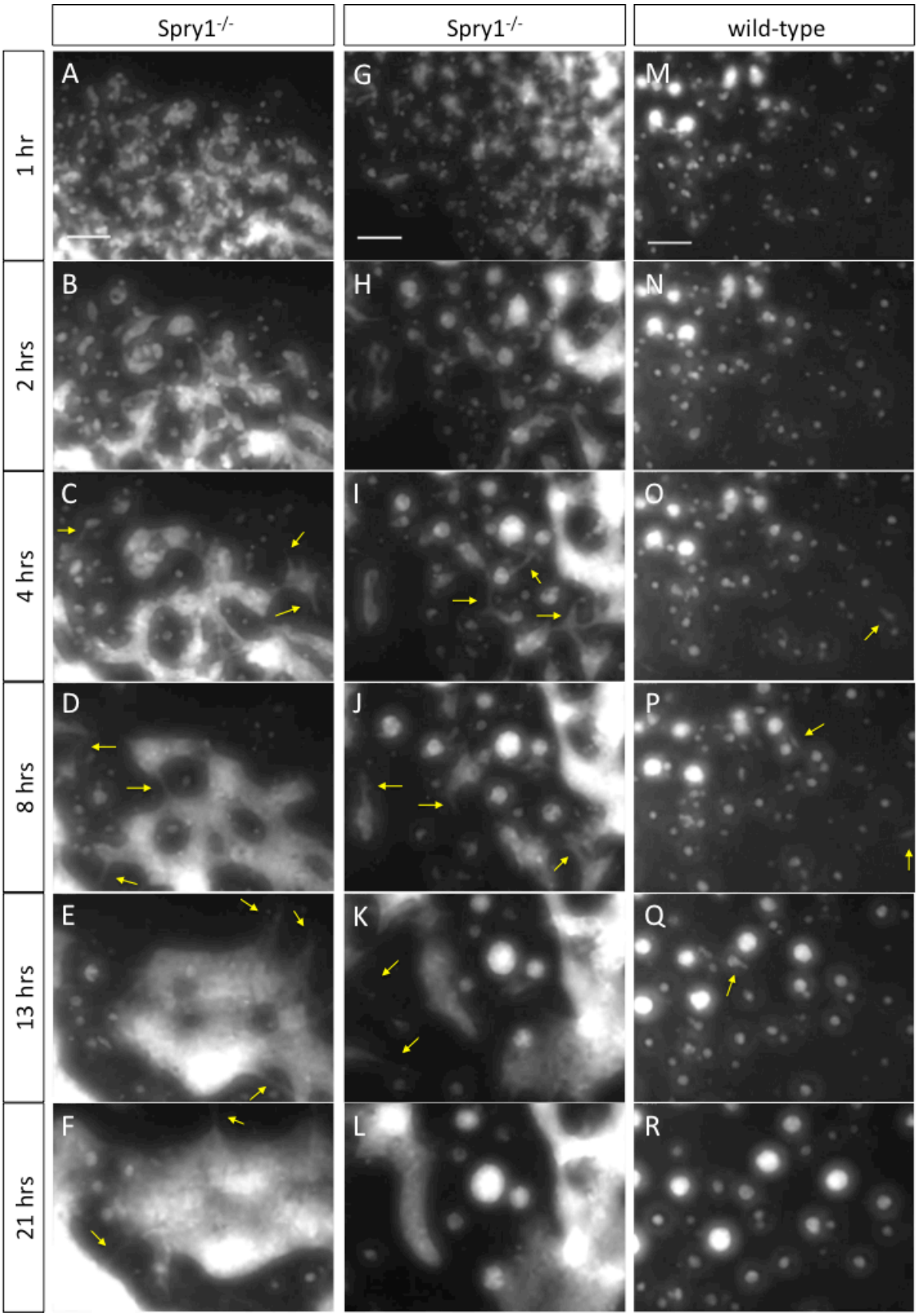
Spry1-/-
Spry1-/-
wild-type
1 hr
2 hrs
4 hrs
8 hrs
13 hrs
21 hrs
A
B
C
D
E
F
G
H
I
J
K
L
M
N
O
P
Q
R

Figure 3.2 – Cellular dynamics during the self-assembly of *Spry1*$^{-/-}$ renal organoids. (A-R) show selected frames from 20x time-lapse movies of reaggregated *Spry1*$^{-/-}$ mutant and WT renal cells carrying *Hoxb7myrVenus* during the self-organization of UB structures. *Spry1*$^{-/-}$ mutant cultures initially contain a denser network of UB cells (A, G) than WT cultures (M). During the subsequent hours, mutant cells self-assemble into large UB structures that continue aggregating with each other to form very large masses of UB epithelia (B-F, H-L). Conversely, WT cells swiftly form UB spheroids that remain distinct from one another during the time-lapse (N-R). The increased aggregation in the mutant coincides with a robust surge of cell extensions that develops among the mutant cells (arrows in C-F and I-K) that is not observed among WT cells, which exhibit moderate levels of cell extensions forming (arrows in O-Q). Scale bar equals 50 microns.

Having shown that the generation of global Spry1$^{-/-}$ mutant renal organoids yields basically similar results—large, broad, cystic areas of UB epithelia, with multiple UB outbuddings—as conventional culture systems, we decided to proceed to construct chimeric reaggregates.

Spry1-/-⇔WT chimeric renal organoids recapitulate the *in vivo* chimera phenotypes

Similar to the global *Spry1*$^{-/-}$ renal organoid analysis, separate single cell-suspensions of renal cells were made from E12.5 *Spry1*$^{-/-}$ or WT kidneys that also carried the Hoxb7myrVenus (green) allele for the visualization of UB epithelia, as diagrammed in **Figure 3.3A**. At the same time, renal cells were also dissociated from E12.5 WT kidneys carrying *Hoxb7cre;Rosa26*$^{Tomato/Tomato}$ (red) as an alternate color UB marker. The three groups of cells were then counted by a hemocytometer and then mixed together accordingly to produce a 1:1 ratio of (green) *Sprouty1-/-* to (red) WT cells and a 1:1 ratio of (green) WT to (red) WT cells as a control **(Figure 3.3A)**. The two cell mixtures were then reaggregated and cultured, and initially exhibited a well-dispersed and evenly mixed distribution of red and green cells **(Figure 3.3B)**. As renal organoid development progressed, both chimeric genotypes develop typical UB structures that displayed fine-

grained mosaicism **(Figures 3.4A-A'', C-C'', E-E'')**. By 3 days of culture, however, this mosaicism resolved into distinct domains based on genotype in the mutant chimeras. *Sprouty1*$^{-/-}$ mutant cells, which upregulate RET signaling, displayed a preference for residence at the tips of

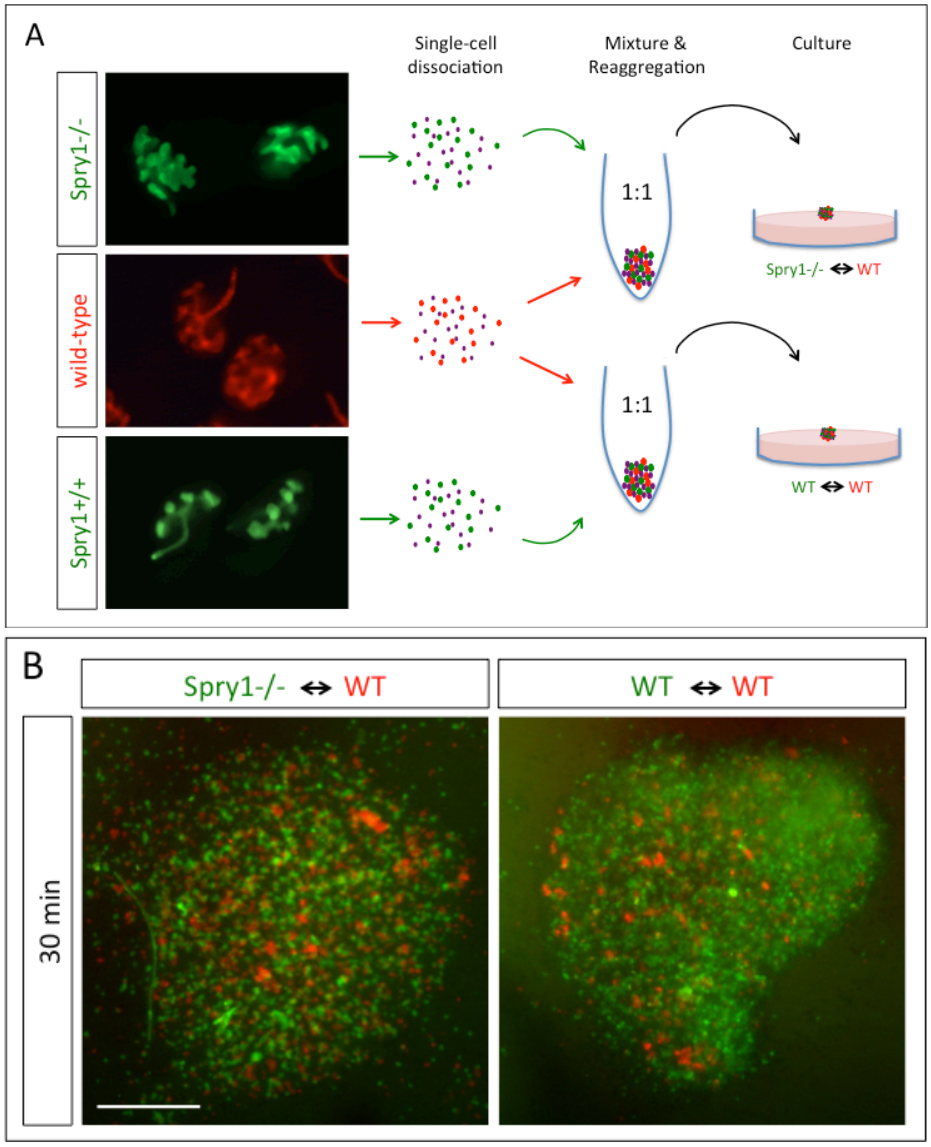

Figure 3.3 – Generation of *Sprouty1*$^{-/-}$⇔WT and WT⇔WT chimeric renal organoids. (A) shows the scheme for creating chimeric renal organoids. E12.5 *Spry1*$^{-/-}$ and *Spry1*$^{+/+}$ (WT) kidneys carrying *Hoxb7myrVenus* were obtained along with E12.5 *Hoxb7cre:Rosa26*$^{Tomato/Tomato}$ (WT) kidneys. The *Spry1*$^{-/-}$ mutant kidney exhibits the typical

phenotype of large dilated UB branches, increased number of branches and irregular branching pattern. The three genotypes were then dissociated separately into single-cell suspensions that were each assessed for cell number using a hemocytometer. Cell suspensions were then mixed accordingly to form 1:1 *Sprouty1*$^{-/-}$ (green)⇔WT (red) suspensions and 1:1 WT (green)⇔WT (red) suspensions. Both cell mixtures were then reaggregated by centrifugation and the pellets were cultured. At the start of culture (30 minutes) both mutant chimera and wild-type control chimera showed a well-dispersed and even distribution of red and green cells (B). Scale bar equals 200 microns.

new UB branches that formed, while WT cells tended to be found in the trunk portions of UB structures **(Figures 3.4B-B'', D-D'')**. In contrast, in the WT ⇔ WT chimera, the salt-and-pepper pattern of red and green cells was maintained at 3 days of culture, and red and green cells had a similar chance of forming part of the tips of branching UB structures **(Figures 3.4F-F'').**

One of the advantages of generating chimeras in the renal organoid system is the ability to easily adjust the level of chimerism to suit one's need. By lowering the proportion of *Sprouty1* mutant cells relative to WT cells we could more easily visualize the behavior of individual mutant cells in a wild-type context. We created *Spry1*$^{-/-}$ ⇔ WT chimeras at a 1:5 ratio and performed time-lapse microscopy of the first 48 hours of renal organoid development. As in the 1:1 chimeras, individual and groups of *Spry1*$^{-/-}$ and WT UB cells again came together to form fine-grained mosaic structures by 18 hours of culture **(Figures 3.5A-D')**. Thereafter the *Spry1*$^{-/-}$ mutant cells could be seen moving into the tip regions of growing UB tubules at the expense of WT cells by 43 hours **(Figures 3.5E-H'')**. By 5 days of culture, mutant cells could still be found at the tips of chimeric UB structures to the relative exclusion of WT cells, which tended to be limited to the trunk regions **(Figures 3.5I-J')**. Moreover, in many instances, once *Spry1*$^{-/-}$ mutant cells were present in

the tips they could also be observed to form elongating UB structures more than their WT counterparts **(Figures 3.5J-K)**. This shows clearly that higher RET-signaling cells outcompete WT cells for residence at the renal organoid tips, as they do *in vivo.*

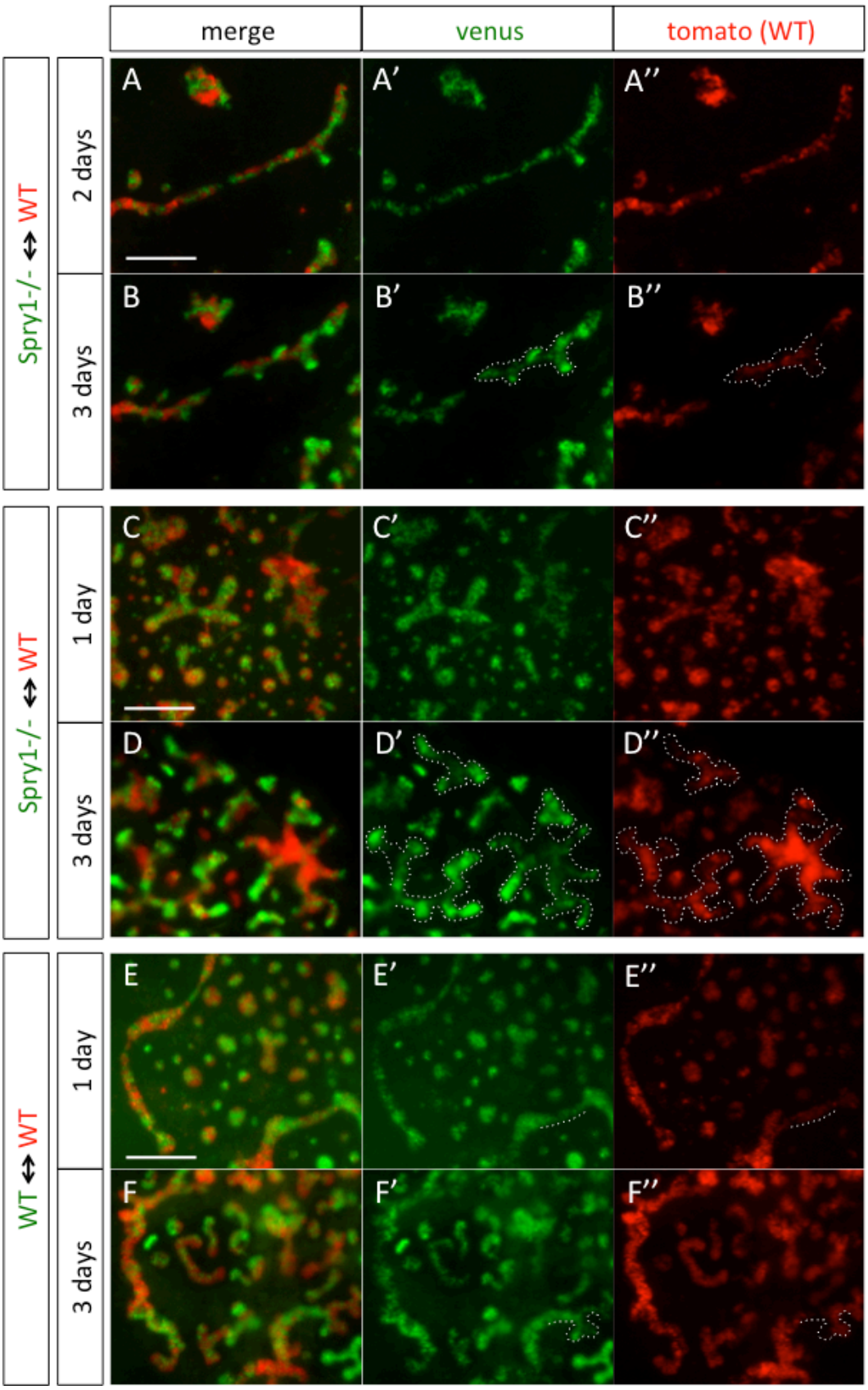
merge
venus
tomato (WT)
Spry1-/- ↔ WT
2 days
3 days
A
A'
A''
B
B'
B''
Spry1-/- ↔ WT
1 day
3 days
C
C'
C''
D
D'
D''
WT ↔ WT
1 day
3 days
E
E'
E''
F
F'
F''

Figure 3.4 – *Spry1*$^{-/-}$ cells preferentially occupy the tips of chimeric renal organoid structures at the expense of WT cells. (A-F'') show a time course of mosaic UB structures in *Spry1*$^{-/-}$⇔WT (A-D'') and WT⇔WT (E-F'') chimeric renal organoids. (A-A''), (C-C''), and (E-E'') display fine-grained mosaic UB structures early in renal organoid development (1 or 2 days-old). By day 3, distinct domains of *Sprouty1*$^{-/-}$ (green) and WT (red) cells become apparent in the mutant chimeras, with mutant cells preferentially taking up residence at the tips of forming or formed UB branches (white dotted lines in B-B''; D-D'')[n=3 cultures]. In 3 day-old WT⇔WT mosaic structures, red and green cells maintain their fine-granularity and red and green cells seem to have equal preference in forming part of the tips of branching UB structures (white dotted lines in F-F''). Scale bar equals 200 microns.

To quantify the contribution of mutant vs. wild type cells to the tips and trunks of the UB tubules, we produced color profiles for 30 randomly chosen "tip" regions and 30 randomly chosen "trunk" regions to further characterize these domains in 3-day chimeric structures (see Experimental Procedures and Appendix A for details). Color profiles were created by calculating the ratio of green versus red pixels within a specific region (channels were evaluated separately and only pixels with intensity values over a background control region were considered). With this analysis, we found that tips in *Sprouty1*$^{-/-}$ ⇔ WT (1:1) chimeras were approximately twice as enriched in mutant (green) pixels when compared to trunks, which were significantly enriched in WT (red) pixels **(Figures 3.6A, B, E)**. We also found tips in mutant chimeras to be significantly more green than tips in WT ⇔ WT chimeras **(Figures 3.6A, C, E)**. No significant difference was found between tip and trunk color profiles of the wild-type control chimeras **(Figures 3.6C, D, E)**.

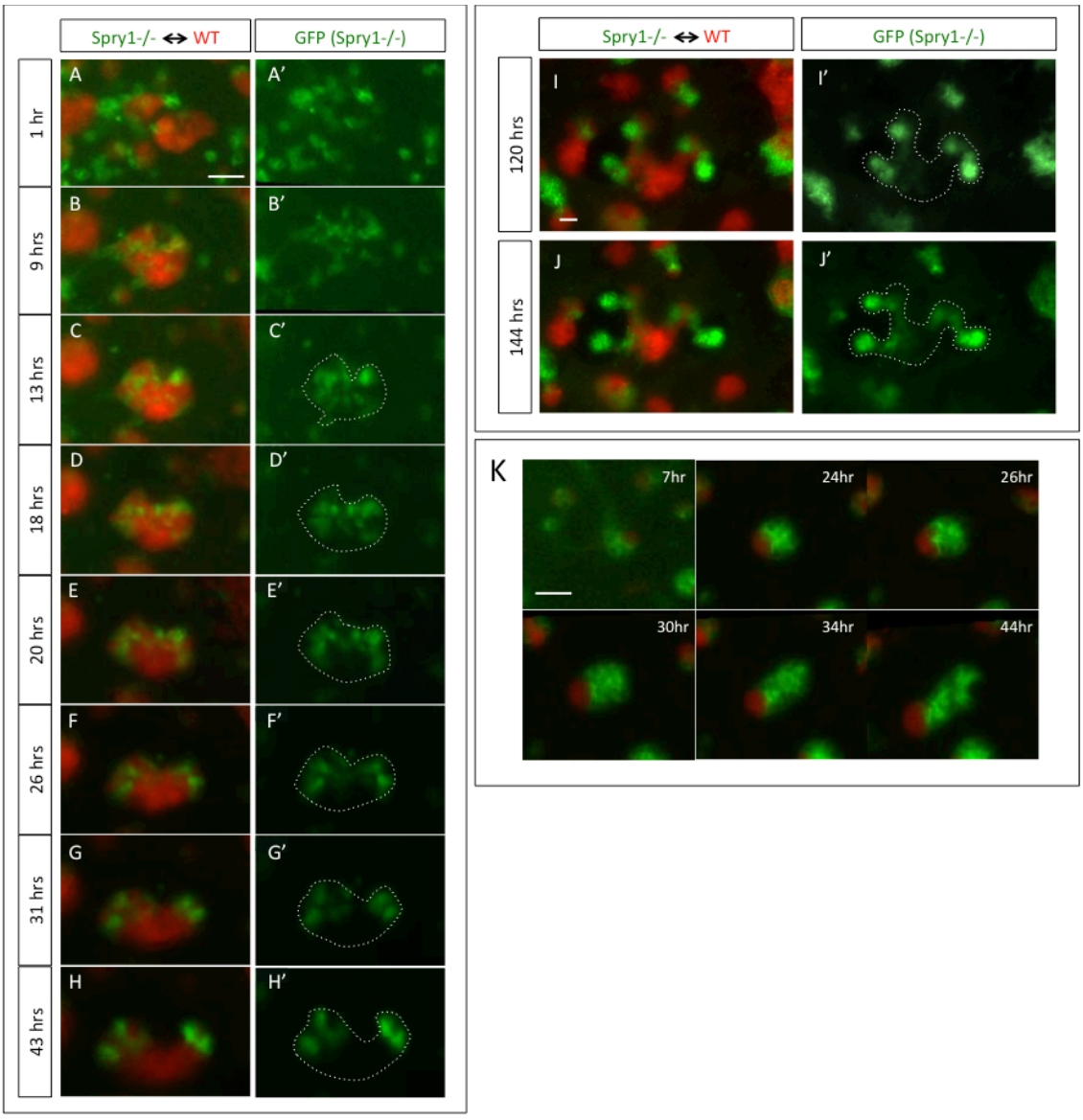

Figure 3.5 – *Sprouty1*$^{-/-}$ cells outcompete WT cells for residence at the tips of growing and branching chimeric renal organoid structures. (A-H') display selected frames from a 43-hour time-lapse of *Spry1*$^{-/-}$ (green)⇔WT (red) mosaic UB structures self-organizing and undergoing UB morphogenesis. (A-B') show the self-assembly of a mosaic UB structure by 9 hours of culture and the UB structure still exhibits fine-grained mosaicism by 18 hours of culture (C-D'). Thereafter, mutant cells reposition to occupy just the tips of an elongating UB tubule at the expense of WT cells (E-H'). (I-J') show the same structure analyzed in (A-H') at 120 (I-I') and 144 hours (J-J') of culture. At both time points, *Spry1*$^{-/-}$ mutant cells can still be observed at the tips of the UB structure that has undergone substantial morphogenetic changes. Mutant tips can be seen undergoing further morphogenetic changes at 144 hours, while the WT "trunk" regions do not grow, elongate, or branch (J-J'). (K) shows selected frames of a 44-hr time-lapse of a chimeric UB structure in which a

region containing mainly *Spry1*$^{-/-}$ cells (green) elongated, while the adjacent region containing mainly WT cells (red) remained relatively constant in size.

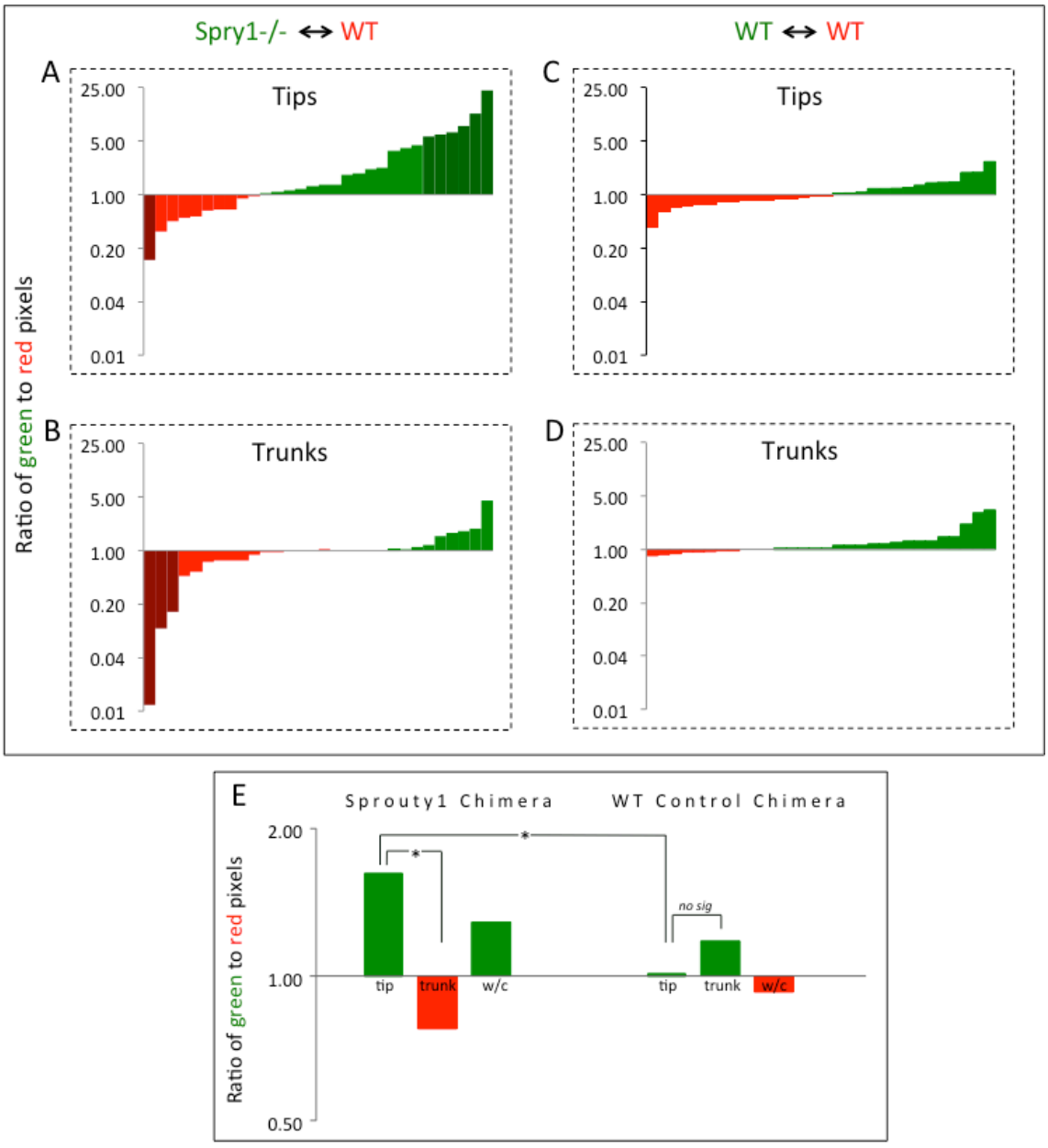

Figure 3.6 – Distribution of wild-type and mutant cells in tip and trunk regions in *Spry1*$^{-/-}$⇔WT and WT⇔WT chimeric UB structures. (A-D) show the ranked ratios of green to red pixels in 30 randomly chosen tip regions (A, C) and 30 randomly chosen trunk regions (B, D) in 3 day-old *Spry1*$^{-/-}$⇔WT (A,B) and WT⇔WT (C, D) chimeric cultures. Regions analyzed took the shape of 40-micron wide circles (each containing 208 pixels in total) and histograms were created for each region (red and green channels were analyzed separately). The ratio of green to red pixels was then calculated to determine the tip or

trunk region's color profile (only pixels with an intensity above that measured in a background control region were used for analysis). Regions containing more green than red pixels are represented as green, and vice versa. Regions in which the ratio of green/red or red/green was >5 are indicated by a darker shade of the predominant color. (E) Shows the average green to red ratios of the specified tip and trunk regions and of the whole culture (w/c) as well (see Experimental Procedures for the calculation methods and Appendix A for raw data). In the *Spry1*$^{-/-}$⇔WT chimera, the tips are, significantly, ~2 times greener than the trunks (which overall had a red profile) (p=.012, using the $\log_{10}$ values of ratios; A, B, E). The tips were also significantly greener (1.6x) than the tips of the WT⇔WT chimera (p=.036, using the $\log_{10}$ values of ratios; A, C, E); the tips and trunks of the wild-type control chimera were not significantly different from each other and many regions in the control chimeras exhibited nearly equal mixes of green and red.

Ret$^{51/cre}$⇔WT chimeric renal organoids recapitulate similar *in vivo* chimera phenotypes

Ret mutant chimeras were also produced and analyzed as an additional test of the use of renal organoids for chimeric analysis. Previously generated *in vivo* chimeras have shown that when Ret null cells (or cells with lower Ret-signaling) are introduced into hosts with higher Ret signaling, the lower Ret signaling cells are outcompeted by higher Ret-signaling cells for residence at the tips of the branching ureteric tree (Chi et al., 2009). Because Ret-null animals exhibit renal agenesis, this would make difficult the procurement of Ret null kidney cells for the generation of chimeric renal organoids. We instead decided to use kidneys that were compound heterozygotes with one hypomorphic allele of *Ret* (*Ret*^{51}) and one null allele. The hypothesis is that *Ret51/Ret-null* cells, with lower Ret signaling, will be out competed by WT cells, with higher Ret-signaling, for residence at the tips of branching UB structures.

Here, the scheme used to generate mosaic renal organoids was slightly different to that used previously. E12.5 *Ret*$^{51/cre}$ kidneys (where *Ret*^{cre} is a null allele) and wildtype littermate kidneys all carrying *Hoxb7venus* were harvested. Each genotype was pooled with wildtype kidneys of a different color UB marker, *Hoxb7cre;Rosa26*$^{Tomato/Tomato}$, at a one kidney to one kidney ratio **(Figure 3.7A)**. Dissociation of these pooled kidneys then created two mosaic single-cell suspensions that were each reaggregated and cultured **(Figure 3.7A)**. At the start of culture both the Ret$^{51/cre}$ ⇔WT chimera and the WT⇔WT chimeras generated showed well-dispersed and evenly mixed distributions of red and green cells. In the mutant chimera, however, there was an abundance of WT (red) cells relative to mutant cells (green)**(Figure 3.7B)**, which is probably due to the reported reduced branch number and kidney volume of Ret51 hypomorphic kidneys (de Graaff et al., 2001) and also observed in our samples prior to dissociation. Although this caused many ureteric bud structures to be non-chimeric and fully WT, we could still examine the relatively fewer chimeric structures that formed.

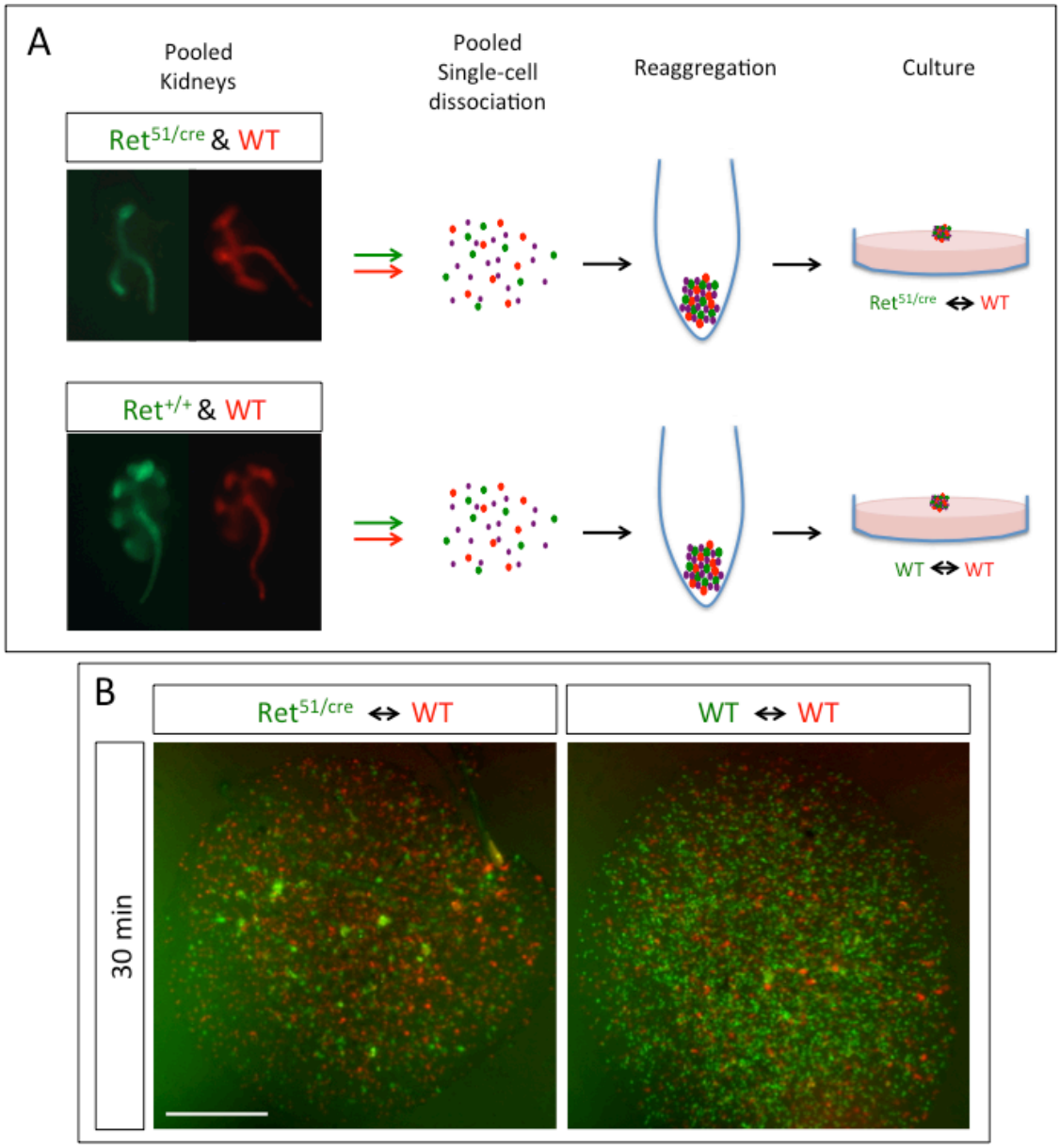

Figure 3.7 – Generation of *Ret*$^{51/cre}$⇔WT and WT⇔WT chimeric renal organoids. (A) shows the scheme for creating chimeric renal organoids, where green dots represent UB cells and purple dots represent other non-UB renal cells. E12.5 *Ret*$^{51/cre}$ and *Ret*$^{+/+}$ (WT) kidneys carrying *Hoxb7myrVenus* were obtained. The *Ret*$^{51/cre}$ mutant kidney displayed a reduced branch number. Each genotype was pooled with E12.5 *Hoxb7cre:Rosa26*$^{Tomato/Tomato}$ (WT) kidneys at a 1 kidney to 1 kidney ratio and then dissociated to form mosaic single-cell suspensions. Both mosaic cell suspensions were then reaggregated by centrifugation and the pellets were cultured. At the start of culture (30 minutes) both mutant chimeric and wild-type control chimeras showed a well-dispersed and even distribution of red and green cells, but the mutant chimera displayed a higher proportion of WT (red) cells (B). Scale bar equals 200 microns.

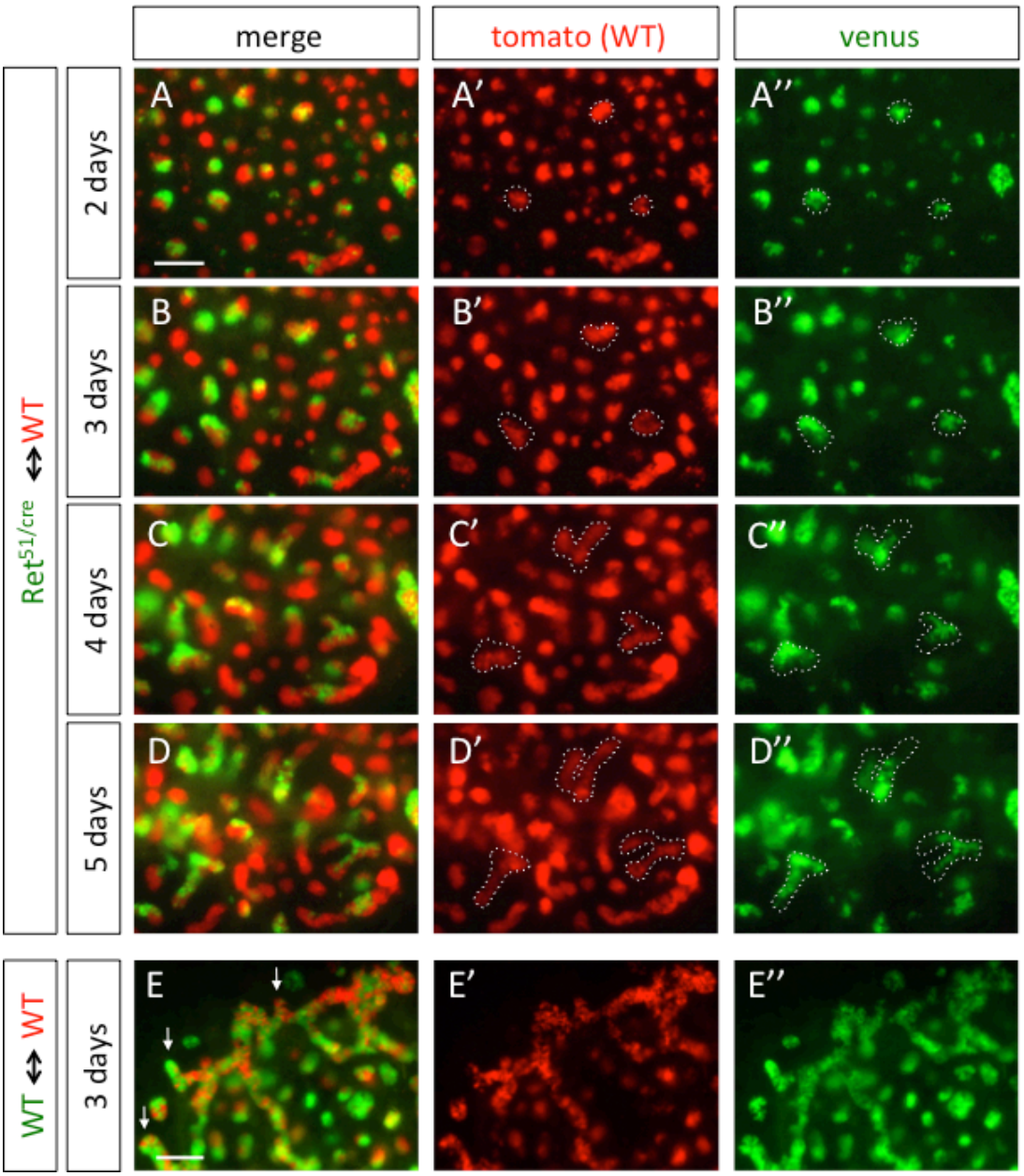

Figure 3.8 – *Ret*$^{51/cre}$ cells show a preference for residence of the tips of branching chimeric renal organoid structures at the expense of WT cells. (A-E'') show a time course of mosaic UB structures in *Ret*$^{51/cre}$⇔WT (A-D'') and WT⇔WT (E-E'') chimeric renal organoids. Mosaic UB structures self-assembled by day 2 (A-A'') but growth and morphogenesis thereafter seemed stunted compared to the littermate wild-type control chimera (E-E'') and other WT renal organoid cultures produced. By day 3, distinct domains of *Ret*$^{51/cre}$ (green) and WT (red) cells became apparent in the mutant chimeras, and by days 4 and 5 (D-D'' and E-E'', respectively), mutant cells preferentially occupied the tips of forming or formed UB branches. In 3 day-old WT⇔WT mosaic structures, red and green cells maintained their fine-granularity (E-E'') and red and green cells seemed to have equal preference in forming part of the tips of branching UB structures (arrows in E). Scale bar equals 100 microns.

We found that *Ret*$^{51/cre}$ cells could still participate in the self-assembly of UB cells and form part of UB spheroids and tubules **(Figures 3.8A-A'')**. Thereafter, both chimeric structures and non-chimeric structures exhibited slow growth compared to other renal organoids created. *Bona fide* branching among UB spheroids was not observed until four days of culture, as opposed to three days normally seen in WT renal organoids **(Figure 3.8C; Chapter 2, Figure 2.3)**. We did notice that, in the chimeric structures that eventually do branch, however, WT cells seem to preferentially occupy the tips at the expense of the *Ret*$^{51/cre}$ mutant cells **(Figures 3.8B-D'').** This is the reverse phenotype of what we see in the *Spry1* chimera study above, but similar to what is seen in *Ret*-null ⇔ WT chimeric kidneys generated *in vivo* (Shakya et al., 2005b; Chi et al., 2009)**.** Also, we found that most chimeric UB structures in the mutant chimeras, whether branching or not, lost their fine-granularity and contained many domains of either mutant or WT cells (**Figures 3.8A-D'')**. This in contrast to the littermate control WT⇔WT chimera which presented a salt-and-pepper pattern throughout the time course and showed no noticeable preference for red or green cells at the tips of UB branches **(Figures 3.8E-E'')**. Indeed, when we performed the same color profile analysis described above on 3-day chimeric cultures, we found that there was no significant difference between tips and trunks with respect to the ratio of red WT cells to green WT cells in the wild-type control chimera **(Figures 3.9C, D, E).** The mutant chimeras, however, showed a strong trend of WT (red) cells being found disproportionately in the tips compared to the trunks **(Figures 3.9A, B, E)**. In summary, *Ret* hypomorphic cells seem to show a deficient ability to form part of the tips of branching UB structures and these results further support the potential for using the renal organoid system in generating mosaic UBs for the study cell autonomous defects.

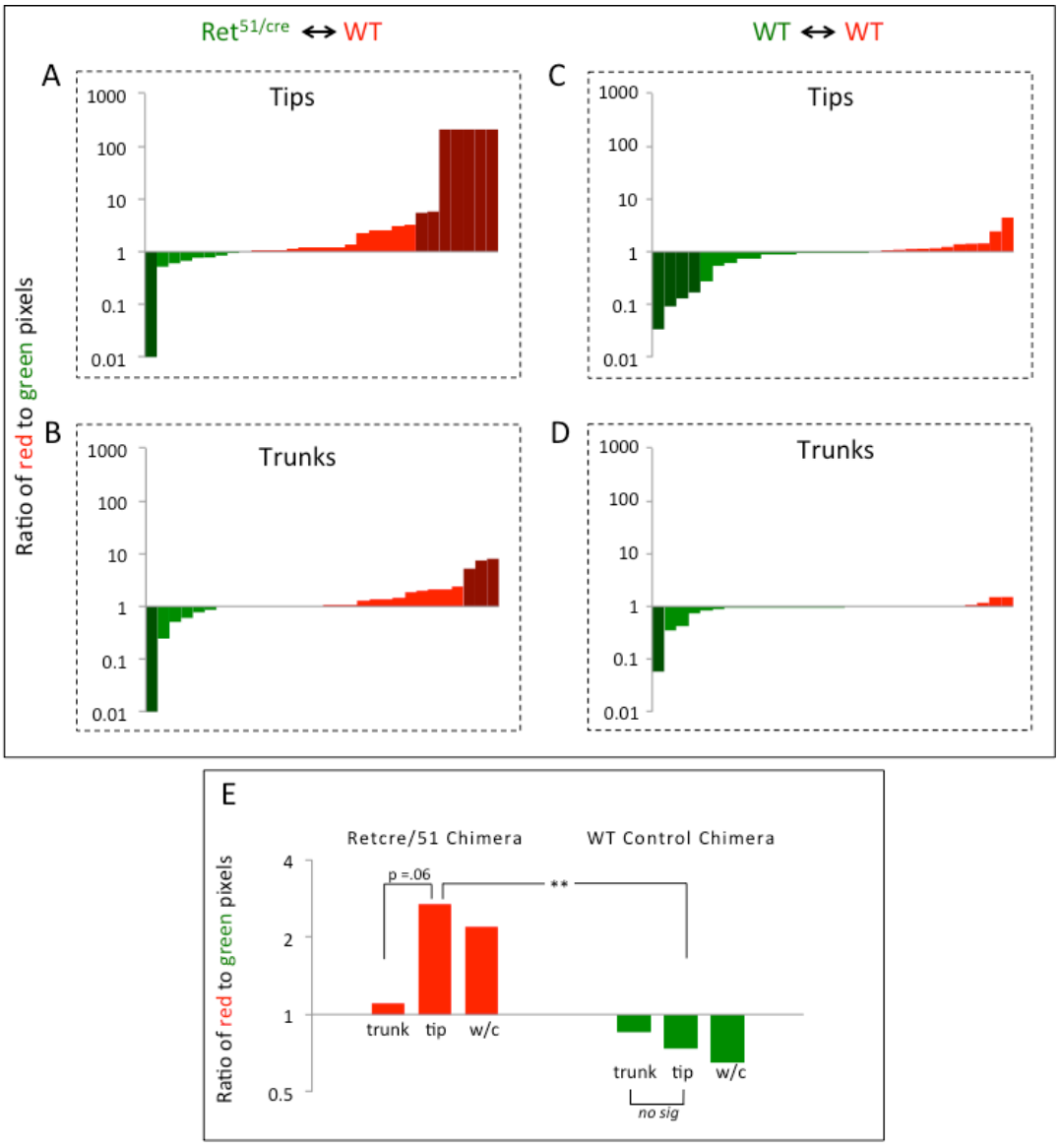

Figure 3.9 – Distribution of wild-type and mutant cells in tip and trunk regions in *Ret*$^{51/cre}$⇔WT and WT⇔WT chimeric UB structures. (A-D) show the ranked ratios of red to green pixels in 30 randomly chosen tip regions (A, C) and 30 randomly chosen trunk regions (B, D) in 3 day-old *Ret*$^{51/cre}$⇔WT (A,B) and littermate WT⇔WT (C, D) chimeric cultures. Analysis was carried out identically to the *Spry1* chimeric data, except that ratios here were calculated red:green (instead of green:red). (E) Shows the averaged green to red ratios of the specified tip and trunk regions and of the whole culture (w/c) as well. In the *Ret*$^{51/cre}$⇔WT chimera, the ratio of red (WT) to green (mutant) pixels tended to be higher in the tips than in the trunks (p=.06, using the $\log_{10}$ values of ratios) Many tips did not have any green (mutant) pixels within (A), whereas this was not the case for the trunks (B). The

tips also had a significantly higher ratio of red (WT) to green (mutant) pixels than the tips of the WT⇔WT chimera (p=.006, using the log_{10} values of ratios)(A, C, E); the tips and trunks of the wild-type control chimera were not significantly different from each other (p=.54) and many regions showed close to a 1:1 mix of green and red (C, D, E). A Student's t-test was performed for each comparison.

DISCUSSION

The complexity of developing *in vivo* chimeric kidneys makes detailed analysis of cell-autonomous cell behaviors at the level of the whole kidney cumbersome and time-consuming. Using the recently devised renal organoid culture method, it is straightforward to make fine-grained chimeras by simply mixing different cell types or by mixing cells transfected with different constructs before reaggregation. Here we have shown that Ret-signaling-dependent cell rearrangements occur in chimeric renal organoids as they do in *in vivo* chimeras (Chi et al., 2009; Kuure et al., 2010; Shakya et al., 2006) using *Spry1*$^{-/-}$ or *Ret*$^{51/cre}$ renal cells in proof-of-concept experiments. Renal organoids globally mutant for *Spry1*$^{-/-}$ display large, cystic masses of UB epithelia with small outbuddings very akin to *in vivo* whole kidney mutants, where very similar branching morphogenesis defects were due to hyperresponsiveness to GDNF/RET signaling (Basson et al., 2005). Moreover, these large masses seem to form from an intense and extensive period of UB self-assembly. This is probably in part due to the seemingly increased number of UB cell extensions forming during this period, which is associated with the accretion of cells during UB self-assembly **(Chapter 2, Figure 2.1)**. Upon the activation of Ret in RET-expressing MDCK cells, there is indeed a dramatic increase in the presence of cellular processes, a reorganization of the cytoskeleton and cell adhesion molecules, and increased cell motility (Tang M-J et al., 1998), so the hyperactive self-assembly phenotype we observe is consistent with the increase in

Ret-signaling in *Spry1* mutants. We cannot exclude the possibility, however, that the "overactive" mutant phenotype observed is the consequence rather than the cause of the apparent denser milieu of UB cells displayed in *Spry1* mutant organoids. This highlights that, as with immortalized cell culture, renal organoid development has the potential to give special insight into the molecular mechanisms that underpin mutant morphologies *in vivo*. A mutant phenotype in kidneys of *Sprouty1*$^{+/-}$ heterozygotes has never been reported (Michos et al., 2010; Basson et al., 2005; Basson et al., 2006). *Sprouty1*$^{-/-}$ homozygous renal organoids display a much more dramatic mutant phenotype than their *in vivo* counterparts, and the basis for this may also allow for the presentation of intermediate phenotypes in heterozygotes. Although further investigation is necessary, this demonstrates how the dissociation and reformation of renal structures via an intermediate single-cell stage may uncover gene dosage requirements that are otherwise compensated for in the context of an intact kidney.

When chimeric renal organoids were made with *Spry1*$^{-/-}$ and WT cells, the mutant cells, with increased Ret-signaling, were able to outcompete the WT cells and preferentially take up residence at the tips of UB structures, where they exhibited an increased growth rate as compared to adjacent WT regions. This distinct phenotype was not detected among wild-type control chimeras, and the visual characterizations of both chimeric cultures were verified by a color profile analysis of different tip and trunk regions. These results are strikingly similar to the pattern observed in *Spry1* chimeras generated *in vivo,* where mutant cells preferentially formed the UB tip domain and the tips of the branching ureteric tree, outcompeting WT cells (Chi et al., 2009), and overall this demonstrates the powerful

utility of renal organoids in studying Ret-signaling-based cell competition that may occur during UB morphogenesis.

We also investigated Ret-signaling-deficient cells and their cell-autonomous effects on UB morphogenesis. *In vivo,* Ret-null cells in WT hosts are unable to form part of the tips of the branching UB. *Ret* null animals exhibit renal agenesis, however, while $Ret^{51/cre}$ kidneys (with one hypomorphic and one null *Ret* allele) are severely hypodysplastic (de Graaf et al., 2001) but nonetheless provide a source of *Ret*-signaling-deficient cells. When $Ret^{51/cre}$ cells were juxtaposed with WT cells in chimeric renal organoids the cultures displayed sluggish growth. This may have been caused by the presence of the mutant cells (perhaps along with a reduction of induced mesenchyme, as low Wnt11 and GDNF expression is observed in $Ret^{51/51}$ kidneys [de Graaf et al., 2001]) since chimeric renal organoids generated with littermate WT control cells presented relatively normal UB morphogenesis. Still, when looking specifically at growing and branching mosaic UB structures within the whole chimeric culture, a preference for WT cells at the branch tips at the expense of $Ret^{51/cre}$ mutant cells was apparent. Although color profile analysis showed that the difference in average color of tips versus trunks only approached significance (p=.06), this may have more to do with the methodology used in the evaluation. The simplest criterion for qualifying as a tip in our analysis included regions positioned on the ends of an elongated tubule. In our color profiling analysis of 3-day old $Ret^{51/cre}$⇔WT chimeric cultures, there was a preponderance UB structures that had not undergone or were in the beginning stages of UB morphogenesis, and this could have hindered our assessment of the ability of different cells to form part of specific domains within the UB. Performing color profile analysis on only complex, branched UB tubules (which formed the

majority of profiled structures in other chimeras) at a later timepoint may yield a more accurate calculation of the visual phenotype that we do, nevertheless, detect in branched mosaic structures.

Because of efficient penetration of siRNAs and other large molecules in this culture system (Unbekandt et al., 2010), the knockdown of UB-specific genes should make it possible to generate fine-grained chimeras of a vast array of genes, bypassing the derivation of a novel knockout or transgenic mouse line for each individual gene (at least for initial assessments of gene function). Additionally, the high-throughput nature of renal organoid chimeric generation can be harnessed as a platform for pharmacological intervention in chimeras to explore the cell-adhesion molecules (Lecuit, 2005; Steinberg, 2007) or cell-signaling pathways (Takahashi, 2001; van Weering et al., 1998; Tang et al., 1998) that may underlie the cell-autonomous cell rearrangements and cell sorting observed. For the study of kidney development in general, and UB morphogenesis in particular, these results validate another technique to add to the growing selection of applications for which the renal organoid system can be useful.

EXPERIMENTAL PROCEDURES

Dissociation of embryonic kidneys. Same as Chapter 2

Pellet culture. Same as Chapter 2

Chimeric Pellet Culture. Same as Chapter 2

Time course and Time-lapse movies. Same as Chapter 2

Color Profiling Analysis. Refer to Appendix A (Page 154) for all data. Three-day old chimeric cultures were used for analysis. Images were converted to black-and-white and given to a third party unaffiliated with the project, and therefore unbiased. This third party was given the criteria for identifying tips and cataloguing the qualifying tips with a number. Tips were defined as either the ends of elongated tubules, or the protruding portion of a kink or bend in the tubule with an internal angle of less than 90°. Thirty non-tip (i.e., trunk) UB regions were also randomly marked on the monochromatic image by the third party before resubmitting to the investigator. Any trunks regions which were located on non-chimeric UB structures were discarded and the third-party was asked to resample for the number of disqualified trunk regions. The number of qualifying tips (the integer set) was entered into an online random integer sequence generator (https://www.random.org), which yielded a random sequence of the integer set, and the first 30 randomized tip numbers were used for analysis. Tips that were part of non-chimeric structures were discarded and the randomized integer set was resampled for the number of disqualified tips. The 30 tip regions and 30 trunks regions analyzed took the shape of 40-micron wide

circles (208 pixels in total; Refer to page 155 in Appendix A for an example) and histograms were created for each region using ImageJ (channels were analyzed separately). With each analyzed region, the ratio of the number of green pixels to the number of red pixels (or red to green pixels) was then calculated to determine the tip or trunk region's "color profile". Only pixels with intensity above a background control region were used for analysis. Ratios for each region analyzed were then plotted on a logarithmic scale where they were ranked in order of magnitude. The color profile ratios for whole cultures were calculated similarly by creating histograms of the whole culture for each channel. The mean of all the red/green (or green/red) ratios was determined by calculating the average for the $\log_{10}$ of each ratio value, and then taking the antilog of this value. The statistical significance of differences between the means for different populations were analyzed by Student's t-test of the $\log_{10}$ values.

CHAPTER 4

The Cell-Autonomous Role of Fgfr2 During Ureteric Bud Morphogenesis

INTRODUCTION

The activation of the GDNF/Ret-signaling pathway is fundamental to UB growth and branching, and in the absence of GDNF, Ret or its co-receptor, Gfrα1, the most frequent consequence is failure of ureteric bud formation (Costantini and Shakya, 2006). It is important to acknowledge, however, that ureters and rudimentary kidneys sometimes form even in the absence of GDNF or Ret (in $Ret^{-/-}$ mice, for example, this happens 30 – 50% of the time, depending on genetic background; Schuchardt et al., 1994; Moore et al., 1996; Sánchez et al., 1996; Schuchardt et al., 1996). This suggests the presence of additional signals that are partially redundant with GDNF in their ability to induce bud outgrowth. Indeed, studies of the Wolffian duct in organ culture show that several members of the fibrobast growth factor (FGF) family, in particular Fgf7 or Fgf10, are competent to induce ureteric budding and adversely affect UB morphogenesis in their absence (Maeshima et al., 2007; Qiao et al., 1999; Zhang et al., 2006). These FGFs have been shown to activate FGF receptors (FGFRs), a gene family of receptor tyrosine kinases (RTKs) with at least 4 signaling members (Powers et al., 2000). In vitro, FGFR activation is associated with many biological responses including proliferation, differentiation, migration, and inhibition of apoptosis (Klint and Claesson-Welsh, 1999). Three of these genes (Fgfrs1-3) are capable of producing multiple receptor isoforms through alternative

splicing of primary transcripts (Powers et al., 2000). FGF7 and FGF10 are secreted by the cortical stroma and MM, respectively, and are ligands with high specificity for Fgfr2 (Bates, 2011). Fgfr2 is strongly expressed in the Wolffian duct and the UB tree (both tips and trunks; the Fgfr2-IIIb isoform) and differentiating nephrons (beginning with renal vesicles) but is present at lower levels in early MM and stromal mesenchyme (the Fgfr2-IIIc isoform) adjacent to the Wolffian duct (Peters et al., 1992; Cancilla et al., 1999; Bates, 2011). Although Fgfr1 is also (lowly) expressed in the ureteric lineage, many studies point to Fgfr2 in the UB as the improtant signaling axis that participates in RTK-signaling for proper UB morphogenesis (Zhao et al., 2004; Maeshima et al., 2007; Michos et al., 2010). *In vivo*, tissue-specific deletion of Fgfr1 have no apparent reanl abnormalities whereas tissue-specific deletion of *Fgfr2* in the UB (*Fgfr2*$^{UB-/-}$) caused a moderate reduction of UB branching leading to renal hypodysplasia (Zhao et al., 2004; Sims-Lucas et al., 2011; Zhang et al, 2006). Double mutants (*Fgfr1/2*$^{UB-/-}$) were indistinguishable from the *Fgfr2* UB-specific knockout. These mice also had an abnormal UB branching pattern, longer UB branches, significantly fewer ampullary tips, and ~70% fewer nephrons than controls, likely due to fewer UB tips to induce nephrogenesis (Zhao et al., 2004).

In other studies, it was discovered that in the absence of both GDNF and Sprouty1 (a negative regulator of RTK signaling) or Ret and Sprouty1, kidney development is grossly normal, with large, well-organized kidneys, normal ureters, a highly branched collecting duct system, and extensive nephrogenesis. The loss of just one allele of Fgf10 from these double mutant mice resulted in renal agenesis, however (Michos et al., 2010). This revealed that Fgfr10/Fgfr2 signaling serves as an alternative signaling pathway to promote RTK signaling, which ultimately leads to UB outgrowth and branching. RET and FGFR2 (and

probably other RTKs) activate a series of shared downstream signaling pathways, including RAS-MAPK-ERK, PI3K-AKT and PLC-γ-Ca++ (Takahashi et al., 2001; Lu et al., 2009; Michos et al., 2010; Okazawa et al., 2015), which together support UB branching morphogenesis. But how do these signaling pathways manifest at the level of WD/UB cell behavior?

Various investigations have determined that Ret-signaling dramatically alters the behavior of UB cells (Shakya et al, 2005b; Chi et al., 2009; Kuure et al., 2010; Paul Riccio et al., manuscript submitted). Indeed, in *in vivo* chimeric studies, UB cells with higher levels of Ret-signaling generated the primary UB tip domain in the Wolffian duct and were shown to outcompete lower Ret-signaling cells for occupation at the tips of the branching UB (Chi et al., 2009). This even held true for *Etv4* and *Etv5,* two downstream transcription factors that appear to mediate the combined effects of several RTKs (RET, FGFR2 and probably others),. In mosaic nephric ducts, individual $Etv4^{-/-};Etv5^{+/-}$ mutant cells were outcompeted by WT cells for residence of the first UB tip (Kuure et al., 2010).

A series of recent, unpublished experiments in our lab has shown that not only is Ret (and Ret–signaling, by extension) needed to mediate formation of the primary ureteric bud tip domain from the Wolffian duct, Ret is also needed for individual cells to remain in the tips of the branching ureteric tree. Using a novel method, MADM (mosaic analysis with double markers; Zong et al., 2005), *Riccio et al.* were able to simultaneously label and knockout Ret in clones of UB cells *in vivo.* Tip cells that became mutant for ($Ret^{-/-}$) in a Ret+/- context were likely to be excluded from the Ret-expressing tip domain during UB branching, while labeled Ret+/+ clones were much more likely to stay in the tips, and to enter new tips as they were formed by branching. This suggested that there is a constant

refinement of the tip cell population during branching morphogenesis so that, as tip cells divide, only those with the highest RTK-signaling are able to remain in the tip progenitor domain, while those with less RTK signaling are left behind to differentiate into trunk cells.

Many of these recent studies have focused on the GDNF/Ret signaling pathway. However, it remains to be seen whether Fgfr2 is, in part, responsible for the RTK-signaling-dependent cell behaviors observed to mediate formation of the ureteric bud tip or whether Fgfr2 is, in part, required for tips cells to be maintained in the tip domain once branching morphogenesis has begun. Indeed, in other branching systems, Fgf receptors have been shown to direct cell behavior cell-autonomously. For instance, in Drosophila tracheal development, there are two functionally distinct classes of cells in budding tracheal branches: cells at the tip that respond directly to secreted FGFs and lead during outgrowth of a branch, and trailing cells that follow the lead cells and form a tube. These roles are not pre-specified, however. There is competition between cells such that those with the highest FGF receptor activity take the lead positions via cell migration, whereas those with less FGF receptor activity assume subordinate positions and form the branch stalk (Ghabrial et al., 2006). Similar studies show that in developing Drosophila air sacs as well, individual cells lacking FGF signaling activities fail to migrate and thus do not stay at the leading edge during branching morphogenesis (Cabernard et al., 2005). In mammalian systems too, Fgfr2 has been shown to participate in competition-based occupancy of the tips of branching organs. During mammary gland development, mosaic deletion of Fgfr2 in epithelial cells of the bifurcating terminal end buds (TEBs) causes those mutant cells to gradually leave the tips as they are out-competed by Fgfr2 heterozygous neighbors for residence of the epithelial tip domain (Lu et al., 2008). This highlights a maintenance role

that Fgfr2 plays in sustaining functional TEBs, as mutant cells that leave this domain survive and persist in the maturing, distal ductal network (Lu et al., 2008).

Here we hypothesize that Fgfr2 contributes to cell rearrangements that occur during UB morphogenesis to form and maintain functional ureteric bud tips. We used the versatile, renal organoid system to generate mosaic UB structures in which *Fgfr2*$^{UB-/-}$ cells are asked to compete with WT cells for residence in the forming tips. We also employed a new, powerful technique, Mosaic mutant Analysis with Spatial and Temporal control of Recombination (or MASTR; Lao et al., 2012), as an independent test for the ability of Fgfr2 null cells to contribute to UB tips in Fgfr2 heterozygous kidneys, *in vivo*. With this system, cells containing floxed alleles of Fgfr2 are simultaneously recombined and marked by a GFPcre fusion protein following FLP-mediated recombination at a defined time point. After several rounds of branching, the distribution of mutant cells within a heterozygous ureteric tree can then be assessed and the importance of Fgfr2-signaling on tip domain maintenance can be elucidated.

RESULTS

Global *Fgfr2*$^{UB-/-}$ renal organoids display a severe reduction in UB morphogenesis

To investigate whether Fgfr2 promotes cell-autonomous cell behavior changes that establish UB tips, we utilized the renal organoid system to generate chimeric UB structures. We have previously shown that this system is suitable for studying Ret-signaling-dependent cell rearrangements that occur in mosaic UBs (Chapter 3). Before generating chimeric organoids, however, we decided to create renal organoids with a knockout of *Fgfr2* in all UB cells, to verify that they display a mutant phenotype, as kidneys lacking *Fgfr2* in the UB do *in vivo*. We reassociated single cells from dissociated *Hoxb7creGFP/+;Hoxb7myrVenus/+;Fgfr2*$^{lox/-}$ kidneys (abbreviated *Fgfr2*$^{UB-/-}$), where only the UB epithelium is null for *Ffgr2*, and from dissociated *Hoxb7myrVenus* (WT) control kidneys. In mutant organoid cultures, *Fgfr2*-null UB cells were able to self-organize into UB structures similar to wildtype cultures after one day of culture (**Figure 4.1B** and **G**). Whereas WT cultures exhibited abundant elongation and bifurcation among their UB structures from 2 to 4 days, *Fgfr2*$^{UB-/-}$ cultures largely did not exhibit these normal UB morphogenetic behaviors over the same time period; indeed only two UB structures displayed branching in the mutant culture (Compare **Figure 4.1C-E** to **I-J**). Mutant UB structures still seemed able to grow in size, however, suggesting that signaling through Fgfr2 may not be required for the proliferative capacity of UB cells, but may instead be needed for other important aspects of UB branching morphogenesis. Consistent with the *Fgfr2*$^{UB-/-}$ renal organoid phenotype, *Fgfr2*$^{UB-/-}$ mutants *in vivo* display a severe reduction in

UB branching but only a relatively small reduction in proliferation (~22%)at branch tips (Zhao et al., 2004).

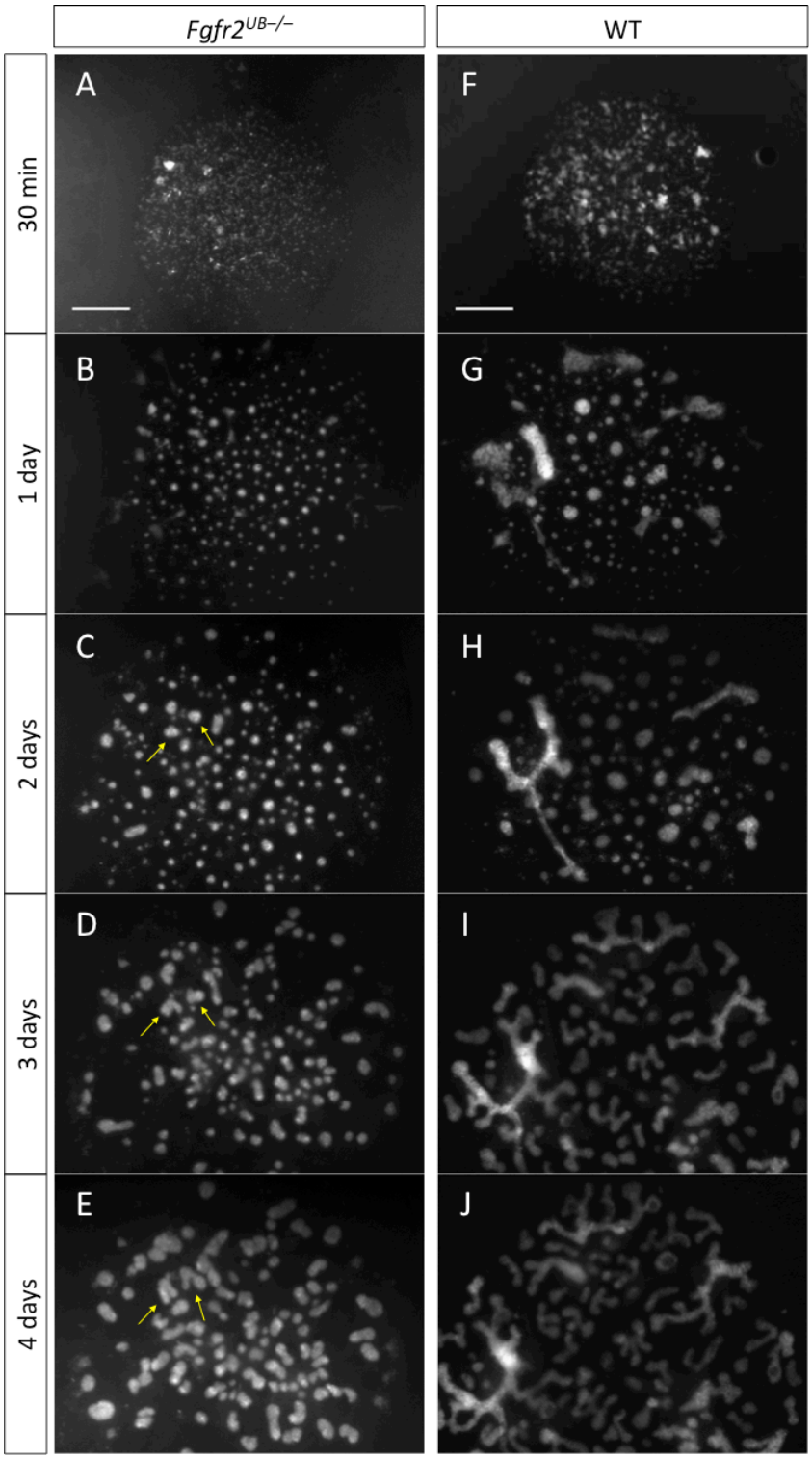

Figure 4.1 – Time course of *Fgfr2*$^{UB-/-}$ mutant renal organoids. (A-J) show images from 30 min to 4 days of *Fgfr2*$^{UB-/-}$ (A-E) and WT (F-J) renal organoid cultures (native fluorescence). At 30-min of culture both *Fgfr2*$^{UB-/-}$ (A) and WT (F) cultures display dispersion of most UB cells, and a day later most UB cells have self-organized into UB structures in mutant (B) ad WT (G) cultures. WT cultures exhibited elongation and branching among UB structures from two to four days of culture (H-J), however, *Fgfr2*$^{UB-/-}$ structures displayed very little elongation and rare branching events during the same time period (yellow arrows, C-E). Mutant UB structures did seem to exhibit growth over the time course. (n=2 *Fgfr2*$^{UB-/-}$ cultures assessed; n= 2 littermate WT control cultures assessed). Scale bar = 200 microns.

Wildtype cells preferentially occupy the UB tips of *Fgfr2*$^{UB-/-}$ ⇔ WT renal organoid chimeras

To generate *Fgfr2*$^{UB-/-}$ ⇔ WT chimeras, separate single cell-suspensions of renal cells were made from E12.5 *Fgfr2*$^{UB-/-}$ and WT (*Fgfr2*$^{+/+}$) kidneys that carried the Hoxb7myrVenus (green) allele for the visualization of UB epithelia, as diagrammed in **Figure 4.2A**. At the same time, renal cells were also dissociated from E12.5 WT kidneys carrying *Hoxb7cre;Rosa26*$^{Tomato/Tomato}$ (red) as an alternate color UB marker. The three groups of cells were then counted by hemocytometer and then mixed together accordingly to produce a 1:1 ratio of (green) *Fgfr2*$^{UB-/-}$ to (red) WT cells and a 1:1 ratio of (green) WT to (red) WT cells as a control **(Figure 4.2A)**. The two cell mixtures were then reaggregated and cultured, and they initially exhibited a well-dispersed and evenly mixed distribution of red and green cells **(Figure 4.2B)**. As renal organoid development progressed, both chimeric genotypes developed typical UB structures that displayed fine-grained mosaicism by 1 day of culture **(Figures 4.3A-A'', D-D'')**. By 2 and 3 days of culture, however, this mosaicism resolved into distinct domains based on genotype in the mutant chimeras. WT

cells preferentially occupied the tips of elongated UB structures that formed and *Fgfr2*$^{UB-/-}$ mutant cells, with no *Fgfr2* signaling, tended to be found in the trunk portions of UB structures **(Figures 4.3B-C")**. By contrast, in the WT⇔WT chimera, the salt-and-pepper pattern of red and green cells was maintained at 2 and 3 days of culture, and red and green cells had a similar chance of forming part of the tips of UB structures **(Figures 4.3E-F").**

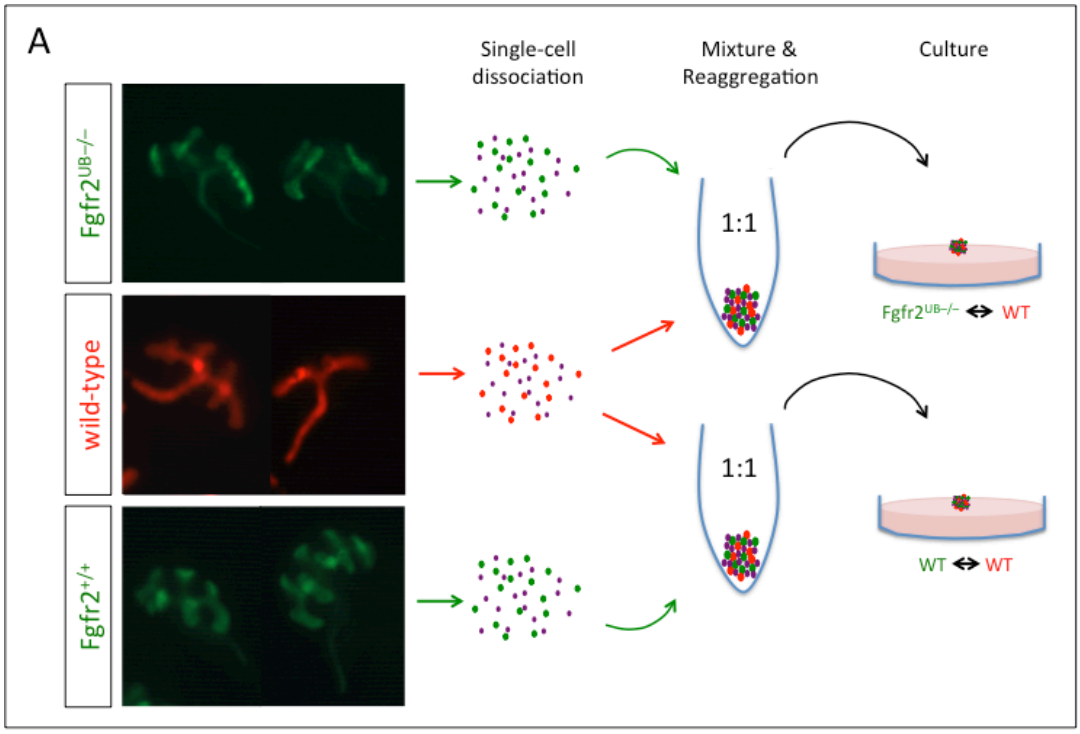

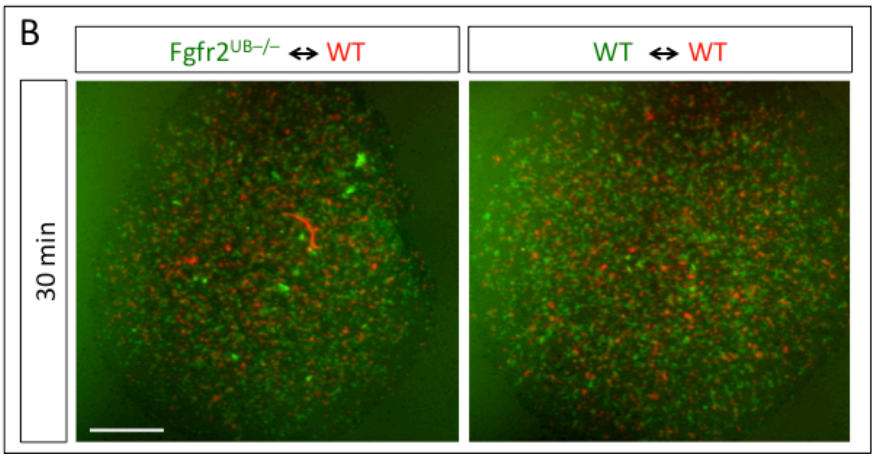

Figure 4.2 – Generation of *Fgfr2*$^{UB-/-}$⇔WT and WT⇔WT chimeric renal organoids. (A) shows the scheme for creating chimeric renal organoids. E12.5 *Fgfr2*$^{UB-/-}$ and *Fgfr2*$^{+/+}$ (WT) kidneys carrying *Hoxb7myrVenus* were obtained along with E12.5 *Hoxb7cre:Rosa26*$^{Tomato/Tomato}$ (WT) kidneys. The cell suspensions were then mixed accordingly to form a 1:1 ratio of *Fgfr2*$^{UB-/-}$ (green)⇔WT (red) suspensions and 1:1 WT (green)⇔WT (red) suspensions. Both cell mixtures were then reaggregated by centrifugation and the pellets were cultured. At the start of culture (30 minutes) both mutant chimera and wild-type control chimera showed a well-dispersed and even distribution of red and green cells (B). Scale bar equals 200 microns.

Green WT cells in control mosaic glands are functionally equivalent to red WT cells, as they could compete with red WT cells to give rise to the whole branched UB epithelium. In another *Fgfr2*$^{UB-/-}$ ⇔WT chimera generated (at a 3:1 ratio), WT cells again formed distinct domains at the tips of UB structures by day 3, and maintained this tip-specific pattern during branching morphogenesis a day later at day 4 (**Figure 4.4A-B''** and **C-D''**). Conversely, littermate WT (green) ⇔WT (red) control chimeras did not display this domain segregation among red and green cells, and no preference was observed for cells with either marker **(Figure 4.4E-F'')**. Analogous to known role of Ret-signaling in cell rearrangements that establish the UB tip domain (Chi et al., 2009), these results reveal a cell-autonomous role for Fgfr2 in the ability of UB cells to contribute to the tip domain during UB morphogenesis in chimeric renal organoids; this presumably reflects a similar role of Fgfr2 in the formation of the UB tip domain *in vivo*

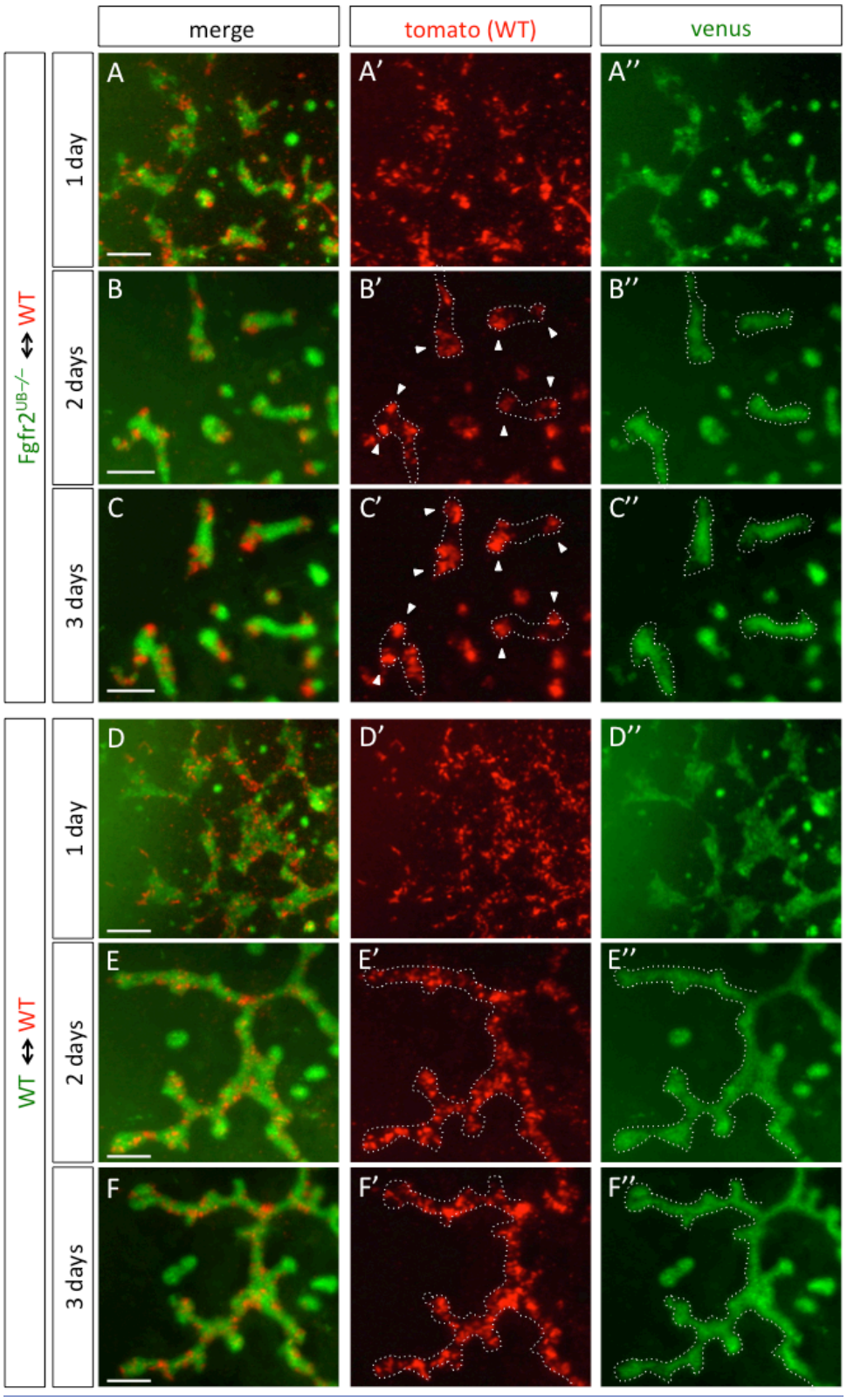
merge
tomato (WT)
venus
Fgfr2UB-/- ↔ WT
WT ↔ WT
1 day
2 days
3 days
A
A'
A''
B
B'
B''
C
C'
C''
D
D'
D''
E
E'
E''
F
F'
F''

Figure 4.3 – Wildtype cells show a preference for residence of the tips of chimeric renal organoid structures at the expense of *Fgfr2*$^{UB-/-}$ cells, after 2-3 days of culture. (A-F'') show a time course of mosaic UB structures in *Fgfr2*$^{UB-/-}$ ⇔WT (A-C'') and WT⇔WT (D-F'') chimeric renal organoids generated at a 1:1 ratio. (A-A'') and (D-D'') display fine-grained mosaic UB structures early in renal organoid development (1 day-old). By day 2 and 3, distinct domains of *Fgfr2*$^{UB-/-}$ (green) and WT (red) cells become apparent in the mutant chimeras, with WT cells preferentially taking up residence at the tips of UB tubules (arrowheads in B'-B'' and C'-C'')[n=3 cultures]. In 2 and 3 day-old littermate control WT⇔WT mosaic structures, red and green cells maintain their fine-granularity and red and green cells seem to have equal preference in forming part of the tips of branching UB structures (E'-E'' and F'-F''). White dotted lines demarcate UB structures. Scale bar = 100m. (n=5 mutant cultures of various chimeric ratios assessed; n=5 WT control cultures of various chimeric ratios assessed).

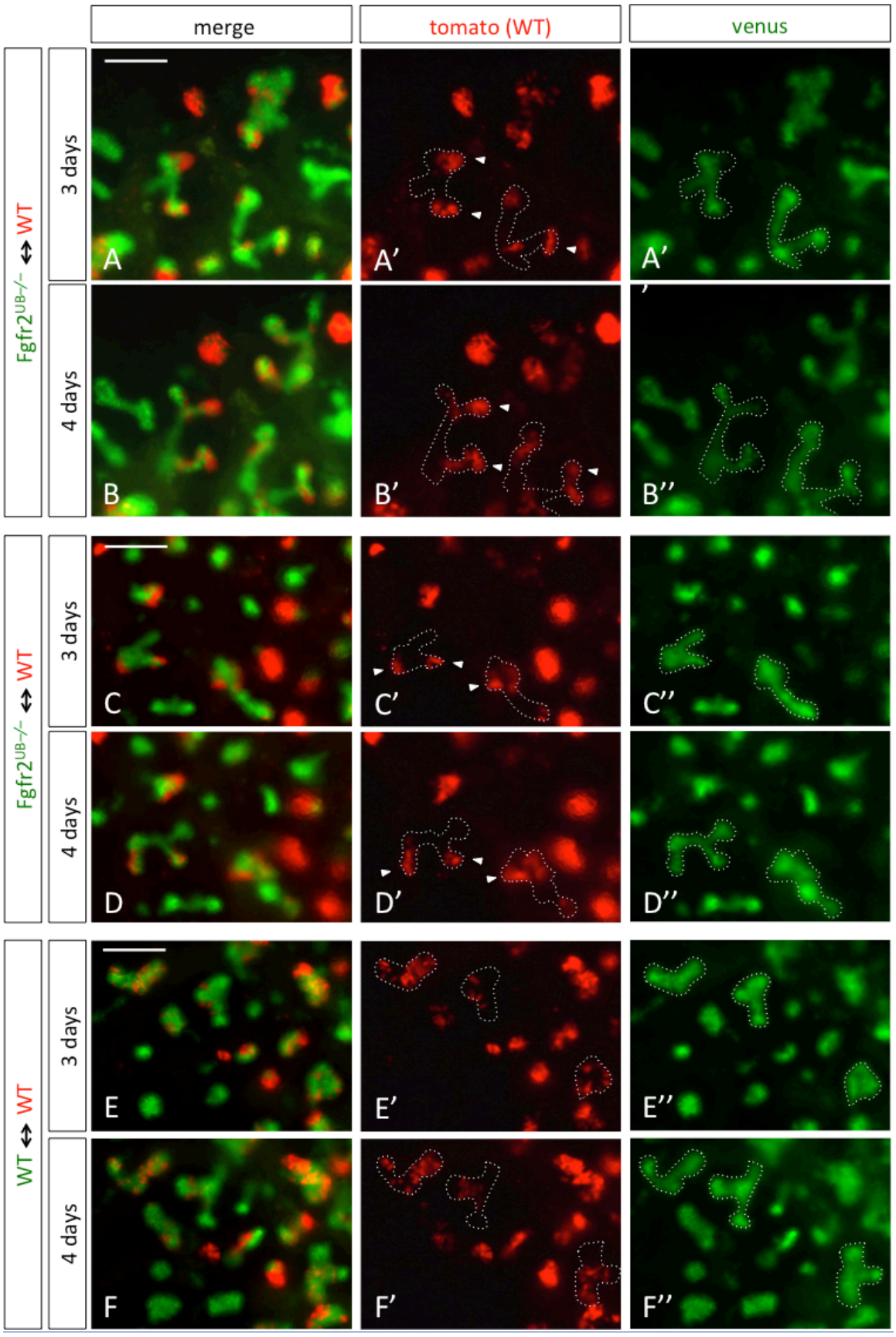
merge
tomato (WT)
venus
Fgfr2UB-/- ↔ WT
WT ↔ WT
3 days
4 days
A
A'
A'
B
B'
B''
C
C'
C''
D
D'
D''
E
E'
E''
F
F'
F''

Figure 4.4 – Wildtype cells show a preference for residence of the tips of chimeric renal organoid structures at the expense of *Fgfr2*$^{UB-/-}$ cells, after 3-4 days of culture. (A-F'') show a time course of mosaic UB structures in *Fgfr2*$^{UB-/-}$⇔WT (A-D'') and WT⇔WT (E-F'') chimeric renal organoids generated at a 3:1 ratio. (A-A'') and (C-C''), display 3 day-old mosaic UB structures with WT cells (red) preferentially occupying the future sites of branching (arrowheads) at the expense of *Fgfr2*$^{UB-/-}$ cells (green). By day 4, many mosaic structures have branched and the preferential residence of WT cells in the tips of new branches was maintained (B-B'';D-D'') Arrowheads correspond to tip specific maintenance of WT cells. By contrast, (E-E'') show control 3 day-old mosaic UB structures with WT (red) cells randomly distributed with no clear domain preference. At day 4, red WT cells maintained their fine-granularity and there seemed to be no preference for red or green cells in forming part of the tips of new UB branches (white dotted lines in F-F''). White dotted lines demarcate UB structures. Scale bar equals 100 microns.

To quantify the results, we produced color profiles for 30 randomly chosen "tip" regions and 30 randomly chosen "trunk" regions (as described in Chapter 3) to further characterize these domains in 3-day-old chimeric structures. Color profiles were created by finding the ratio of red versus green pixels within a specific region (channels were evaluated separately and only pixels with intensity values over a background control region were considered). With this analysis, we found that tips in *Fgfr2*$^{UB-/-}$ ⇔WT (1:1) chimeras were approximately twice as enriched in red (WT) pixels when compared to trunks, which were significantly enriched in green (mutant) pixels **(Figures 4.5A, B, E)**. We also found tips in mutant chimeras to be significantly more green than tips in WT ⇔ WT chimeras **(Figures 4.5A, C, E)**. No significant difference was found between tip and trunk color profiles of the wild-type control chimeras **(Figures 4.5C, D, E)**.

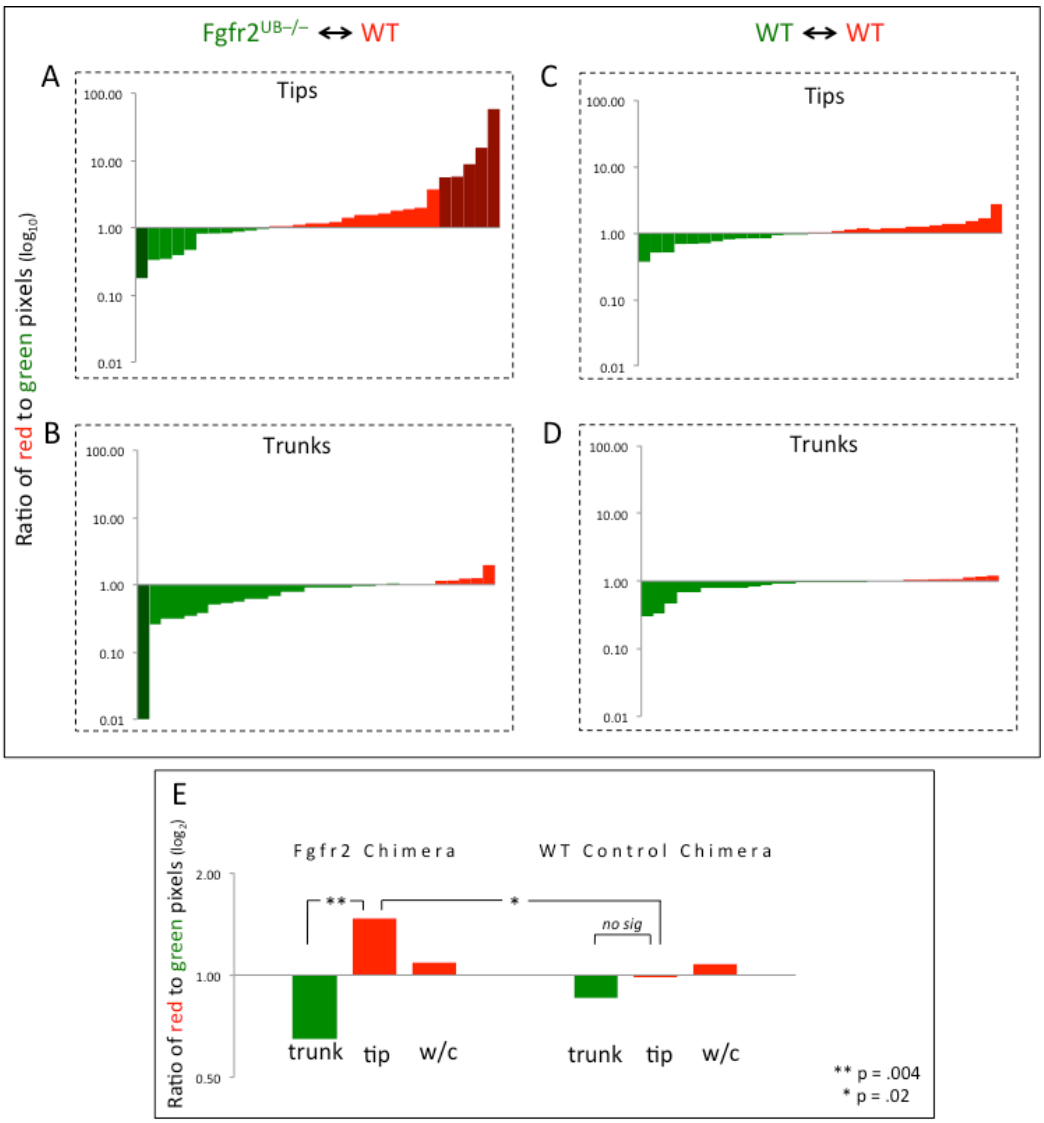

Figure 4.5 – Color profiles of tip and trunk regions in *Fgfr2*$^{UB-/-}$ ⇔WT and WT⇔WT chimeric UB structures. (A-D) show the ranked ratios of green to red pixels in 30 randomly chosen tip regions (A, C) and 30 randomly chosen trunks (B, D) regions in 3 day-old *Fgfr2*$^{UB-/-}$ ⇔WT (A,B) and WT⇔WT (C, D) chimeric cultures. Regions analyzed took the shape of 40-micron wide circles (208 pixels in total) and histograms were created for each region (channels were analyzed separately). The ratio of red to green pixels was then calculated to determine the tip or trunk region's color profile (only pixels with an intensity above a background control region were used for analysis). Regions that were more red were represented by red bars and those that were greener were represented by green bars. Regions that were very green (5 times greener than red) or very red (5 times redder than green) were noted by a darker shade of the corresponding color. (E) Shows the averaged green to red ratios of the specified tip and trunk regions and of the whole culture (w/c) as well (see Experimental Procedures in Chapter 3 for the calculation methods and Appendix for raw data). In the *Fgfr2*$^{UB-/-}$ ⇔WT chimera, the tips were approximately two times redder than the trunks which were significantly greener (p=.004; A, B, E). The tips were

also significantly redder than the tips of the WT⇔WT chimera (p=.02; A, C, E); the tips and trunks of the wild-type control chimera were not significantly different from each other and many regions exhibited close to equal mixes of red and green.

Cells lacking *Fgfr2* become slightly less abundant in heterozygous UB tips.

As an independent test for the importance of *Fgfr2* in UB tip cells *in vivo*, the novel MASTR approach (Lao et al., 2012) was employed to mosaically delete *Ffgr2* and track the mutant UB cells during kidney development. To this end, embryos containing three pertinent genetic alleles were obtained: 1) an inducible *Flp* transgene driven by the *Rosa26* promoter (R^{FlpoER}), 2) a Rosa26 MASTR allele containing a STOP cassette flanked by frt sites preceding *GFPcre* and also driven by the *Rosa26* promoter (R^{MASTR}), and 3) either $Fgfr2^{lox/-}$ (mutant) or $Fgfr2^{+/-}$ (control). Activation of FlpoER by tamoxifen results in recombination of the R^{MASTR} allele in a subset of cells in the embryo; the GFPcre fusion protein is then expressed in these cells; the GFP of GFPcre allows us to visualize the cells in which recombination occurred, while the strong Cre activity of GFPcre has a very high probability of deleting the Fgfr2 flox allele in the same cells (Lao et al., 2012). Other studies have often attempted to use the conventional Cre/loxP system to recombine both the floxed gene to be mutated and a separate floxed reporter allele as a marker of mutation. But differential Cre activity on these floxed genes and floxed reporter alleles can lead to unwanted labeled control cells or unlabeled mutants. By contrast, the MASTR technique preserves the spatiotemporal control of the conventional cre/loxP systems but has the added advantage of gene mutation and cell-labeling being essentially linked inextricably by virtue of the GFPcre.

Pregnant females carrying $R^{FlpoER/MASTR}$;$Fgfr2^{lox/-}$ (experimental) and $R^{FlpoER/MASTR}$;$Fgfr2^{+/-}$ (control) embryos were injected with tamoxifen at approximately E10.5; this will induce recombination when the primary UB tip domain has already been established. The kidneys were subsequently analyzed at E13.5, after the UB had had the chance to undergo several rounds of branching morphogenesis. Both mutant and control mosaic kidneys appeared grossly normal with no significant difference in the number of UB branches (data not shown), consistent with a low level of recombination of the $Fgfr2^{lox}$ allele. Because the GFP fluorescence of GFPcre was too low to visualize clearly, we used whole-mount immunofluorescence with an antibody against GFP to identify cells in which recombination had occurred. Because recombination occurs in cells scattered throughout the kidney (and the embryo), including the metanephric mesenchyme, we could not visualize GFP+ UB cells clearly in whole mount preparations. Therefore, we used confocal microscopy to obtain "optical sections" through the kidneys, in which the UB was labeled with anti-Calbindin1.

This analysis revealed that mutant ($Fgfr2^{-/-}$) recombinant cells were not absolutely excluded from the heterozygous ureteric bud tips, as most tip regions contained numerous mutant cells **(Figure 4.6A-A')**, although several tips were devoid of any mutant cells **(Figure 4.6B-C')**. This was in slight contrast to $R^{FlpoER/MASTR}$;$Fgfr2^{+/-}$ control embryos where, unsurprisingly, heterozygous recombinant cells were again found in moderate quantities in most heterozygous UB tips **(Figure 4.6D-E')**, though some tips contained a great abundance of marked cells **(Figure 4.6 F-G')**. The distribution of MASTR-labeled cells in tips and trunks are given in **Table 4.1**. To quantify the contribution of MASTR-labeled cells to the UB tips, we counted the fraction of GFP+ cells in the UB tips relative to the total

number of GFP+ cells anywhere in the UB. In the control kidneys, an average of 52% +/- 4.3% (SD) of GFP+ UB cells were located in the tips, while in the experimental kidneys only 38% +/- 8.5% (SD) of the GFP+ UB cells were located in the tips, a significant difference (P=0.035; **Figure 4.7**). This reveals a small, cell-autonomous deficiency in the ability of *Fgfr2* mutant cells to contribute to and/or remain in the UB tips.

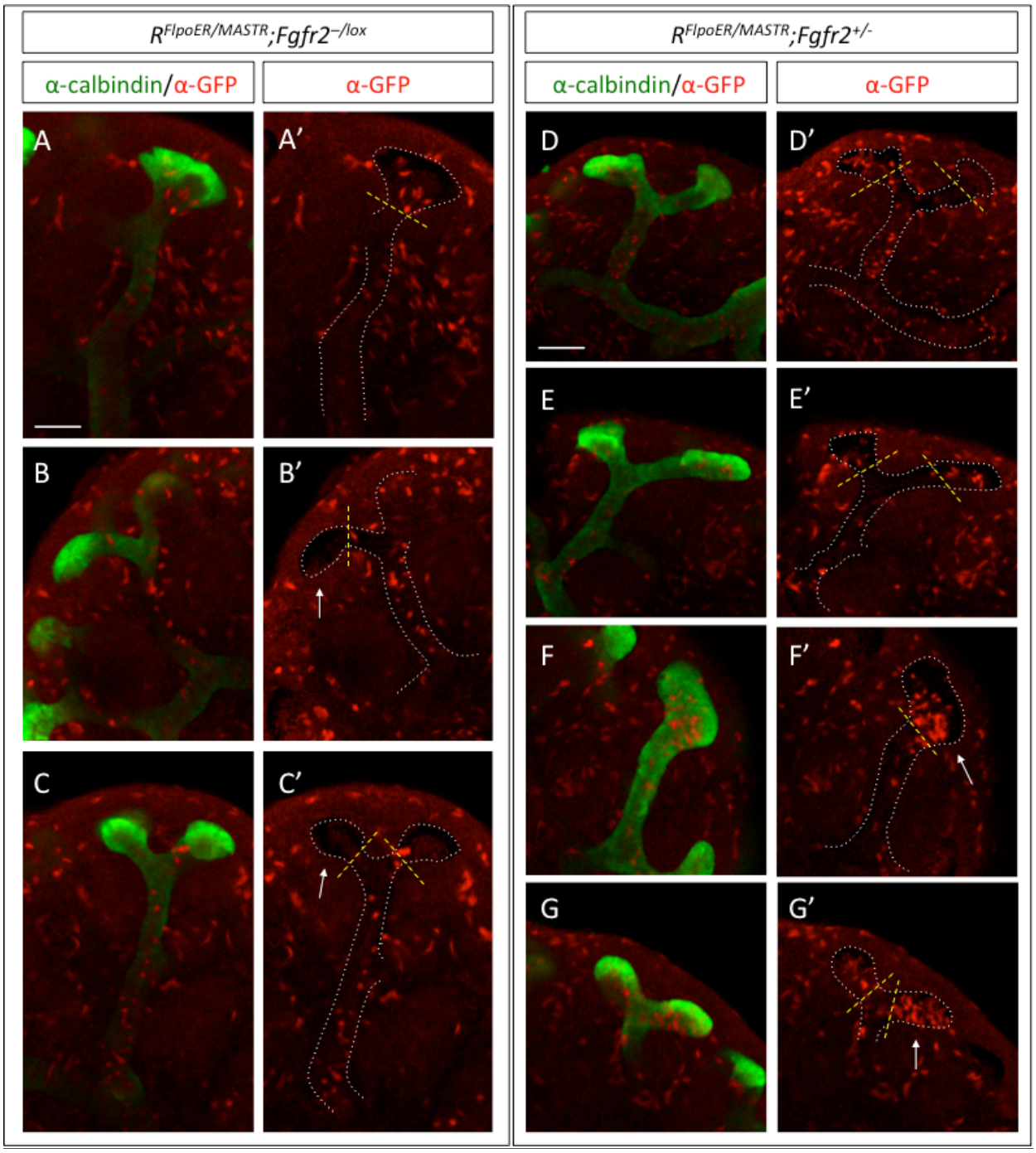

Figure 4.6 – Prevalence of recombinant cells in $R^{FlpoER/MASTR}$;$Fgfr2^{lox/-}$ and $R^{FlpoER/MASTR}$;$Fgfr2^{+/-}$ UB tips. (A-G') Immunofluorescence images (single optical sections) of representative UB tips and adjacent trunk regions from E13.5 $R^{FlpoER/MASTR}$;$Fgfr2^{lox/-}$ experimental (A-C') or $R^{FlpoER/MASTR}$;$Fgfr2^{+/-}$ (D-G') control embryos treated with 4mg of Tamoxifen at E10.5. (A-A') Most UB branches (green; α-Calbindin) in $R^{FlpoER/MASTR}$;$Fgfr2^{lox/-}$ kidneys displayed some mutant recombinant cells (red; α-GFP) in their tips. Numerous tips in these kidneys were devoid of mutant cells, however (arrows; B-C'). In $R^{FlpoER/MASTR}$;$Fgfr2^{+/-}$ kidneys, almost all UB branches contained some recombinant cells in

their tips (D-E'), however numerous tips contained an abundance of recombinant cells (arrows; F-G'). Ureteric epithelium is demarcated by white dotted lines in (A'-G'); tips and trunks are divided by yellow dashed lines. Scale bar equals 100 microns; confocal images.

A

Control	# of Tips	# of Tip Recombinants	# of Trunk Recombinants	Total
Kidney 1	31	193	218	411
Kidney 2	75	321	295	616
Kidney 3	69	460	339	799

B

Mutant	# of Tips	# of Tip Recombinants	# of Trunk Recombinants	Total
Kidney 1	47	91	120	211
Kidney 2	39	102	162	264
Kidney 3	79	183	402	585

Table 4.1 – The distribution of recombinant UB cells in $R^{FlpoER/MASTR}$; $Fgfr2^{lox/-}$ and $R^{FlpoER/MASTR}$;$Fgfr2^{+/-}$ kidneys. After induction with 4mg of Tamoxifen at E10.5, the number of recombinant cells in E13.5 tips and trunks of $R^{FlpoER/MASTR}$;$Fgfr2^{+/-}$ (control; n=3 kidneys; A) and $R^{FlpoER/MASTR}$;$Fgfr2^{lox/-}$ (mutant; n=3 kidneys; B) kidneys was tabulated to calculate the total number of recombinants in each kidney. The number of tips for each kidney is also given.

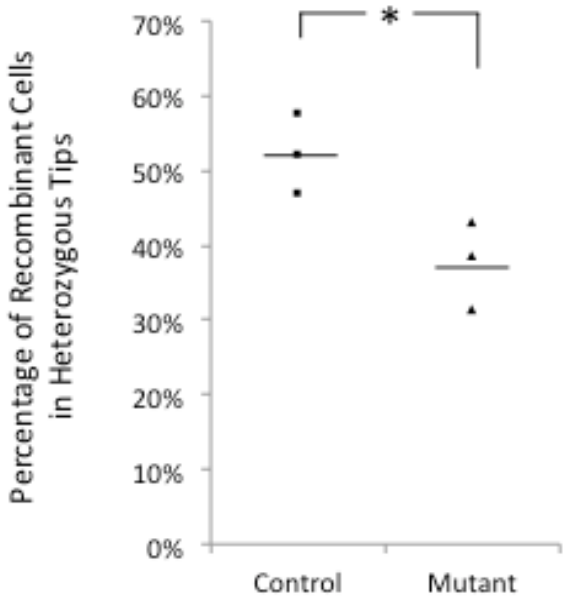

Figure 4.7 – The fraction of recombinant UB cells in the UB tips of *R*$^{FlpoER/MASTR}$; *Fgfr2*$^{lox/-}$ and *R*$^{FlpoER/MASTR}$;*Fgfr2*$^{+/-}$ kidneys. After induction with 4mg of Tamoxifen at E10.5, the number of recombinant cells in E13.5 tips and trunks of *R*$^{FlpoER/MASTR}$;*Fgfr2*$^{+/-}$ (control; n=3 kidneys) and *R*$^{FlpoER/MASTR}$;*Fgfr2*$^{lox/-}$ (mutant; n=3 kidneys) kidneys was tabulated. The percentage of recombinant cells in UB tips (i.e., recombinant cells in tips/recombinant cells in tips + trunks) was then calculated for each kidney and is displayed along with the mean. Mutant recombinant cells were slightly less prevalent (avg 38% vs. 52%) in tips relative to trunks, than control recombinants. Student's t-test; *P* = .035.

DISCUSSION

RTK-signaling through *Fgfr2* has been known to play an important role in UB branching morphogenesis, although its importance appears to be secondary to that of Ret signaling. The cell-autonomous effects of RTK-signaling mediated by *Fgfr2* have not previously been studied in the kidney, however. Here we show that cell competition between WT and *Fgfr2*$^{-/-}$ mutant UB cells in fine-grained mosaic renal organoid structures resulted in segregation of the WT and mutant cells into different domains: WT cells preferentially occupied the future sites of branching and were preferentially maintained in the tips of the branching organoids. These observations show that individual cells lacking Fgfr2 display a large defect in the ability to contribute to forming UB branches. This suggests that Fgfr2-signaling may aid in establishing the UB tip domain, together with the Ret-signaling-dependent domain segregation observed in chimeric Wolffian ducts *in vivo* (Shakya et al, 2005b; Chi et al., 2009; Kuure et al., 2010) and chimeric organoids (Chapter 3).

There are various potential mechanisms by which Fgfr2 may influence cell behavior, including effects on cell proliferation or survival, directed cell migration, or differential cell adhesion (Meyer et al. 2009). UB tip cells are distinguished from trunk cells by a much higher rate of proliferation, as assayed by incorporation of BrdU (Fisher et al., 2001; Meyer et al., 2004; Micheal et al., 2004) and WT cells in a forming tip domain may simply proliferate more than *Fgfr2*$^{-/-}$ cells, resulting in the phenotype we observed. In E10.5 embryos with a targeted deletion of Fgfr2 in the Wolffian ducts, there was indeed a large

reduction (~50%) in proliferation in the coelom side (non-MM side) of the Wolffian ducts; however, on the side of the WD facing the metanephric mesenchyme, where the primary tip domain forms, there was no significant difference in proliferation rates between controls and WD-targeted *Fgfr2* mutants (Okazawa et al., 2015). When taken together with the previously observed small difference in proliferation rates (~22%) and cell death rates in UB tips of E13.5 *Fgfr2*$^{UB-/-}$ and WT kidneys developed *in vivo* (Zhao et al., 2004), cell proliferation or survival are not likely the main mechanisms of domain segregation during the formation of UB tips, although they cannot be fully excluded. Also, the significant deficiency of WT cells in trunk regions of *Fgfr2*$^{UB-/-}$ ⇔*WT* chimeric UB structures argues against a simple, tip proliferation-based model; cell migration and/or adhesion are more likely mechanisms given the observed segregation of WT and mutant cells into different domains. In some situations, cells sort out based on differing expression of adhesion molecules, such as E-cadherin (Steinberg, 2007). Fgfr2-signaling might alter the adhesive properties of cells, so that WT cells are passively sorted from mutant cells, based on adhesive differences, however it seems unlikely that adhesive differences alone can explain WT cells sorting to the site where new branches form, which suggests directed cell migration may be involved. Indeed, cell rearrangements have been observed in other chimeric UBs involving other RTK-signaling molecules, specifically *Ret*, or *Etv4* and *Etv5* (Chapter 3; Chi et al., 2009; Kuure et al., 2010). Time-lapse microscopy of mosaic *Fgfr2*$^{UB-/-}$ ⇔WT UBs in the future may help resolve the precise mechanism that leads to the non-random distribution of WT and mutant UB cells.

We also used the MASTR approach to investigate the requirement of *Fgfr2* for the maintenance of cells in UB tips, during kidney development *in vivo*. In this system, *Fgfr2*

mutant mosaicism was induced at E10.5, a stage at which the primary UB tip domain has already formed (Chi et al., 2009). In E13.5 kidneys, we found a slight but significant reduction in the fraction of recombinant *Fgfr2-/-* UB cells in the UB tips, compared to controls (38% vs. 52%). The defects displayed by *Fgfr2* mutant cells in this system were considerably milder than we had observed in the chimeric renal organoid system, where *Fgfr2*$^{-/-}$ cells were largely excluded from the UB tips. There are at least two potential differences in the experimental methods that may account for the different results. First, in the chimeric organoids, the mutant and WT UB cells were mixed together and formed UB epithelial tubules, which then gave rise to tip and trunk domains; but in the MASTR experiments the mutant cells were generated starting at E10.5, after the primary UB tip domain had already formed, and some of the mutant cells presumably arose in the UB tip. Therefore, in order to contribute to the UB tips at E13.5, the mutant cells only had to remain in the tip domain for several days, but they did not have to enter the tip domain while it was first being generated. As discussed further below, it is possible that Fgfr2 is more important for the cell rearrangements that generate the UB tip domain than it is for the maintenance of the UB tip. Second, in the chimeric organoids the *Fgfr2-/-* mutant cells were competing with fully wild type (*Fgfr2*$^{+/+}$) cells, whereas in the MASTR experiments the *Fgfr2*$^{-/-}$ (GFP+) mutant cells were competing with *Fgfr2*$^{+/-}$ cells (as MASTR recombination was carried out in *Fgfr2*$^{lox/null}$ kidneys). The smaller difference between signaling levels in the two competing cell populations in the MASTR experiments may have accounted for the milder defect displayed by *Fgfr2*$^{-/-}$ cells in this experimental assay. It is possible to perform MASTR starting with *Fgfr2*$^{lox/lox}$ kidneys, and we will do this in future experiments; we expect that the results will show a more severe defect in *Fgfr2*$^{-/-}$ cells.

As both assays showed a defect (although varying in severity) in the contribution of *Fgfr2*$^{-/-}$ cells to UB tips, the next question is: what is the mechanism by which the mutant cells are (partially or fully) displaced by wild type (or *Fgfr2*$^{+/-}$) cells? One possibility is that the mutant cells are displaced due to a defect in cell movements required to stay at the tip during branching, while a different possibility is that the mutant tip cells proliferate less than WT or *Fgfr2*$^{+/-}$ tip cells, and over time are outnumbered. The cell movement model would best be tested by time lapse microscopy of chimeric organoid cultures; in the case of *Spry1* chimeras (Chapter 3), time-lapse imaging showed that *Spry1*$^{-/-}$ cells moved from an apparently random distribution, earlier in the cultures, to preferentially occupy the tips. We attempted to make time-lapse movies of the Fgfr2 chimeric organoids, but so far have been unsuccessful. Time lapse imaging of MASTR kidneys in culture is not yet feasible, as the GFPcre encoded by the MASTR locus, which labels the recombinant cells, can only be easily visualized after antibody staining. An improved version of the MASTR allele, encoding a more strongly fluorescent protein, is needed for such experiments.

The other possible explanation is that *Fgfr2*$^{-/-}$ UB tip cells proliferate more slowly than wild type tip cells, so the mutant cells are gradually overgrown by the WT tip cells. Indeed, this was the explanation proposed to explain the effects of loss of *Fgfr2*$^{-/-}$ cells in mosaic mammary gland epithelium (Lu et al., 2009). In *Fgfr2*$^{UB-/-}$ E13.5 kidneys, it was reported that the UB tip cells showed a slightly lower rate of proliferation (13% fewer BrdU+ cells) than tip cells in WT kidneys (Zhao et al., 2004). Whether this slight difference is enough to account for the virtual absence of *Fgfr2*$^{-/-}$ cells in the UB tips of chimeric organoids is unclear, but it could presumably account for the milder difference seen in MASTR kidneys.

Unlike Ret, Fgfr2 expression does not normally become restricted to the tips of the branching epithelium, but is instead found throughout the tips and trunks during UB morphogenesis. In light of this, proliferation regulated by Fgfr2-signaling in the tips could differ from that of the trunks despite its uniform expression. Indeed, in the branching mammary epithelium, Fgfr2 is also expressed in the terminal end buds (the tips) and throughout the ductal epithelium. However, FGFR2-signaling functions specifically in terminal end bud cells to stimulate them to proliferate frequently enough in order to generate both cells at the tips of branching epithelium and cells in the extending duct (Lu et al., 2009). Attempts to measure the relative proliferation of WT and mutant cells in the UB tips and trunks of MASTR kidneys were so far unsuccessful, but should be feasible.

A third possibility is a defect in cell survival, as a slight increase in cell death was reported in *Fgfr2*$^{UB-/-}$ E13.5 UB tips (Zhao et al., 2004). Although we saw no visual evidence of apoptosis among mutant recombinant cells, there seemed to be an overall lower prevalence of MASTR-labeled mutant cells than control cells even when accounting for kidney size (data not shown) or the number of tips of each kidney **(Table 4.1)**, therefore a fuller investigation is warranted. Future proliferation and cell death assays in mosaic kidneys should help clarify the cause of the slight reduction of mutant *Fgfr2* cells in host WT tips, and the possibility still remains that other cellular behaviors or properties, such as differences in cell adhesion, contribute to the Fgfr2-dependent cell competition observed in UB tips.

Together these data are consistent with a possible model in which Fgfr2 plays a relatively more prominent role in organizing the primary tip domain and a lesser,

supporting role in maintaining the UB branch tips. In Ret knockout mice, almost 40% of embryos show budding of the primary UB, and additional deletion of *Fgfr2* completely abolishes UB formation (Michos et al., 2010; Schuchardt et al., 1994). Similarly, although renal agenesis was rare in Fgf10 homozygotes (15%), removing one Gdnf allele (*Fgf10*$^{-/-}$;*Gdnf*$^{+/-}$) caused 100% agenesis (Michos et al., 2010), indicating that Fgf10 and Gdnf normally cooperate to promote UB outgrowth from the WD. Furthermore, Fgf10 expression is sufficient in inducing ectopic WD budding of the cultured mouse urogenital system, even in a *Gdnf*$^{-/-}$ embryo (Michos et al., 2010). These previous observations indicate partial redundancy between RET and FGFR2 signaling in the initial formation of the UB.

It has previously been demonstrated that adjacent E10.5 Wolffian duct cells often have varying levels of phospho-ERK, a read-out of RTK-signaling (Chi et al., 2009) and this likely allows for high-RTK-signaling cells to sort to the primary tip domain at the onset of normal UB morphogenesis. Fgfr2-signaling may normally help modulate the overall levels of RTK-signaling in individual cells to promote their segregation to the progenitor tip domains in the WD and the UB. Actually, Fgfr2 has been shown to regulate *Etv* expression (downstream of RTK-signaling) in E10.5 Wolffian ducts (Okazawa et al., 2015). Other unstudied RTKs and other MM-derived signals are very likely to play a role in this process as well since the WD can still become pseudo-stratified in various Fgf10/GDNF double mutants that exhibit renal agenesis (Michos et al., 2010).

Later during branching morphogenesis, deletion of Fgfr2-signaling causes a slight reduction in cell proliferation in UB tips (Zhao et al., 2004), as already mentioned. Further

analysis is needed to clarify whether this is the primary cause for the reduction in the distribution of Fgfr2 mutant cells within control tips, as previously described.

RTK-signaling though Fgfr2 is a known secondary signaling network during UB morphogenesis. Similar to Ret and other shared signaling components that form the main signaling axis, Fgfr2 mediates cell-autonomous cell behaviors that cause cells to sort to different domains, which may ultimately help refine the epithelial progenitor domains that regulate UB development.

EXPERIMENTAL PROCEDURES

Dissociation of embryonic kidneys. Same as Chapter 2.

Pellet culture. Same as Chapter 2.

Chimeric Pellet Culture. Same as Chapter 2.

Time course. Same as Chapter 2.

Color Profiling Analysis. Same as Chapter 3.

Mouse Manipulation. Tamoxifen (Sigma T5648, 4 mg) was administered by intraperitoneal injection

Whole-mount Immunofluorescence Staining. E13.5 kidneys were fixed in 4% paraformaldehyde (PFA) (overnight, 4°C) and washed in PBS (3 x 10min). Samples were then incubated in 10% Normal Donkey Serum in TSP (0.1% Triton X-100, 0.05% Saponin, PBS)(overnight, 4°C) before incubation in the following primary antibodies: Rabbit anti-GFP (Invitrogen, 1:400) and Goat anti-Calbindin (Santa Cruz, 1:200). Primary antibody was diluted in TSP and 10% Normal Donkey Serum (NDS) and incubation was for 4 days at 4°C followed by TSP washes (3 x 40min, RT). Secondary antibodies (Cy3 Donkey anti-Rabbit, Cy2 Donkey anti-Goat, respectively; Jackson ImmunoResearch) were diluted in TSP and 10% NDS and samples were incubated for 3 days at 4°C followed by TSP washes (3x, 40min, RT).

Confocal Microscopy and Statistics. Samples were then methanol-dehydrated, cleared with the agent BABB (Benzyl alcohol : Benzyl benzoate; 1:1) (Fisher Scientific) for confocal microscopy, and optical sections at 3-micron intervals were imaged through the whole kidneys. All recombinant cells within the ureteric trees were then counted and tabulated and the percentage of recombinant cells in the tips were then calculated in mutant ($R^{FlpoER/MASTR}$;$Fgfr2^{lox/-}$;n=3) and WT ($R^{FlpoER/MASTR}$;$Fgfr2^{lox/-}$;n=3) samples. The averaged percentages for the kidneys of each genotype were compared with a Student's t-test.

CHAPTER 5

The Role of Matrix Metalloproteinase 14 in Early Kidney Development

INTRODUCTION

While many signaling proteins and transcription factors that control ureteric bud growth and branching have been discovered, the genes they regulate, which carry out cellular functions, and thus mediate important cell behaviors, are largely unknown. GDNF-Ret signaling is required for normal expression of *Etv4* and *Etv5*, critical components of the gene regulatory network that leads to proper UB branching during kidney development (Lu et al., 2009). In the kidney and other contexts, these transcriptional regulators have also been implicated in cell migration, such as in the radial migration of cortical neurons and in invasive cancer cells (Firlej et al., 2008; Hasegawa et al., 2004; Kuure et al., 2010). In exploring the downstream genes potentially regulated by *Etv4* and *Etv5*, *Lu et al., 2009* identified several genes whose expression in the ureteric bud depends on *Etv4* and *Etv5*. Among them was membrane-type matrix metalloproteinase 1 (*MT1-MMP* or *Mmp14*), which had previously been shown to be directly regulated by Etv4 in other cell types (Cowden Dahl et al., 2007). Indeed, *Mmp14* gene and protein expression is significantly reduced in both $Etv4^{-/-};Etv5^{+/-}$ and *Ret*-hypomorphic kidneys, both of which display renal hypoplasia and reduced branching (Lu et al., 2009; de Graaff et al., 2001).

MMP14 is a transmembrane endopeptidase and is part of a family of matrix metalloproteinases (MMPs) that contributes to growth, development, and wound healing(Vu et al., 2000). Along with its expression in the ureteric bud (as early as E11.5), its

protein expression has also been detected in the metanephric mesenchyme (MM), but this detection is thought to be caused by protein shedding, whereby the catalytic domain of membrane bound-MMP14 on UB cells is cleaved and causes detection in the MM (Toth et al., 2002). While many MMPs are secreted, MMP14 is one of a subset that contain a transmembrane domain and are thus located at the cell surface.

MMP14 is known to degrade components of the extracellular matrix (ECM), including type I, II and III collagens, fibronectin, vitronectin, laminins 111 and 332, fibrin and proteoglycans (Seiki, 2003). MMP14 can additionally cleave other cell surface proteins such as CD44 (Kajita et al., 2001), transglutaminase (Belkin et al., 2001), αv integrin (Deryugina et al., 2002), syndecan-1 (Endo et al., 2003), and low-density lipoprotein receptor related protein (Rozanov et al., 2004). These extremely divergent substrates for MMP14 make it an important regulator of the pericellular environment and allow it to regulate multiple cellular functions, such as promoting invasion, cell migration and proliferation and other aspects of branching morphogenesis (Barbolina et al., 2008). Until recently, it had been thought that matrix metalloproteinases, in general, participate in these processes simply by degrading components of the extracellular matrix (ECM). However, it is now apparent that MMP activity is much more specific and can cause the release of growth factors from the ECM, all of which influence cellular behavior (Vu et al., 2000).

MMP14 can also associate with other cell surface and cytoplasmic proteins and participate in signaling pathways that affect various cellular activities. One such activity is

cell migration, in which MMP14 has also been shown to have a clear role. For example, in many metastasizing cancers, MMP14 is upregulated (along with ETV4, as previously mentioned) and expressed in cells at the invasive front of the tumor where it confers cancer cells with the ability to penetrate the basal membrane and migrate to different sites (Seiki, 2003; Timoshenko et al., 2014). Additionally, when engineered mammary epithelial tubules were populated (in a random manner) with cells that have varying levels of MMP14 expression, the cells with the most MMP14 expression sorted to the ends of the cylindrical tubule, possessing greater cell motility and outcompeting those with less MMP14 expression (Mori et al., 2009). Cell migration, itself, requires several components: activation of cytoskeletal motor function to provide cell movement, alteration of adhesive sites and cell-surface adhesive molecules to provide traction, clearing of ECM to break down physical barriers, and the presence of chemoattractants to guide migration (Vu et al., 2000). MMP14 may potentially regulate any of these processes. Interestingly, the cellular rearrangements observed in engineered epithelial tubules were independent of the catalytic domain but absolutely required the hemopexin domain, implicated in binding to and signaling through other cell surface receptors, such as CD44 (Barbolina et al., 2008; Mori et al., 2009). Likewise, in the developing mammary glands, MMP14 is expressed in the invading edges of the terminal end buds (TEBs) of the ductal epithelium. In this tissue, it has been shown to activate MAP-Kinase signaling and regulate Integrin β1-dependent branching morphogenesis independent of its catalytic domain (Mori et al., 2013). This further demonstrates that MMP14 can act as a signaling module in branching organs.

Mmp14 knockout mice die postnatally at day 14, exhibiting hypoplastic kidneys with fewer branches and a severe reduction in cell proliferation (Riggins et al., 2010), among other abnormalities. Although increased deposition of ECM components has been observed in mutant kidneys (Riggins et al., 2010), the precise mechanisms that cause the branching defects, and whether these mechanisms are cell-autonomous, are not known, and the precise role of MMP14 in branching morphogenesis remains to be elucidated. We decided to take an approach that has been fruitful in studies of several other genes involved in ureteric bud branching: to generate chimeras in which a subset of cells lack *Mmp14* and examine their ability to contribute to the Wolffian duct and ureteric bud in developing chimeric kidneys.

Stimulation of the Ret receptor tyrosine kinase by GDNF can promote cell proliferation in the ureteric bud tip cells of cultured kidneys (Pepicelli et al., 1997). GDNF could also direct the chemotactic migration of cultured Madin-Darby canine kidney (MDCK) cells that were engineered to express Ret (Tang et al., 1998). Additionally, Ret signaling promotes cell movements; in the Wolffian duct that give rise to the first ureteric bud tip, initiating kidney development (Chi et al., 2009b). As mentioned, these cellular behaviors have been found to be mediated, at least in part, by ETV4 and ETV5 expression (Kuure et al., 2010). In forming chimeras in whch a subset of the WD/UB cells carried the *Etv4*$^{-/-}$;*Etv5*$^{+/-}$ mutant alleles in a wild-type host, it was observed that the mutant cells were unable to contribute to the primary ureteric bud tip domain of the WD or to the tips of UB branches, and were instead relegated to the UB trunks. In contrast, when *Etv4*$^{-/-}$;*Etv5*$^{+/-}$ embryonic stem (ES) cells were injected into *Ret*-hypomorphic hosts they contributed extensively to the UB tips as well as the trunks. These studies showed that an early role of ETV4/5

expression is to promote competitive cellular rearrangements in the caudal region of the Wolffian duct, and that they act in a cell-autonomous fashion. As MMP14 is also implicated in cell proliferation and cell migration (Mori et al., 2009; Riggins et al., 2010) and is known to be regulated by ETV4 and ETV5 expression, it was important to explore whether these ETV4/5-related cellular behaviors are mediated in some manner by MMP14. Similar to the Ret and Etv4/5 experiments above, chimeras generated with *Mmp14* mutant and WT cells revealed that MMP14 does not act cell-autonomously to initiate or promote cell rearrangements during UB morphogenesis, as there was an ample contribution of mutant cells to the tips of the branching ureteric trees of E12.5 and E14.5 chimeric kidneys

GDNF can induce the formation of supernumerary UB outgrowths when expressed ectopically in kidney cultures (Shakya et al., 2005a). Studies have also shown,that excessive RET-signaling, through a constitutively active form of the protein, can cause unrestricted growth of the ureteric bud (Srinivas et al., 1999). These studies demonstrate that not only does normal UB branching morphogenesis require GDNF and RET, but that UB outgrowth and branching are a specific consequence of these signals. As mentioned, the absence of MMP14 yields less proliferation of UB cells, less branching, and an increase in basement membrane components (Riggins et al., 2010). It remains to be seen, however, whether MMP14 parallels its upstream effectors and can specifically promote proliferation in the developing UB, stimulate branching, or influence the specific pattern of growth and branching. Therefore, in addition to chimera studies of MMP14 loss-of-function, I performed gain of function studies in which I attempted to overexpress MMP14 in a subset of UB cells in order to explore whether MMP14 imparts any these inductive qualities in a cell autonomous fashion. We hypothesized that cells with increased MMP14 expression

might exhibit increased cell motility, might segregate from WT cells and sort to the tips, and perhaps form extra, ectopic branches as excessive disintegration of the basement membrane proceeds.

RESULTS

Testing the requirement for Mmp14 during cellular rearrangements in the Wolffian duct and ureteric bud

To investigate whether MMP14 is required for cell rearrangements in the Wolffian duct/UB and branching morphogenesis of the ureteric bud, we tracked the behavior of fluorescently marked mutant cells compared to their WT host cells in chimeric ureters and kidneys. *Mmp14*$^{-/-}$ embryonic stem cells that also carried the *Hoxb7:myr-venus* transgene, which expresses a yellow fluorescent protein in the WD and UB (Chi et al., 2009a) ,were first generated. These cells were then injected in to wild-type blastocysts, which were implanted into pseudopregnant foster mothers and allowed to develop to E12.5. The kidneys were then excised, stained with anti-calbindin to allow visualization of the entire ureteric bud epithelium, and anti-GFP to label the *Mmp14-/-* ES cell derived ureteric bud cells, and imaged.

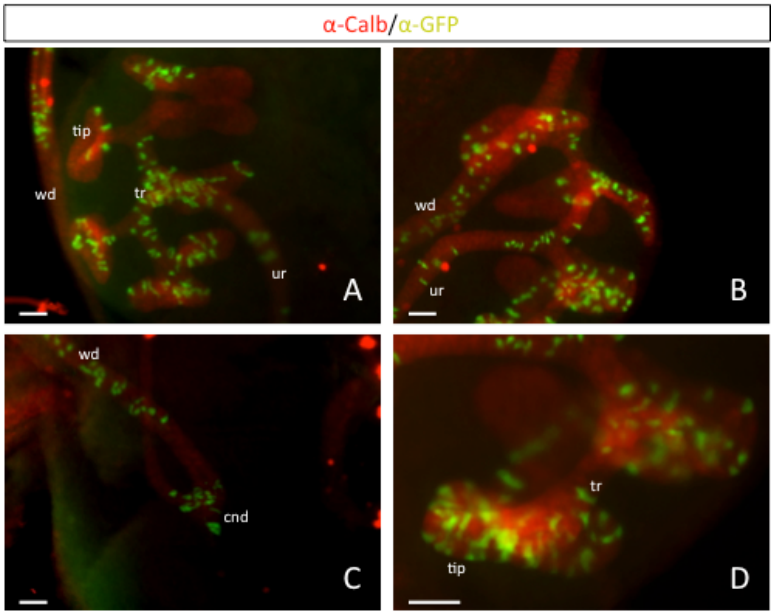

Figure 5.1 - Distribution of *Mmp14*$^{-/-}$ cells in chimeric Wolffian duct and ureteric bud epithelium at E12.5. Whole-mount immunofluorescence images of *Mmp14*$^{-/-}$ <-> WT chimeric kidneys and ureters from E12.5 embryos (A-D) stained with α-GFP (green) to reveal mutant cells, with α-calbindin (red) to label all WD and UB cells. Mutant cells contribute to the Wolffian ducts (A-C), ureters (A, B), ureteric bud trunks (A, B, D), and tips (A, B, D) of all chimeric embryos analyzed (*n*=3/3 embryos). cnd, common nephric duct; tip, ureteric tree tip; tr, ureteric tree trunk; ur, ureter; wd, Wolffian duct. Scale bar eaquals 100 microns

Figure 5.1 shows whole-mount images of chimeras at E12.5. In contrast to *Ret* (Shakya et al., 2005b), *Sprouty1* (Chi et al., 2009) and *ETV4/5* (Kuure et al., 2010) mutant cells, *Mmp14* mutant cells show no apparent domain segregation from the WT cells in the ureteric bud. Cells lacking *Mmp14* can clearly contribute to the trunks and tips of the branching ureteric bud at E12.5. As shown in the whole-mount images (Fig 5.1 A-C), *Mmp14* mutant cells were also found in the Wolffian duct and common nephric duct, with an apparently random distribution of mutant cells throughout the ureteric tree. This contrasts sharply with the behavior of Ret-/- or Etv4-/-;Etv5+/- cells.

The ability of Mmp14-/- cells to remain at the UB tips in E12.5 kidneys made it unnecessary to examine earlier-stage chimeric embryos, because (based on all previous studies) if the cells were absent from the UB tips at an earlier stage, they would not repopulate the tips at E12.5. However, we considered the possibility that a very minor defect in cell competition might not yet be revealed at E12.5, and might take more time to become visible. Therefore, additional chimeric embryos were examined at E14.5 **(Figure 2)**.

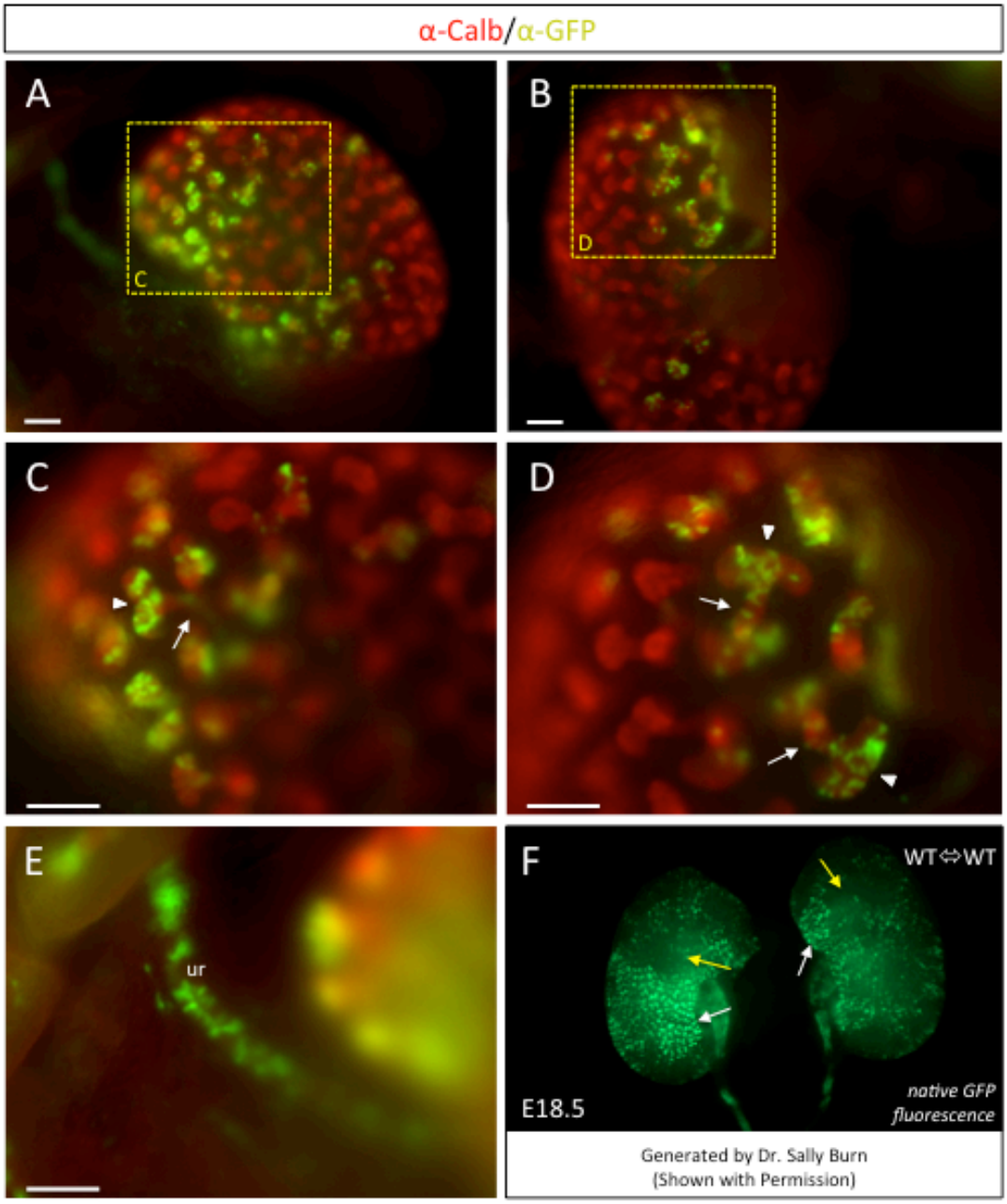

Figure 5.2 - Distribution of *Mmp14*$^{-/-}$ cells in chimeric ureteric bud epithelium at E14.5. Whole-mount immunofluorescence images of *Mmp14*$^{-/-}$ <-> WT chimeric kidneys from E14.5 embryos (A-E) stained with anti-GFP (green) to reveal mutant cells, with anti-calbindin (red) to label all UB cells. C and D are enlargements of the kidneys in A and B, respectively. Mutant cells contribute to the ureters (E), trunks (A-D; arrows), and tips (A-D; arrowheads) of all chimeric kidneys analyzed (*n*=2/2 kidneys). *Courtesy of Dr. Sally Burn*, (E) shows E18.5 kidneys from a WT⇔WT embryo in which WT ES cells carrying *Hb7GFP* were injected into a WT host blastocyst. A patchwork pattern of UB tip contribution was observed, with regions of high contribution of GFP+ cells to the UB tips (white arrows) adjacent to regions with little or no contribution to of GFP+ cells to the UB tips (yellow arrows). ur, ureter. Scale bar equals 200 microns.

At this later stage, and similar to E12.5, *Mmp14* mutant cells are still able to contribute to the tips and trunks of the branching ureteric tree, as well as the Wolffian duct **(Figure 5.2A-E)**. A patchwork contribution of *Mmp14* mutant cells to WT UB tips was observed, with some UB segments displaying a high contribution of mutant cells adjacent to other segments that were devoid of mutants. This pattern is consistent with other later-stage WT⇔WT chimeric kidneys generated (**Figure 5.2F;** Courtesy of Dr. Sally Burn).

Exploring the role of MMP14 in promoting ureteric bud growth by gain-of-function studies

To determine whether MMP14 expression is sufficient to stimulate UB growth and branching, we attempted to overexpress the protein in a subset of UB cells by viral infection and to observe changes in cell behavior. We used a retroviral vector (MMP14 vector) to stably express a single bicistronic mRNA containing mouse *Mmp14*, an internal ribosomal entry site (IRES), and *myr-Venus* expression marker to produce virus in cultured cell; a separate control virus expressing myr-Venus without *Mmp14* was similarly produced (Venus Control vector; **Figures 5.3A and B**).

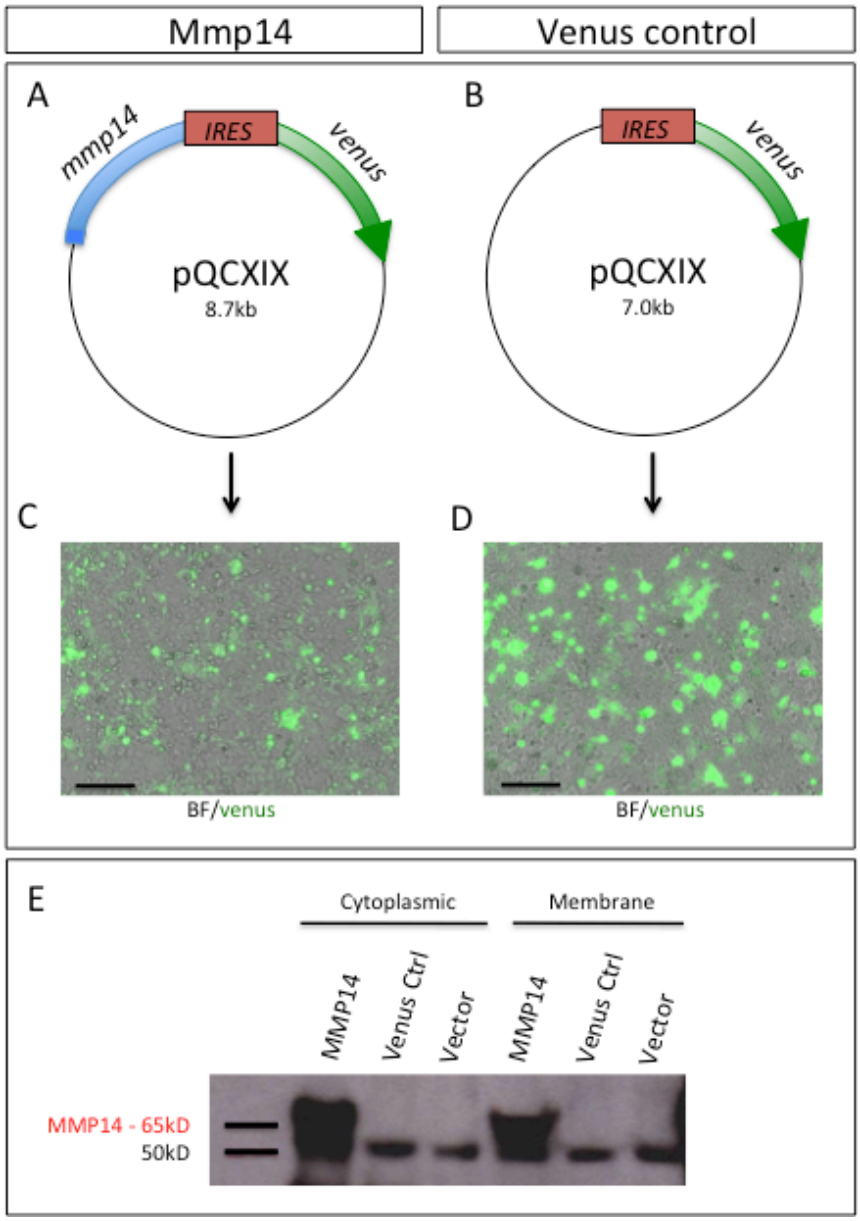

Figure 5.3 – Transfection of retroviral vectors reveals functional plasmids that can overexpress MMP14. (A) and (B) show vector diagrams of the *mmp14-IRES-myrVenus* (MMP14) and *IRES-myrVenus* (Venus Control) retroviral plasmids, respectively. In (C)and (D) HEK293 cells were transfected with MMP14-*IRES-myrVenus* and Venus Control plasmids, respectively, and expression of the Venus marker reveals functional retroviral plasmids. Western blotting against MMP14 in cell lysate (cytoplasmic) and cell debris (membrane) protein fractions obtained from transfected HEK293 cells revealed MMP14 protein expression only in cells transfected with the MMP14 vector and not the Venus Control or the pQCXIX backbone vectors (E). 50kD band was non-specific binding that showed protein was loaded.

Initial transfection into Human Embryonic Kidney (HEK293) cells for the production of virus revealed a robust expression of *myr-Venus* and a functional plasmid **(Figures 5.3C and D)**. Western blotting against MMP14 protein was then performed on cells transfected with either the MMP14 vector, the Venus Control vector, or a third *'empty'* control vector lacking both the *Mmp14* and *myr-Venus* constructs. Both cell lysates (enriched for cytoplasmic protein) and cellular debris (enriched for membrane-bound proteins) were prepared and probed, but only cells transfected with the MMP14 vector contained the metalloproteinase in both fractions **(Figure 5.3E)**. This result further confirmed the production of MMP14 by the viral plasmid and confirmed its potential use in overexpressing MMP14 in ureteric bud cells.

Virus was subsequently collected from the supernatant of HEK293 cells transfected with either the MMP14 or Venus Control vectors and viral titers revealed moderate concentrations of viral preparations: MMP14 viral preparation yield – 3.3×10^6 colony-forming units (cfu)/mL and Venus Control viral preparation yield – 1.6×10^5 cfu/mL. Both viruses were able to infect HEK293 cells, as visualized by Venus marker expression, indicating proper viral assembly and suitable infectability **(Figure 5.4)**.

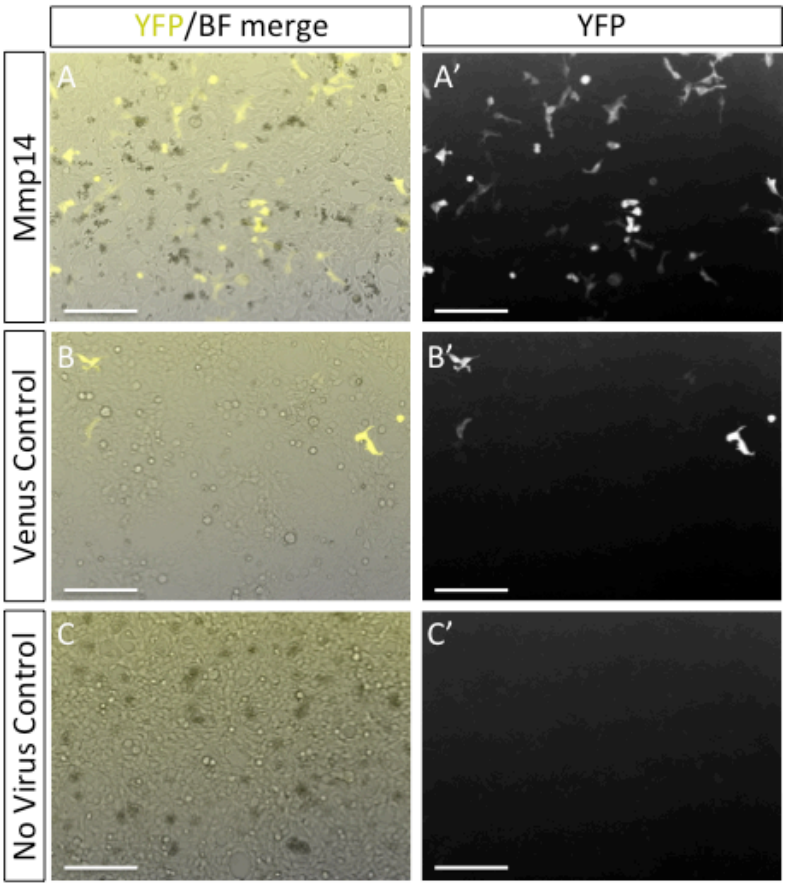

Figure 5.4 – Infection of HEK293 cells with MMP14 and Venus Control virus reveals functional virus and viral infectablility. Venus expression in infected HEK293 cells are visualized under YFP fluorescence (A'-C') and under YFP fluorescence with bright field (A-C) two days after infection with either MMP14 virus (A, A') or Venus Control virus (B, B'). HEK293 cells not infected with virus did not show any fluorescing cells (C, C').

Multiple trials of injecting MMP14 or Venus Control virus into the lumens of *Hoxb7:cre;Rosa26*$^{Tomato/Tomato}$ explant kidneys at e11.5 did not prove fruitful. **Table 1A** describes the various modifications executed in attempting to troubleshoot the infection of UB cells via luminal injection. These included utilizing older kidneys to decrease the risk of damage during injection, adding glycerol to the viral preparation in order to prevent viral particles from potentially adhering to the walls of the glass capillary used for injection, and

A

Attempt #	Infection Type	Protocol & Modifications	Result
1	Whole Kidney Virus Infection	used femtojet to introduce nanoliters of viral prep + polybrene into the E11.5 ureteric lumen	No marker expression
2	Whole Kidney Virus Infection	Same as Attempt #1 and injected virus into older kidneys (e12.5)	No marker expression
3	Whole Kidney Virus Infection	Same as Attempt #2 and added Glycerol (1:12) to viral prep to prevent virions from adhering to the walls of the glass capillary used for injection	No marker expression
4	Whole Kidney Virus Infection	Same as Attempt #3 and used new viral preps, immuno-stained for Venus two days post-injection	No marker expression

B

Attempt #	Infection Type	Protocol & Modifications	Result
5	Renal Organoid Viral Infection	After reaggregation and placement on filter added 10ul of viral prep + polybrene on cultures and placed in 37°C incubator	Marker expression observed by Day 2 but both MMP14- and Venus Control-infected cultures died. Non-infected controls were normal
6	Renal Organoid Viral Infection	Same as Attempt #5 but only 5 ul of viral prep + polybrene	Marker expression observed by Day 2 but both MMP14- and Venus Control-infected cultures died. Non-infected controls were normal
7	Renal Organoid Viral Infection	Before reagg, added 5ul of viral prep to kidney cell suspension and incubated at RT for 20 min. Any potential toxins should stay in supernatant after reagg.	Very limited marker expression observed by Day 2 but both MMP14- and Venus Control-infected cultures still malaised and died.
8	Renal Organoid Viral Infection	Same as Attempt #7 except incubated virus in 37°C incubator for 30 min (10 sec. agitation every 10 min).	Marker expression observed by Day 2 but both MMP14- and Venus Control-infected cultures died. Non-infected controls were normal

Table 5.1 – Troubleshooting retroviral infection of UB epithelia for the overexpression of MMP14. (A) describes the modifications of the viral infection protocol undertaken in unsuccessful attempts to infect UB cells via the lumen of E11.5 or E12.5 embryonic explant kidneys. (B) describes the modifications made to the viral infection protocol to promote the survival of E12.5 renal organoid cultures after effective infection of UB cells.

also included immunostaining for Venus two days post-injection to screen for potential low expression of our desired constructs from the retroviral plasmid. None of these troubleshooting actions yielded proper infection of epithelial cells in the UB. We therefore attempted to infect UB cells in other contexts, in renal organoids and in single-cell suspensions, in order to demonstrate the infectability of UB cells by our viral constructs and to achieve overexpression of MMP14 in a ureteric bud context.

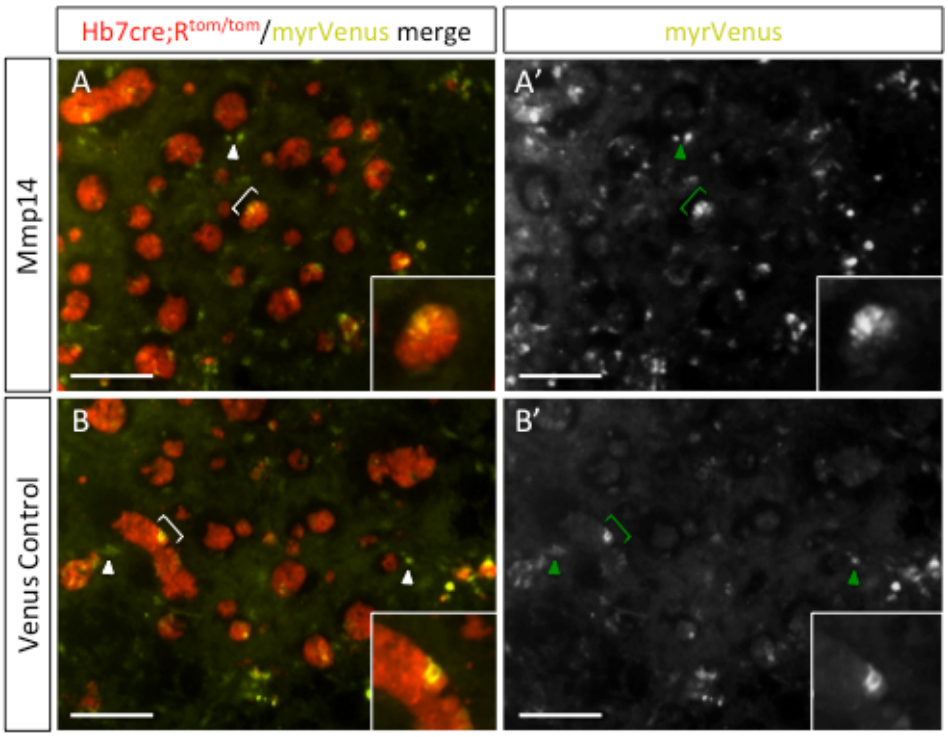

Figure 5.5 – Infection of renal organoid cultures demonstrates the infectablitly of primary renal cells. Venus expression in UB cells (brackets) and non-UB cells (arrowheads) in 2-day old renal organoid cultures infected with MMP14 virus (A, A') or Venus Control virus (B, B') at the onset of 37°C incubation (0hr). (A') and (B') show venus expression of the respective regions in (A) and (B), which show venus expression (yellow) in the context of the ureteric bud marker *Hoxb7cre;Rosa26*$^{Tomato/Tomato}$ (red).

To pursue the question of whether MMP14 is sufficient in conferring increased cell motility, the ability of cells to sort to the ureteric bud tips, and in stimulating UB growth and branching, we decided to turn to the renal organoid system previously shown to be suitable for the study of cell rearrangements during UB morphogenesis. To this end, freshly made cultures were incubated in a droplet of either Mmp14 or Venus Control viral preparations or control media just after reaggregation, at the onset of 37°C incubation (0hr). When examined at 48 hours post-reaggregation, both Mmp14- and Venus Control-infected cultures showed infection of non-UB and UB cells, as visualized by Venus expression **(Figure 5.5)**, but these cultures quickly deteriorated for unknown reasons. During the subsequent 48 hours, the infected cultures dramatically decreased in overall size, and the ureteric bud structures lost their tubular configuration and decreased in size as well **(Figure 5.6A-B'')**. In contrast, cultures incubated in control media showed relatively normal growth and branching **(Figure 5.6C-C'')**.

In further atttempts, viral preparations were briefly administered to embryonic kidney cells at the single-cell suspension stage just before reaggregation. This would dilute (~20-fold) any potential toxin in the viral supernatant into the much larger volume of medium used in the single-cell suspension. After reaggregation the cultures were washed in fresh medium and then cultured as normal, but we still observed the same deterioration phenotype previously described in virus-infected renal organoids. **Table 1B** describes the adjustments to the viral infection protocol for renal organoids that were made in efforts to promote the survival of renal organoid cultures infected with MMP14 and Venus Control virus.

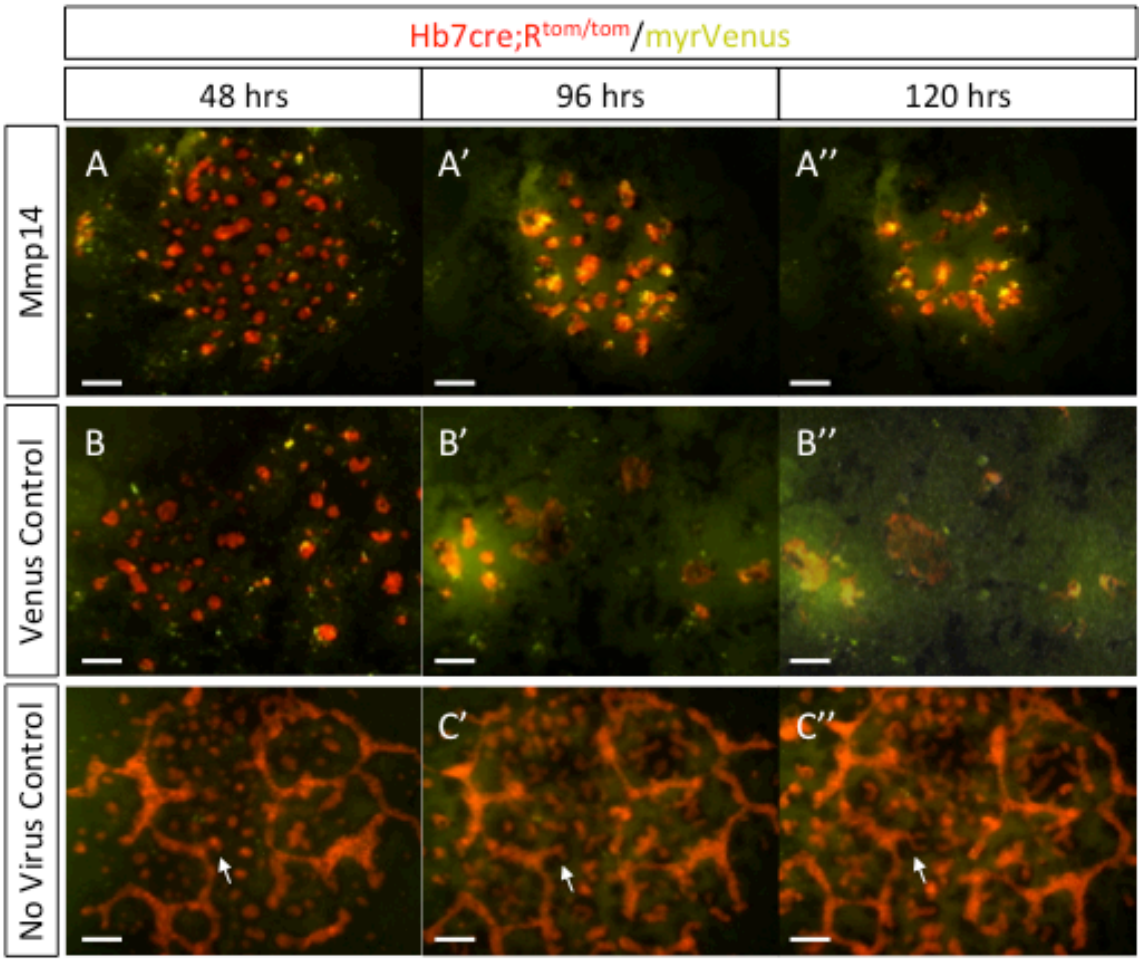

Figure 5.6 – The disintegration of renal organoid cultures infected with MMP14 and Venus Control virus. (A-A'') and (B-B'') show the dramatic decline in size and integrity of renal organoid cultures infected with MMP14 and Venus Control retrovirus, respectively, at 48hrs (A and B), 96hrs (A' and B'), and 120hrs (A'' and B'') post-infection. In contrast, renal organoids cultures incubated in a vehicle control, with no virus, exhibited normal growth and branching (arrows in C-C'') during the same time interval.

DISCUSSION

During kidney development, MMP14 has been shown to act downstream of Ret signaling via the transcription factors *Etv4* and *Etv5*, and has been shown to be required for extracellular matrix degradation, cell proliferation, and proper ureteric bud morphogenesis (Barbolina et al., 2008; Vu et al., 2000; Riggins et al., 2010). Etv4/5 have been shown to be involved in important, cell-autonomous cell movements that occur during normal kidney development (Kuure et al., 2010), and a body of literature has also suggested that that might be the case for MMP14 in the kidney as well (Mori et al., 2009; Lu et al., 2009; Chi et al., 2009). Indeed, MMP14 has been implicated in cell migration during development and in normal physiology (Vu et al., 2000), and studies on mammary epithelia demonstrate that MMP14 can modulate cell migration cell-autonomously (Mori et al., 2009).

Here, by generating *in vivo* chimeras in which UB cells are either mutant or WT for MMP14, we have discovered that MMP14 is not required for the cellular rearrangements that initiate and promote UB morphogenesis, as mutant cells were frequently found in the tip progenitor domains of E12.5 branching UBs. This is in contrast to upstream signaling proteins and regulators, such as RET and ETV4/5, which confer cells with the ability to form part of the tip progenitor domain. In similar *in vivo* chimera experiments, $Ret^{-/-}$ or $Etv4^{-/-};Etv5^{+/-}$ cells were outcompeted by WT cells and excluded from the tip domains, instead taking up residence in the trunk portions of the branching ureteric tree. One possibility is that MMP14 is required, but the effects are not cell-autonomous. The wildtype cells present may somehow be able to compensate for the lack of MMP14 in the relatively fewer mutant cells and therefore no discernible UB phenotype would be revealed.

Alternatively, MMP14 may not play a role in the cell rearrangements that occur in the Wolffian duct and ureteric bud that establish and maintain the progenitor tip domains during UB morphogenesis.

We were concerned that, if the behaviors imparted to WD/UB cells by *Mmp14* are small in scope, potentially weak cell competition may not have had enough time at E12.5 to produce domain segregation. Weak cell competition has been illustrated in previous experiments involving chimeras. When *Ret*$^{-/-}$ cells were mixed with WT cells, they were almost entirely absent from the UB tips, but when mixed with *Ret*-hypomorphic cells, they contributed more extensively to the tips (Chi X et al., 2009). The fact that *Ret*$^{-/-}$ cells can contribute to the UB tip domain in a *Ret*-hypomorphic background suggests that the difference in signaling levels between *Ret* null and hypomorphic cells is not great enough for the hypomorphic cells to fully out-compete the null cells. To address these concerns we harvested kidneys at E14.5, during a dramatic upsurge in the rate of UB branching morphogenesis (with many rounds of branching leading to exponential rise in tip number and kidney volume; Short KM et al., 2014) and still found *Mmp14* null cells at many of the ureteric tree tips. Thus, we observed no evidence that *Mmp14-/-* cells have a competitive disadvantage with regard to wild type cells, in their ability to contribute to, and remain at, the ureteric bud tips..

Our attempt to overexpress MMP14 in a subset of ureteric bud cells via retroviral infection was unsuccessful. The MMP14 retroviral plasmid was indeed capable of expressing MMP14 protein and the Venus marker when transfected into HEK293 cells in

culture and, once virus was produced and concentrated, it was able to infect HEK293 cells as well. But the viral preparations were unable to infect UB cells when injected into the lumens of early embryonic kidneys after many attempts and troubleshooting modifications, including injecting into slightly older kidneys (E12.5), creating new viral preparations, immunostaining for Venus in case of weak expression, and adding glycerol to the viral preparation to prevent any virion adhesion to the walls of the glass capillary used for injection. Conversely, when renal organoid cultures were incubated with viral preparations, there was successful infection of both UB cells and non-UB cells, indicating that the virus produced was functional and had adequate infectivity. Though effective, infection of UB cells in the renal organoid system involved incubation in 5 or 10ul of the viral preparations (with a few thousand virions) and only accomplished infection of a very small percentage of the UB cells in the culture. In contrast, *in vivo* kidney injections involve injecting less then a microliter of viral preparation and this amount may be too minute for a sufficient amount of infectious particles to be released into the lumen. The viral preps were concentrated to a titer on the order of 10^6 cfu/mL for the MMP14 virus and 10^5 cfu/mL for the Venus Control virus. As the amount viral preparation that was actually injected was on the nanoliter scale, this would translate to only a few dozen infectious units or less being injected into the lumen.

Furthermore, the rationale for using retroviruses to infect UB cells and overexpress MMP14 was its unique ability to stably express our genetic constructs by integrating into the host cell genome, but one of the pitfalls of the retroviral system is that it only transduces dividing cells (Coffin JM et al., 1997). This may reduce the amount of target cells that can be infected in the UB when compared to the rapidly dividing HEK293 cells that

were used to determine the viruses' titers. This low availability of target cells, compounded with the very small number of infectious particles being delivered into the lumen, may be the reason we did not observe any infection of UB cells in *in vivo* kidneys. Lentiviruses, on the other hand, are a subset of the retroviral family that contain additional accessory proteins that enable integration in the absence of cell division (Cooray S et al., 2012) and thus may be more suitable for the delivery of our genetic constructs as it would greatly increase the multiplicity of infection in branching ureteric buds.

Though the MMP14 and Venus Control retroviruses were able to infect UB cells in renal organoid cultures, both infected cultures soon thereafter deteriorated while cultures incubated in control media were left intact with UB structures even growing and branching. It is possible that something in the cell infection, the proviral transcription and integration, and/or the proviral expression process hindered the survival of the UB structures and, therefore, the culture as a whole. Alternatively, there may have been a toxin in the viral preparation that was being concentrated, along with the viruses, that had adverse effects on culture survival. To address the latter hypothesis, the volume of viral preparations used for incubation was reduced from 10ul to 5ul and a chemical often added to viral preparations to increase infectability, Polybrene, was removed since excessive exposure has been shown to be toxic to cells in other systems (Lin P et al., 2011). Additionally, dissociated renal cells were briefly incubated in ~20-fold dilutions of viral preparations, and the pellets were washed just after reaggregation before culturing. Both approaches were exercised in an attempt to greatly reduce the renal cells' exposure to any potential

toxins in the viral preparation (which contains medium conditioned by the packaging cells) but failed to aid in the survival of infected cultures. Although a toxin cannot be ruled out, the results support the notion that something in the retroviral infection process itself is adversely affecting the viability of the renal organoid cultures, thereby preventing the analysis of infected UB cells.

To further understand the role that MMP14 has in kidney development, future studies will have to focus on the biochemical attributes of MMP14 itself. Great knowledge will be gained in revealing the proteins that interact with MMP14 and the signaling cascades they promote or inhibit. Catalytic domain cleavage and phosphorylation events should also be thoroughly explored as they may have a profound effect on the behavior of MMP14 and the cells that express it. The knockout of MMP14 does not cause renal agenesis and the moderate branching defects it does cause suggests that there are other players involved in cell movements in the WD and UB. Indeed, MMP2 and MMP9 are known to be expressed in the kidney (Pohl et al., 2000) with a similar temporal expression pattern to MMP14, and *Mmp9* has been shown to be directly regulated by *Etv4* in other cellular contexts (Cowden Dahl et al., 2007). A double- or triple-knockout of various MMPs with MMP14 may be needed to observe the severe phenotype seen in *Etv4/5* or *Ret* mutants. MMP14 does play a prominent role in UB branching morphogenesis and these experiments will provide us with a more comprehensive understanding of its function in early kidney development.

EXPERIMENTAL PROCEDURES

Embryonic Stem Cell Lines. Wildtype and *Mmp14*$^{-/-}$ ES cells carrying *Hoxb7:myr-Venus* were derived similarly to Shakya et al., 2005. These mice were a gift of Dr. M Seiki (Ohtake et al., 2006). Brielfy, Mmp14$^{+/-}$ (MGI: 3687379) males and females carrying Hoxb7:myrVenus (MGI:4415296) were mated to each other. Embryos were recovered at the blastocyst stage and individual embryos were placed in culture to derive embryonic stem cell lines. ES clones were genotyped for Mmp14$^{-/-}$ and Hoxb7:myrVenus. The ES cell lines were derived by Zaiqi Wu, a technician in the lab.

Generation of Chimeras. Blastocysts were first derived from wildtype 129 mice and were injected with *Mmp14*$^{-/-}$ ES cells (also carrying *Hoxb7:myrVenus*). Chimeric blastocysts were then implanted into wildtype pseudopregnant hosts. Chimeric embryos generated by blastocyst injection were recovered at E12.5 and E14.5 and urogenital systems were dissected, cultured for 3 or 4 hours on a filter, and then fixed.

Immunofluorescence Microscopy. Urogenital systems were fixed in 4% paraformaldehyde (PFA) (1 hr, 4°C), and washed 3x in PBS on a filter. Samples were then incubated in TSP (0.1% Triton X-100, 0.05% Saponin, PBS)(3x, 10min, room temperature) before incubation in the following primary antibodies: Goat anti-Calbindin (Invitrogen, 1:200) and Rabbit anti-GFP (Invitrogen, 1:500). Primary antibody was diluted in TSP and 10% Normal Donkey Serum (NDS) and incubation lasted 3hrs at room temperature (RT) followed by TSP washes (3x, 10min, RT). Secondary antibodies (Cy3 Donkey anti-Goat, Cy2 Donkey anti-Rabbit, Jackson ImmunoResearch) were diluted in TSP and 10% NDS and samples were incubated for one hour at RT followed by TSP washes (3x, 10min, RT).

Samples were then mounted onto slides using Fluoro-gel and imaged by by Zeiss AxioObserver Z1. 5x and 10x objectives were used.

Generation of Retroviral Vector for Overexpression. To generate the "MMP14" viral vector, In-Fusion® (Clonetech) cloning was used to clone mouse *Mmp14* cDNA into the BamHI cloning site upstream of the Internal Ribosomal Entry Site (IRES) of the pQCXIX retroviral vector (Clonetech). *Myr-venus* DNA was simultaneously cloned into the MluI site downstream of the IRES. Previously acquired *mmp14* cDNA and *myr-venus* DNA were both amplified by PCR using primers designed with 16bp overhangs (in red below) that are complimentary to the ends of the linearized plasmid backbone. The primers designed for *mmp14* were:

5'-CTTAATTAACGGATCCATGTCTCCCGCCCCTCGA-3' (forward)

5'-TTCGCTGCTGGACAAGGTCTGAGGATCCGGAATTCCGC-3' (reverse)

The primers designed for *myr-venus* were:

5'-AAGCTTGATCACGCGTATGGGAAGCAGCAAGAGCAAG-3' (forward)

5'-GGCATGGCACGAGCTGTACAAGTAAACGCGTCTCGAGATAT-3' (reverse).

The protocol for combining all cloned fragments then proceeded as described in the In-Fusion® HD Cloning Kit User Manual The final product was then transformed into *E. Coli* Stellar Competent Cells (HST08 strain) for amplification and confirmed by a diagnostic digest of the final product with. The same protocol was executed in order to generate the "Venus Control" viral vector by cloning only *myr-venus* segments with into downstream MluI site.

Viral Production. MMP14 virus was generated by co-transfecting the MMP14 viral plasmid and a separate plasmid containing vesicular stomatitis virus G protein (VSV-G), an envelope protein, into HEK293GP cells using polyethylenimine (PEI). Before transfection the HEK293GP cells were seeded in 10-cm plates (Corning) at 50% confluency in 7 ml KCM for 16 h at 37 °C, 5% CO_2. The transfection reagent was made with serum-free media (Opti-MEM®; Life Technologies) containing 10µg of the MMP14 viral plasmid, 5µg of the VSV-G plasmid, and 1x PEI. Fresh KCM was given to the cells immediately before transfection. Transfection efficiency was then assessed by Venus marker expression 48 h after transfection and supernatant containing virus was collected at 48, 72 and 96 h after transfection. Venus Control virus was produced similarly using the Venus Control viral plasmid.

Virus Purification, Concentration and Titration. Cell debris was first removed from the viral preparations by low speed centrifugation (2,000 rpm for 5min at RT). The supernatant was then filtered with .45µm pore size Steriflip filters (Millipore) and then filtered with Amicon Ultra-100K centrifugal filters (Millipore) for 15min in a swinging bucket centrifuge (Beckman TJ-6). Viral preparations were then further concentrated by ultracentrifugation at 40,000 rpm for 2 h at 4°C (Beckman TLA100.3 rotor). The pellets were then resuspended in 50mL KCM, aliquoted, and stored at -80°C. Serial 10-fold dilutions of MMP14 and Venus Control virus were then made and added to HEK293GP cells seeded onto 24-well plates (Corning) at 50% confluency 16 h before infection. The number of infected cells (visualized by Venus expression) in wells with well-isolated infected cells was then calculated.

Viral Infection. MMP14 or Venus Control virus preparation was loaded into pulled borosilicate glass capillaries in the presence of 4μg/ml Polybrene and injected into the lumens of *Hoxb7:cre;Rosa26*$^{Tomato/Tomato}$ or WT kidneys at E11.5 or E12.5. This was performed using a FemtoJet (Eppendorf) and kidneys swelled in response to injection. Some viral preparations were also supplemented with 50% Glycerol at a 1:5 ratio before injection. Infection was then assessed by the presence of the myr-Venus marker under GFP or YFP fluorescence.

Protein Extraction and Preparation. Approximately 6.5 x 10^6 HEK293 cells were transfected via Polyethylenimine (PEI) with 15 μg of MMP14 or 15 μg of Venus Control retroviral vector. These cells were washed with cold PBS 72 h after transfection. RIPA lysis buffer was then added to the culture plates and the cells were scraped off with a cell scraper (BD Falcon), collected into an Eppendorf tube, and incubated for 30 min at 4°C. The samples were subsequently centrifuged at 12,000 rpm for 10 min and the supernatants poured into new Eppendorf tubes. The supernatants (Cell Lysate) and the pellets (Cell Debris with cell membrane enrichment) were tested for protein concentration using the Bradford Assay. The sample were then diluted in sample buffer (10% glycerol, 10% SDS, 5% β-mercaptoethanol, 0.1% bromophenol blue, 500 mM Tris base, pH 6.75) at a 1:1 ratio, boiled at 96°C for 5 min, and then stored at -20°C for Western Blotting analysis.

Western blot Analysis. A total of 30 μg of protein in sample buffer was heated to 96°C for 5 min, cooled and loaded in each well of a 10% bisacrylamide (Biorad) gel and run at 40-100 V for 1 hr or until the protein ladder markers (Precision Plus -BioRad) were well separated. Protein was transferred to a methanol- activated PVDF (Millipore) membrane at

12 V for 45 min using an ECL semi dry transfer unit (Amersham Biosciences TE77). Membranes were then rinsed once in 1X PBS/0.05% Tween-20 (PBST), blocked in 3% milk and incubated with 1:2000 rabbit anti-MMP14 primary antibody (Epitomics). Blots were washed for 10m at RT (3x) in PBST and then incubated for 3 h with Donkey HRP-conjugated anti-rabbit (Jackson ImmuonoResearch) secondary antibody at a concentration of 1:10000, and re-washed. Protein bands were then detected by chemiluminescence (Millipore).

CHAPTER 6

DISCUSSION

Conclusions and Future Directions

Here, we have demonstrated the efficacy of renal organoids for studying the cellular basis of ureteric bud morphogenesis. After the dissociation of embryonic kidneys into single cells and their subsequent reaggregation, ureteric bud cells self-assemble into UB structures by sending out long processes, migrating and aggregating with other UB cells to form epithelial vesicles. These structures then undergo events typical of *in vivo* UB morphogenesis including elongation into single-layered epithelial tubes, luminal cell division, terminal bifurcation, the expression and maintenance of tip markers at the ends of branching UB structures, and remodeling of older branch generations. We also discovered that ureteric bud organoids experience similar Ret-signaling-dependent cell rearrangements that are found in engineered *in vivo* chimeras and are likely to be the basis on which the normal progenitor tip domain is established and maintained. When *Sprouty1*$^{-/-}$ UB cells (with higher Ret-signaling) were mixed with WT UB cells (with lower Ret-signaling) for the production of finely-grained, mosaic renal organoids, *Sprouty1*$^{-/-}$ cells were found to outcompete WT cells for residence at the tips of the resulting UB structures. Similarly, fine-grained chimeric organoids generated with Ret-signaling-deficient UB cells and WT cells (*Ret*$^{51/-}$⇔WT) displayed sharp domain segregated based on the level of Ret-signaling, with a strong tendency of WT cells to reside in UB tips. These results recapitulated those observed in *Sprouty1*$^{-/-}$⇔WT chimeras produced *in vivo* (Chi et al.

2009) or are consistent with other Ret-signaling-deficient chimeric kidneys (*Ret*$^{-/-}$⇔WT or *Etv4*$^{-/-}$; *Etv5*$^{+/-}$⇔WT; Shakya et al., 2005b; Kuure et al., 2010), validating renal organoids as a suitable system to study cell rearrangements and cell sorting that occur during UB morphogenesis.

Using the versatile renal organoid system, we extended these findings to include Fgfr2, another RTK known to be involved in ureteric bud morphogenesis (Zhao et al., 2004; Bates, 2011) and known to synergize with the Ret-signaling pathway (Michos et al., 2010; Maeshima et al., 2007; Okazawa et al., 2015). Fgfr2$^{UB-/-}$⇔WT renal organoid chimeras displayed distinct domain segregation, with WT cells preferentially residing in the tips of branching UB structures at the expense of *Fgfr2*$^{UB-/-}$ mutant cells. As with the in vivo and organoid chimeric data reported thus far on RTK-signaling, this suggests that RTK-signaling through Fgfr2, as well, may help UB cells properly organize in the WD to form the primary tip at the onset UB morphogenesis. On the other hand, using the novel MASTR technique, mosaic deletion of *Fgfr2* during branching morphogenesis (after the creation of the primary UB) resulted in only a slight reduction of mutant recombinant cells in UB tips a few branch generations later. This indicated that the function of Fgfr2 in maintaining the progenitor UB branch tips during this phase of kidney organogenesis may be less critical than it is in the initial formation of the UB tips; however, more experimentation is needed, such as juxtaposing *Fgfr2*-/- cells with WT cells, rather than heterozygous cells).

Mmp14, one of the recently discovered downstream components of Ret-signaling in the UB (Lu et al., 2009), is a transmembrane metalloproteinase that has been linked to epithelial cell migration in a wide range of tissues (Firlej et al., 2008; Hasegawa et al., 2004:

Barbolina et al., 2008). Also, when in competition with low Mmp14-expressing cells, high Mmp14-expressing cells segregate to the tips of engineered mammary epithelial tubules via cell-autonomous cell migration (Mori et al., 2009). In the developing kidney, however, this does not seem to be the case. When we generated chimeric embryos, we observed contribution of *Mmp14*-null cells to the tips of branching E12.5 and E14.5 WT ureteric buds at a level comparable to that seen in control chimeras. A retroviral-mediated upregulation of Mmp14 was also attempted to address the potential sufficiency of Mmp14 in affecting the morphogenetic behaviors of UB cells. These attempts failed, however, as retroviral delivery was either inefficient in intact kidneys or toxic in renal organoids. Lentiviral infection in kidney explants or plasmid transfection during renal organoid production may help to circumvent these complications in order to elucidate a possible cellular basis of Mmp14 function during UB morphogenesis.

Taken together, our research opens the door to a promising and productive future for the renal organoid system in the study of kidney development. The easy generation of mosaic renal structures in this system, by the simple mixing of cells, will allow investigators to potentially discover the cell-autonomous effects of RTK-signaling mediators other than Ret or Fgfr2. For instance, *Met* is expressed in the UB tips and encodes an RTK for Hepatocyte growth factor, secreted by the metanephric mesenchyme (Lu et al., 2009; Ishibe et al., 2009). During motor neuron development, Met-signaling has been shown to *non*-cell-autonomously regulate *Etv* expression, which is required to recruit motor neurons to motor pools (Helmbacher et al., 2003). In UB-specific mutants of *Met*,

there is a small decrease in UB branching (Ishibe et al., 2009). It is not clear, though, from these kidney-wide experiments, whether Met-signaling is needed autonomously for a cell to follow a UB-tip specific fate, or whether it is needed for a population of cells to be able to set up the conditions in which properly functioning UB tips can form. These possibilities could be tested by the production of chimeric renal tissues in which *Met*$^{-/-}$ UB cells are mixed with WT cells. Additionally, very little is known about the role of the downstream effectors of RTK-signaling (such as Mmp14) on WD or UB cell behavior and how they lead to epithelial morphogenesis. These unknown potential functions can also be revealed by investigating cell competition in mosaic organoids. Because of the arduous nature of producing chimeras *in vivo*, renal organoid chimera generation will allow for a higher-throughput analysis of many important genes that may form the cellular basis of UB branching morphogenesis. Also, RNA interference has already proven to be useful in this new system (Unbekandt et al., 2010), as siRNAs and other large molecules have less problems of penetration in cell suspensions than they do in intact organs. Thus, the downregulation of a multitude of UB-specific genes could be leveraged to create mosaic organoids on a large scale. In this regard, this approach may possibly serve as a platform for the introduction of pharmacological agents to further shed light on the molecules involved in cell-autonomous cell behavior changes. It has been found that knockout of a single gene may lead to the upregulated expression of related or redundant pathways, resulting in phenotypic compensation that can preclude any study of cell-autonomous effects in single-gene knockouts. For example, the expression level of *Fgf7* was higher in *Ret*$^{-/-}$ mice that exhibited UB formation than those that did not (Maeshima et al., 2007), and conditional deletion of *Met* in the UB leads to an upregulation of Egfr, another membrane-

bound RTK in the UB (Ishibe et al., 2009). Thus, easy RNAi-mediated double downregulation of potentially redundant pathways in mosaic renal organoids could circumvent this problem and could greatly improve our understanding of the cellular basis of gene function.

Branching morphogenesis is an essential developmental process that is responsible for the formation of a variety of epithelial organs, from the trachea and air sacs in the fly to the mammary gland, lung, kidney and salivary gland in vertebrates (Affolter et al., 2003). RTK-signaling-based cell competition may be an evolutionarily conserved mechanism of epithelial branching morphogenesis (Shakya et al., 2005b; Kuure et al., 2010; Ghabrial et al., 2006; Cabernard et al., 2005; Lu et al., 2008), and this mechanism may be used to refine and focus the progenitor domains of epithelial trees for proper, directed growth and branching. Mosaic renal organoids can thus serve as a model for illuminating this process, and the underlying genes involved, in an effort to improve health outcomes when there is dysfunction in kidney morphogenesis or other branched organs.

REFERENCES

al-Awqati Q, Goldberg MR. (1998). Architectural patterns in branching morphogenesis in the kidney. *Kidney Int*. 1998 Dec;54(6):1832-42.

Affolter M, Bellusci S, Itoh N, Shilo B, Thiery JP, Werb Z. (2003). Tube or not tube: remodeling epithelial tissues by branching morphogenesis. *Dev Cell*. 2003 Jan;4(1):11-8.

Auerbach R, Grobstein C. (1958) Inductive interaction of embryonic tissues after dissociation and reaggregation. *Exp Cell Res* 1958; 15: 384–397.

Barak H, Rosenfelder L, Schultheiss TM, Reshef R. (2005). Cell fate specification along the anterior-posterior axis of the intermediate mesoderm. *Dev Dyn*. 2005 Apr; 232(4):901-14.

Barak H, Huh SH, Chen S, Jeanpierre C, Martinovic J, Parisot M, Bole-Feysot C, Nitschké P, Salomon R, Antignac C, Ornitz DM, Kopan R. (2012). FGF9 and FGF20 maintain the stemness of nephron progenitors in mice and man. *Dev Cell.* 2012 Jun 12; 22(6):1191-207.

Barbolina MV, Stack MS. (2008). Membrane Type 1-Matrix Metalloproteinase: Substrate Diversity in Pericellular Proteolysis. *Seminars in cell & developmental biology*. 2008;19(1):24-33. doi:10.1016/j.semcdb.2007.06.008.

Barros E J, Santos O F, Matsumoto K, Nakamura T, Nigam S K. (1995). Differential tubulogenic and branching morphogenetic activities of growth factors: implications for epithelial tissue development. *Proc Natl Acad Sci* USA 92:4412–4416

Basson MA, Akbulut S, Watson-Johnson J, Simon R, Carroll TJ, Shakya R, Gross I, Martin GR, Lufkin T, McMahon AP, Wilson PD, Costantini FD, Mason IJ, Licht JD. (2005). Sprouty1 is a critical regulator of GDNF/RET-mediated kidney induction. *Dev Cell*. 2005 Feb;8(2):229-39.

Basson MA, Watson-Johnson J, Shakya R, Akbulut S, Hyink D, Costantini FD, Wilson PD, Mason IJ, and Licht JD. (2006). Branching morphogenesis of the ureteric epithelium during kidney development is coordinated by the opposing functions of GDNF and Sprouty1. *Dev. Biol*. 299, 466–477.

Bates C. (2011). Role of fibroblast growth factor receptor signaling in kidney development. *American Journal of Physiology - Renal Physiology.* 2011 Vol. 301 no. 2, F245-F251

Belkin AM1, Akimov SS, Zaritskaya LS, Ratnikov BI, Deryugina EI, Strongin AY. (2001). Matrix-dependent proteolysis of surface transglutaminase by membrane-type metalloproteinase regulates cancer cell adhesion and locomotion. *J Biol Chem*. 2001 May 25;276(21):18415-22. Epub 2001 Mar 2.

Blank U, Brown A, Adams DC, Karolak MJ, Oxburgh L. (2009). BMP7 promotes proliferation of nephron progenitor cells via a JNK-dependent mechanism. *Development.* 2009 Nov; 136(21):3557-66.

Bouchard M, Souabni A, Mandler M, Neubüser A, Busslinger M. (2002). Nephric lineage specification by Pax2 and Pax8. *Genes Dev*. 2002 Nov 15; 16(22):2958-70.

Brown AC, Adams D, de Caestecker M, Yang X, Friesel R, Oxburgh L. (2011). FGF/EGF signaling regulates the renewal of early nephron progenitors during embryonic development. *Development*. 2011 Dec; 138(23):5099-112.

Bunn HF. (2013). Erythropoietin. *Cold Spring Harb Perspect Med*. 2013 Mar 1; 3(3):a011619.

Cabernard C and Affolter M. (2005). Distinct roles for two receptor tyrosine kinases in epithelial branching morphogenesis in Drosophila. *Dev. Cell* 9, 831– 842.

Cancilla B, Ford-Perriss MD, Bertram JF. (1999). Expression and localization of fibroblast growth factors and fibroblast growth factor receptors in the developing rat kidney. *Kidney Int* 56: 2025–2039, 1999.

Cantley L G, Barros E J, Gandhi M, Rauchman M, Nigam S K. (1994). Regulation of mitogenesis, motogenesis, and tubulogenesis by hepatocyte growth factor in renal collecting duct cells. *Am J Physiol* 267:F271–F280

Cebrian C, Borodo K, Charles N, and Herzlinger DA. (2004). Morphometric index of the developing murine kidney. *Dev Dyn* 231:601–608.

Chi X, Hadjantonakis A-K, Hyink D, Costantini F. (2009a). A transgenic mouse that reveals cell shape and arrangement during ureteric bud branching. *Genesis (New York, NY : 2000)*. 2009;47(2):61-66. doi:10.1002/dvg.20452.

Chi X, Michos O, Shakya R, Riccio P, Enomoto H, Licht JD, Asai N, Takahashi M, Ohgami N, Kato M, Mendelsohn C, Costantini F. (2009). Ret-dependent cell rearrangements in the Wolffian duct epithelium initiate ureteric bud morphogenesis. *Dev Cell.* 2009 Aug;17(2):199-209. doi: 10.1016/j.devcel.2009.07.013.

Chia I, Grote D, Marcotte M, Batourina E, Mendelsohn C, Bouchard M. (2011). Nephric duct insertion is a crucial step in urinary tract maturation that is regulated by a Gata3-Raldh2-Ret molecular network in mice. *Development*. 2011 May; 138(10):2089-97.

Coffin JM, Hughes SH, Varmus HE, editors (1997). Retroviruses. Cold Spring Harbor (NY): Cold Spring Harbor Laboratory Press

Coles HS, Burne JF, Raff MC. (1993).Large-scale normal cell death in the developing rat kidney and its reduction by epidermal growth factor. *Development*. 1993; 118: 777–784.

Cooray S, Howe SJ, Thrasher AJ. (2012). Retrovirus and lentivirus vector design and methods of cell conditioning. *Methods Enzymol*. 2012; 507:29-57. doi: 10.1016/B978-0-12-386509-0.00003-X

Corish P, Tyler-Smith C. (1999). Attenuation of green fluorescent protein half-life in mammalian cells. *Protein Eng*. 1999 Dec;12(12):1035-40.

Costantini F. (2006). Renal branching morphogenesis: concepts, questions, and recent advances. *Differentiation*. 2006 Sep; 74(7):402-21.

Costantini F. (2012). Genetic controls and cellular behaviors in branching morphogenesis of the renal collecting system. *Wiley interdisciplinary reviews Developmental biology*. 2012;1(5):693-713. doi:10.1002/wdev.52.

Costantini F, Shakya R. (2006). GDNF/Ret signaling and the development of the kidney. *Bioessays*. 2006 Feb; 28(2):117-27.

Costantini F, Kopan R. (2010) Patterning a complex organ: branching morphogenesis and nephron segmentation in kidney development. *Developmental Cell*. 2010;18(5):698-712. doi:10.1016/j.devcel.2010.04.008.

Cowden Dahl KD, Zeineldin R, Hudson LG. PEA3 Is Necessary for Optimal Epidermal Growth Factor Receptor–Stimulated Matrix Metalloproteinase Expression and Invasion of Ovarian Tumor Cells. *Molecular cancer research : MCR*. 2007;5(5):413-421. doi:10.1158/1541-7786.MCR-07-0019.

Davies, JA. (1994). Control of Calbindin-D-28K expression in developing mouse kidney. *Dev. Dyn*. 199, 45-51.

Davies JA, Ladomery M, Hohenstein P, Michael L, Shafe A, Spraggon L, Hastie N. (2004). Development of an siRNA-based method for repressing specific genes in renal organ culture and its use to show that the Wt1 tumour suppressor is required for nephron differentiation. *Hum Mol Genet*. 2004 Jan 15;13(2):235-46. Epub 2003 Nov 25.

Davies JA, Unbekandt M. (2012). siRNA-mediated RNA interference in embryonic kidney organ culture. *Methods in Molecular Biology*, 886 (2012), pp. 295–303

de Graaff E, Srinivas S, Kilkenny C, D'Agati V, Mankoo BS, Costantini, F, and Pachnis V. (2001). Differential activities of the RET tyrosine kinase receptor isoforms during mammalian embryogenesis. *Genes Dev*. 15, 2433– 2444.

Derman MP, Cunha MJ, Barros EJ, Nigam SK, Cantley L G. (1995). HGF-mediated chemotaxis and tubulogenesis require activation of the phosphatidylinositol 3-kinase. *Am J Physiol* 268:F1211–F1217

Deryugina EI, Ratnikov BI, Postnova TI, Rozanov DV, Strongin AY. (2002). Processing of integrin alpha(v) subunit by membrane type 1 matrix metalloproteinase stimulates migration of breast carcinoma cells on vitronectin and enhances tyrosine

phosphorylation of focal adhesion kinase. *J Biol Chem*. 2002 Mar 22;277(12):9749-56. Epub 2001 Nov 27.

Drawbridge J, Meighan CM, Mitchell EA. (2000). GDNF and GFRalpha-1 are components of the axolotl pronephric duct guidance system. *Dev Biol*. 2000 Dec 1; 228(1):116-24.

Dressler GR. (2006). The cellular basis of kidney development. *Annu Rev Cell Dev Biol*. 2006; 22:509-29.

Dressler GR. (2009). Advances in early kidney specification, development and patterning. *Development (Cambridge, England)*. 2009;136(23):3863-3874.

Ehrenfels CW, Carmillo PJ, Orozco O, Cate RL, and Sanicola M. (1999). Perturbation of RET signaling in the embryonic kidney. *Dev Genet* 24:263–272.

Elberg G, Guruswamy S, Logan CJ, Chen L, Turman MA. (2007). Plasticity of epithelial cells derived from human normal and ADPKD kidneys in primary cultures. *Cell Tissue Res*. 2008 Feb;331(2):495-508. Epub 2007 Nov 15.

Endo K, Takino T, Miyamori H, Kinsen H, Yoshizaki T, Furukawa M, Sato H. (2003). Cleavage of syndecan-1 by membrane type matrix metalloproteinase-1 stimulates cell migration. *J Biol Chem*. 2003 Oct 17;278(42):40764-70. Epub 2003 Aug 6.

Firlej V, Ladam F, Brysbaert G, Dumont P, Fuks F, de Launoit Y, Benecke A, Chotteau-Lelievre A. (2008). Reduced tumorigenesis in mouse mammary cancer cells following inhibition of Pea3- or Erm-dependent transcription. *J Cell Sci.* 2008 Oct 15;121(Pt 20):3393-402. doi: 10.1242/jcs.027201. Epub 2008 Sep 30.

Fisher CE, Michael L, Barnett MW, Davies JA. (2001). Erk MAP kinase regulates branching morphogenesis in the developing mouse kidney. *Development* 128(21):4329–4338

Ghabrial AS and Krasnow MA. (2006). Social interactions among epithelial cells during tracheal branching morphogenesis. Nature 441, 746–749.

Grobstein C. (1953). Inductive epitheliomesenchymal interaction in cultured organ rudiments of the mouse. *Science*. 1953 Jul 10;118(3054):52-5.

Grobstein C. (1956). Trans-filter induction of tubules in mouse metanephrogenic mesenchyme. *Exp Cell Res*. 1956 Apr;10(2):424-40

Gross I, Morrison DJ, Hyink DP, Georgas K, English MA, Mericskay M, Hosono S, Sassoon D, Wilson PD, Little M, Licht JD. (2003). The receptor tyrosine kinase regulator Sprouty1 is a target of the tumor suppressor WT1 and important for kidney development. *J. Biol. Chem*. 278, 41420–41430.

Grote D, Souabni A, Busslinger M, Bouchard M. (2006). Pax 2/8-regulated Gata 3 expression is necessary for morphogenesis and guidance of the nephric duct in the developing kidney. *Development*. 2006 Jan; 133(1):53-61.

Grote D, Boualia SK, Souabni A, Merkel C, Chi X, Costantini F, Carroll T, Bouchard M. (2008). Gata3 acts downstream of beta-catenin signaling to prevent ectopic metanephric kidney induction. *PLoS Genet.* 2008 Dec; 4(12):e1000316.

Hasegawa H, Ashigaki S, Takamatsu M, Suzuki-Migishima R, Ohbayashi N, Itoh N, Takada S, Tanabe Y. (2004). Laminar patterning in the developing neocortex by temporally coordinated fibroblast growth factor signaling. *J. Neurosci.* 24, 8711-8719

Helmbacher F, Dessaud E, Arber S, deLapeyriere O, Henderson CE, Klein R, et al. (2003). Met signaling is required for recruitment of motor neurons to PEA3-positive motor pools. *Neuron*. 2003;39:767–777.

Hendry CE, Vanslambrouck JM, Ineson J, Suhaimi N, Takasato M, Rae F, et al. (2013). Direct transcriptional reprogramming of adult cells to embryonic nephron progenitors. *Journal of the American Society of Nephrology*, 24 (9) (2013), pp. 1424–1434

Hoy WE, Bertram JF, Denton RD, Zimanyi M, Samuel T, Hughson MD. (2008). Nephron number, glomerular volume, renal disease and hypertension. *Curr Opin Nephrol Hypertens*. 2008. May; 17(3):258-65.

Ishibe S, Karihaloo A, Ma H, Zhang J, Marlier A, Mitobe M, Togawa A, Schmitt R, Czyczk J, Kashgarian M, Geller DS, Thorgeirsson SS, Cantley LG. (2009) Met and the epidermal growth factor receptor act cooperatively to regulate final nephron number and maintain collecting duct morphology. *Development*. 2009 Jan; 136(2):337-45.

Jain S, Encinas M, Johnson EM Jr, and Milbrandt J. (2006). Critical and distinct roles for key RET tyrosine docking sites in renal development. *Genes Dev* 20:321–333.

Jijiwa M, Fukuda T, Kawai K, Nakamura A, Kurokawa K, Murakumo Y, Ichihara M, and Takahashi M. (2004). A tar- geting mutation of tyrosine 1062 in Ret causes a marked decrease of enteric neurons and renal hypoplasia. *Mol Cell Biol* 24:8026– 8036.

Kajita M, Itoh Y, Chiba T, et al. Membrane-Type 1 Matrix Metalloproteinase Cleaves Cd44 and Promotes Cell Migration. *The Journal of Cell Biology*. 2001;153(5):893-904.

Kanwar, YS, Carone, FA, Kumar, A, Wada, J, Ota, K, Wallner, EI. (1997). Role of extracellular matrix, growth factors and proto-oncogenes in metanephric development. *Kidney Int.* 1997 52: 589–606

Karner CM, Das A, Ma Z, Self M, Chen C, Lum L, Oliver G, Carroll TJ. (2009) Canonical Wnt9b signaling balances progenitor cell expansion and differentiation during kidney development. *Development.* 2011 Apr; 138(7):1247-57.

Klint, P, Claesson-Welsh, L. (1999). Signal transduction by fibroblast growth factor receptors. *Front Biosci*. 4, D165–D177.

Kuure S, Chi X, Lu B, Costantini F. (2010a). The transcription factors Etv4 and Etv5 mediate formation of the ureteric bud tip domain during kidney development. *Development (Cambridge, England)*. 2010;137(12):1975-1979. doi:10.1242/dev.051656.

Kuure S, Cebrian C, Machingo Q et al (2010b) Actin depolymerizing factors cofilin1 and destrin are required for ureteric bud branching morphogenesis. *PLoS Genet* 6:e1001176

Kuure S. (2012). Analysis of migration in primary ureteric bud epithelial cells. *Methods Mol Biol*. 2012;886:147-55. doi: 10.1007/978-1-61779-851-1_13.

Laeno AMA, Tamashiro DAA, Alarcon VB. (2013). Rho-Associated Kinase Activity Is Required for Proper Morphogenesis of the Inner Cell Mass in the Mouse Blastocyst. *Biology of Reproduction*. 2013;89(5):122. doi:10.1095/biolreprod.113.109470.

Lao Z, Raju GP, Bai CB, Joyner AL. (2012). Mosaic mutant Analysis with Spatial and Temporal control of Recombination (MASTR): a new technique for determining the fate of mutant cells using conditional floxed alleles in mice. *Cell Reports*. 2012;2(2):386-396.

Lecuit, T. (2005). Adhesion remodeling underlying tissue morphogenesis. *Trends Cell Biol*. 15, 34–42.

Lee W-C, Berry R, Hohenstein P *et al*. (2008). siRNA as a tool for investigating organogenesis. *Organogenesis* 2008; 4: 176–181.

Li Z, Jerebtsova M, Liu XH, Tang P, Ray PE. (2006). Novel cystogenic role of basic fibroblast growth factor in developing rodent kidneys. *Am J Physiol Renal Physiol*. 2006 Aug; 291(2):F289-96.

Liang CC, Park AY, Guan JL. (2007). In vitro scratch assay: a convenient and inexpensive method for analysis of cell migration in vitro. *Nat Protoc.* 2:329–333

Lin P, Correa D, Lin Y, Caplan AI (2011) Polybrene Inhibits Human Mesenchymal Stem Cell Proliferation during Lentiviral Transduction. *PLoS ONE* 6(8): e23891. doi:10.1371/journal.pone.0023891

Lin Y, Zhang S, Rehn M, Itaranta P, Tuukkanen J, Heljasvaara R, Pelto- keto H, Pihlajaniemi T, and Vainio S. (2001). Induced repatterning of type XVIII collagen expression in ureter bud from kidney to lung type: association with sonic hedgehog and ectopic surfactant protein C. *Development* 128, 1573–1585.

Lu BC, Cebrian C, Chi X, Kuure S, Kuo R, Bates CM, Arber S, Hassell J, MacNeil L, Hoshi M, et al. (2009). Etv4 and Etv5 are required downstream of GDNF and Ret for kidney branching morphogenesis. *Nat. Genet.* 41, 1295-1302

Lu P, Ewald AJ, Martin GR, Werb Z. (2008). Genetic mosaic analysis reveals FGF receptor 2 function in terminal end buds during mammary gland branching morphogenesis. *Developmental Biology*. 2008;321(1):77-87. doi:10.1016/j.ydbio.2008.06.005.

Maeshima A, Sakurai H, Choi Y, Kitamura S, Vaughn DA, Tee JB, et al. (2007). Glial cell-derived neurotrophic factor independent ureteric bud outgrowth from the Wolffian duct. *J Am Soc Nephrol*. 2007;18:3147–3155.

Majumdar A, Vainio S, Kispert A, McMahon J, McMahon AP. (2003). Wnt11 and Ret/Gdnf pathways cooperate in regulating ureteric branching during metanephric kidney development. *Development*. 2003;130:3175–3185.

Marose TD, Merkel CE, McMahon AP, Carroll TJ. (2008). Beta-catenin is necessary to keep cells of ureteric bud/Wolffian duct epithelium in a precursor state. *Dev Biol.* 2008 Feb 1; 314(1):112-26.

Merlet-Bénichou C, Gilbert T, Vilar J, Moreau E, Freund N, and Lelièvre-Pégorier M. (1999). Nephron number: variability is the rule. Causes and consequences. *Lab Invest*. 79, 515-527.

Meyer TN, Schwesinger C, Bush KT, Stuart RO, Rose DW, et al. 2004. Spatiotemporal regulation of morphogenetic molecules during in vitro branching of the isolated ureteric bud: toward a model of branching through budding in the developing kidney*. Dev Biol* 275:44 – 67.

Meyer TN, Schwesinger C, Sampogna RV et al. (2006) Rho kinase acts at separate steps in ureteric bud and metanephric mesenchyme morphogenesis during kidney development. *Differentiation* 2006; 74: 638–647.

Michael L, and Davies JA. (2004). Pattern and regulation of cell proliferation during murine ureteric bud development. *J. Anat*. 204, 241–255.

Michos O, Cebrian C, Hyink D, et al. (2010). Kidney Development in the Absence of Gdnf and Spry1 Requires Fgf10. Beier DR, ed. *PLoS Genetics.* 2010;6(1):e1000809. doi:10.1371/journal.pgen.1000809.

Montesano, R, Schaller, G, Orci, L. (1991). Induction of epithelial tubular morphogenesis in vitro by fibroblast-derived soluble factors. *Cell* 1991 66: 697–711

Moore MW, Klein RD, Farinas I, Sauer H, Armanini M, et al. (1996). Renal and neuronal abnormalities in mice lacking GDNF. *Nature* 382:76 – 79.

Mori H, Gjorevski N, Inman JL, Bissell MJ, Nelson CM. (2009). Self-organization of engineered epithelial tubules by differential cellular motility. *Proceedings of the National Academy of Sciences of the United States of America*. 2009;106(35):14890-14895. doi:10.1073/pnas.0901269106.

Mori H, Lo AT, Inman JL, et al. Transmembrane/cytoplasmic, rather than catalytic, domains of Mmp14 signal to MAPK activation and mammary branching morphogenesis via binding to integrin β1. *Development (Cambridge, England)*. 2013;140(2):343-352. doi:10.1242/dev.084236.

Nagy A. (2002). Cre recombinase: the universal reagent for genome tailoring. Genesis. 2000 Feb;26(2):99-109.

Nguyen HQ, Danilenko DM, Bucay N, DeRose ML, Van GY, Thomason A, Simonet WS. (1996). Expression of keratinocyte growth factor in embryonic liver of transgenic mice

causes changes in epithelial growth and differentiation resulting in polycystic kidneys and other organ malformations. *Oncogene*. 1996 May 16; 12(10):2109-19.

Ohuchi H, Hori Y, Yamasaki M, Harada H, Sekine K, Kato S, Itoh N. (2000). FGF10 acts as a major ligand for FGF receptor 2 IIIb in mouse multi-organ development. *Biochem Biophys Res Commun*. 2000 Nov 2; 277(3):643-9.

Ohtake Y, Tojo H, Seiki M. (2006). Multifunctional roles of MT1-MMP in myofiber formation and morphostatic maintenance of skeletal muscle*. J Cell Sci*. 2006 Sep 15;119(Pt 18):3822-32. Epub 2006 Aug 22.

Okada H, Danoff TM, Kalluri R, Neilson EG .(1997). Early role of Fsp1 in epithelial-mesenchymal transformation. *Am J Physiol Renal Physiol*. 42:F563–F574

Okazawa M, Murashima A, Harada M, et al. (2015). Region-specific regulation of cell proliferation by FGF receptor signaling during the Wolffian duct development. *Developmental Biology*. 2015;400(1):139-147.

Pachnis V, Mankoo B, and Costantini F. (1993). Expression of the c-ret proto-oncogene during mouse embryogenesis. *Development* 119, 1005–1017.

Packard A, Georgas K, Michos O, Riccio P, Cebrian C, Combes AN, Ju A, Ferrer-Vaquer A, Hadjantonakis AK, Zong H, Little MH, Costantini F. (2013). Luminal mitosis drives epithelial cell dispersal within the branching ureteric bud. *Dev Cell*. 2013 Nov 11;27(3):319-30. doi: 10.1016/j.devcel.2013.09.001. Epub 2013 Oct 31.

Pepicelli CV, Kispert A, Rowitch DH, McMahon AP. (1997). GDNF induces branching and increased cell proliferation in the ureter of the mouse. *Dev Biol*. 1997 Dec 1;192(1):193-8.

Peters KG, Werner S, Chen G, Williams LT. (1992) Two FGF receptor genes are differentially expressed in epithelial and mesenchymal tissues during limb formation and organogenesis in the mouse. *Development* 114: 233–243, 1992.

Pichel JG, Shen L, Sheng HZ, Granholm AC, Drago J, Grinberg A, Lee EJ, Huang SP, Saarma M, Hoffer BJ, Sariola H, Westphal H. (1996). Defects in enteric innervation and kidney development in mice lacking GDNF. *Nature*. 1996 Jul 4; 382(6586):73-6.

Pohl M, Sakurai H, Bush K, Nigam S. (2000). Matrix metalloproteinases and their inhibitors regulate in vitro ureteric bud branching morphogenesis. *American Journal of Physiology - Renal Physiology* Nov 2000, 279 (5) F891-F900

Powers, CJ, McLeskey, SW, Wellstein, A. (2000). Fibroblast growth factors, their receptors and signaling. *Endocr.-Relat. Cancer* 7, 165 – 197.

Qiao J, Uzzo R, Obara-Ishihara T, Degenstein L, Fuchs E, Herzlinger D. (1999). FGF-7 modulates ureteric bud growth and nephron number in the developing kidney. *Development*. 1999 Feb; 126(3):547-54.

Qiao J, Bush KT, Steer DL, Stuart RO, Sakurai H, Wachsman W, Nigam SK. (2001). Multiple fibroblast growth factors support growth of the ureteric bud but have different effects on branching morphogenesis. *Mech Dev*. 2001 Dec; 109(2):123-35.

Quaggin SE, Kreidberg JA. (2008). Development of the renal glomerulus: good neighbors and good fences. *Development*. 2008 Feb; 135(4):609-20.

Riccio PN, Michos O. (2012). Dissecting and culturing and imaging the mouse urogenital system. *Methods Mol Biol*. 2012;886:3-11. doi: 10.1007/978-1-61779-851-1_1.

Riggins KS, Mernaugh G, Su Y, Quaranta V, Koshikawa N, Seiki M, Pozzi A, and Zent R, MT1-MMP-mediated basement membrane remodeling modulates renal development (2010). Exp Cell Res. 316(17): p. 2993-3005.

Rosselot C, Spraggon L, Chia I, Batourina E, Riccio P, Lu B, Niederreither K, Dolle P, Duester G, Chambon P, Costantini F, Gilbert T, Molotkov A, Mendelsohn C. (2010). Non-cell-autonomous retinoid signaling is crucial for renal development. *Development*. 2010 Jan; 137(2):283-92.

Rozanov DV, Hahn-Dantona E, Strickland DK, Strongin AY. (2004). The low density lipoprotein receptor-related protein LRP is regulated by membrane type-1 matrix metalloproteinase (MT1-MMP) proteolysis in malignant cells. *J Biol Chem*. 2004 Feb 6;279(6):4260-8. Epub 2003 Nov 25.

Sakurai H, Nigam S K. (1997). Transforming growth factor-beta selectively inhibits branching morphogenesis but not tubulogenesis. *Am J Physiol.* 272:F139–F146

Sánchez MP, Silos-Santiago I, Frisén J, He B, Lira SA, Barbacid M. (1996). Renal agenesis and the absence of enteric neurons in mice lacking GDNF. *Nature*. 1996 Jul 4; 382(6586):70-3.

Santos OF, Moura LA, Rosen EM, Nigam SK. (1993a). Modulation of HGF-induced tubulogenesis and branching by multiple phosphorylation mechanisms. *Dev Biol*. 159:535–548

Santos OF, Nigam SK. (1993b) HGF-induced tubulogenesis and branching of epithelial cells is modulated by extracellular matrix and TGF-beta. *Dev Biol*. 160:293–302

Santos-Araújo C, Leite-Moreira A, Pestana M. (2015). Clinical value of natriuretic peptides in chronic kidney disease. *Nefrologia*. 2015 May-Jun;35(3):227-33..

Saxen. (1987). Organogenesis of the Kidney. *Cambridge University Press*.

Schaeren-Wiemers, N & Gerfin-Moser, A. (1993) A single protocol to detect transcripts of various types and expression levels in neural tissue and cultured cells: in situ hybridization using digoxigenin-labelled cRNA probes. *Histochemistry* 100, 431–440 (1993).

Schuchardt A, D'Agati V, Larsson-Blomberg L, Costantini F, Pachnis V. (1994). Defects in the kidney and enteric nervous system of mice lacking the tyrosine kinase receptor Ret. *Nature*. 1994 Jan 27; 367(6461):380-3.

Schuchardt A, D'Agati V, Pachnis V, and Costantini, F. (1996). Renal agenesis and hypodysplasia in ret-k- mutant mice result from defects in ureteric bud development. *Development*. 122:1919–1929.

Seiki M. (2003). Membrane-type 1 matrix metalloproteinase: a key enzyme for tumor invasion. *Cancer Lett*. 2003 May 8;194(1):1-11

Shah MM, Tee JB, Meyer T, Meyer-Schwesinger C, Choi Y, Sweeney DE, Gallegos TF, Johkura K, Rosines E, Kouznetsova V, Rose DW, Bush KT, Sakurai H, Nigam SK. (2009). The instructive role of metanephric mesenchyme in ureteric bud patterning, sculpting, and maturation and its potential ability to buffer ureteric bud branching defects. *Am J Physiol Renal Physiol*. 2009 Nov; 297(5):F1330-41.

Shakya, R, Jho, EH, Kotka P, Wu Z, Kholodilov N, Burke R, D'Agati, V and Costantini, F. (2005a). The role of GDNF in patterning the excretory system. *Dev Biol* 283:70–84.

Shakya, R., Watanabe, T., and Costantini, F. (2005b). The role of GDNF/Ret signaling in ureteric bud cell fate and branching morphogenesis. *Dev Cell.* 8, 65–74.

Schedl, A. (2007) Renal abnormalities and their developmental origin. *Nature Reviews*. Genetics 8..10 (Oct 2007): 791-802.

Short KM, Combes AN, Lefevre J, Ju AL, Georgas KM, Lamberton T, Cairncross O, Rumballe BA, McMahon AP, Hamilton NA, Smyth IM, Little MH. (2014) Global Quantification of Tissue Dynamics in the Developing Mouse Kidney. *Dev Cell*. 2014 Apr 28; 29(2):188-202. doi: 10.1016/j.devcel.2014.02.017.

Sims-Lucas S, Argyropoulos C, Kish K, McHugh K, Bertram JF, Quigley R, Bates CM. (2009). Three-dimensional imaging reveals ureteric and mesenchymal defects in Fgfr2-mutant kidneys. *J Am Soc Nephrol*. 2009 Dec; 20(12):2525-33.

Sims-Lucas S, Cusack B, Eswarakumar VP, Zhang J, Wang F, Bates CM. (2011). Independent roles of Fgfr2 and Frs2α in ureteric epithelium. *Development (Cambridge, England).* 2011;138(7):1275-1280.

Sparks MA, Crowley SD, Gurley SB, Mirotsou M, Coffman TM. (2014). Classical Renin-Angiotensin System in Kidney Physiology. *Comprehensive Physiology*. 2014;4(3):1201-1228. doi:10.1002/cphy.c130040.

Srinivas S, Goldberg MR, Watanabe T, D'Agati V, al- Awqati Q. and Costantini F. (1999a). Expression of green fluorescent protein in the ureteric bud of transgenic mice: a new tool for the analysis of ureteric bud morphogenesis. *Dev Genet.* 24:241–251.

Srinivas S, Wu Z, Chen CM, D'Agati V, and Costantini F. (1999b). Dominant effects of RET receptor misexpression and ligand-independent RET signaling on ureteric bud development. *Development* 126, 1375-1386.

Steinberg, M.S. (2007). Differential adhesion in morphogenesis: a modern view. *Curr. Opin. Genet*. Dev. 17, 281–286.

Strutz F, Okada H, Lo CW, Danoff T, Carone RL, Tomaszewski JE, Neilson EG. (1995). Identification and characterization of a fibroblast marker—Fsp1. *J Cell Biol*. 130:393–405

Takahashi, M. (2001). The GDNF/RET signaling pathway and human diseases. *Cytokine Growth Factor Rev*. 12:361-373.

Tang M-J, Worley D, Sanicola M, Dressler GR. (1998). The RET–Glial Cell-derived Neurotrophic Factor (GDNF) Pathway Stimulates Migration and Chemoattraction of Epithelial Cells . *The Journal of Cell Biology*. 1998;142(5):1337-1345.

Timoshenko OS, Gureeva TA, Kugaevskaia EV, Solov'eva NI. (2014). [Membrane type 1 matrix metalloproteinase (MT1-MMP) and the regulators of its activity as invasive factors in squamous cell cervical carcinomas]. *Biomed Khim*. 2014 Nov-Dec;60(6):683-8.

Toth M, Hernandez-Barrantes S, Osenkowski P, Bernardo MM, Gervasi DC, Shimura Y, Meroueh O, Kotra LP, Gálvez BG, Arroyo AG, Mobashery S, Fridman R. (2002). Complex pattern of membrane type 1 matrix metalloproteinase shedding. Regulation by autocatalytic cells surface inactivation of active enzyme. *J Biol Chem*. 2002 Jul 19;277(29):26340-50. Epub 2002 May 9.

Uetani N, Bouchard M. (2009). Plumbing in the embryo: developmental defects of the urinary tracts. *Clin Genet*. 2009 Apr; 75(4):307-17.

van Weering, D. H., and J. L. Bos. (1998). Signal transduction by the receptor tyrosine kinase Ret. *Recent Results Cancer Res*. 154:271-281

Vega QC, Worby CA, Lechner MS, Dixon JE, Dressler GR. (1996). Glial cell line-derived neurotrophic factor activates the receptor tyrosine kinase RET and promotes kidney morphogenesis. *Proceedings of the National Academy of Sciences of the United States of America*. 1996;93(20):10657-10661.

Vu T, Werb Z. (2000). Matrix metalloproteinases: effectors of development and normal physiology. *Genes & Dev.* 2000 14: 2123-2133. doi:10.1101/gad.815400

Watanabe K, Ueno M, Kamiya D et al. (2007) A ROCK inhibitor permits survival of dissociated human embryonic stem cells. *Nat Biotechnol.* 2007; 25: 681–686.

Watanabe T, Costantini F. (2004) Real-time analysis of ureteric bud branching morphogenesis in vitro. *Dev Biol* 271:98–108.

Weiss AC, Airik R, Bohnenpoll T, Greulich F, Foik A, Trowe MO, Rudat C, Costantini F, Adams RH, Kispert A. (2014) Nephric duct insertion requires EphA4/EphA7 signaling from the pericloacal mesenchyme. Development. 2014 Sep;141(17):3420-30. doi: 10.1242/dev.113928.

Xia Y, Nivet E, Sancho-Martinez I, Gallegos T, Suzuki K, Okamura D, Wu MZ, Dubova I, Esteban CR, Montserrat N, Campistol JM, Izpisua Belmonte JC. (2013). Directed differentiation of human pluripotent cells to ureteric bud kidney progenitor-like cells. *Nat Cell Biol*. 2013 Dec;15(12):1507-15. doi: 10.1038/ncb2872. Epub 2013 Nov 17.

Xinaris C, Benedetti V, Rizzo P, Abbate M, Corna D, Azzollini N, Conti S, Unbekandt M, Davies JA, Morigi M, Benigni A, Remuzzi G. (2012). In vivo maturation of functional renal organoids formed from embryonic cell suspensions. *J Am Soc Nephrol*. 2012 Nov;23(11):1857-68. doi: 10.1681/ASN.2012050505. Epub 2012 Oct 18.

Zhang X, Ibrahimi OA, Olsen SK, Umemori H, Mohammadi M, Ornitz DM. (2006). Receptor specificity of the fibroblast growth factor family. The complete mammalian FGF family. *J Biol Chem*. 2006;281:15694–15700.

Zhao H, Kegg H, Grady S, Truong HT, Robinson ML, Baum M, Bates CM. (2004). Role of fibroblast growth factor receptors 1 and 2 in the ureteric bud. *Dev Biol.* 2004 Dec 15; 276(2):403-15.

Zong H, Espinosa JS, Su HH, Muzumdar MD, Luo L. (2005). Mosaic analysis with double markers in mice. Cell. 2005;121:479–492.

Appendix A - Catalogue of tips and trunks and their color histograms (randomized subset). Refer to Experimental Procedures Chapter 3 for more detailed methods. Tips were catalogued in blue, trunk regions were catalogued in yellow. For each chimeric culture 30 tip regions and 30 trunks regions analyzed took the shape of 40-micron wide circles (208 pixels in total; Refer to page … for an example), and histograms were created for each region using ImageJ (channels were analyzed separately) and these histograms are shown here. Background control regions were chosen in areas containing the highest nonspecific fluorescence in each culture. "Green Pixels" or "Red Pixels" refers to the number of pixels with an intensity above all the pixels in the background control region probed. "G/R" is the Green:Red pixel ratio and "R/G" is the Red:Green pixel ratio. Includes *Spry1*$^{-/-}$⇔WT, *Ret*$^{51/cre}$⇔WT, *Fgfr2*$^{UB-/-}$⇔WT, and WT⇔WT cultures.

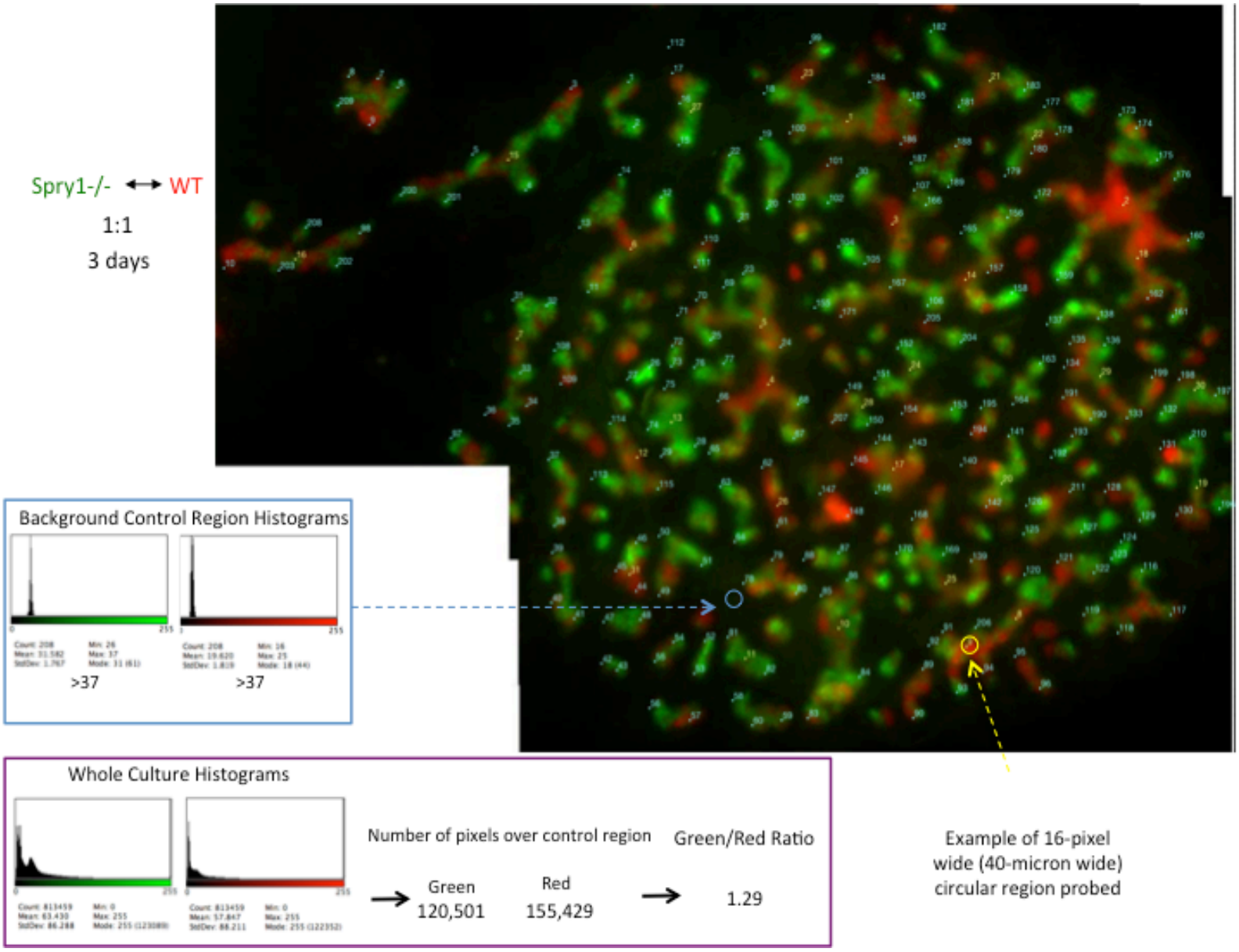
Spry1-/- ↔ WT
1:1
3 days
Background Control Region Histograms
>37
>37
Whole Culture Histograms
Number of pixels over control region
Green/Red Ratio
Green
120,501
Red
155,429
1.29
Example of 16-pixel wide (40-micron wide) circular region probed

Tip	Green Histogram	Red Histogram	Green Pixels	Red Pixels	G/R
6	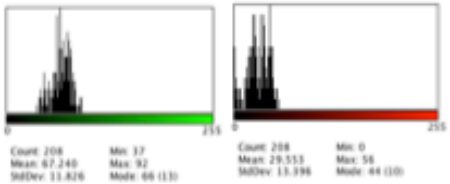		207	55	3.76
7	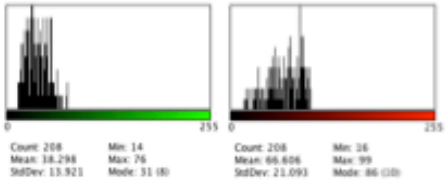		94	180	0.52
13	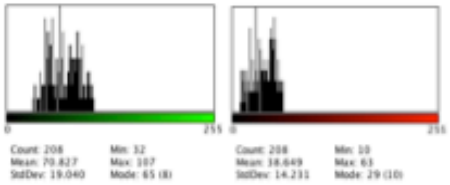		200	106	1.89
14	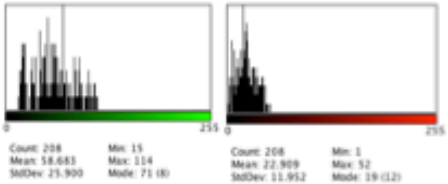		157	24	6.54
18	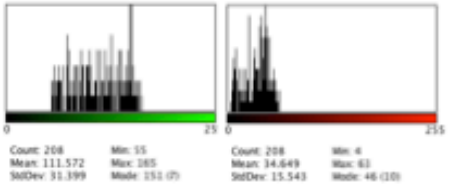		208	95	2.19

Tip	Green Histogram	Red Histogram	Green Pixels	Red Pixels	G/R
39	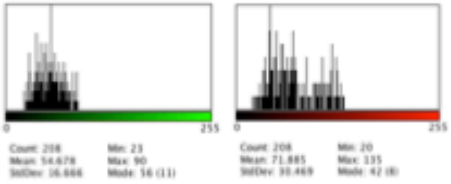		162	183	0.89
50	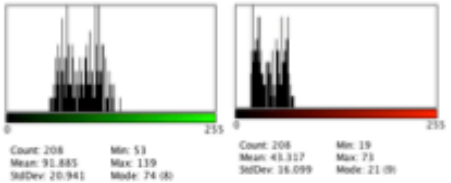		208	116	1.79
51	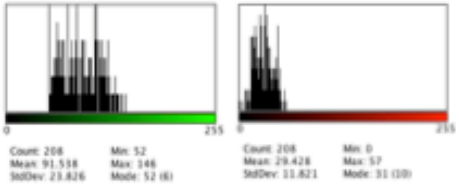		208	46	4.52
57	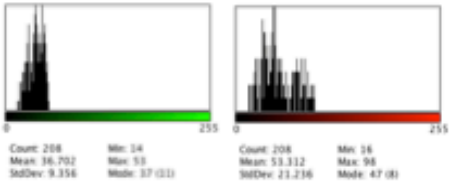		88	143	0.62
59	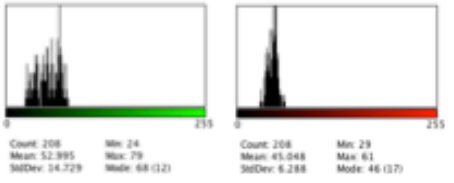		156	163	0.96

Spry1-/- ↔ WT (Tips)

Tip	Green Histogram	Red Histogram	Green Pixels	Red Pixels	G/R
63	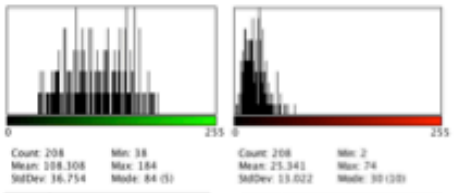		206	26	7.92
70	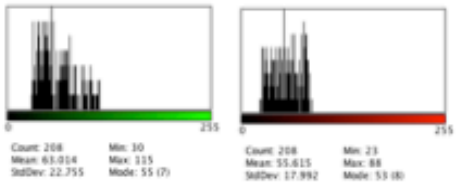		176	157	1.12
72	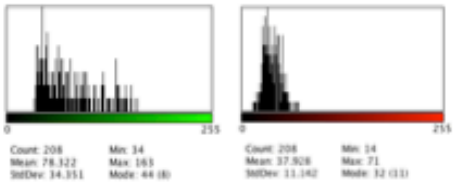		192	87	2.21
77	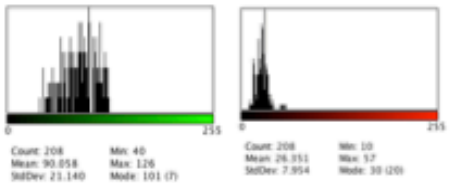		208	9	23.11
90	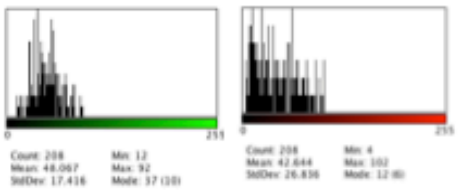		139	103	1.35

Tip	Green Histogram	Red Histogram	Green Pixels	Red Pixels	G/R
98	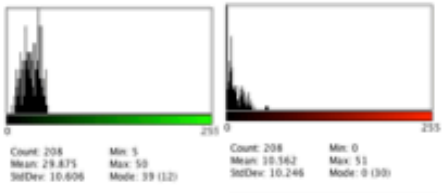		46	4	11.50
109	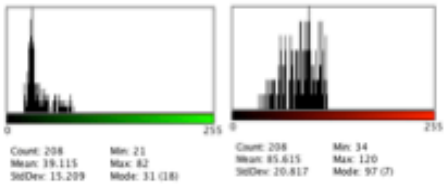		67	206	0.33
110	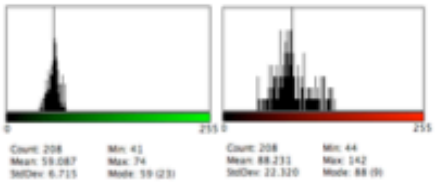		83	166	0.50
128	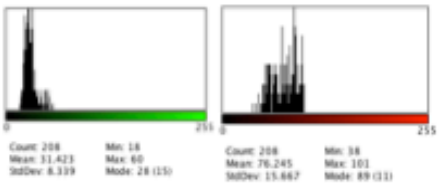		29	207	0.14
136	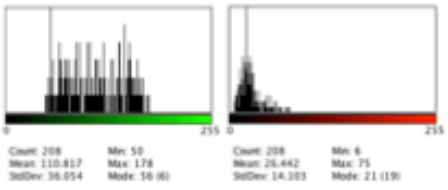		208	34	6.12

Spry1-/- ↔ WT (Tips)

Tip	Green Histogram	Red Histogram	Green Pixels	Red Pixels	G/R
149	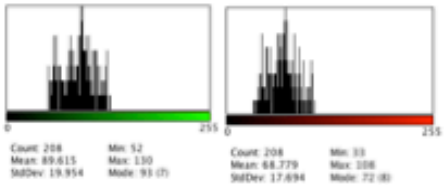		208	201	1.03
156	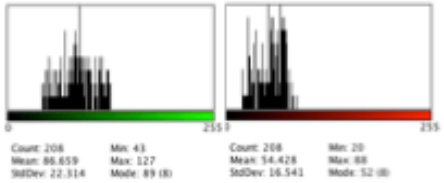		208	160	1.30
158	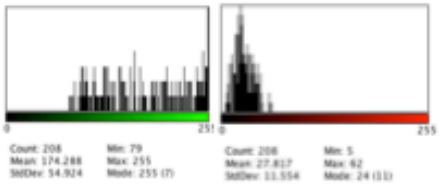		208	36	5.78
161	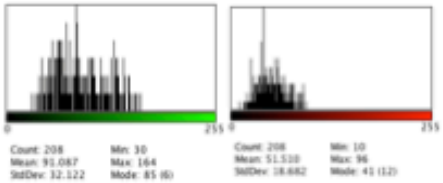		204	149	1.37
181	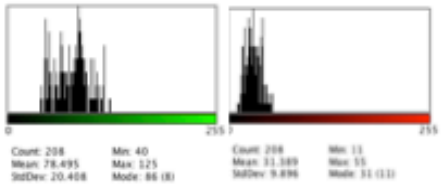		208	51	4.08

Tip	Green Histogram	Red Histogram	Green Pixels	Red Pixels	G/R
191	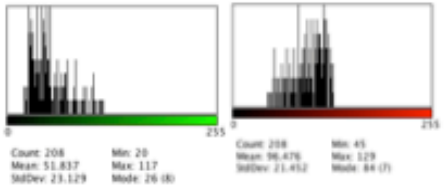		133	208	0.64
194	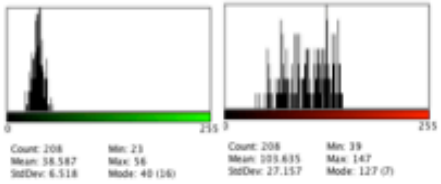		93	207	0.45
197	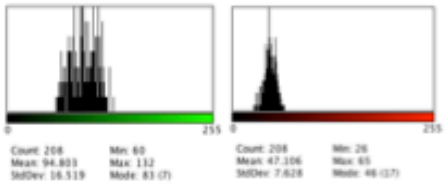		208	176	1.18
207	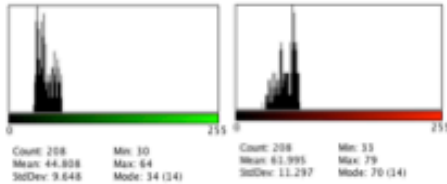		130	202	0.64
211	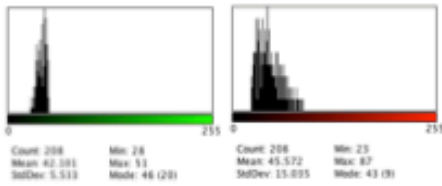		139	125	1.11

Spry1-/- ↔ WT (Tips)

Trunk	Green Histogram	Red Histogram	Green Pixels	Red Pixels	G/R
1	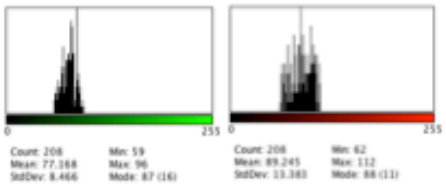		208	208	1.00
2	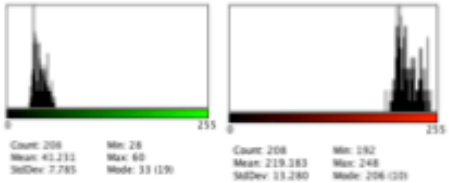		110	208	0.53
3	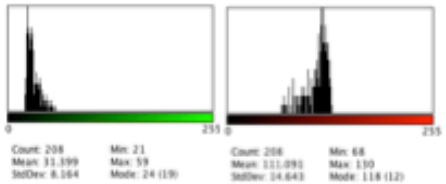		33	208	0.16
4	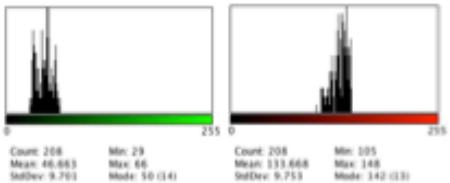		148	208	0.71
5	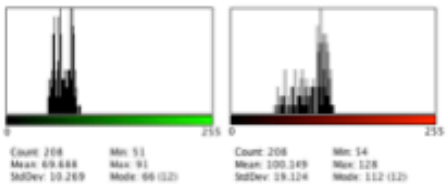		208	208	1.00

Trunk	Green Histogram	Red Histogram	Green Pixels	Red Pixels	G/R
6	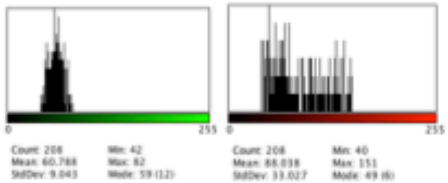		208	208	1.00
7	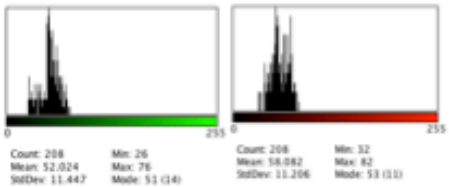		174	197	0.88
8	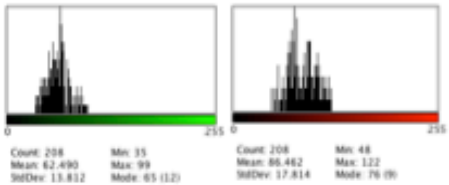		201	208	0.97
9	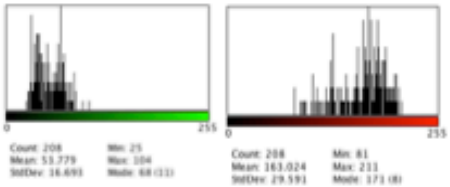		152	208	0.73
10	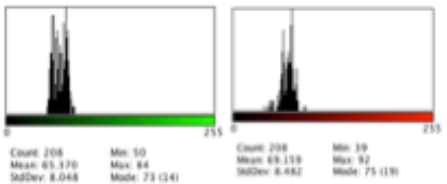		208	207	1.00

Spry1-/- ↔ WT (Trunks)

Trunk	Green Histogram	Red Histogram	Green Pixels	Red Pixels	G/R
11	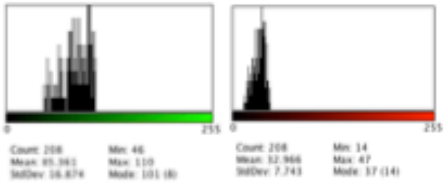		208	46	4.52
12	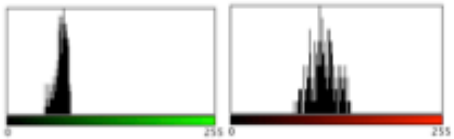		208	208	1.00
13	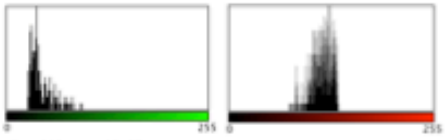		97	208	0.47
14	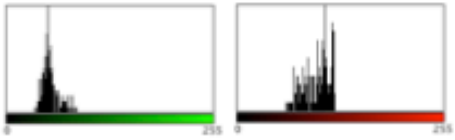		202	208	0.97
15	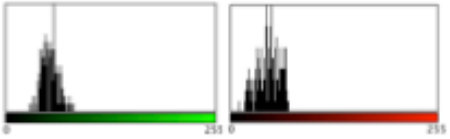		143	197	0.73

Trunk	Green Histogram	Red Histogram	Green Pixels	Red Pixels	G/R
16	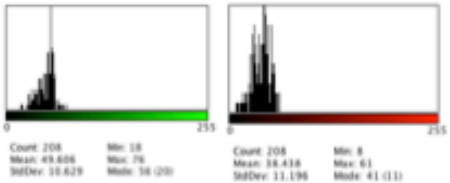		169	109	1.55
17	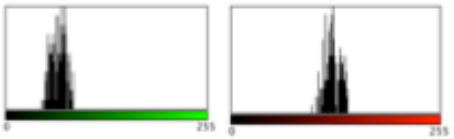		208	208	1.00
18	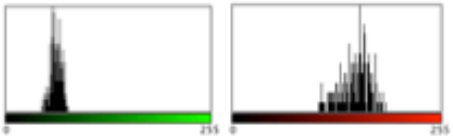		208	208	1.00
19	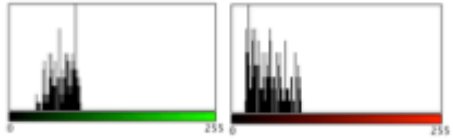		202	112	1.80
20	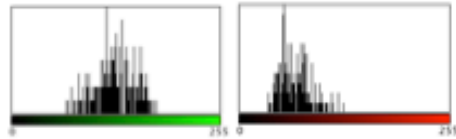		208	204	1.02

Spry1-/- ↔ WT (Trunks)

Trunk	Green Histogram	Red Histogram	Green Pixels	Red Pixels	G/R
21	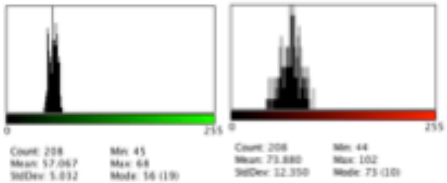		208	208	1.00
22	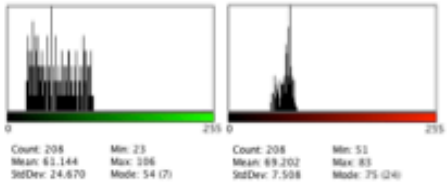		153	208	0.74
23	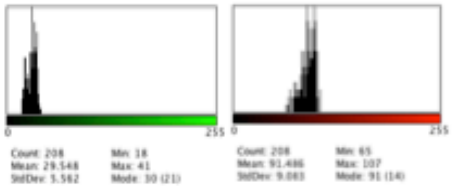		2	208	0.01
24	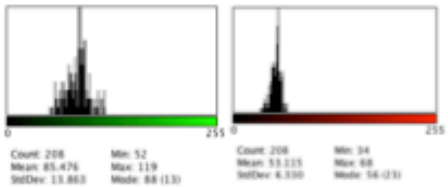		208	200	1.04
25	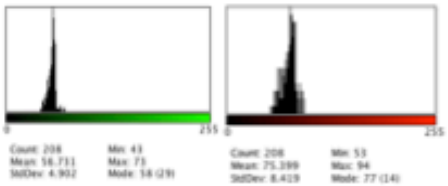		208	208	1.00

Trunk	Green Histogram	Red Histogram	Green Pixels	Red Pixels	G/R
26	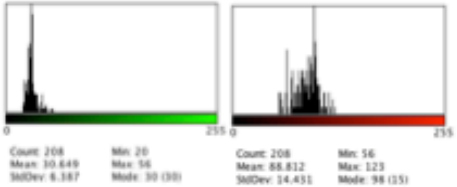		20	208	0.10
27	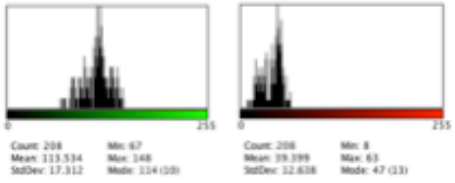		208	122	1.70
28	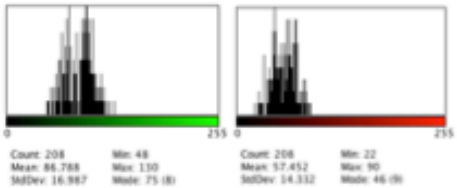		208	186	1.12
29	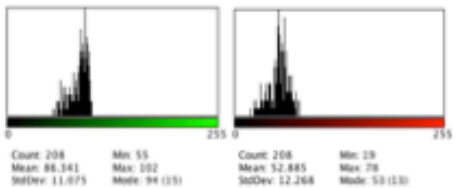		208	175	1.19
30	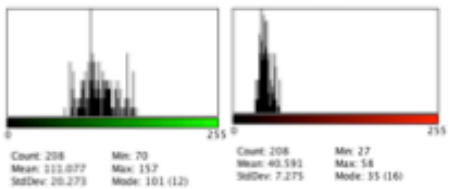		208	107	1.94

Spry1-/- ↔ WT (Trunks)

WT ↔ WT

1:1

3 days

Background Control Region Histograms

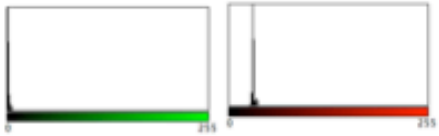

>37 >37

Whole Culture Histograms

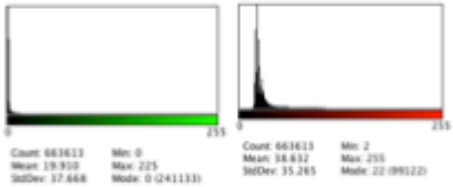

Number of pixels
over control region

Green	Red
129,999	139,990

Green/Red Ratio

0.929

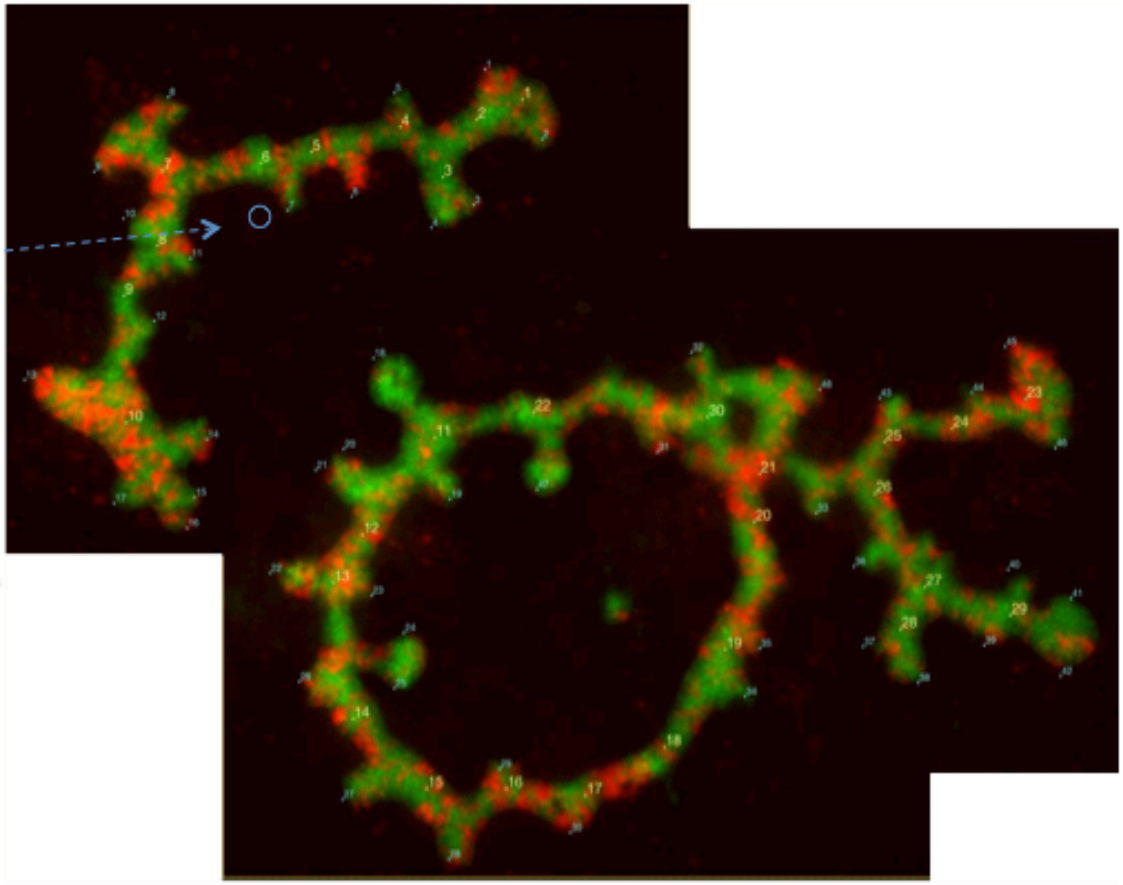

Tip	Green Histogram	Red Histogram	Green Pixels	Red Pixels	G/R
1	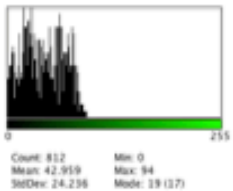	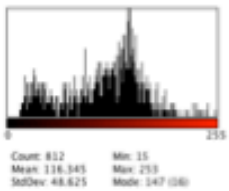	111	185	0.60
2	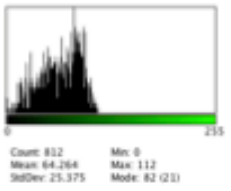	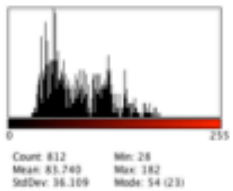	168	193	0.87
4	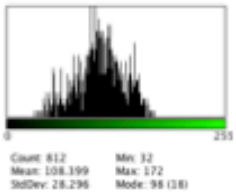	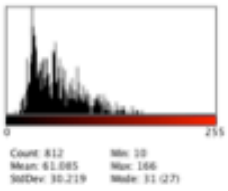	207	145	1.43
5	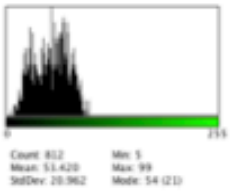	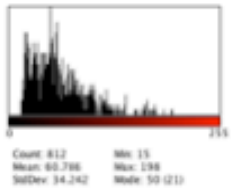	147	145	1.01
7	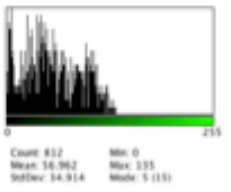	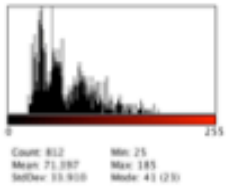	137	172	0.80

Tip	Green Histogram	Red Histogram	Green Pixels	Red Pixels	
9	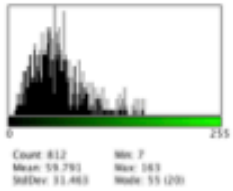	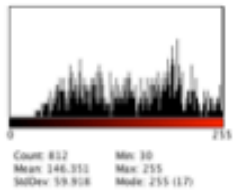	152	206	0.74
14	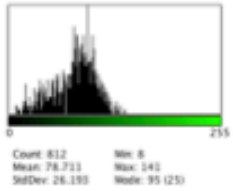	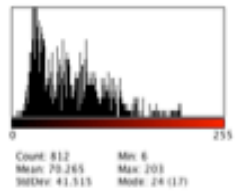	187	140	1.33
15	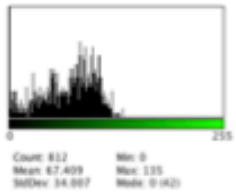	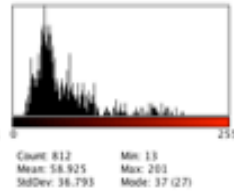	161	134	1.20
16	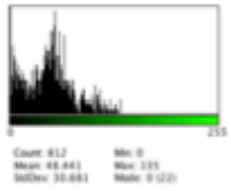	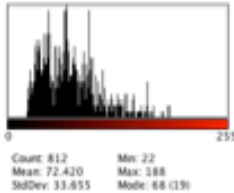	130	173	0.75
18	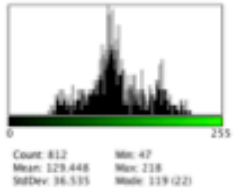	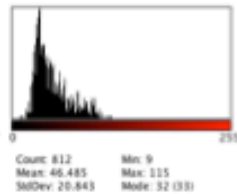	208	107	1.95

WT ↔ WT (Tips)

Tip	Green Histogram	Red Histogram	Green Pixels	Red Pixels	G/R
20	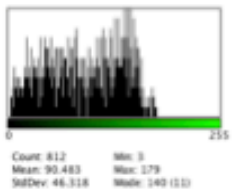	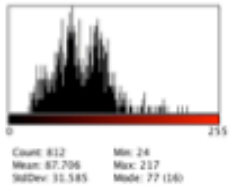	171	196	0.87
22	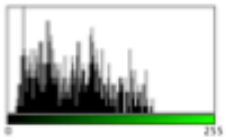	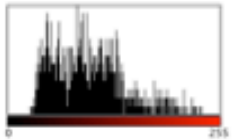	163	197	0.83
23	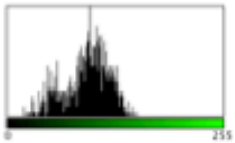	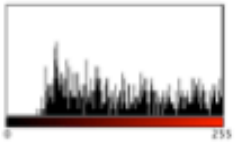	202	208	0.97
24	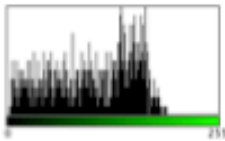	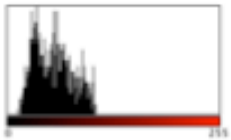	174	140	1.24
25	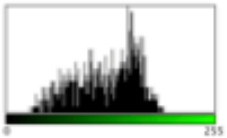	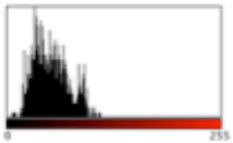	205	141	1.46

Tip	Green Histogram	Red Histogram	Green Pixels	Red Pixels	
26	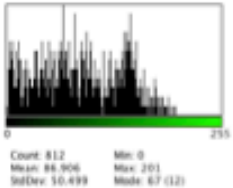	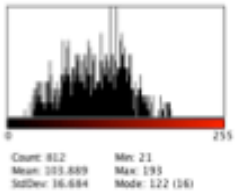	164	198	0.83
28	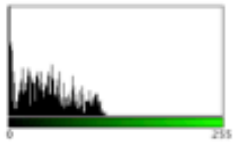	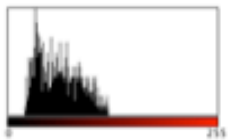	103	153	0.67
29	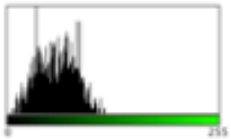	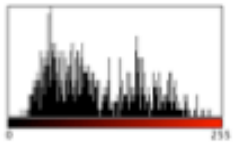	158	192	0.82
32	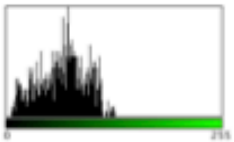	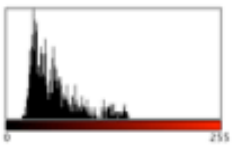	166	138	1.20
33	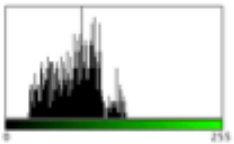	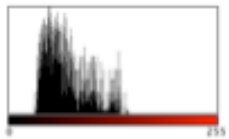	192	193	0.99

WT ↔ WT (Tips)

Tip	Green Histogram	Red Histogram	Green Pixels	Red Pixels	G/R
34	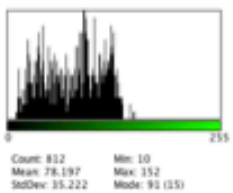	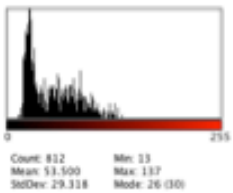	168	116	1.45
36	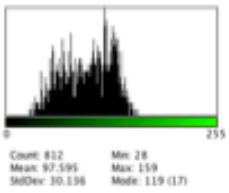	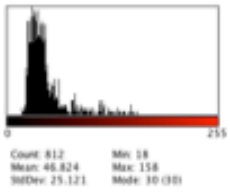	204	104	1.96
37	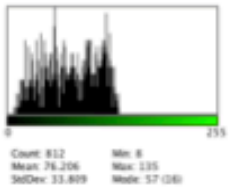	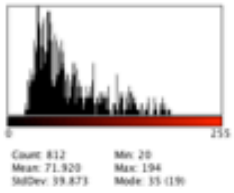	172	164	1.05
38	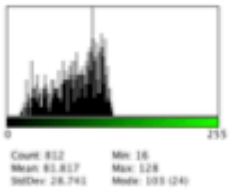	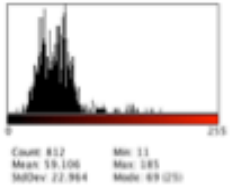	183	170	1.08
40	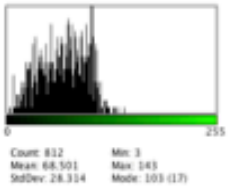	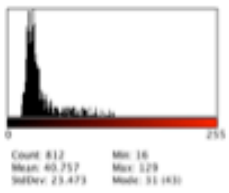	169	63	2.70

Tip	Green Histogram	Red Histogram	Green Pixels	Red Pixels	
42	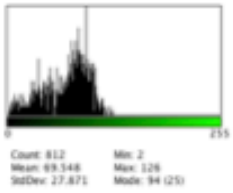	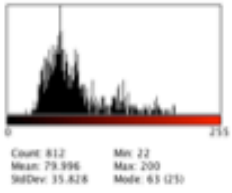	169	199	1.45
43	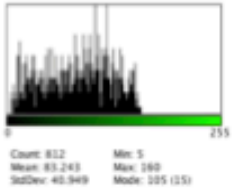	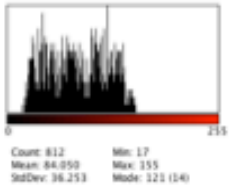	168	180	1.96
45	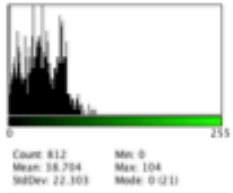	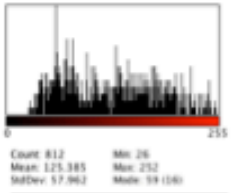	74	202	1.05
46	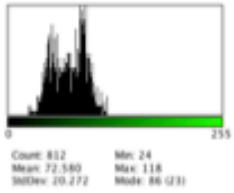	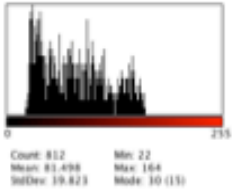	201	166	1.08
48	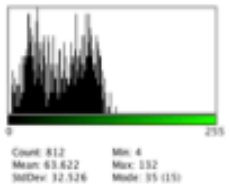	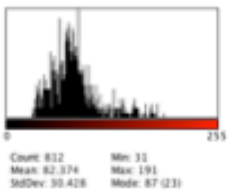	143	201	2.70

WT ↔ WT (Tips)

Tip	Green Histogram	Red Histogram	Green Pixels	Red Pixels	G/R
1	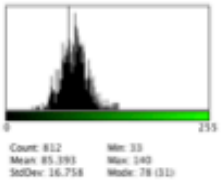	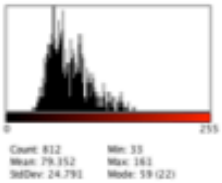	207	206	1.00
2	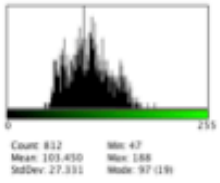	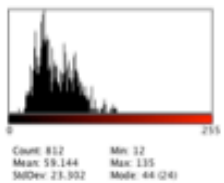	208	164	1.27
3	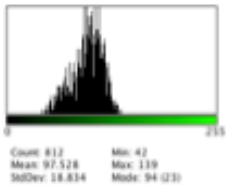	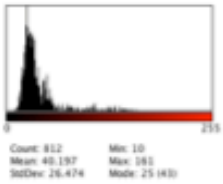	208	62	3.34
4	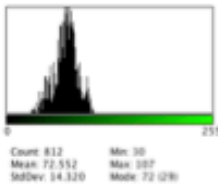	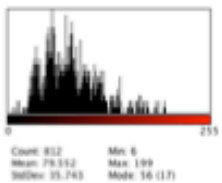	205	182	1.13
5	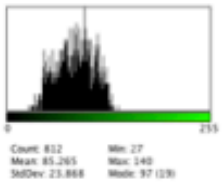	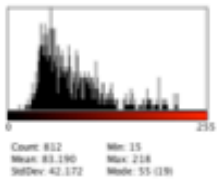	204	195	1.05

Tip	Green Histogram	Red Histogram	Green Pixels	Red Pixels	G/R
6	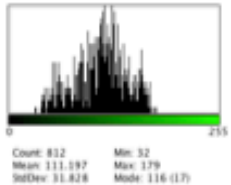	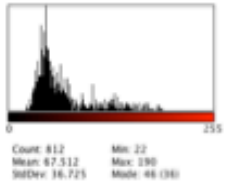	207	175	1.18
7	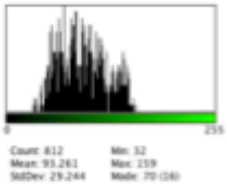	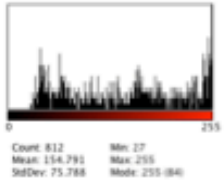	206	199	1.04
8	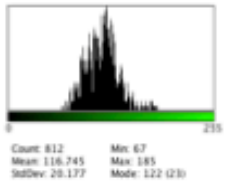	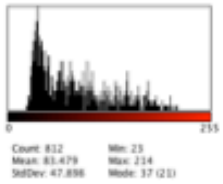	208	164	1.27
9	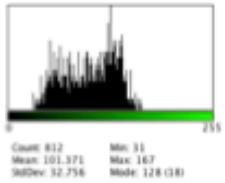	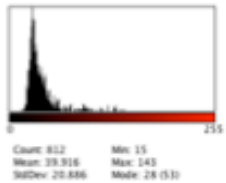	205	67	3.05
10	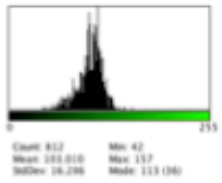	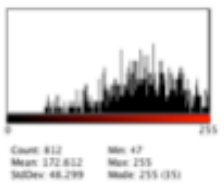	208	208	1.00

WT ↔ WT (Trunks)

Tip	Green Histogram	Red Histogram	Green Pixels	Red Pixels	G/R
11	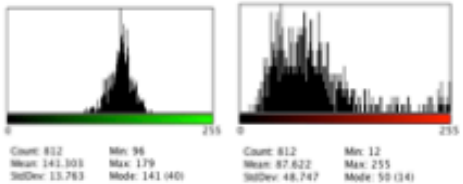		208	186	1.12
12	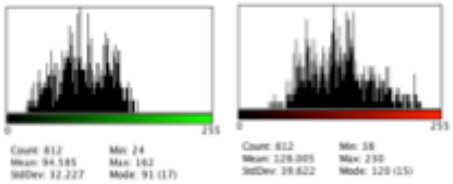		200	208	0.96
13	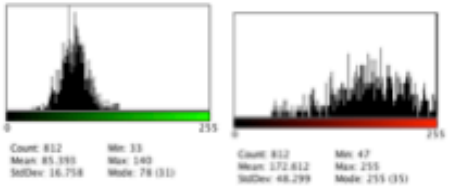		208	208	1.00
14	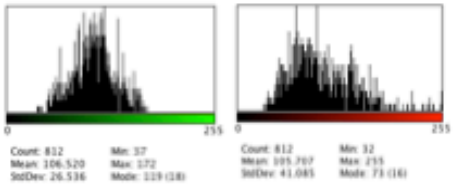		207	206	1.01
15	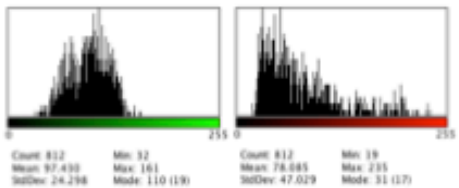		207	164	1.26

Tip	Green Histogram	Red Histogram	Green Pixels	Red Pixels	G/R
16	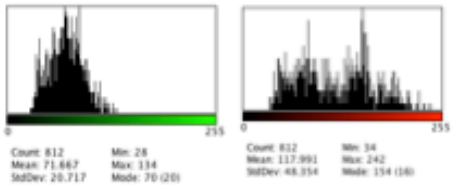		193	205	0.94
17	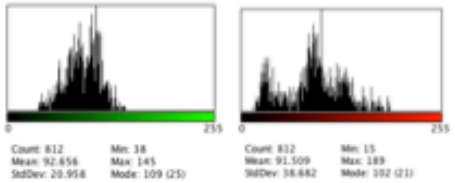		207	177	1.17
18	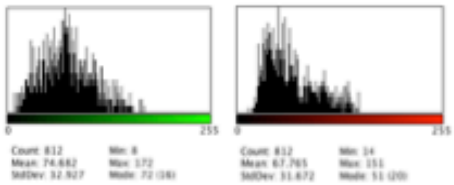		175	165	1.06
19	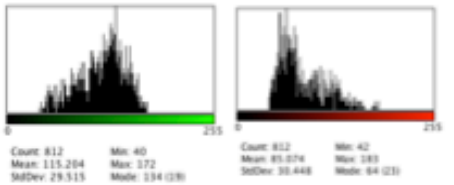		208	208	1.00
20	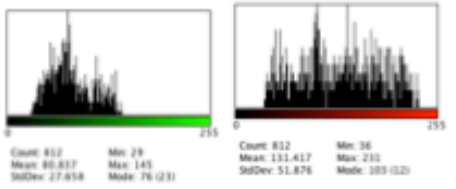		200	206	0.97

WT ↔ WT (Trunks)

Tip	Green Histogram	Red Histogram	Green Pixels	Red Pixels	G/R
21	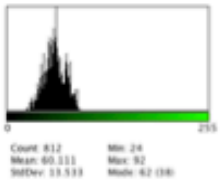	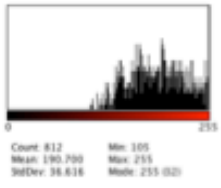	194	208	0.93
22	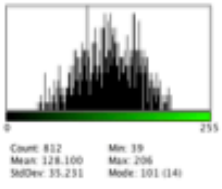	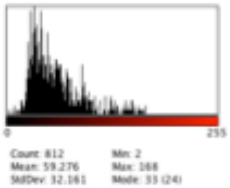	208	141	1.47
23	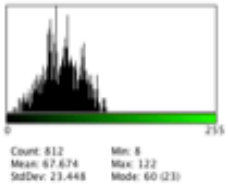	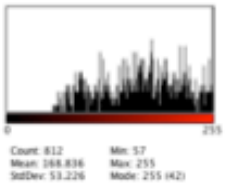	183	208	0.88
24	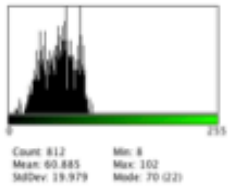	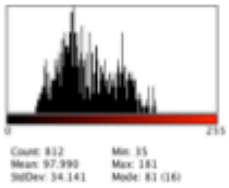	171	206	0.83
25	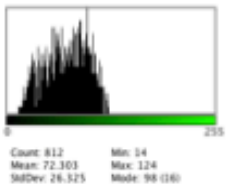	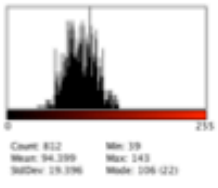	178	208	0.86

Tip	Green Histogram	Red Histogram	Green Pixels	Red Pixels	G/R
26	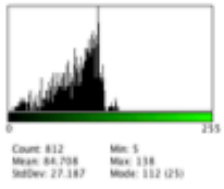	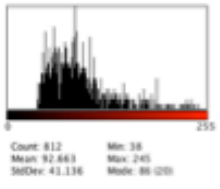	192	206	0.93
27	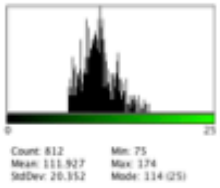	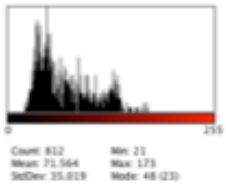	208	168	1.24
28	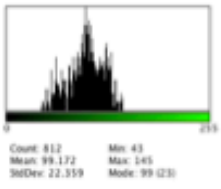	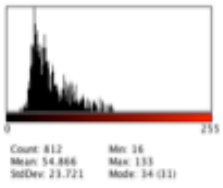	208	141	1.48
29	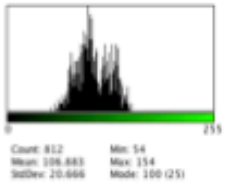	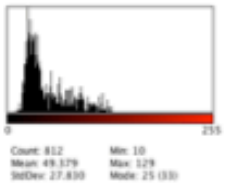	208	97	2.15
30	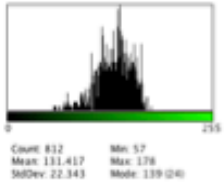	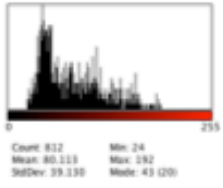	208	188	1.11

WT ↔ WT (Trunks)

Ret51/cre ↔ WT

1:1

3 days

Background Control Region Histograms

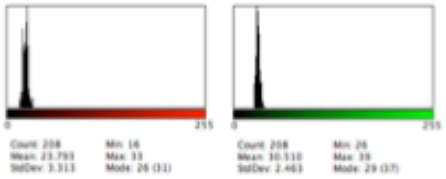

>39 >39

Whole Culture Histograms

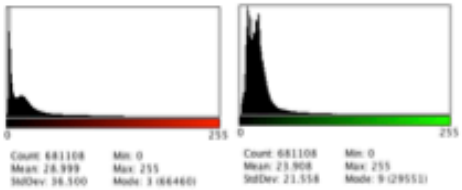

Number of pixels
over control region

Red	Green
149,379	68,464

Red/Green Ratio

2.18

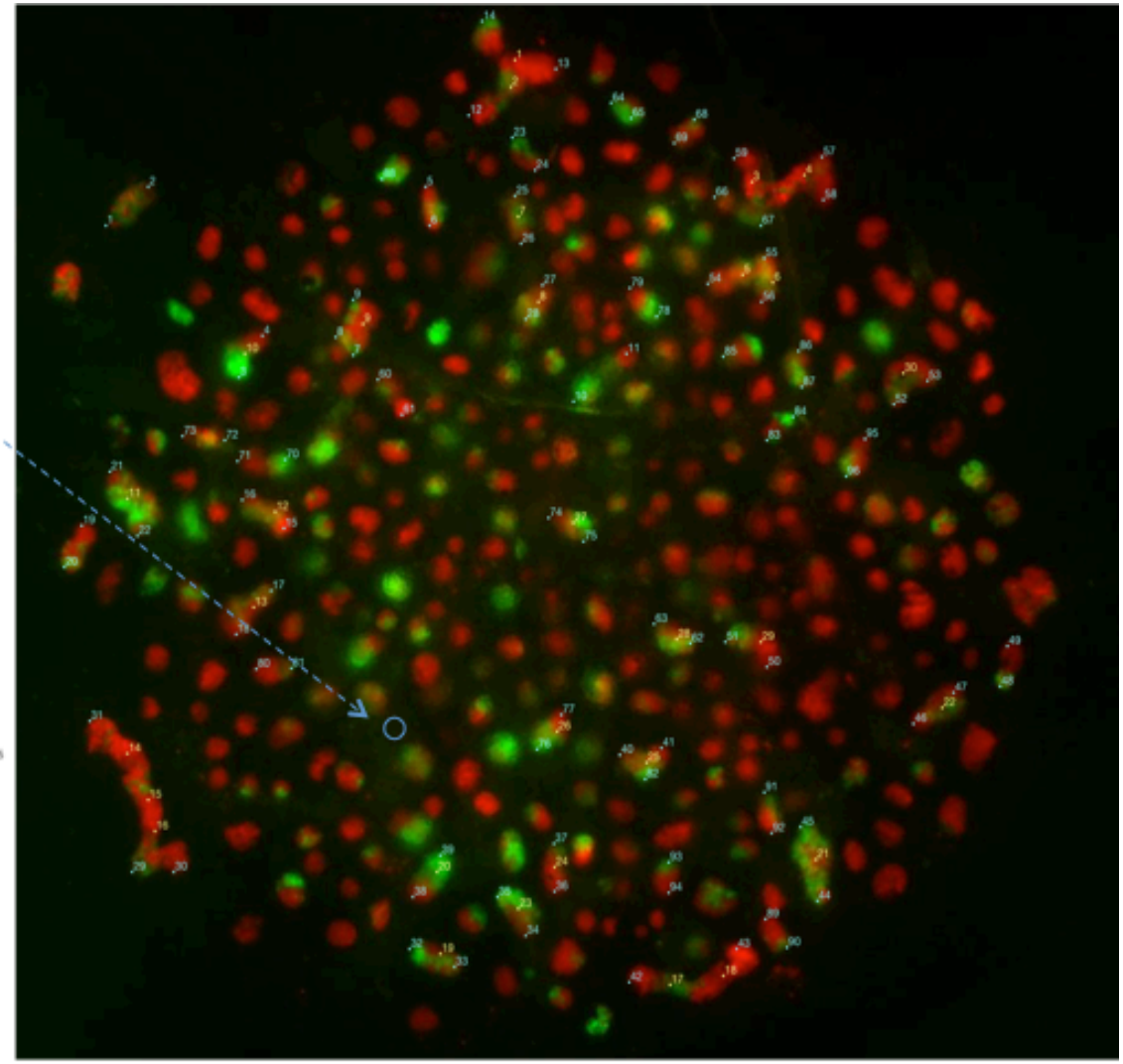

Tip	Red Histogram	Green Histogram	Red Pixels	Green Pixels	R/G
4	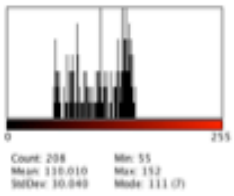	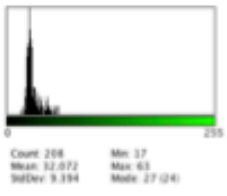	208	38	5.47
5	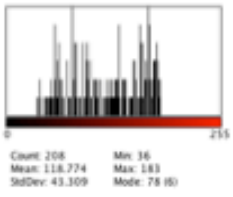	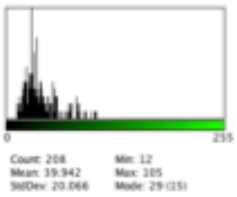	204	79	2.58
9	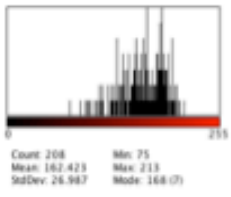	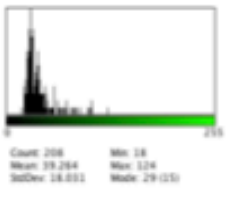	208	64	3.25
12	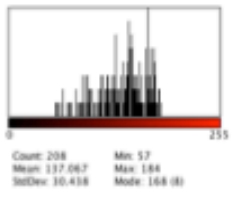	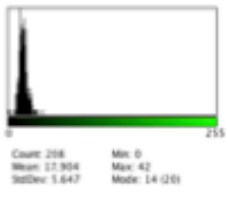	208	1	208
16	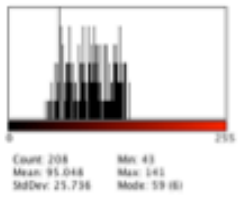	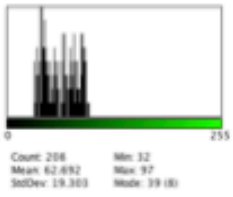	208	180	1.16

Tip	Red Histogram	Green Histogram	Red Pixels	Green Pixels	
18	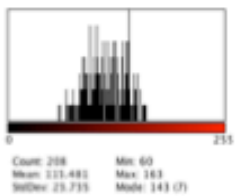	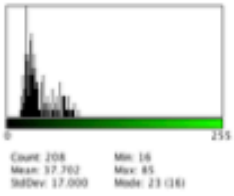	208	68	3.06
23	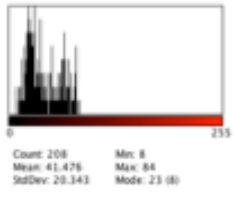	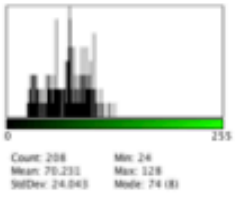	92	178	0.52
25	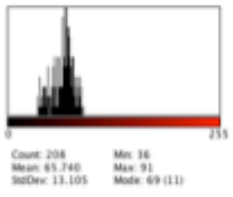	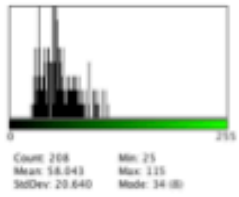	200	166	1.20
35	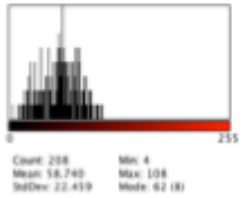	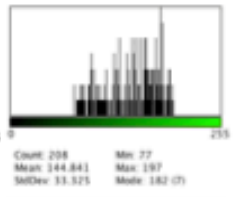	161	208	0.77
37	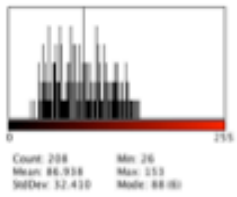	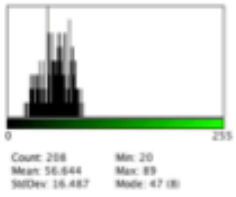	199	170	1.17

Ret51/cre ↔ WT (Tips)

Tip	Red Histogram	Green Histogram	Red Pixels	Green Pixels	R/G
38	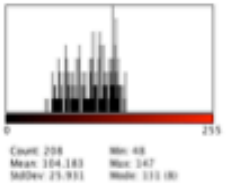	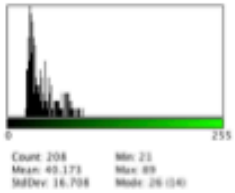	208	81	2.57
39	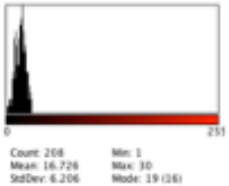	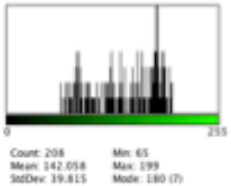	0	208	0.00
42	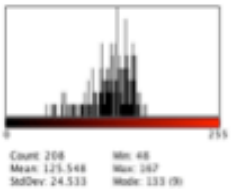	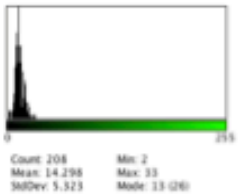	208	1	208
50	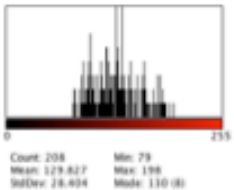	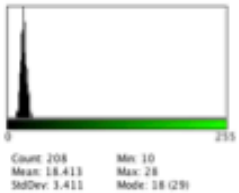	208	1	208
52	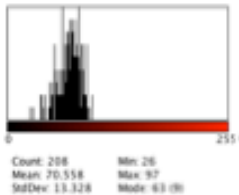	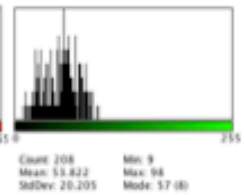	202	151	1.34

Tip	Red Histogram	Green Histogram	Red Pixels	Green Pixels	
54	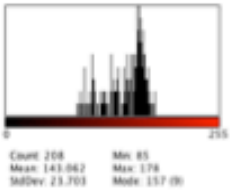	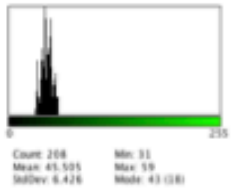	208	171	1.22
55	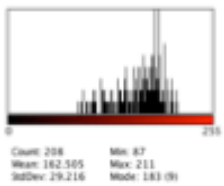	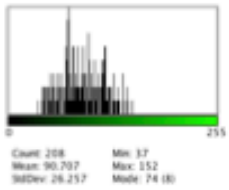	208	207	1.00
56	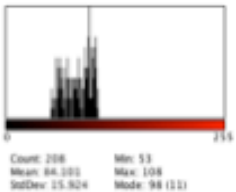	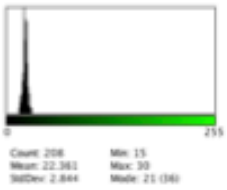	208	1	208
57	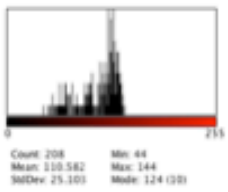	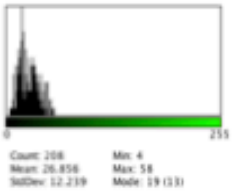	208	36	5.78
58	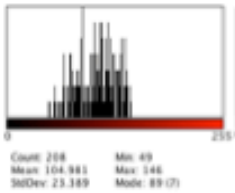	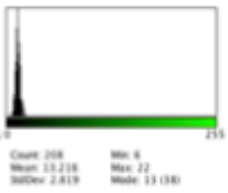	208	1	208

Ret51/cre ↔ WT (Tips)

Tip	Red Histogram	Green Histogram	Red Pixels	Green Pixels	R/G
62	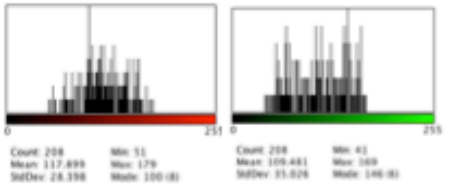		208	208	1.00
67	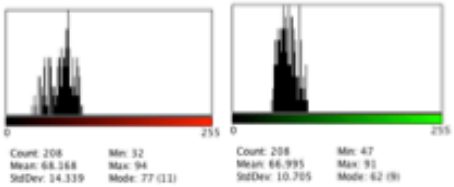		204	208	0.98
72	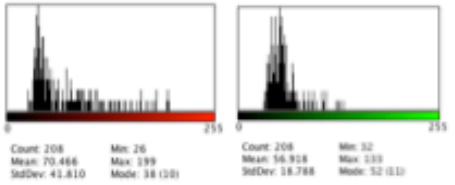		155	184	0.84
74	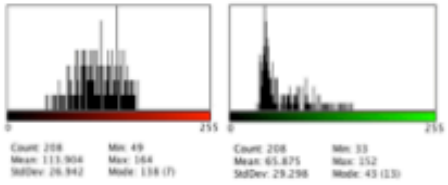		208	190	1.09
76	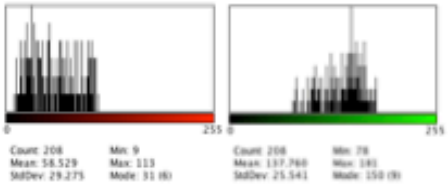		139	208	0.67

Tip	Red Histogram	Green Histogram	Red Pixels	Green Pixels	R/G
79	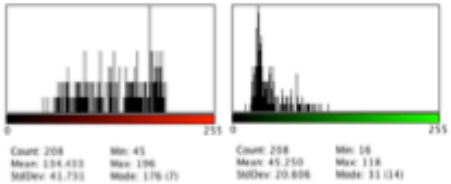		208	94	2.21
81	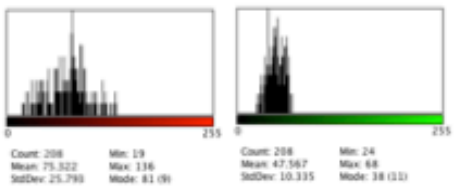		187	155	1.21
82	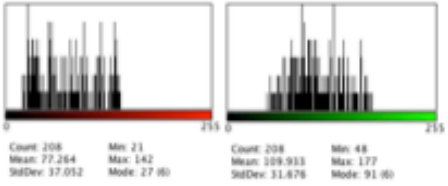		159	208	0.76
84	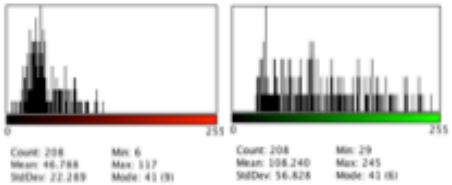		113	188	0.60
86	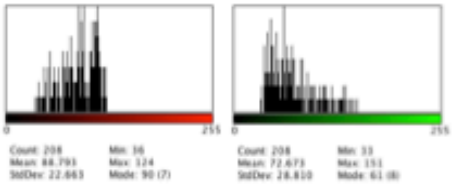		206	195	1.06

Ret51/cre ↔ WT (Tips)

Trunk	Red Histogram	Green Histogram	Red Pixels	Green Pixels	R/G
1	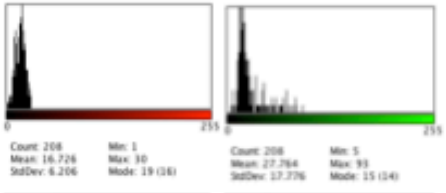		1	39	0.03
2	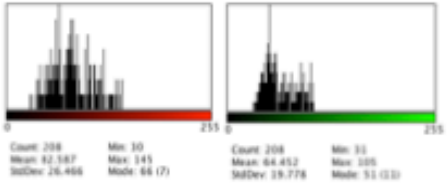		203	195	1.04
3	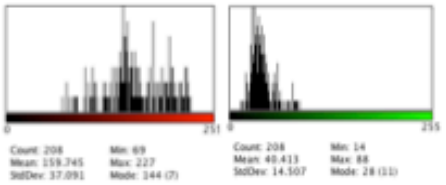		208	89	2.34
4	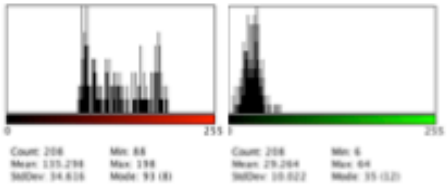		208	26	8.00
5	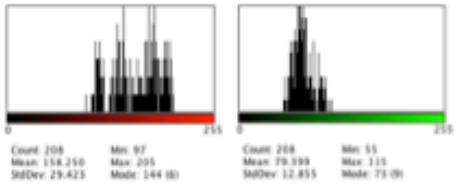		208	208	1.00

Trunk	Red Histogram	Green Histogram	Red Pixels	Green Pixels	R/G
6	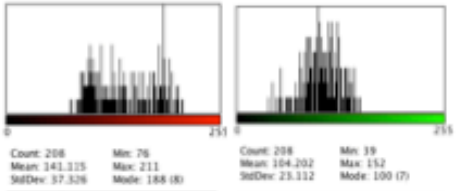		208	207	1.00
7	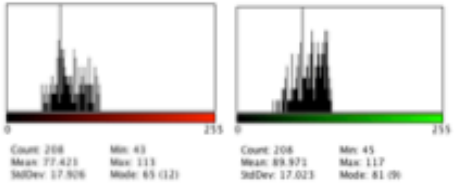		208	208	1.00
8	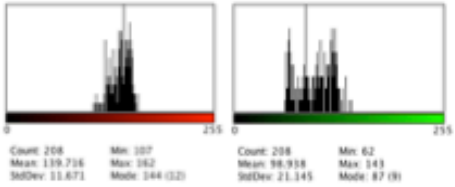		208	208	1.00
9	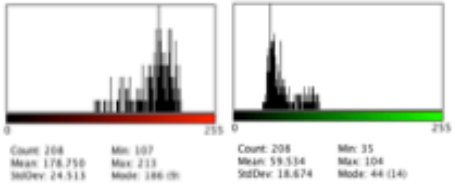		208	202	1.03
10	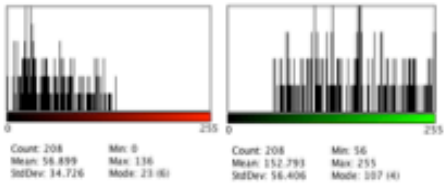		125	208	0.60

Ret51/cre ↔ WT (Trunks)

Trunk	Red Histogram	Green Histogram	Red Pixels	Green Pixels	R/G
11	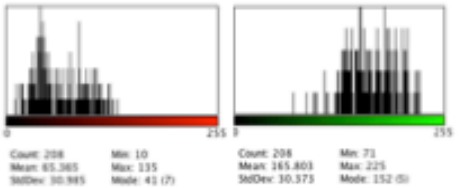		160	208	0.77
12	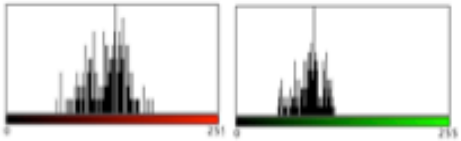		208	208	1.00
13	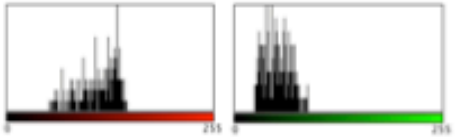		208	152	1.37
14	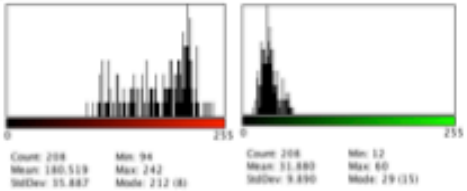		208	40	5.20
15	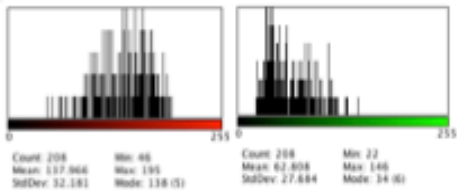		208	157	1.32

Trunk	Red Histogram	Green Histogram	Red Pixels	Green Pixels	
16	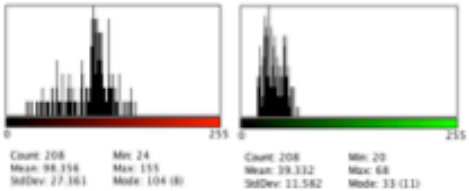		201	95	2.12
17	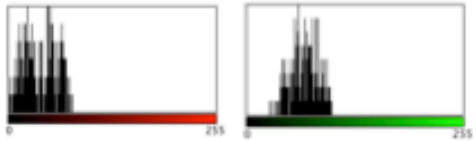		102	202	0.50
18	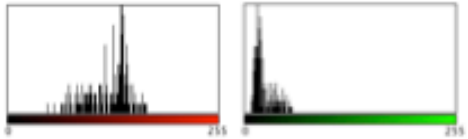		208	28	7.43
19	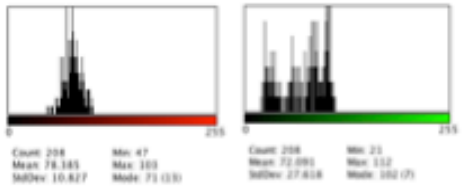		208	164	1.27
20	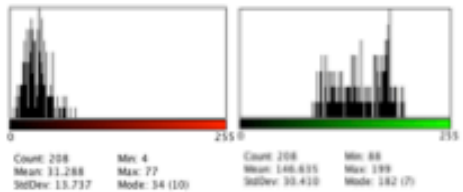		51	208	0.25

Ret51/cre ↔ WT (Trunks)

Trunk	Red Histogram	Green Histogram	Red Pixels	Green Pixels	R/G
21	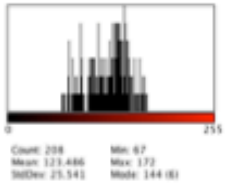	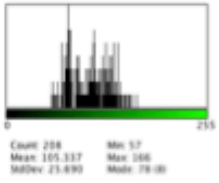	208	208	1.00
22	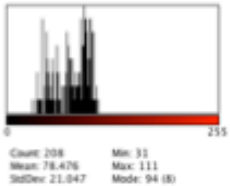	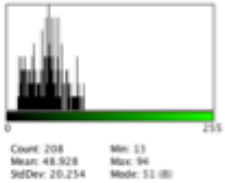	201	139	1.45
23	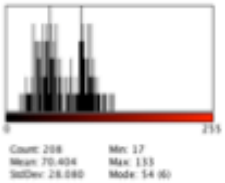	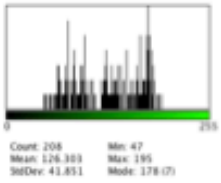	178	208	0.86
24	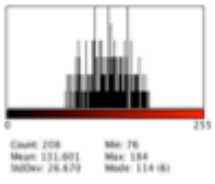	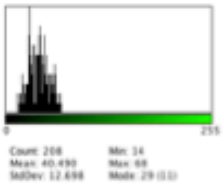	208	110	1.89
25	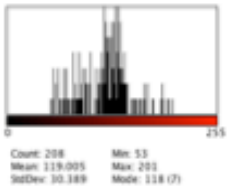	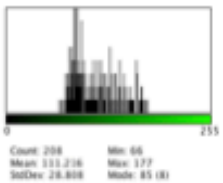	208	208	1.00

Trunk	Red Histogram	Green Histogram	Red Pixels	Green Pixels	R/G
26	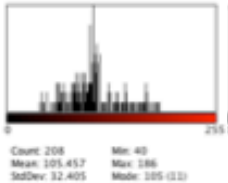	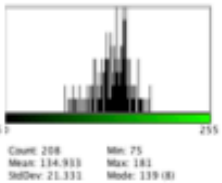	208	208	1.00
27	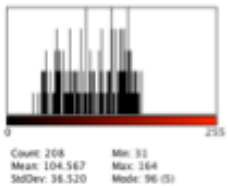	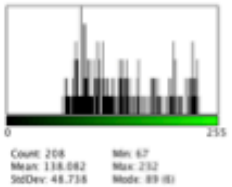	208	206	1.01
28	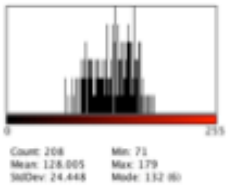	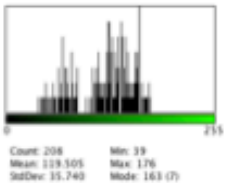	208	207	1.00
29	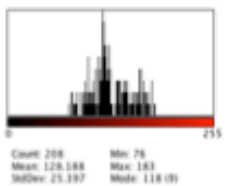	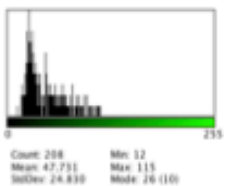	208	103	2.02
30	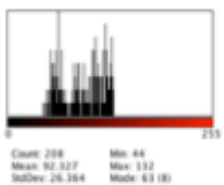	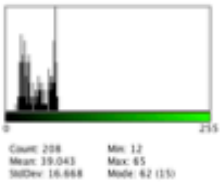	208	99	2.10

Ret51/cre ↔ WT (Trunks)

WT ⟷ WT

1:1

3 days

Background Control Region Histograms

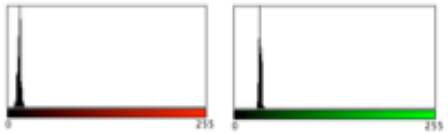

>21 >38

Whole Culture Histograms

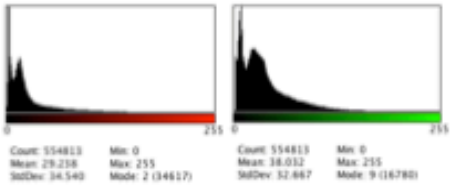

Number of pixels
over control region

Red	Green
125,146	192,546

Red/Green Ratio

.65

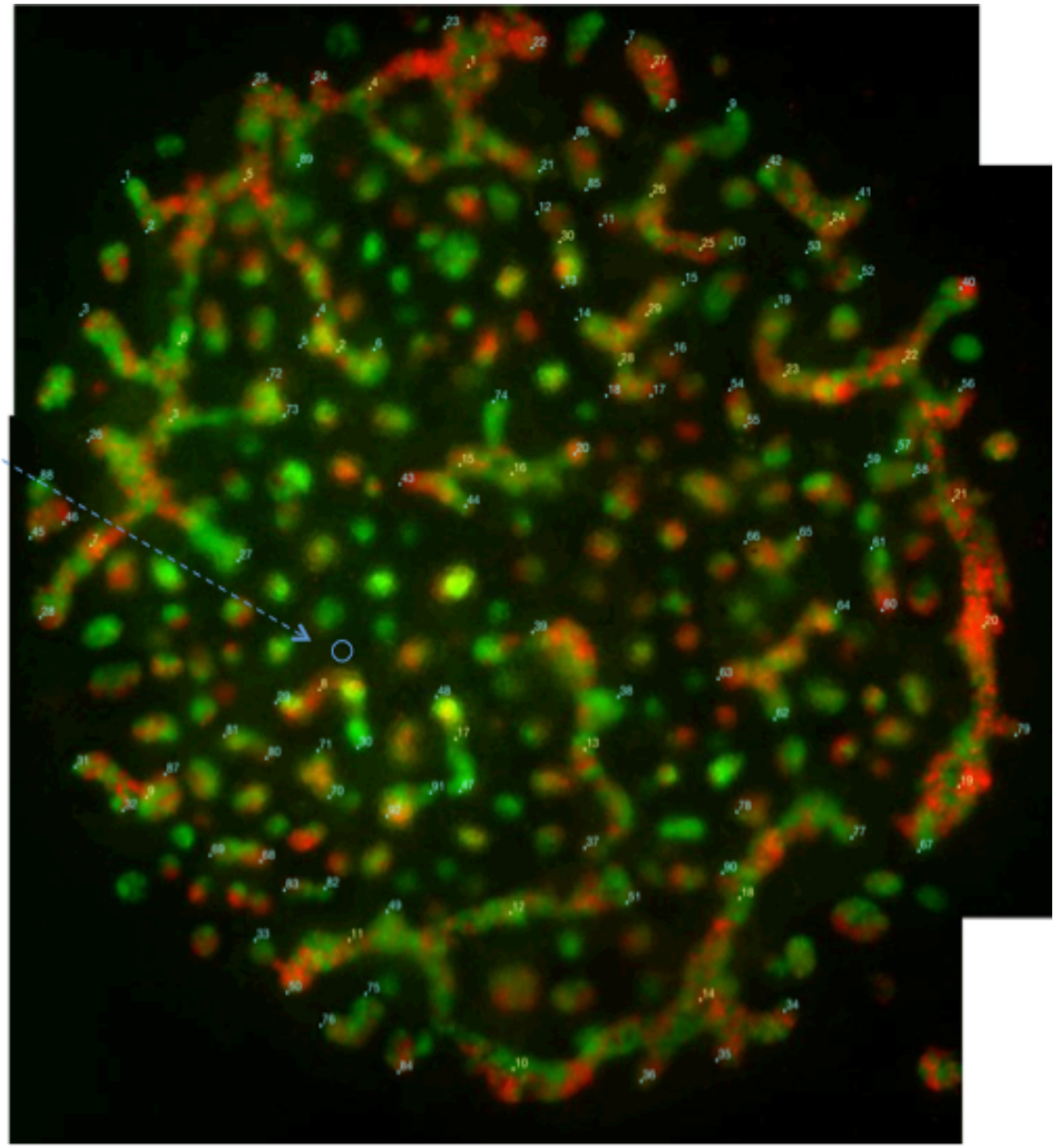

Tip	Red Histogram	Green Histogram	Red Pixels	Green Pixels	R/G
2	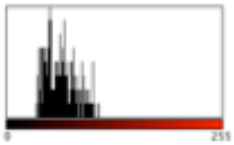	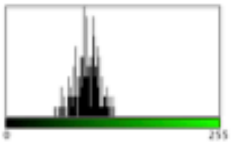	197	197	0.95
3	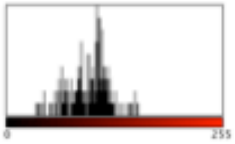	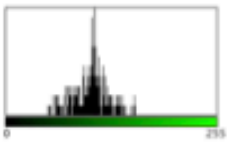	205	205	0.99
4	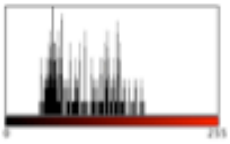	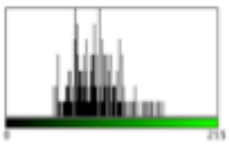	208	208	1.00
5	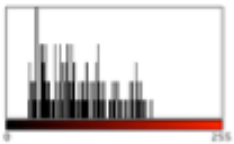	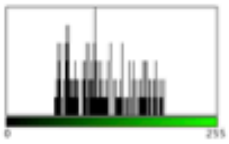	181	181	0.87
7	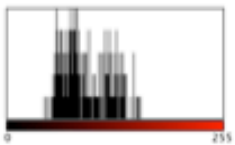	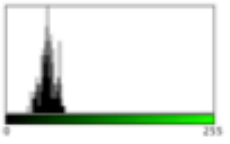	208	208	1.14

Tip	Red Histogram	Green Histogram	Red Pixels	Green Pixels	
8	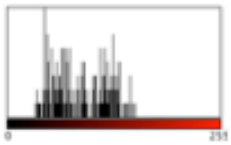	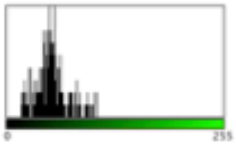	201	163	1.23
16	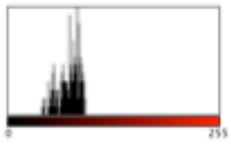		208	145	1.43
21		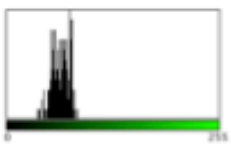	125	205	0.61
23	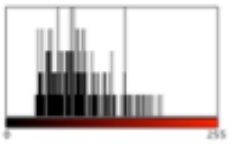	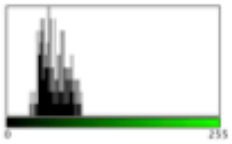	199	183	1.09
24	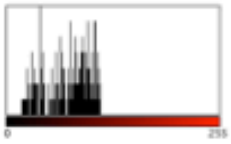	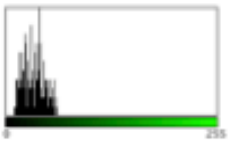	175	72	2.43

WT ↔ WT (Tips)

Tip	Red Histogram	Green Histogram	Red Pixels	Green Pixels	R/G
30	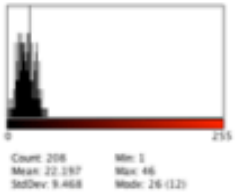	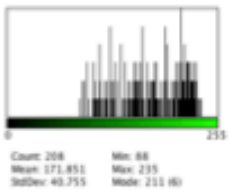	7	208	0.03
36	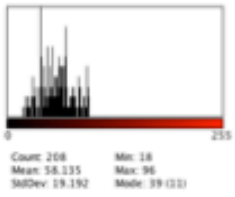	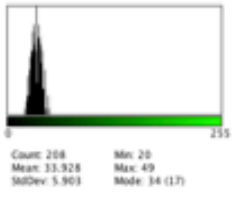	168	38	4.42
37	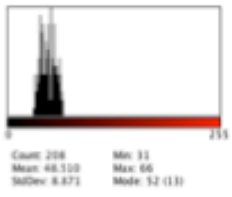	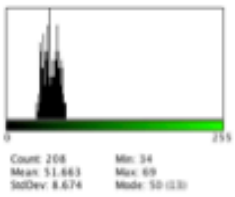	167	191	0.87
40	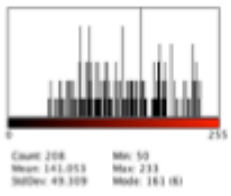	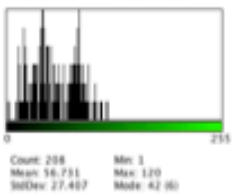	208	147	1.41
42	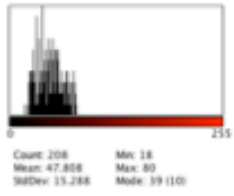	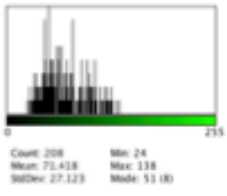	136	186	0.73

Tip	Red Histogram	Green Histogram	Red Pixels	Green Pixels	
47	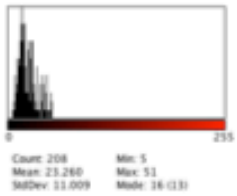	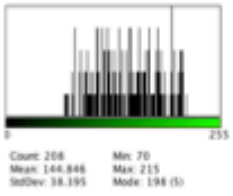	27	208	0.13
49	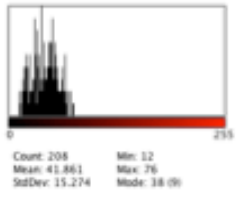	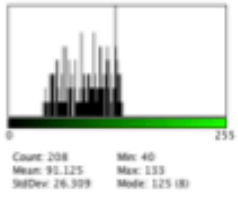	115	208	0.55
50	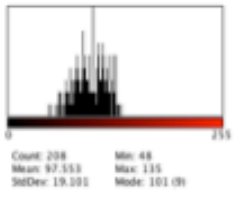	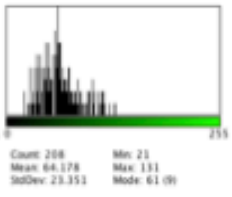	208	179	1.16
63	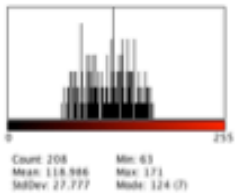	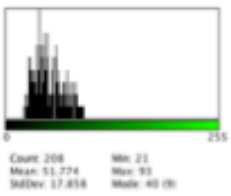	208	150	1.39
64	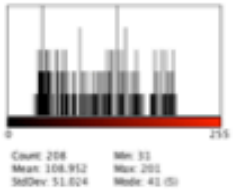	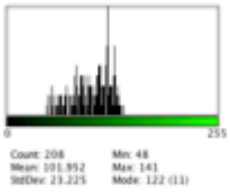	195	208	0.94

WT ↔ WT (Tips)

Tip	Red Histogram	Green Histogram	Red Pixels	Green Pixels	R/G
65	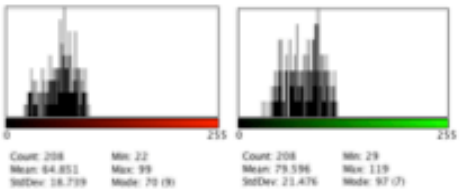		181	205	0.88
66	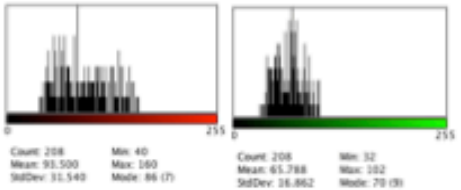		208	202	1.03
72	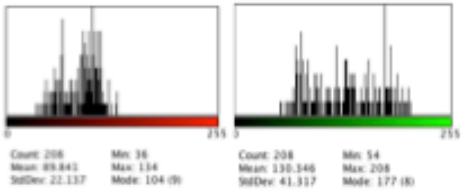		206	208	0.99
73	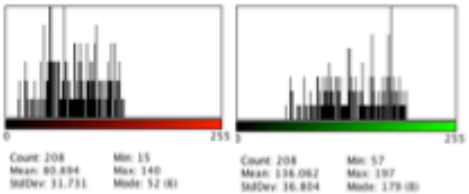		190	208	0.91
75	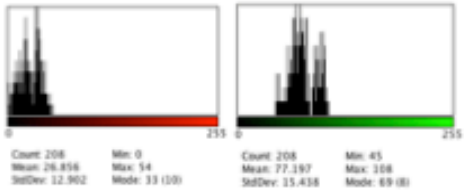		35	208	0.17

Tip	Red Histogram	Green Histogram	Red Pixels	Green Pixels	
81	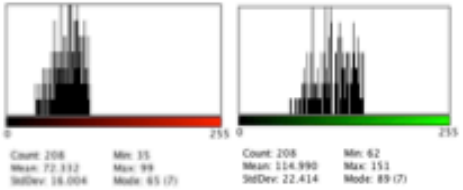		201	208	0.97
83	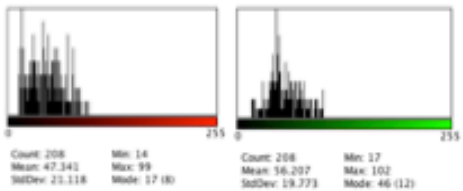		125	173	0.72
84	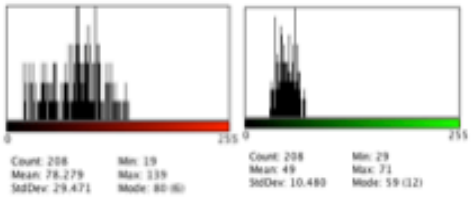		183	163	1.12
88	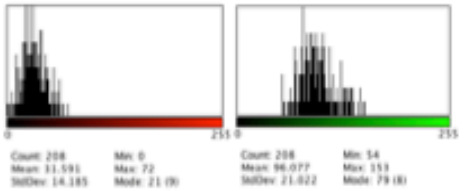		57	208	0.27
89	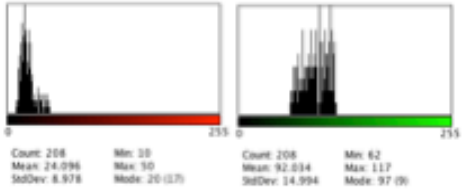		19	208	0.09

WT ↔ WT (Tips)

Trunk	Red Histogram	Green Histogram	Red Pixels	Green Pixels	R/G
1	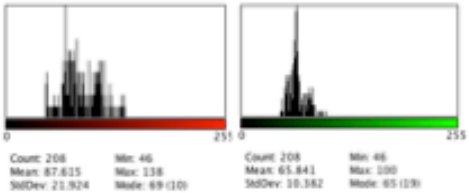		208	208	1.00
2	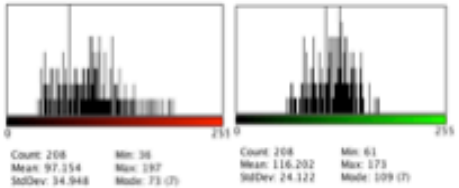		206	206	0.99
3	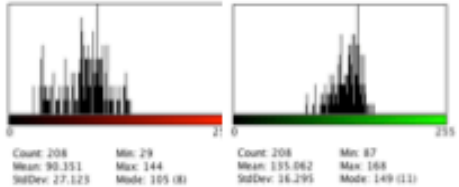		200	200	0.96
4	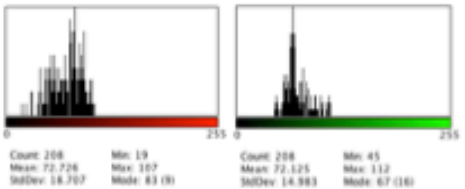		199	199	0.96
5	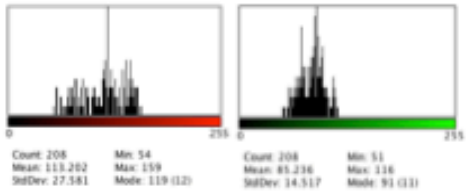		208	208	1.00

Trunk	Red Histogram	Green Histogram	Red Pixels	Green Pixels	
6	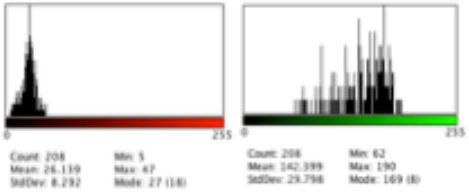		12	208	0.06
7	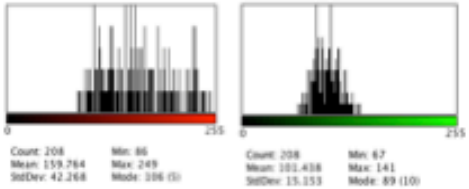		208	208	1.00
8	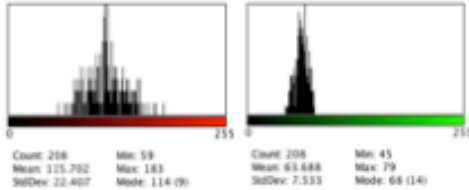		208	208	1.00
9	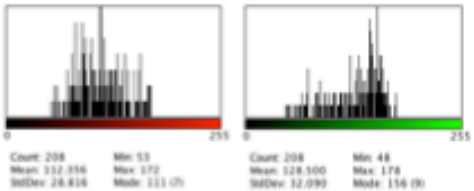		208	208	1.00
10	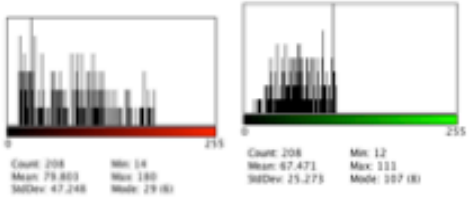		150	176	0.85

WT ↔ WT (Trunks)

Trunk	Red Histogram	Green Histogram	Red Pixels	Green Pixels	R/G
11	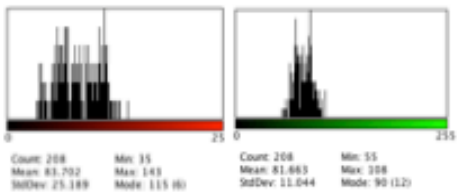		202	208	0.97
12	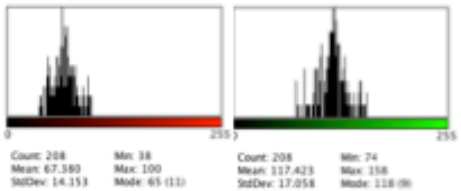		205	208	0.99
13	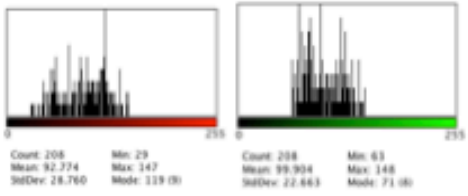		202	208	0.97
14	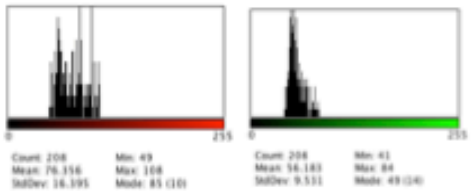		208	208	1.00
15	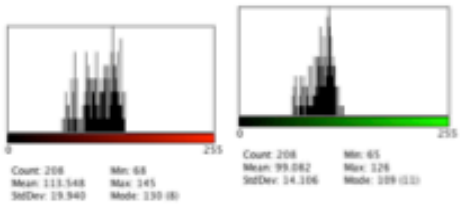		208	208	1.00

Trunk	Red Histogram	Green Histogram	Red Pixels	Green Pixels	
16	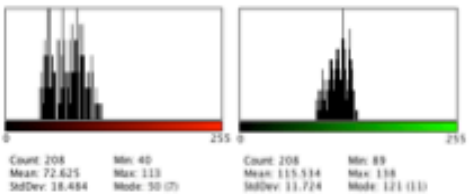		208	208	1.00
17	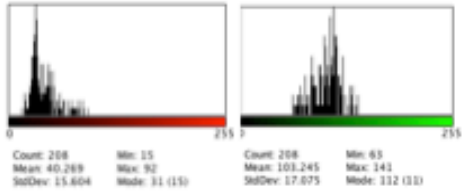		87	208	0.42
18	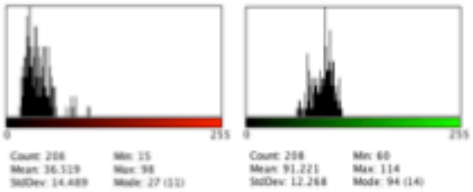		73	208	0.35
19	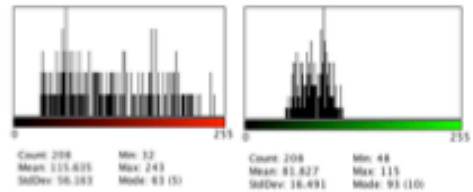		195	208	0.94
20	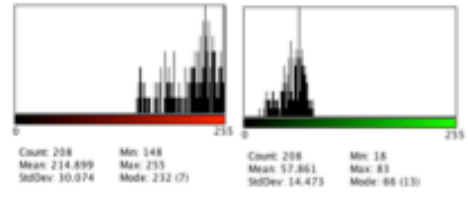		208	178	1.17

WT ↔ WT (Trunks)

Trunk	Red Histogram	Green Histogram	Red Pixels	Green Pixels	R/G
21	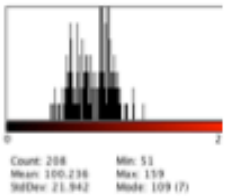	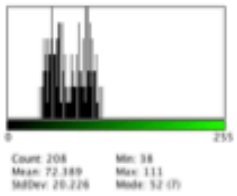	208	206	1.01
22	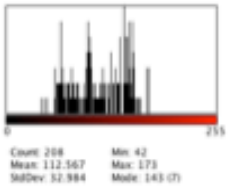	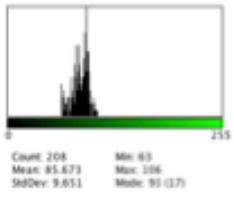	208	208	1.00
23	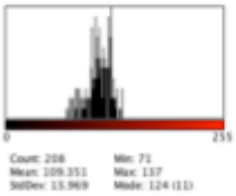	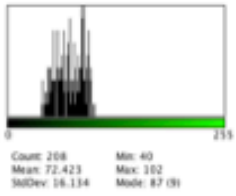	208	208	1.00
24	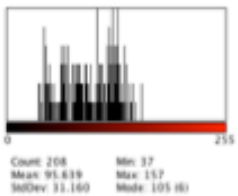	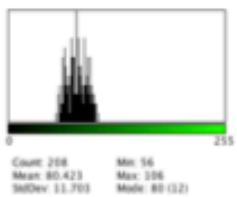	204	208	0.98
25	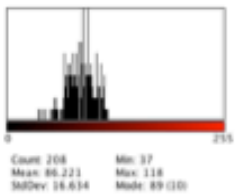	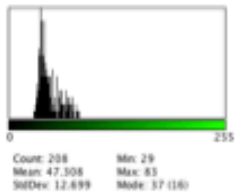	206	137	1.50

Trunk	Red Histogram	Green Histogram	Red Pixels	Green Pixels	
26	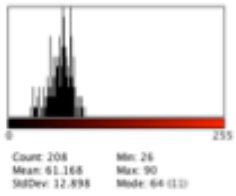	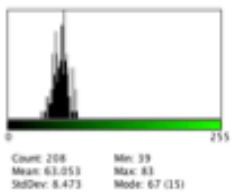	194	207	0.94
27	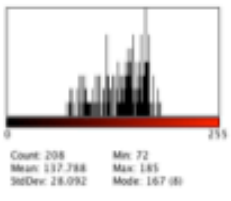	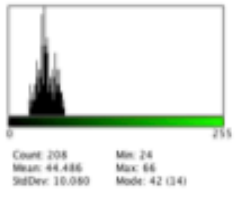	208	139	1.50
28	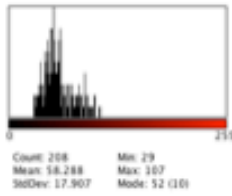	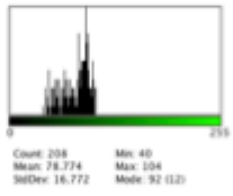	181	208	0.87
29	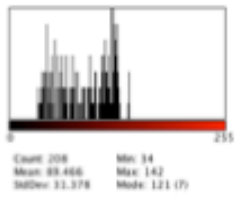	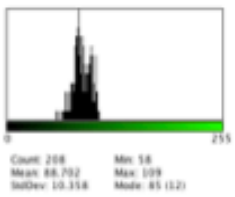	198	208	0.95
30	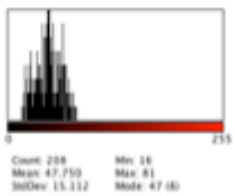	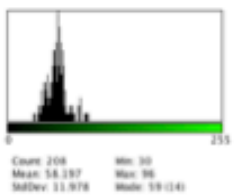	147	199	0.74

WT ↔ WT (Trunks)

Fgfr2$^{UB-/-}$ ⟷ WT

1:1

3 days

Background Control Region Histograms

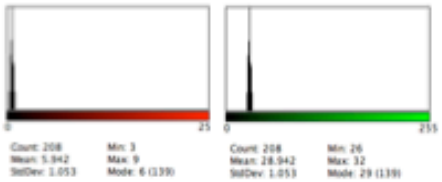

>32 >32

Whole Culture Histograms

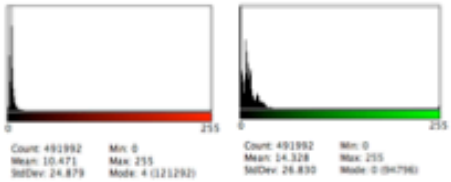

Number of pixels
over control region

Red	Green
28,903	26,557

Red/Green Ratio

1.088

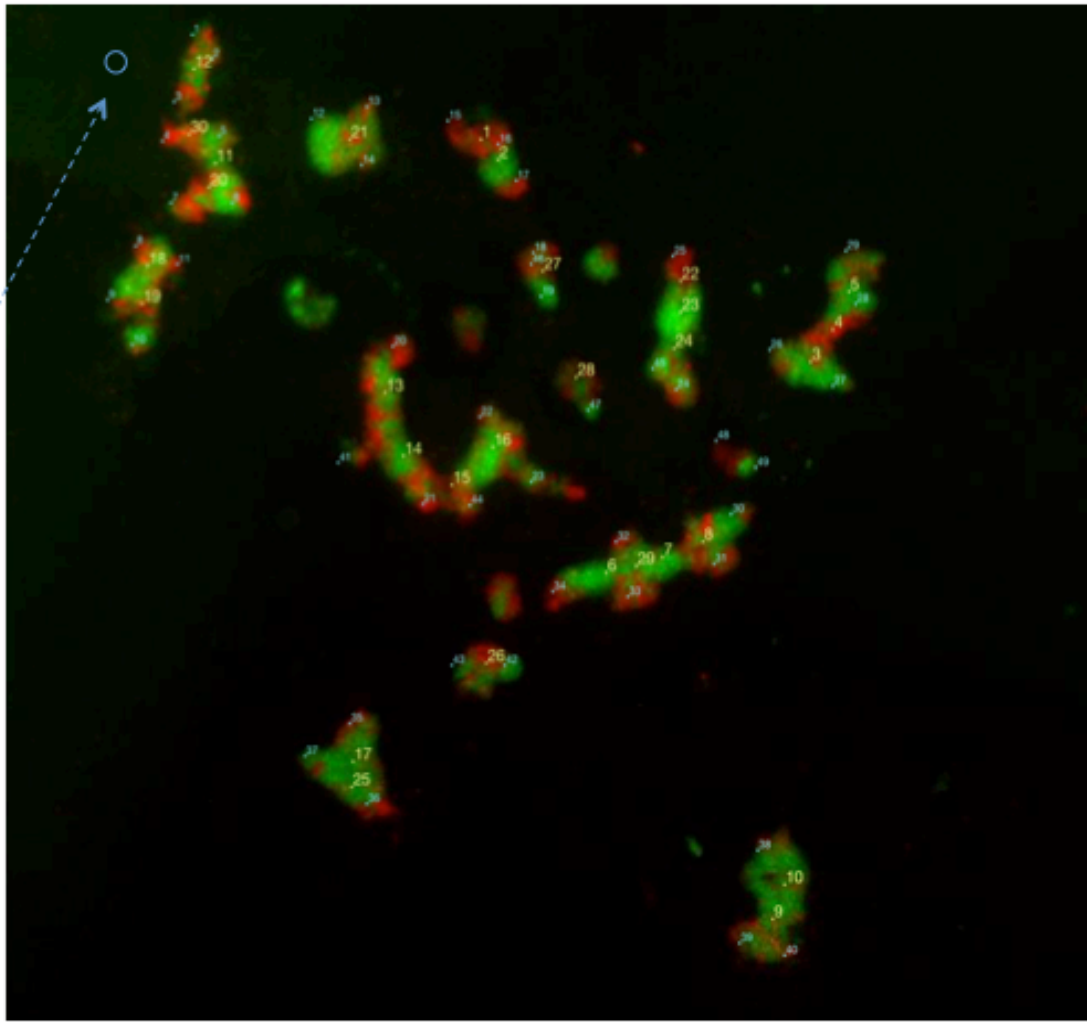

Tip	Red Histogram	Green Histogram	Red Pixels	Green Pixels	R/G
1	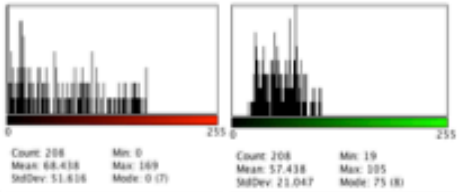		126	154	0.82
3	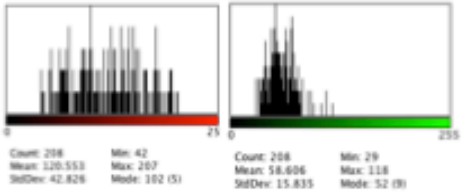		208	186	1.12
4	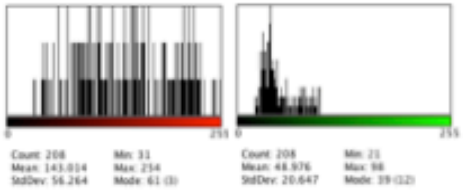		208	112	1.86
6	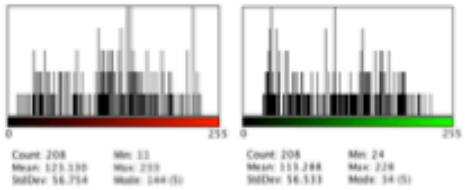		188	180	1.04
7	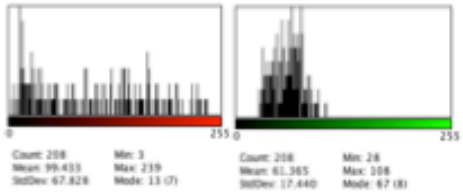		147	181	0.81

Tip	Red Histogram	Green Histogram	Red Pixels	Green Pixels	
8	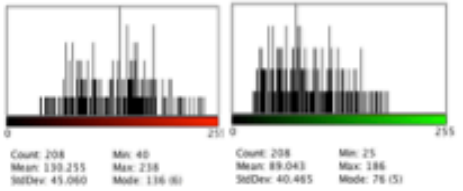		208	184	1.13
10	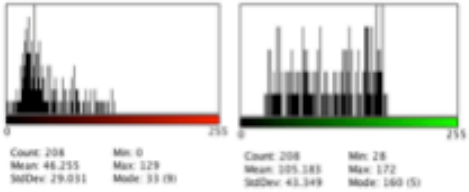		90	194	0.46
11	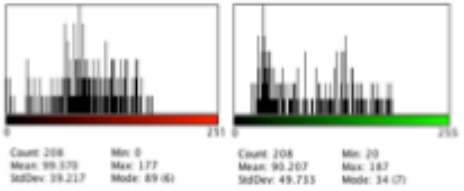		191	161	1.19
13	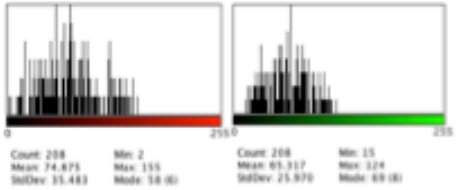		172	164	1.05
14	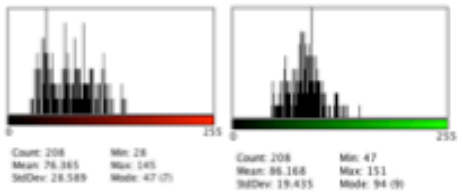		188	208	0.90

$Fgfr2^{UB-/-}$ ↔ WT (Tips)

Tip	Red Histogram	Green Histogram	Red Pixels	Green Pixels	R/G
15	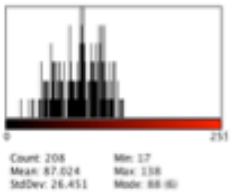	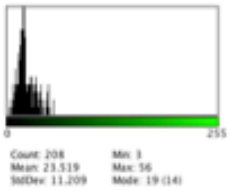	202	23	8.78
16	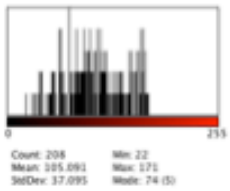	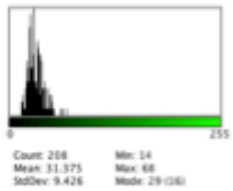	201	35	5.74
18	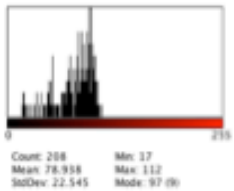	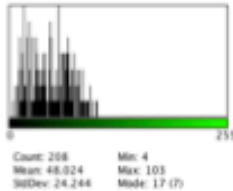	192	125	1.54
20	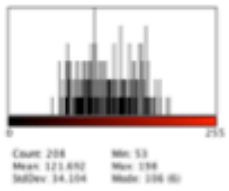	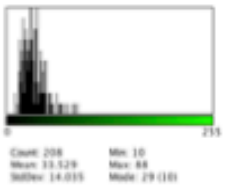	208	56	3.71
22	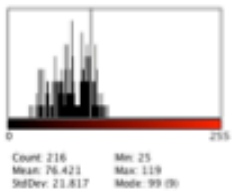	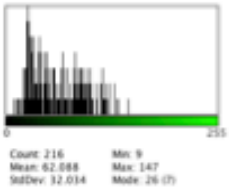	201	146	1.38

Tip	Red Histogram	Green Histogram	Red Pixels	Green Pixels	
23	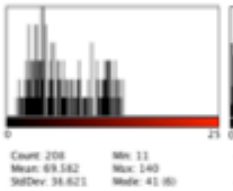	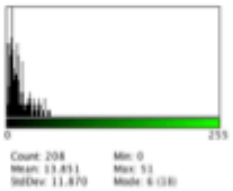	154	10	15.40
24	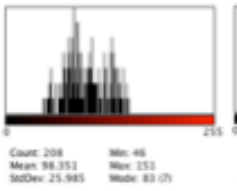	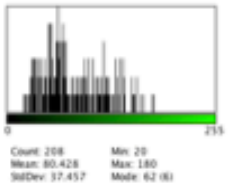	208	181	1.15
27	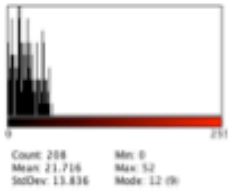	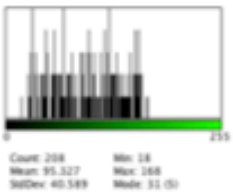	33	187	0.18
28	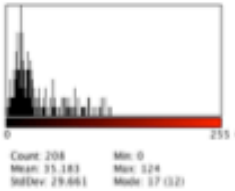	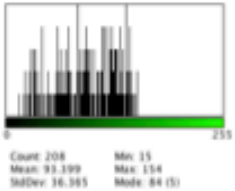	61	185	0.33
29	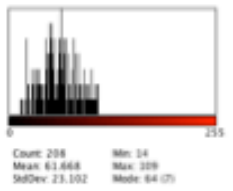	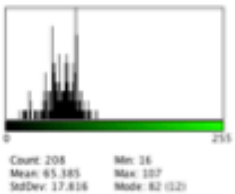	170	196	0.87

Fgfr2$^{UB-/-}$ ↔ WT (Tips)

Tip	Red Histogram	Green Histogram	Red Pixels	Green Pixels	R/G
33	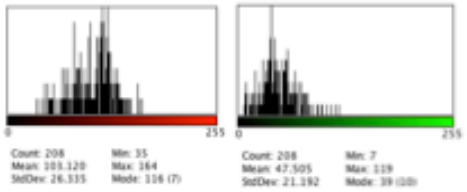		206	124	1.66
36	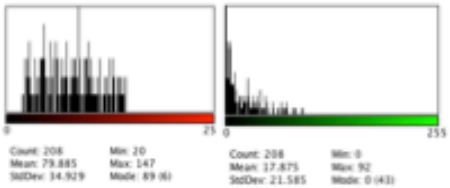		179	32	5.59
37	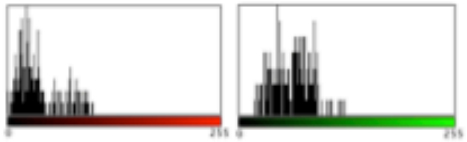		66	169	0.39
38	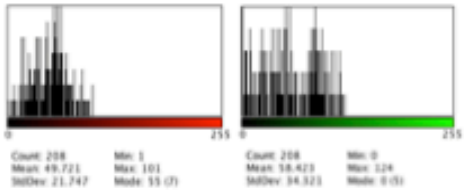		137	141	0.97
39	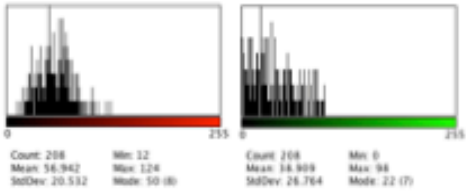		164	90	1.82

Tip	Red Histogram	Green Histogram	Red Pixels	Green Pixels	
41	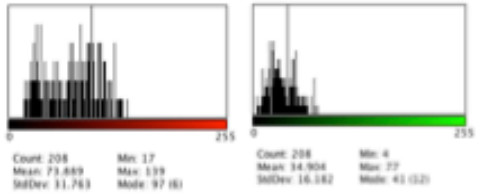		163	81	2.01
42	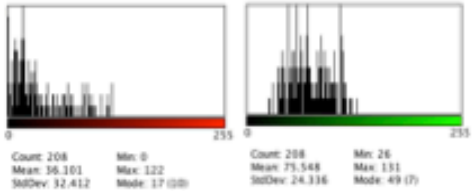		67	196	0.34
44	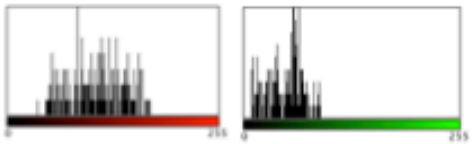		207	133	1.56
45	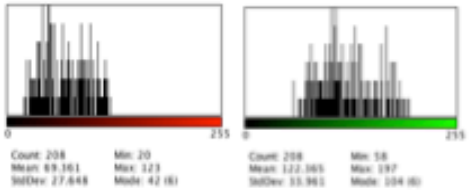		172	208	0.83
49	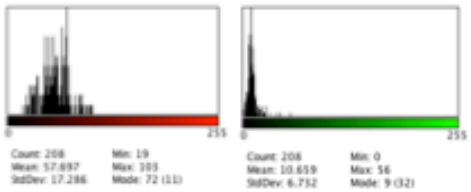		174	3	58.00

$Fgfr2^{UB-/-}$ ⟷ WT (Tips)

Trunk	Red Histogram	Green Histogram	Red Pixels	Green Pixels	R/G
1	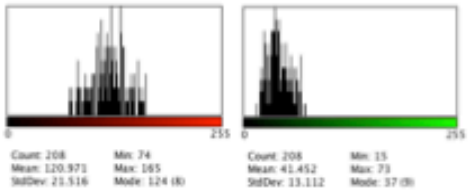		208	106	1.96
2	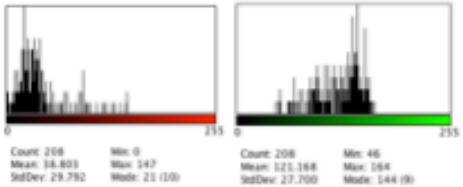		65	208	0.31
3	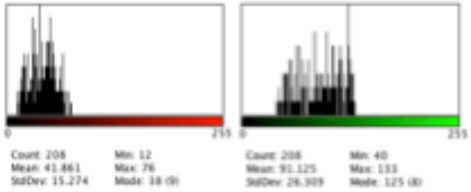		107	208	0.51
4	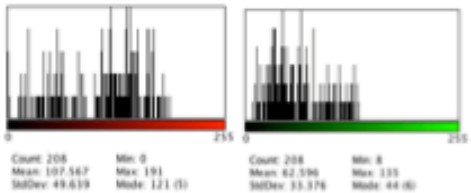		184	147	1.25
5	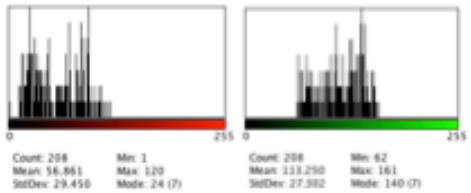		129	208	0.62

Trunk	Red Histogram	Green Histogram	Red Pixels	Green Pixels	
6	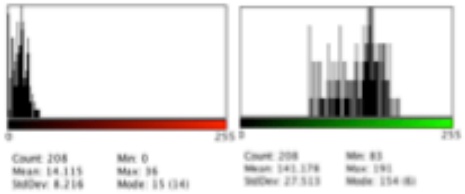		0	208	0.00
7	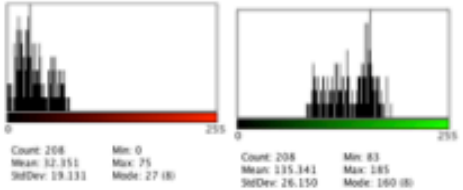		66	208	0.32
8	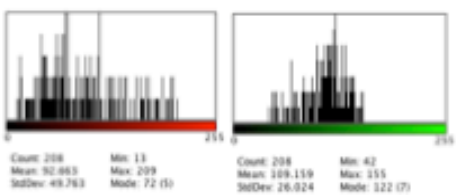		186	208	0.89
9	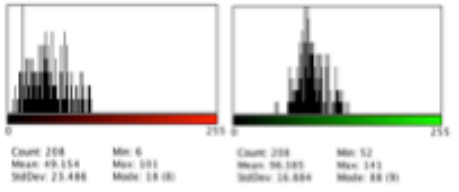		131	208	0.63
10	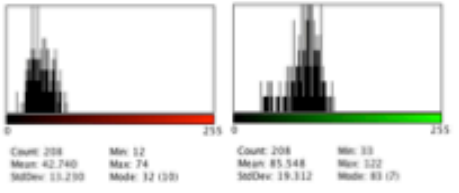		113	202	0.56

$Fgfr2^{UB-/-}$ ⟷ WT (Trunks)

Trunk	Red Histogram	Green Histogram	Red Pixels	Green Pixels	R/G
11	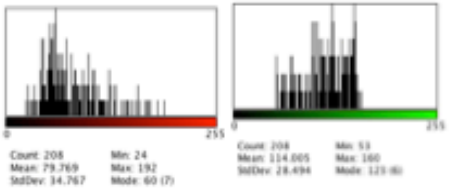		198	208	0.95
12	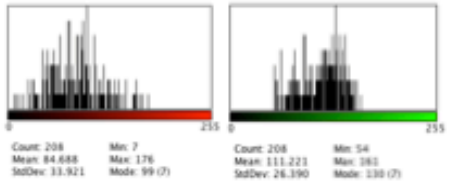		192	208	0.92
13	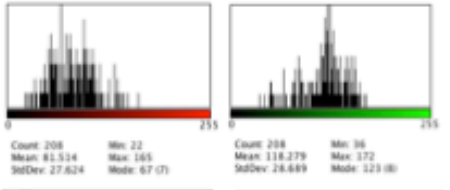		199	207	0.96
14	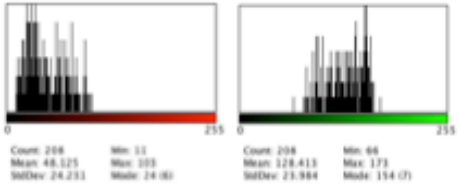		110	208	0.53
15	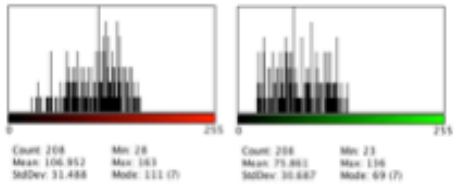		202	177	1.14

Trunk	Red Histogram	Green Histogram	Red Pixels	Green Pixels	R/G
16	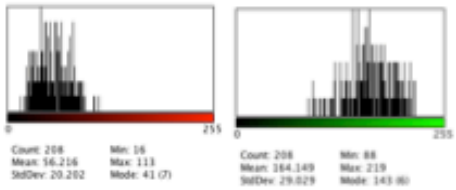		161	208	0.77
17	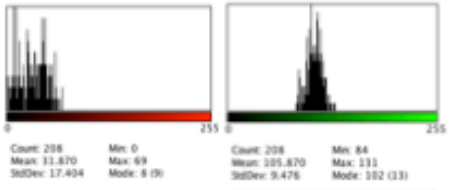		80	208	0.38
18	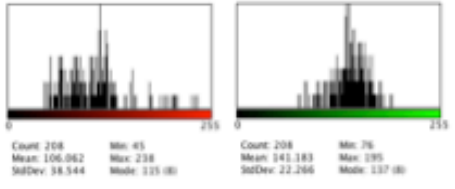		208	208	1.00
19	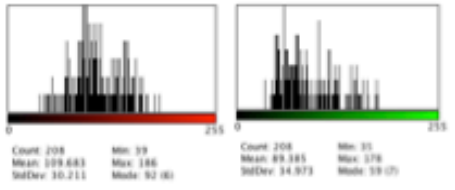		207	206	1.00
20	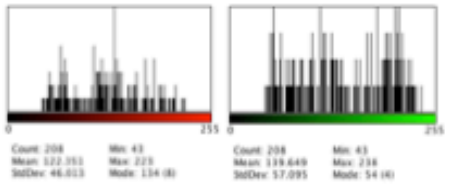		208	208	1.00

$Fgfr2^{UB-/-}$ ⟷ WT (Trunks)

Trunk	Red Histogram	Green Histogram	Red Pixels	Green Pixels	R/G
21	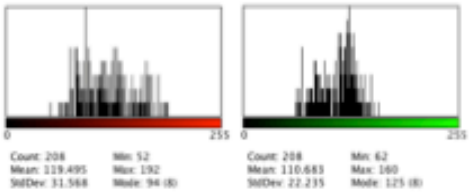		208	208	1.00
22	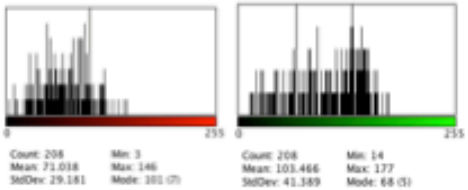		175	189	0.93
23	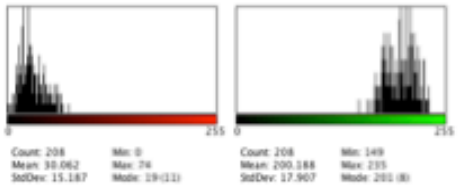		53	208	0.25
24	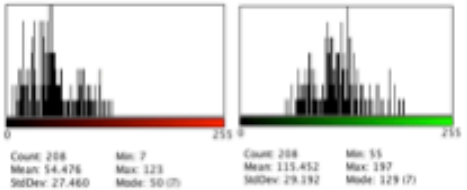		143	208	0.69
25	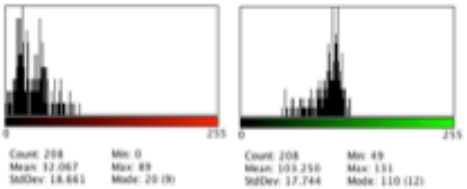		72	208	0.35

Trunk	Red Histogram	Green Histogram	Red Pixels	Green Pixels
26	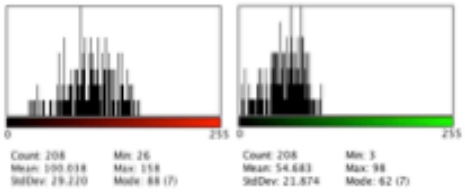		200	162
27	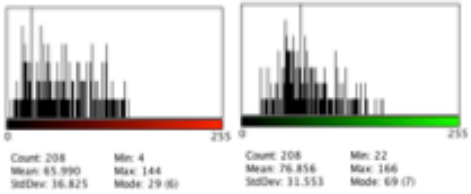		148	190
28	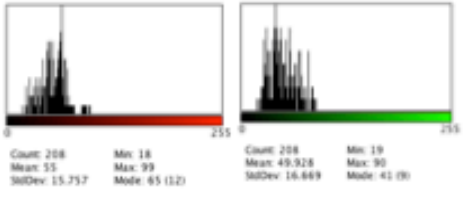		172	149
29	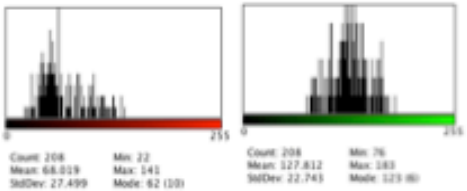		189	208
30	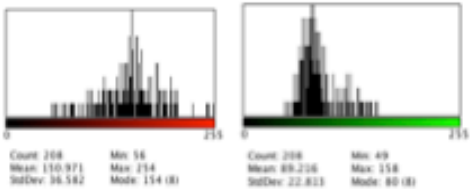		208	208

$Fgfr2^{UB-/-}$ ↔ WT (Trunks)

WT ↔ WT

1:1

3 days

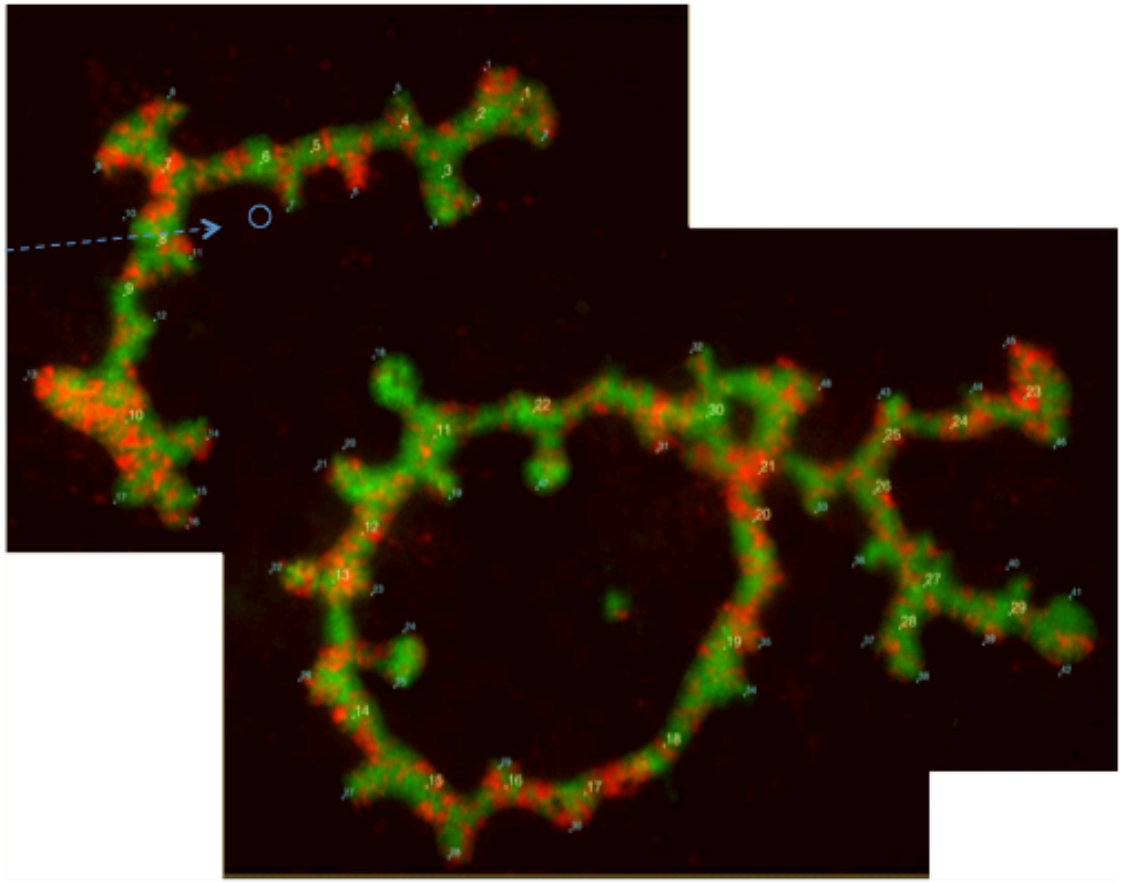

Background Control Region Histograms

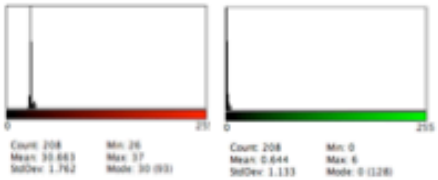

>37 >37

Whole Culture Histograms

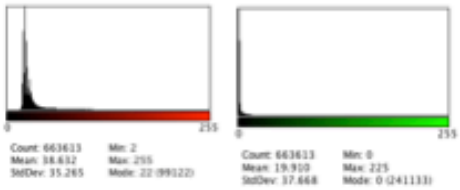

Number of pixels
over control region

Red	Green
139,990	129,999

Red/Green Ratio

1.077

Tip	Red Histogram	Green Histogram	Red Pixels	Green Pixels	R/G
1	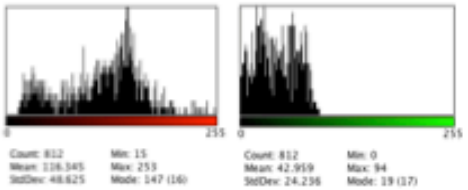		185	111	1.7
2	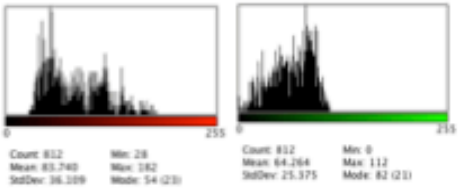		193	168	1.1
4	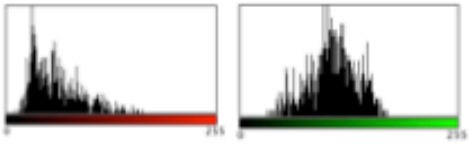		145	207	0.7
5	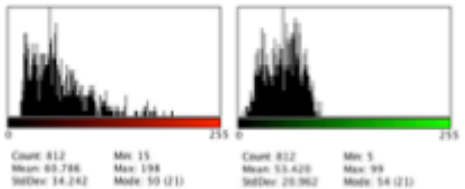		145	147	1.0
7	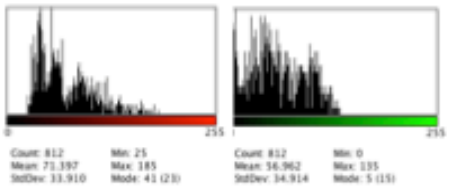		172	137	1.3

Tip	Red Histogram	Green Histogram	Red Pixels	Green Pixels	
9	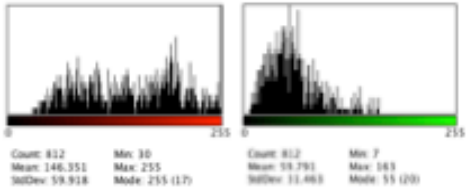		206	152	1.4
14	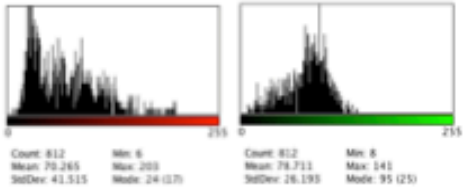		140	187	0.8
15	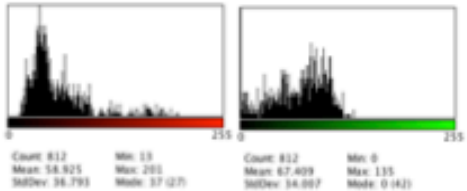		134	161	0.8
16	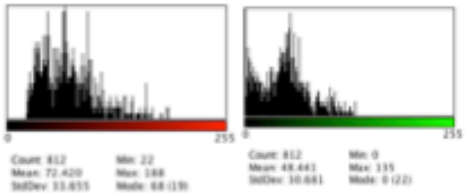		173	130	1.3
18	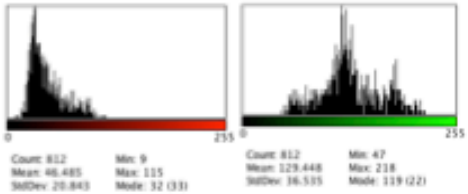		107	208	0.5

WT ↔ WT (Tips)

Tip	Red Histogram	Green Histogram	Red Pixels	Green Pixels	R/G
20	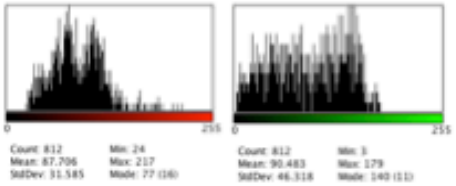		196	171	1.1
22	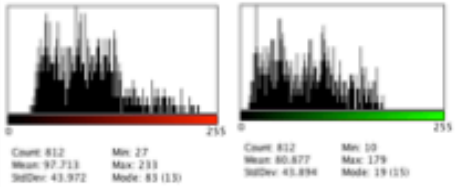		197	163	1.2
23	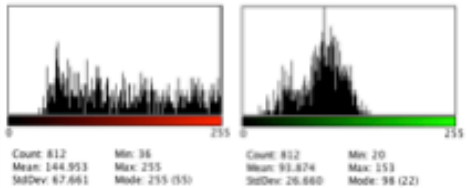		208	202	1.0
24	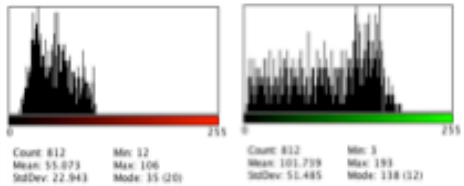		140	174	0.8
25	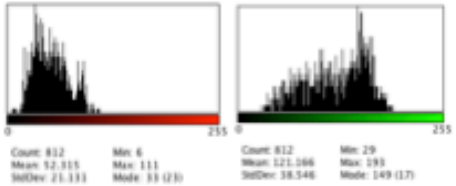		141	205	0.7

Tip	Red Histogram	Green Histogram	Red Pixels	Green Pixels	R/G
26	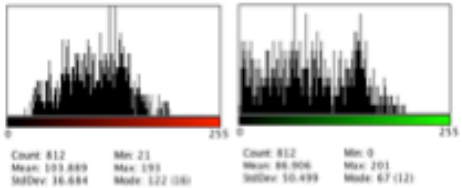		198	164	1.2
28	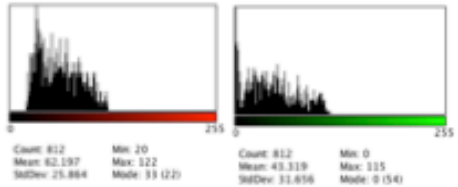		153	103	1.5
29	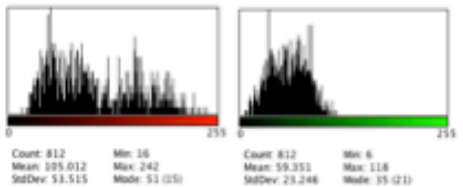		192	158	1.2
32	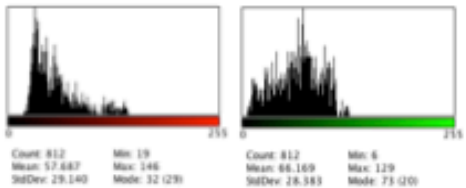		138	166	0.8
33	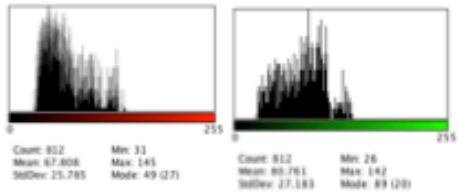		193	192	1.0

WT ↔ WT (Tips)

Tip	Red Histogram	Green Histogram	Red Pixels	Green Pixels	R/G
34	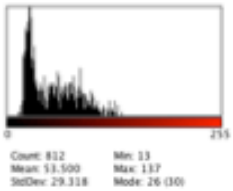	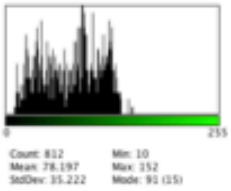	116	168	0.7
36	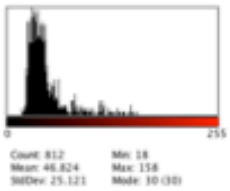	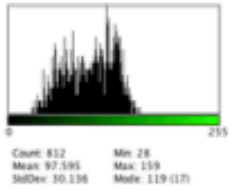	104	204	0.5
37	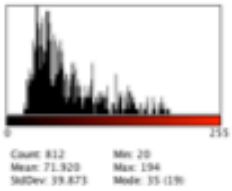	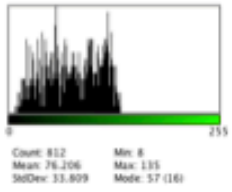	164	172	1.0
38	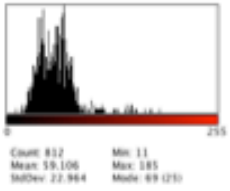	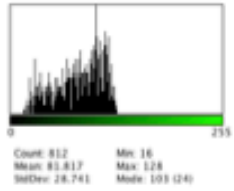	170	183	0.9
40	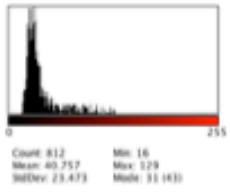	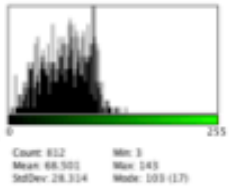	63	169	0.4

Tip	Red Histogram	Green Histogram	Red Pixels	Green Pixels	
42	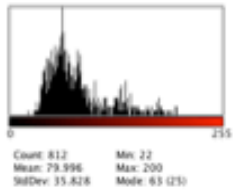	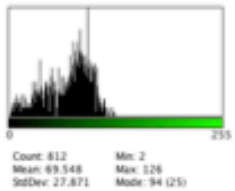	199	169	1.2
43	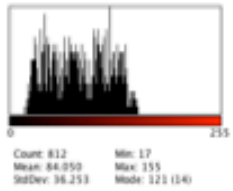	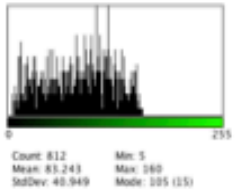	180	168	1.1
45	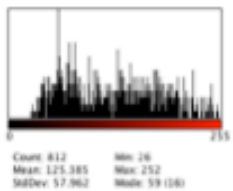	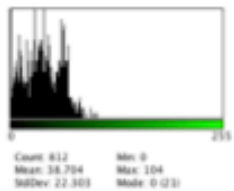	202	74	2.7
46	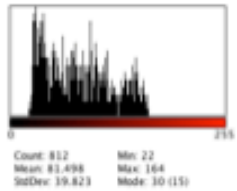	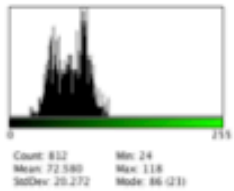	166	201	0.8
48	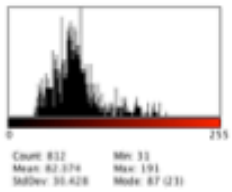	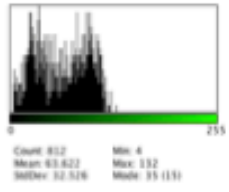	201	143	1.4

WT ↔ WT (Tips)

Trunk	Red Histogram	Green Histogram	Red Pixels	Green Pixels	R/G
1	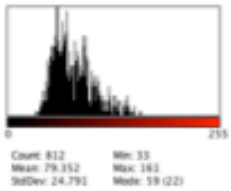	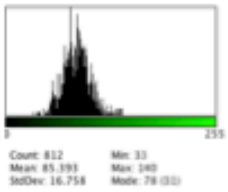	206	207	1.00
2	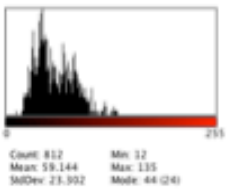	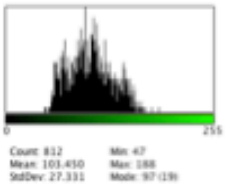	164	208	0.79
3	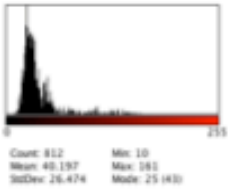	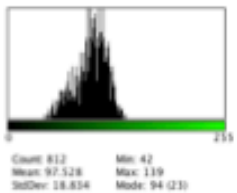	62	208	0.30
4	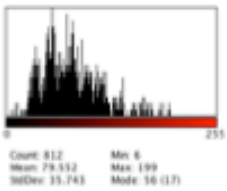	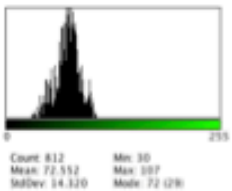	182	205	0.89
5	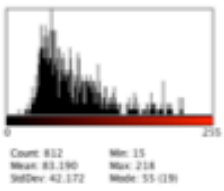	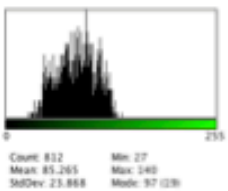	195	204	0.95

Trunk	Red Histogram	Green Histogram	Red Pixels	Green Pixels	R/G
6	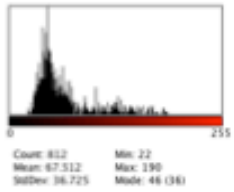	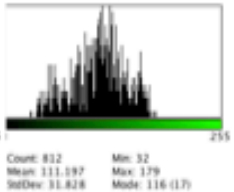	175	207	0.85
7	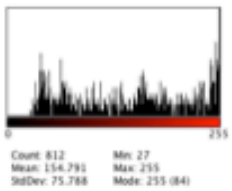	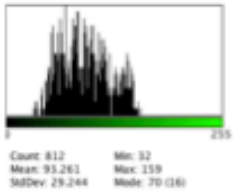	199	206	0.97
8	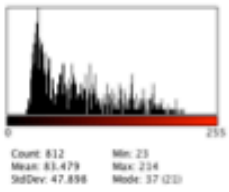	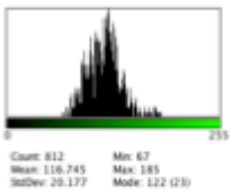	164	208	0.79
9	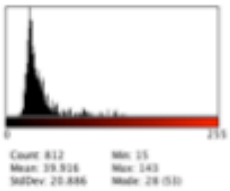	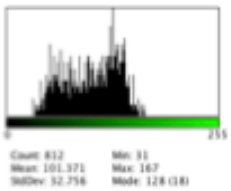	67	205	0.33
10	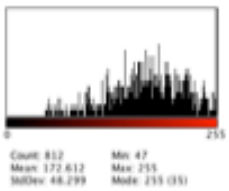	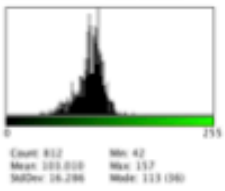	208	208	1.00

WT ↔ WT (Trunks)

Trunk	Red Histogram	Green Histogram	Red Pixels	Green Pixels	R/G
11	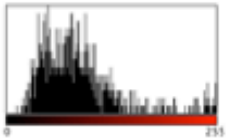	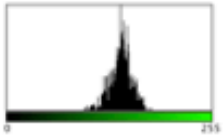	186	208	0.89
12	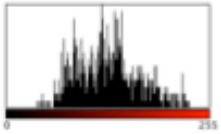	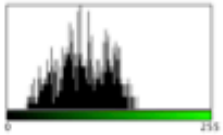	208	200	1.04
13	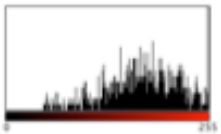	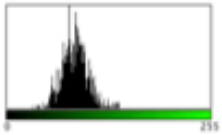	208	208	1.00
14	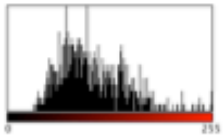	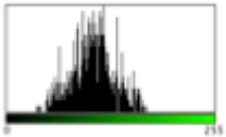	206	207	0.99
15	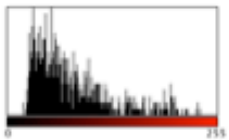	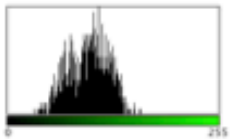	164	207	0.79

Trunk	Red Histogram	Green Histogram	Red Pixels	Green Pixels	R/G
16	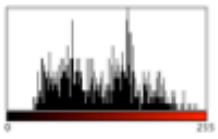	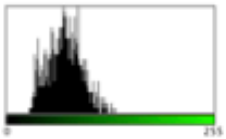	205	193	1.06
17	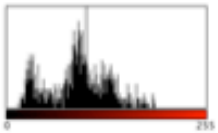	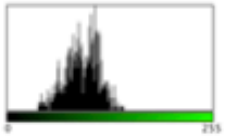	177	207	0.86
18	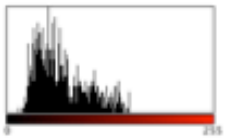	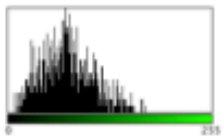	165	175	0.94
19	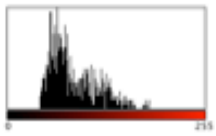	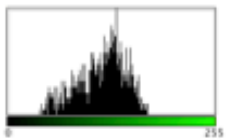	208	208	1.00
20	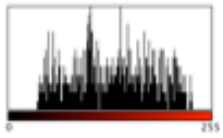	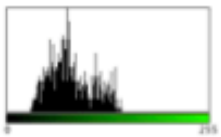	206	200	1.03

WT ↔ WT (Trunks)

Trunk	Red Histogram	Green Histogram	Red Pixels	Green Pixels	R/G
21	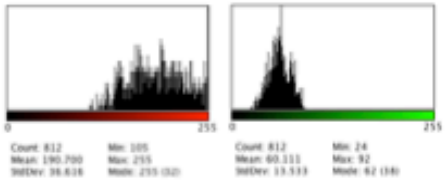		208	194	1.07
22	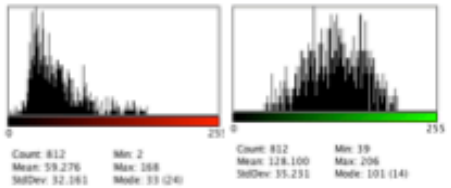		141	208	0.68
23	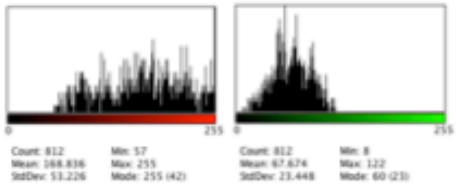		208	183	1.14
24	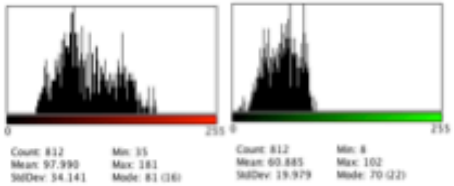		206	171	1.21
25	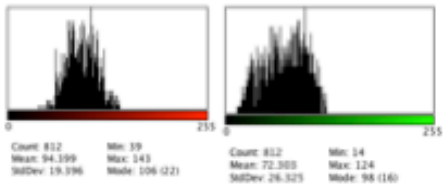		208	178	1.17

Trunk	Red Histogram	Green Histogram	Red Pixels	Green Pixels	R/G
26	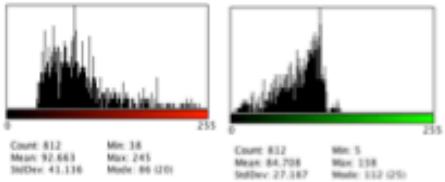		206	192	1.07
27	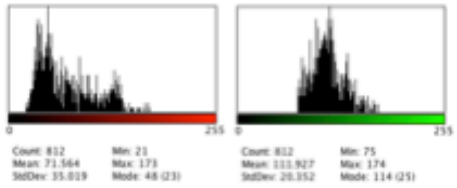		168	208	0.81
28	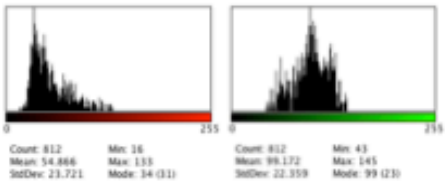		141	208	0.68
29	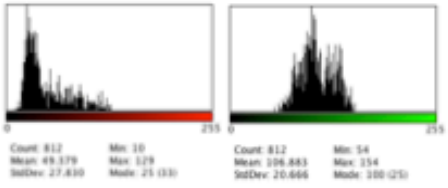		97	208	0.46
30	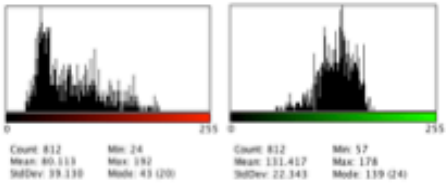		188	208	0.90

WT ↔ WT (Trunks)